AN ANALYTICAL MODEL OF A VEHICLE OCCUPANT FOR USE IN CRASH SIMULATIONS

by

Bruce Michael Bowman

APPENDIX C

AN ANALYTICAL MODEL OF A VEHICLE OCCUPANT FOR USE IN CRASH SIMULATIONS

ACKNOWLEDGMENTS

I would like to express my gratitude to all those who were associated with the research presented here. I wish to thank, in particular:

Professor Samuel K. Clark, Chairman of the doctoral committee, for his guidance throughout this study.

Professors Robert L. Hess, Robert C. Juvinall, and Wei H. Yang and Doctor D. Hurley Robbins, members of the doctoral committee, for their advice and assistance.

Doctor Verne L. Roberts and Doctor James H. McElhaney of the Biosciences Division of The University of Michigan Highway Safety Research Institute, which provided financial support for this investigation.

Mr. Robert O. Bennett for his guidance in various computational aspects of this research and for aid in using the HSRI 3-D computer model.

Mr. Nabih Alem for his assistance in the reduction of experimental data.

And, finally, Sue Stewart for typing the final manuscript.

TABLE OF CONTENTS

Page

ACKNOWLEDGMENTS ii

LIST OF FIGURES vi

LIST OF APPENDICES xii

NOMENCLATURE xiii

ABSTRACT xxi

Chapter

1 INTRODUCTION 1

2 INVESTIGATORY MODELS 5

3 THE ANALYTICAL MODEL 9

3.1 The Kinetic Linkage 9
3.2 The Generalized Coordinates 14
3.3 The Basic Joint Model 17

3.3.1 Joint Stop Moments 20
3.3.2 Elastic Moments 22
3.3.3 Muscle Tension Moments 24

4 THE DIFFERENTIAL EQUATIONS OF MOTION 26

4.1 Lagrange's Equations 26
4.2 The Rotation Matrix 27
4.3 The Angular Velocity Vector 29
4.4 Torso Kinetic Energy 31

4.4.1 Translational Terms in the Equations of Motion 35
4.4.2 Rotational Terms in the Equations of Motion .. 37

4.5 Head Kinetic Energy 38

4.5.1 Translational Terms in the Equations of Motion 41
4.5.2 Rotational Terms in the Equations of Motion .. 42

4.6 Torso Potential Energy and Dissipation Functions and Contributions to the Equations of Motion 42

4.6.1 Torso Gravitational Terms 42
4.6.2 Torso Joint Stop Terms for Bending 43
4.6.3 Torso Joint Stop Terms for Twisting 54

Chapter Page

4.6.4 Torso Elastic Terms for Bending 58
4.6.5 Torso Elastic Terms for Twisting 63

4.7 Neck-Linkage Potential Energy and Dissipation Functions and Contributions to the Equations of Motion .. 64

4.7.1 Head Gravitational Terms 64
4.7.2 Neck-Torso Joint Stop Terms for Bending 65
4.7.3 Neck-Head Joint Stop Terms for Bending 68
4.7.4 Head-Torso Joint Stop Terms for Twisting 75
4.7.5 Neck-Torso Elastic Terms for Bending 77
4.7.6 Neck-Head Elastic Terms for Bending 79
4.7.7 Head-Torso Elastic Terms for Twisting 83
4.7.8 Neck Stretching Terms 83

4.8 Muscle Tension 84

4.8.1 Muscle Tension Moments 88
4.8.2 Muscle Tension Forces 89

5 THE NUMERICAL SOLUTION 90

6 PRELIMINARY TEST RUNS OF THE COMPUTER MODEL 93

7 FORCED MOTION 101

7.1 The Forcing Feature 101
7.2 Uses of the Forcing Feature 103

7.2.1 Excitation 103
7.2.2 Elimination of Non-participating Degrees of Freedom 103
7.2.3 Constraining the Mathematical Model 104

7.3 Verification for Simple Forced Motion Problems 105

8 PRELIMINARIES FOR CRASH SIMULATIONS 107

8.1 Selection of Vehicle Occupant Parameter Values 107

8.1.1 Body Parameters 107
8.1.2 Joint Parameters 109

8.2 Neck Initial Conditions 118

9 THE PHILOSOPHY OF MODEL VERIFICATION 120

10 VERIFICATION OF THE VEHICLE OCCUPANT MODEL 123

10.1 Frontal Impact 123
10.2 Side Impact 141

Chapter Page

10.3 Side Impact with Zero Elastic Neck Moments 161
10.4 Side Impact with Non-Zero Muscle Tension 171
10.5 Oblique Impact: Excitation at Lower Torso 188
10.6 Oblique Impact: Excitation at Upper Torso 207

11 CONCLUSIONS AND SUGGESTIONS FOR EXTENDED RESEARCH 213

11.1 Conclusions 213
11.2 Suggestions for Extended Research 214

LIST OF FIGURES

Figure Page

1. Two-dimensional "chain" systems for investigating extensible and inextensible spine model formulations 6

2. Profile of the kinetic linkage of the crash victim model (n=3) 12

3. Profile of the kinetic linkage of the crash victim model, with two leg elements (n=5) 13

4. Inertial Euler angles for element i 15

5. The "generalized pitching angle" and the "heading angle" for bending at a typical torso joint 19

6. Stop angle "ellipse" for a ball-and-socket joint 21

7. Illustration of the relative positions of spinal joints and the center of mass for torso element i 32

8. Vector constraint loop for elimination of (x_2, y_2, z_2) 33

9. The head-neck-torso linkage 39

10. View along k_{i+1}, showing heading angle Θ_i 45

11. Heading angle Θ_i as the angle between i_{i+1} and the projection of $\vec{v}$ on the i_{i+1}-j_{i+1} plane 45

12. Stop angle "ellipse" 47

13. Neck-torso joint coordinates 66

14. Neck-head joint coordinates 66

15. A linear Maxwell element forced by $x(t)$, $x = x_2 - x_1$ 85

16. A free system to be forced by $x_1(t)$ 102

17. Extreme voluntary forward bending of torso 114

18. A sector 114

19. Extreme voluntary fore-aft bending of torso 117

20. Extreme voluntary lateral bending of torso 117

21. Frontal impact: before and after t = 0 124

Figure Page

22. Profile of the vehicle occupant with some of its dimensions (in feet) 133

23. Frontal impact time history for pitching 134

24. Torso pitching for frontal impact 135

25. Head pitching for frontal impact 136

26. Pitching angle for head relative to torso 137

27. Relative pitching angle at neck-torso joint (N-T) 138

28. Relative pitching angle at neck-head joint (N-H) 139

29. Components of neck compression force in e_1 140

30. HSRI 3-D and dummy head yaw for side impact 142

31. HSRI 3-D and dummy head pitch for side impact 143

32. HSRI 3-D and dummy head roll for side impact 144

33. HSRI 3-D and VOM head yaw for side impact 150

34. HSRI 3-D and VOM head pitch for side impact 151

35. HSRI 3-D and VOM head roll for side impact 152

36. Head yaw relative to torso for side impact: VOM and HSRI 3-D 153

37. Head pitch relative to torso for side impact: VOM and HSRI 3-D 154

38. Head roll relative to torso for side impact: VOM and HSRI 3-D 155

39. Generalized pitching angle R and heading angle Θ at neck-torso joint (N-T) for side impact 156

40. Generalized pitching angle R' and heading angle Θ' at neck-head joint (N-H) for side impact 157

41. HSRI 3-D torso roll for side impact 158

42. Neck length compression force for side impact 158

43. Elastic spring moment at neck-torso joint (N-T) for side impact 159

Figure Page

44. Elastic spring moment at neck-head joint (N-H) for side impact 159

45. Head x-position for side impact 160

46. Head y-position for side impact 160

47. Head z-position for side impact 160

48. Head yaw for side impact, with and without elastic neck moments 163

49. Head pitch for side impact, with and without elastic neck moments 164

50. Head roll for side impact, with and without elastic neck moments 165

51. Relative head yaw for side impact, with and without elastic neck moments 166

52. Relative head pitch for side impact, with and without elastic neck moments 167

53. Relative head roll for side impact, with and without elastic neck moments 168

54. Generalized pitching angle R and heading angle Θ at neck-torso joint (N-T) for side impact, with zero elastic neck moments 169

55. Generalized pitching angle R' and heading angle Θ' at neck-head joint (N-H) for side impact, with zero elastic neck moments 170

56. Head yaw for side impact with non-zero muscle tension 176

57. Head pitch for side impact with non-zero muscle tension ... 177

58. Head roll for side impact with non-zero muscle tension 178

59. Relative head yaw for side impact with non-zero muscle tension 179

60. Relative head pitch for side impact with non-zero muscle tension 180

61. Relative head roll for side impact with non-zero muscle tension 181

Figure Page

62. Muscle tension moment for generalized pitching at the neck-torso joint (N-T) 182

63. Muscle tension moment for generalized pitching at the neck-head joint (N-H) 182

64. Muscle tension moment for twisting at the head-torso joint (H-T) 182

65. Generalized pitching angle R and heading angle Θ at neck-torso joint (N-T) for side impact, with non-zero muscle tension 183

66. Generalized pitching angle R' and heading angle Θ' at neck-head joint (N-H) for side impact, with non-zero muscle tension 184

67. Neck-torso joint stop moments, with and without muscle tension 185

68. Neck-head joint stop moments for zero muscle tension 186

69. Neck-head joint stop moments for non-zero muscle tension .. 187

70. Simultaneous oblique impact by two vehicles 189

71. Vehicle yawing velocity and acceleration profiles 193

72. Vehicle yaw for double oblique impact at 50 mph 194

73. Torso wind-up for oblique impact: excitation at lower torso 197

74. Yaw for second torso element relative to first torso element 198

75. Yaw for third torso element relative to second torso element 199

76. Generalized pitching angle R_1 and heading angle Θ_1 at first torso joint for oblique impact 200

77. Generalized pitching angle R_2 and heading angle Θ_2 at second torso joint for oblique impact 201

78. HSRI 3-D and VOM head yaw for oblique impact: excitation at lower torso 202

Figure Page

79. HSRI 3-D and VOM head pitch for oblique impact: excitation at lower torso 203

80. HSRI 3-D and VOM head roll for oblique impact: excitation at lower torso 204

81. Head yaw relative to torso for oblique impact: excitation at lower torso 205

82. Head pitch relative to torso for oblique impact: excitation at lower torso 206

83. Head roll relative to torso for oblique impact: excitation at lower torso 206

84. HSRI 3-D and VOM head yaw for oblique impact: excitation at upper torso 208

85. HSRI 3-D and VOM head pitch for oblique impact: excitation at upper torso 209

86. HSRI 3-D and VOM head roll for oblique impact: excitation at upper torso 210

87. Head yaw relative to torso for oblique impact: excitation at upper torso 211

88. Head pitch relative to torso for oblique impact: excitation at upper torso 212

89. Head roll relative to torso for oblique impact: excitation at upper torso 212

90. A simple dynamic system with Maxwell element 229

91. Twisting test 232

92. Pitching test, elastic k 235

93. Pitching test, joint stop c 237

94. A Maxwell element 243

95. A three-parameter solid 244

96. Muscle at a joint 246

Figure Page

97. Two-dimensional analogue for joint stop resistance to bending at a typical torso joint 258

98. Joint stop resistance to twisting at a typical torso joint (top view of two connected body elements) 259

99. Two-dimensional analogue for elastic resistance to bending deformation away from equilibrium at a typical torso joint 260

100. Elastic resistance to twisting deformation away from equilibrium at a typical torso joint (top view of two connected elements) 261

101. Resistance to change of neck length 262

LIST OF APPENDICES

Page

LIST OF REFERENCES 216

APPENDIX A DERIVATIVES 220

APPENDIX B SOLUTION FOR MUSCLE TENSION FORCE BY REDUCTION TO QUADRATURE 229

APPENDIX C A SIMPLE DYNAMIC SYSTEM INVOLVING A MAXWELL ELEMENT . 233

APPENDIX D ANALYTICAL SOLUTIONS FOR SPECIAL CASES 235

APPENDIX E ESTIMATION OF NECK MUSCLE TENSION PARAMETER VALUES .. 250

APPENDIX F TWO-DIMENSIONAL ANALOGUES OF THE BASIC BALL-AND-SOCKET JOINT CHARACTERISTICS 258

NOMENCLATURE

a_1, a_2, a_3	Constant coefficients in c and k for Maxwell element
a,b	Body dimensions
a,b	Vehicle dimensions
a,b	Quantities defined for convenience
$a_{jk,i}$	Element of $[A_i]$; j^{th} row, k^{th} column
A	Area of an average cervical disc
$[A_i]$	Rotation matrix which takes e into e_i
$[A'_{i+1}]$	Rotation matrix which takes e_i into e_{i+1}
$[A]^{-1}$	Inverse of matrix [A]
$[A]^T$	Transpose of matrix [A]
A_{ij}	Matrix coefficients defined for convenience
Arg	Argument
b_{ik}	A quantity defined for convenience
b_{ij}	Elements of [B]
[B]	A matrix defined for convenience
c	Damping coefficient
$c_{i,j}$	Damping coefficient for j^{th}-order moment terms at joint i
c_1, c_2, c_3	Time-dependent factors defined for convenience
CG	Center of gravity
d	Distance of N-H backward from z_h-axis
d	Denominator
D	Rayleigh dissipation function
DISS	Dissipated energy

e	The basis of unit vectors for inertial frame
e_i	The basis of unit vectors for i^{th} rotating frame
$\hat{e}$	A unit vector
E	Young's modulus
E	Total energy
f	Joint stop angle as a function of heading angle
f_o	A natural frequency
$f(t)$	A curve to be fit by Lagrange interpolation
f_o, f_1, f_2	Local ordinate values for a curve to be fit by Lagrange interpolation
$\{f\}$	A vector of forces and moments
$\vec{F}_1, \vec{F}_2$	Force vectors for a Maxwell element
$F, F^{(\ell)}$	Static muscle tension force parameter indicating degree of muscle contraction
F	Tension in a Maxwell element
F	Force for neck Kelvin element
F	A force
F	Any function of generalized coordinates alone
g	Acceleration of gravity
G_{ki}	Coefficient of $\ddot{q}_i$ in the k^{th} Lagrange equation
$[G]$	Matrix with elements G_{ki}
h	Subscript or superscript indicating "head"
h	Average thickness for a cervical disk
h_1, h_2	Integration step sizes
$h(t)$	A quantity defined for convenience

H_k	The part of the first term in the k^{th} Lagrange equation containing no $\ddot{q}_i$
H-T	Head-torso joint, for twisting
HSRI	Subscript indicating results from the University of Michigan Highway Safety Research Institute 3-D model
i, j, k	Unit vectors for inertial frame
i_i, j_i, k_i	Unit vector for i^{th} rotating frame
i	Subscript indicating torso element i
$i+1$	Subscript indicating torso element next to and below element i
(i)	Superscript indicating i^{th} mass
$\overline{I}^{(i)}$	Inertia tensor for i^{th} body element (defined in i^{th} rotating coordinate frame)
I_i, J_i, K_i	Diagonal components of inertia tensor $\overline{I}^{(i)}$
$I_{pk}^{(i)}$	Components of $\overline{I}^{(i)}$ in e_i
$I_{jl,i}$	Components of inertia tensor $\overline{I}^{(i)}$ in e
I	A moment of inertia
I	An integral
J	An impulse integral
k	Spring coefficient
$k_{i,j}$	Spring coefficient for j^{th}-order moment terms at joint i
k_i'	k_i in e_{i+1}^o components after a rotation along with e_{i+1} into e_{i+1}^o
k'	Axial stiffness of an average cervical disc
KE	Kinetic energy

l	Neck length
$\vec{l}$	Neck length vector, N-T to N-H
$\hat{l}$	Unit vector for $\vec{l}$
$\hat{l}', \hat{l}''$	Vectors at N-T and N-H analogous to k_i'
l_{eq}	Equilibrium neck length
l_i	Length of torso element i
l	A vehicle dimension
(ℓ)	Superscript for linear muscle tension parameters
$\vec{L}_o$	Angular momentum vector with respect to origin of the inertial frame
$\vec{L}^{(v)}$	Linear component of $\vec{L}_o$
$\vec{L}^{(\omega)}$	Angular component of $\vec{L}_o$
L_x, L_y, L_z	Inertial components of $\vec{L}_o$
L	Effective moment arm for muscle at a joint
L_i	A polynomial for Lagrange interpolation
m_i	Mass of element i
m, M	A mass
M, K, C	Mass, spring and damping elements for a "black box"
M, M_i	A component of the total moment at a joint
$M, M^{(\theta)}$	Static muscle tension moment parameter at a joint indicating degree of muscle contraction
M	A moment
MT	Subscript indicating "muscle tension"
n	Number of torso and leg elements
n	Numerator

N	Number of degrees of freedom
N-H	Neck-head joint
N-T	Neck-torso joint
P_x, P_y, P_z	Inertial components of total linear momentum
P_{ij}	A quantity defined for convenience
$q_k, \dot{q}_k, \ddot{q}_k$	k-th generalized coordinate, velocity and acceleration
$\{\ddot{q}\}$	A vector of accelerations
Q_k	Generalized force for q_k
r	z_h - component of N-H; approximately one-half of the longitudinal head length
$\vec{r}$	Inertial position vector
R_i, R, R'	Generalized pitching angles at torso joint i, N-T, and N-H, respectively
$\vec{R}$	Position vector for a center of mass
R_1, R_2	Radii of curvature
sgn x	$\frac{x}{\lvert x \rvert}$, +1 or -1
S_i, S, S'	Angle of pitching deformation at torso joint i, N-T and N-H
t	Time
t_r	Duration of impact phase for oblique collision vehicle kinematics
t_{max}	Time at which obliquely struck vehicle comes to rest
t_o, t_1, t_2	Local abscissa values for a curve to be fit by Lagrange interpolation

t_o	Distance of N-T backward from CG for torso element 1, in e_1
t_i	Distance of CG for torso element i forward from joint i, in e_i
t	Subscript indicating "torso"
T	Kinetic energy
T	Superscript indicating "transpose"
v_o	An initial velocity
v	Final velocity for impacting vehicle, after separation
$\vec{v}$	A vector defined for convenience
VOM	The (n + 1)-mass "vehicle occupant model"
V	Potential energy
W	A weight
x_i, y_i, z_i	Inertial coordinates of center of mass of i^{th} element
x,y,z	Coordinates which define the position of N-H with respect to N-T, in e_1
x,y,z	Cartesian coordinates, in general
x_1, x_2	Coordinates of two points
x	Length of a Maxwell element
X(t)	An excitation

$\alpha_f, \alpha_b, \alpha_s$	Joint stop angles to front, back and side
$\alpha_i, \beta_i, \gamma_i$	Components of $\vec{\omega}_i$ in e_i
γ	Damping ratio
δ	A deformation

δ_{pk}	Kronecker delta; 1 if $p = k$ and 0 if $p \neq k$
Δ	Ramp length for joint stop damping coefficients
ε	A non-dimensional quantity relating to energy or momentum conservation
ϵ	A small value of time
η	Fraction of initial kinetic energy lost in a collision
θ	A measured value for extreme voluntary torso bending or twisting
$\theta^{N-T}, \theta^{N-H}$	Relative pitch angles at N-T and N-H (defined only for the planar case)
θ_1, θ_2	Distributed joint stop angles
$\bar{\theta}$	Extreme voluntary torso twist per unit length
(θ)	Superscript for angular muscle tension parameters
$\Theta_i, \Theta, \Theta'$	Heading angles at torso joint i, N-T, and N-H, respectively
λ	Lagrange multiplier
μ	Coefficient of friction
φ	Phase angle
φ_1, φ_2	Circular segment angles
$\psi_i, \theta_i, \varphi_i$	Inertial yaw, pitch, and roll Euler angles for element i
$\psi'_{i+1}, \theta'_{i+1}, \varphi'_{i+1}$	Relative yaw, pitch, and roll Euler angles for element $i + 1$ with respect to e_i
$\psi_h, \theta_h, \varphi_h$	Inertial head yaw, pitch, and roll Euler angles
$\psi^h, \theta^h, \varphi^h$	Yaw, pitch, and roll Euler angles for head relative to upper torso element

ψ_{i+1}^{0}	$\psi'_{i+1}(0)$
ψ_1, ψ_2	Central angles for sectors
$\dot{\psi}_r$	Yawing velocity of obliquely struck vehicle at $t = t_r$
$[\Psi_i],[\Theta_i],[\Phi_i]$	Intermediate rotation matrices
$\vec{\omega}_i$	Angular velocity vector for element i
$\vec{\omega}$	Angular velocity vector
ω	A forcing frequency
ω	A natural frequency
^{0}	Superscript indicating evaluation at $t = 0$

ABSTRACT

This investigation is concerned with development of an improved analytical model of a vehicle occupant for use in digital computer three-dimensional crash simulation studies. The vehicle occupant is treated as a discrete parameter, viscoelastic system.

Three-dimensional models in current use are, in various respects, simplistic representations of the human body as a mechanical system. An attempt is made here to improve upon some of their shortcomings. The new features of primary importance are: 1) a more realistic joint model; 2) the capability for positioning joints off the center line of body elements; 3) a two-joint, extensible neck to replace the conventional simple ball-and-socket joint neck; 4) an n-mass torso which allows for twisting and bending; and, 5) allowance for the effect of muscle contraction on the crash kinematics as a function of the degree of voluntary or involuntary "tightening" of the muscles, based upon experimental findings.

The solution of the (3n + 9)-degree-of-freedom free motion problem is formulated as a system of Lagrange equations. As the immediate objective of this investigation is not the development of improved restraint systems - the ultimate goal of mathematical crash simulations - but rather development of a better model of the vehicle occupant for use in such simulations, no provision is made for exciting the occupant model by way of contact with a vehicle interior. However, the analysis does allow for forcing the system through any of the generalized coordinates, i.e., tabular or functional time histories may be provided in order to eliminate any coordinate as a degree of freedom. An IBM 360/67 computer is used to obtain the solution of the differential equations of motion.

The investigation of several crash situations shows that the proposed model is able to predict several experimentally observed characteristics of crash kinematics which cannot be accounted for with simpler models. The model is felt to be, on the one hand, a significantly improved approximation to the human crash victim and, on the other hand, not disproportionately burdensome in terms of either demands of the model for required bioparameter values or the cost of solution for crash kinematics.

CHAPTER 1

INTRODUCTION

In recent years there has been much interest in mathematical modeling of vehicle-occupant systems for crash simulation studies. The objective of such investigations is to obtain guidance in designing vehicle structures and restraint systems which will minimize the extent of injury sustained by occupants in a crash situation.

Models of a wide range of complexity have been described in the literature. Occupant models have ranged from one-dimensional, one-degree-of-freedom representations to three-dimensional representations having many degrees of freedom. Numerous models involving occupants with three of fewer degrees of freedom have been developed (1, 2, 3, 4, 5, 6, 7, 8), all in one or two dimensions. Roberts and Robbins (9) have studied a simple three-dimensional system with one mass and four degrees of freedom. These simpler simulations have not been precursors of the more complex simulations, but instead have been designed to investigate specific aspects of the collision dynamics.

The earliest known model of intermediate complexity was developed by McHenry (10). McHenry formulated and solved a two-dimensional (planar) problem with six degrees of freedom for occupant motion and a fore-aft crash acceleration history for the vehicle. This work was later extended by McHenry and Naab (11, 12) to a very similar model having a vehicle occupant with ten degrees of freedom. A nine-degree-of-freedom, two-dimensional occupant model (without vehicle) was developed by Roberts, Ward, and Nahum (13); the hip point is restrained from translational motion, and fore-aft forcing functions are applied at the head and chest. Becker and Robbins (14) reproduced the McHenry and Naab analysis with slight modification of some features of the model. This model was further extended by Robbins, Bennett, and Roberts (15). Notably, they add an averaging technique which makes possible a dependable numerical integration of discontinuous forces.

While the aforementioned two-dimensional simulations are reasonably sophisticated, they are limited to investigation of either front-end or rear-end collisions, with motion of the crash victim in the vertical, fore-aft plane. The study of more general crash conditions requires a vehicle-occupant system modeled in three dimensions.

Thompson (16) did the earliest known work in three-dimensional simulation. The crash victim was modeled as an eight-degree-of-freedom, three-mass system. Occupant response and overall vehicle crush could be investigated for a two-car collision from any direction. A much more complete study was made by Young (17), whose analysis allows for a vehicle motion of a general nature, i.e., three linear and three angular degrees of freedom in an inertial frame. A three-dimensional vehicle interior is idealized by twenty-five planar surfaces. A twelve-mass vehicle occupant with thirty-one degrees of freedom is modeled. Two arms and two legs are included, each having two masses, and the three-mass torso is joined to a one-mass head-neck element. Although formulated as a three-dimensional problem, Young's model has been exercised only in two dimensions. Thus, there is an effective reduction to ten degrees of freedom, and this simulation becomes nearly identical to the most advanced two-dimensional models (11, 15). The validity of Young's model seems to be restricted to the planar case because of the analytical representation of the joints of the crash victim.* The most recent three-dimensional simulation was done by Robbins, Bennett, and Roberts

---

*See Section 3.3.2, pages 23 and 24.

(18). A completely general, six-degree-of-freedom vehicle acceleration history can be provided to describe a crash. A vehicle interior can be defined having up to twenty-five planar surfaces, which may be fixed or moving with respect to the vehicle. Up to ten "contact ellipsoids" may be fixed to the crash victim at arbitrary positions for interaction with the vehicle interior. The twelve-degree-of-freedom crash victim has three rigid masses, which represent head, torso, and legs connected at "neck" and "hip" joints. This model is fully operational in three dimensions.

It is felt that the three-dimensional crash victim models developed to date are, in various respects, simplistic representations of the human body as a mechanical system. An attempt is made in this investigation to improve upon some of their shortcomings. The new features of primary importance are: 1) a more realistic joint model; 2) the capability for positioning joints off the center line of body elements; 3) a two-joint, extensible neck to replace the conventional simple ball-and-socket joint neck; 4) an n-mass torso which allows for twisting and bending; and, 5) allowance for the effect of muscle tension as a function of the degree of voluntary or involuntary "tightening" of the muscles, based upon experimental findings. As the purpose of this study is to develop a more sophisticated vehicle occupant model and not specifically to investigate the kinematics of crash situations, provision is not made for interaction of the occupant with a vehicle interior. A rather general forcing capability has been provided, however, for studying the dynamic response of the model. Also, since flexible neck and torso representations are the primary concern, leg elements have not been included explicitly as a part of the system studied, although the capability of their inclusion is implicit in the analysis.

Certain work which provided guidance in selection of the torso model is discussed in Chapter 2. Chapters 3 and 4 together provide a complete description of the analytical model. Chapter 3 is intended to provide a general description of the basic features of the entire model. These features are described in greater detail, analytically and pictorially, in Chapter 4, along with development of the differential equations of motion, and use of the Table of Contents should be invaluable for finding detailed information in Chapter 4 regarding any specific feature of the model. Chapter 5 discusses the numerical solution of the equations of motion. In Chapter 6 is described the means by which the equations of motion, as derived and as implemented in the computer program, were verified. The manner in which forcing excitation of the vehicle occupant model is provided is discussed in Chapter 7. The material in Chapters 8 and 9 is preparatory to the set of final model verification computer exercises described in detail in Chapter 10. Appendices A through E provide considerable detail on various aspects of this investigation which are discussed less fully in the text. Appendix F illustrates the basic joint characteristics of the three-dimensional analytical model in terms of two-dimensional analogues.

CHAPTER 2

INVESTIGATORY MODELS

The investigation of several two-dimensional mechanical systems preceded development of the complete three-dimensional head-neck-torso model. These systems were designed mainly to answer certain questions regarding analytical approach to the torso problem and computational feasibility.

The primary candidates for the torso model were: 1) an extensible spine model and 2) an inextensible spine model. These were investigated by numerically solving the equations of motion for a "chain" of n links connected at their end points by either springs or pins, respectively. (See Figure 1.) A sinusoidal displacement was imposed at one extremity of the chain. The two systems have, respectively, 3n - 2 and n degrees of freedom.

It was seen immediately, as expected, that the motion of the system with springs connecting the links could be made to approach, as closely as desired, the motion of the system with pin joints by choosing larger and larger values for the spring rates. Since the extension (or compression) of the spine with respect to its unstrained length must be relatively small even in a violent crash situation, the spring rates which would account for extension of the spine in a torso model would be relatively "large." Hence, as far as the gross motion is concerned, the inextensible spine model should be a reasonable substitute for the more realistic extensible spine model.

The primary advantage in using the extensible spine model would seem to be the immediate availability of forces of tension and compression along the spine. But in the limit, as spring rates approach

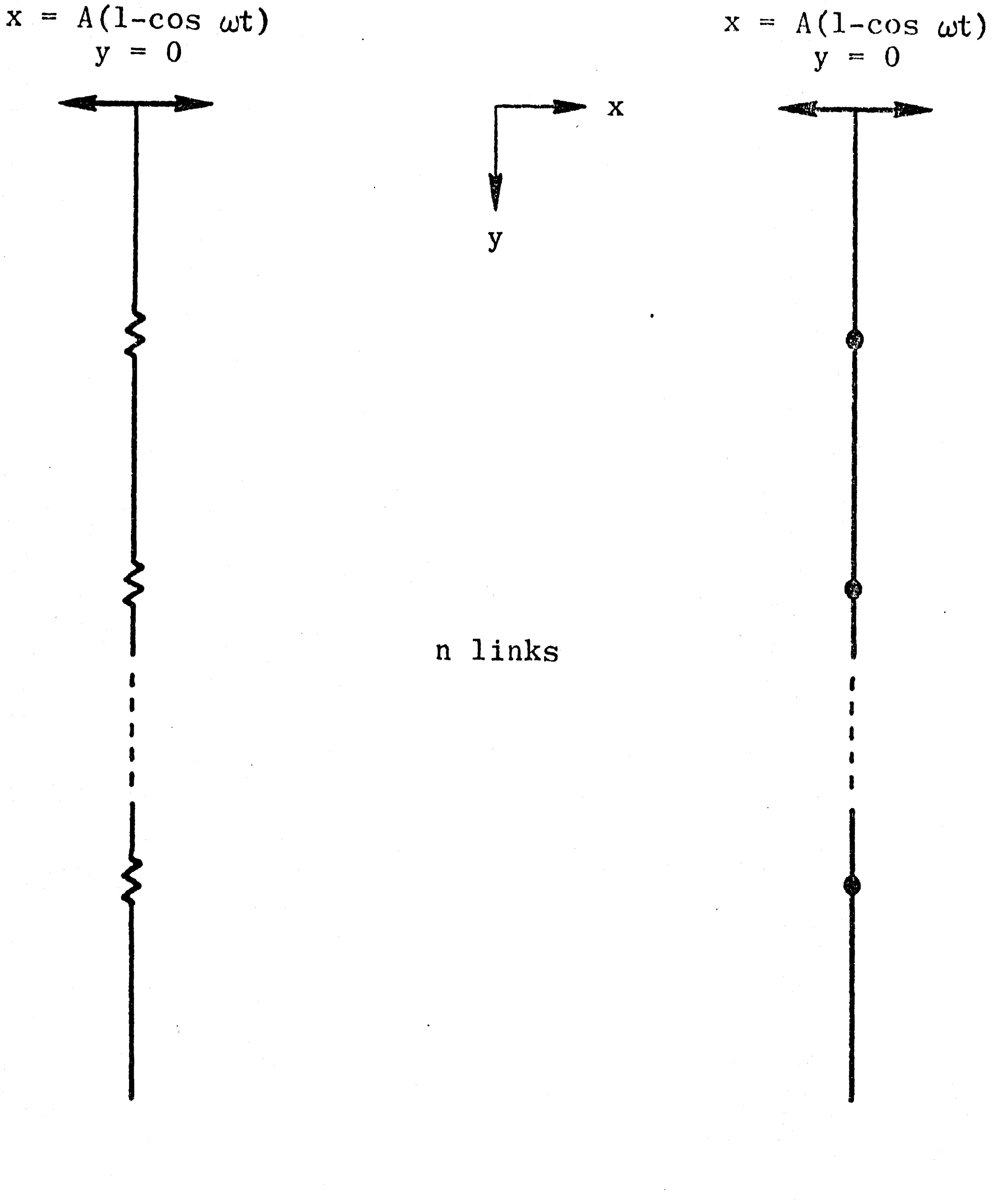
$x = A(1-\cos \omega t)$
$y = 0$
$x = A(1-\cos \omega t)$
$y = 0$
x
y
n links

Figure 1. Two-dimensional "chain" systems for investigating extensible and inextensible spine model formulations.

infinity, these forces become precisely the constraint forces which are immediately available if the pin joint model is solved as a (3n - 2)-degree-of-freedom system in terms of Lagrange multipliers. Since knowing the tension and compression forces in the spine is of potential value as an injury predictor, this second approach to the inextensible spine problem was tried as an alternative to the other two models. The motion obtained by this method of solution was identical, of course, to that obtained by the numerically simpler method for the pin joint problem. The constraint forces determined in this manner had local positive and negative peak values that were quite similar to spring forces in the extensible spine model.

It was thus determined that there is no great advantage of the extensible spine model over the Lagrange multiplier formulation of the inextensible spine model. Each, however, has significant disadvantages in comparison with the first formulation of the pin joint problem. First, it is noted that solution of the latter involves solving a system of n simultaneous linear algebraic equations each time that the integration algorithm requires new values for time derivatives, while the previously mentioned formulations involve systems of size 3n - 2 and 5n - 4, respectively. The system for the Lagrange multiplier formulation is the largest because not only are none of the degrees of freedom analytically eliminated but also two Lagrange multipliers for each joint are present as unknowns (with the generalized accelerations) in the equations of motion. Since a significant percentage of the total number of operations required to perform the integration over unit time will be attributable to the inversion of the algebraic system, and since the number of multiplication operations for the inversion of a system of order N is nearly proportional to N^3, it is clear that the costs of determining the motion for the various formulations will differ greatly. For n equal to 3, the relative cost ratios will be nearly 27:343:1331, or 1:12.7:49.3.

The extensible spine model has a disadvantage over and above the one just discussed. The system of differential equations for this formulation has an inherent "instability" in that any numerical integration algorithm must require smaller and smaller time steps as larger values for spring rates are chosen. Physically, this is a manifestation of the greater and greater natural frequencies associated with the mechanical system. Since integration time steps will in general be smaller than for the other formulations, the cost will be increased from what it would have been otherwise in approximate proportion to the increase in number of time steps required for integration over unit time.

In consequence of the foregoing cost considerations, it was decided that only an inextensible spine can be considered as practical for the three-dimensional torso model and that constraint forces resulting directly from a Lagrange multiplier formulation are a luxury that cannot be afforded. It did become clear, by the time that computer solution of the complete three-dimensional model was completed, that cost would in fact have been prohibitive for either of the other proposed formulations.

An additional purpose in investigating the "chain" linkage discussed in the foregoing was to see if large numbers of degrees of freedom might possibly lead to unstable numerical solution of the equations of motion. As many as ten links were tried for the Lagrange multiplier formulation, corresponding to a forty-sixth order algebraic system and a fifty-sixth order system of differential equations. There was no indication of divergence in the numerical solution.

CHAPTER 3

THE ANALYTICAL MODEL

In this chapter the general features of the analytical model are described. Greater detail is presented in Chapter 4, in which the equations of motion are developed.

3.1 THE KINETIC LINKAGE

Selection of an inextensible spine as a component of the torso model has already been discussed in Chapter 2. The neck model used here was adopted after consideration of the findings of several investigators.

The head-to-torso linkage used to date in crash victim models has consistently been a simple hinge (pin) in the case of two-dimensional models or a simple ball-and-socket joint in the case of three-dimensional models. In such models the only mode of relative movement of the head with respect to the torso is one of rotation. It has been pointed out, however, by Ewing, et al. (19), that the relative motion in flexion (i.e., forward rotation of the head-neck) includes in addition a translation component. Tisserand and Wisner (20) similarly conclude that translation can be significant in extension (backward rotation of the head-neck). Significant rotation occurs in an impact only after the translation phase, which is observed as the initial part of the motion.

Translation terms will result if a head-to-torso linkage having two or more "joints" is selected. A six- or seven-joint neck might make a good model since the cervical spine has seven vertebral bodies.* It is felt, however, that a two-joint neck is a good compromise against the cost disadvantage (and others) or a more complex neck. Tarrière and Sapin (22) point out that, with regard to the flexion-extension of the head, there are two main axes of rotation. One is situated at the base of the neck and passes through the middle of the articulation of the seventh cervical vertebra with the first thoracic vertebra. The other is located at the base of the cranium and passes through the middle of the atlanto-occipital articulation. Therefore, a model with ball-and-socket joints at these positions provides the mechanism for the two primary flexion-extension modes as well as for the translation mode; such a model is developed in this investigation.

---

*Jackson notes that there are thirty-four joints (of sorts) in the neck (21)(p.77).

It should perhaps be made clear that Tarrière and Sapin do not develop a mathematical model for a two-joint neck. The (two-dimensional) one-joint model that they present does not (cannot) allow for a translational mode for relative head motion, but the authors give the following reasons for hypothesizing a single axis of rotation at the seventh-cervical/first-thoracic vertebral articulation: "1. Articular mechanics show that rotation occurs around this axis for movements of large amplitude. The center of rotation descends from the upper portion of the cervical column to the lower portion as the amplitude of the movement increases. 2. The pathological anatomy of the injuries found in traffic accidents shows that most dislocations (luxations or fractures) occur at the last cervical vertebra." They also note that it can be difficult to determine the range of importance of viscoelastic coefficients if too many degrees of freedom are considered; and this is certainly true. But the first argument given by Tarrière and Sapin is not necessarily valid for dynamic situations (indeed, the findings of Ewing and Tisserand and

Wissner would seem to indicate that it is not); the argument therefore does not successfully justify omitting a joint at the atlanto-occipital articulation from the mathematical model.

A further characteristic of previous neck models has been the lack of a "stretching" mode. Schulman, et al. (23), have shown, however, that the neck can stretch considerably in a moderately violent crash situation. It was decided, therefore, to represent the neck length as a massless Kelvin element deformable in the directions of its end points. Neck mass may be neglected or distributed as desired between the head and torso.

A profile showing the linkage selected for this investigation is shown in Figure 2. Three torso masses are shown here although the analysis is done for a general number, n. In this figure the lower torso element should be thought of as the pelvic mass and the middle torso element as the midsection. The upper element probably should extend nearly to the bottom of the rib cage.

It is mentioned in Chapter 1 that this study is directed at development of neck and torso models and that legs are therefore not included. The analysis is general enough, however, that additional "torso" elements can be provided for representing thigh and lower leg elements of a single leg. The hip joint for connecting this leg to the pelvic element is of necessity on the sagittal plane although it may be positioned anywhere on that plane. Figure 3 shows a linkage with leg elements.

It is further noted here that the shape of the body elements is irrelevant to this study since, as mentioned earlier, the interaction of the man with a vehicle interior is not under investigation. The "shape" of body elements does enter indirectly, of course, in the values of the various mass moments of inertia.

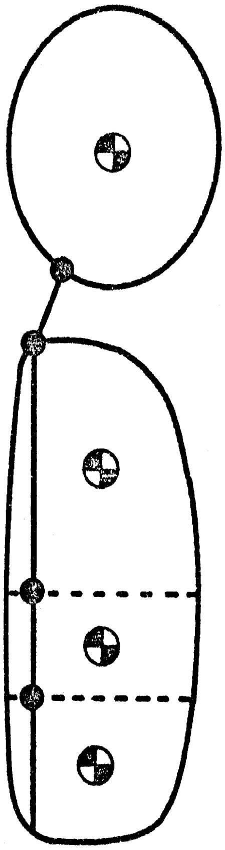

Figure 2. Profile of the kinetic linkage of the crash victim model (n=3).

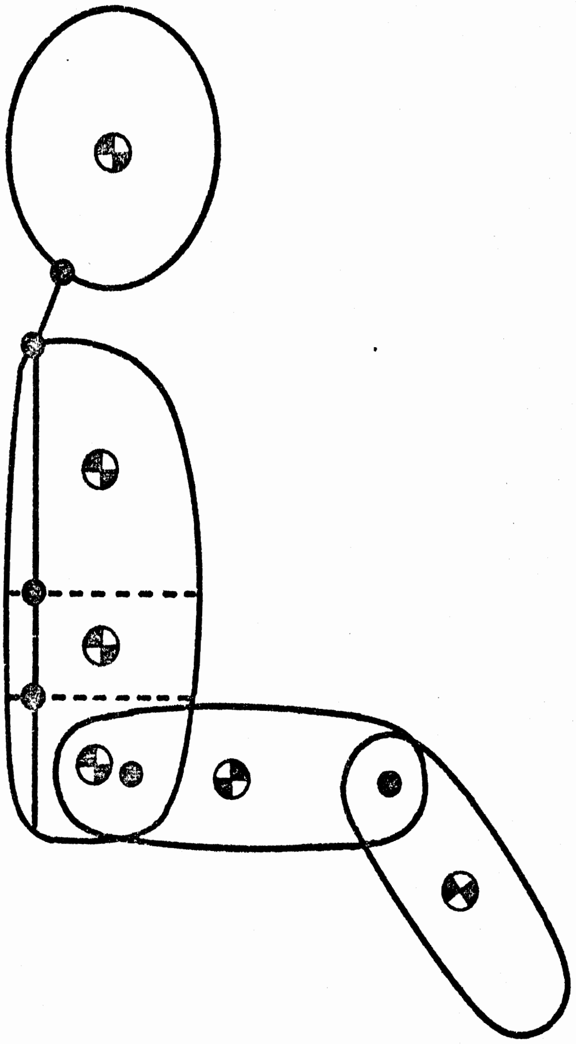

Figure 3. Profile of the kinetic linkage of the crash victim model, with two leg elements (n=5).

3.2 THE GENERALIZED COORDINATES

The n torso masses are joined by n - 1 ball-and-socket joints along the "spine." The distances between successive joints are constants, thus giving the torso alone 6 + 3(n - 1) degrees of freedom. The uppermost mass is assigned six generalized coordinates, x_{CG}, y_{CG}, z_{CG} (CG = center of gravity), and Euler angles ψ (yaw), θ (pitch), and φ (roll), all inertial. The 3(n - 1) constraints then allow each of the other torso masses to be described by three additional Euler angles. Since an extensible neck model has been selected, six additional coordinates are required to fix the position and orientation of the head. Three are inertial Euler angles for the head. The remaining three have been chosen as the cartesian coordinates of the neck-head joint (N-H) with respect to the rotating frame of reference fixed to the first (upper) torso mass but with origin displaced to the neck-torso joint (N-T). (The computer program accepts the corresponding spherical coordinates as initial conditions, however, and also calculates the spherical coordinates from the internal cartesian coordinates for the purpose of output.)

There are many valid definitions for Euler angle coordinates. They are defined as follows for this analysis.

Let

$$e_i = \begin{Bmatrix} i_i \\ j_i \\ k_i \end{Bmatrix} \tag{3.3.1}$$

be the basis for a rotating frame fixed to body element i, where i = 1, 2, ..., n, n + 1, there being n torso elements and one head element.

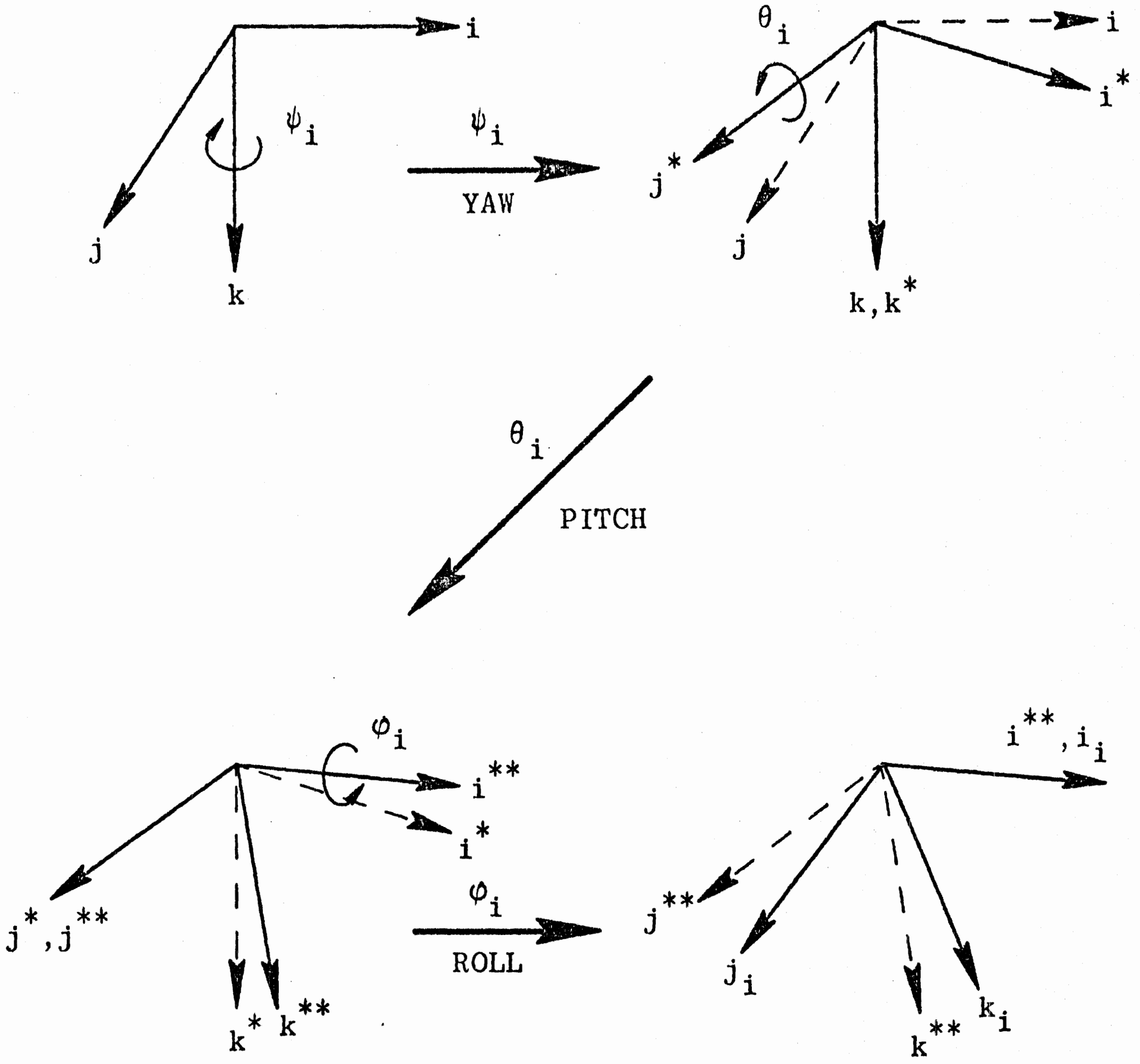
i
j
k
ψ_i
ψ_i
YAW
θ_i
i
i^*
j^*
j
k, k^*
θ_i
PITCH
φ_i
i^{**}
i^*
j^*, j^{**}
k^*
k^{**}
φ_i
ROLL
i^{**}, i_i
j^{**}
j_i
k^{**}
k_i

Figure 4. Inertial Euler angles for element i.

Let

$$e = \begin{Bmatrix} i \\ j \\ k \end{Bmatrix} \tag{3.3.2}$$

be for a selected inertial frame, and consider, temporarily, a coincidence of the rotating frame with the inertial frame. The orientation of body element i can now be described uniquely for the range $-\frac{\pi}{2} < \theta_i < \frac{\pi}{2}$ by Euler angle rotations $\psi_i(t)$, $\theta_i(t)$, $\phi_i(t)$ - yaw, pitch, and roll - taken successively about the k, j^*, and i^{**} axes, where (*) indicates the first intermediate position and (**) indicates the second intermediate position. The orthogonal bases are "right-handed" and all rotations are taken as "right-handed," arbitrarily. These rotations are illustrated in Figure 4.

"Relative" yaw, pitch, or roll angles for element i with respect to element j can be defined similarly by replacing the inertial basis e by e_j. Relative Euler angles are used at several places in the analysis, but not as generalized coordinates.

A few comments are made here regarding the body axes, e_i. The i^{th} body element will have an inertia tensor $\overline{I}_i$. Principal axes are chosen for body coordinate axes (so as to diagonalize all inertia tensors). It follows, then, since any axis of symmetry of a body is a principal axis and since some "longitudinal" axis of any (nearly symmetrical) torso element should be approximately an axis of symmetry, that one body axis for each element is approximately a longitudinal axis of symmetry. This axis is designated as $\pm k_i$, $+k_i$ taken arbitrarily as "downward." Similarly, i_i is an axis out of the "front" of the i^{th} body element and j_i is an axis out of the "right side" of the body element. Finally, if constant mass density is assumed for each rigid body element of the model, then each mass center, which would be precisely at some intersection of axes of symmetry, must lie approximately at an intersection of human body principal axes. Mass centers for the model elements are assumed, as in all previous models, to be exactly at such intersections, i.e., at the origins of body coordinate axes.

For completeness the notation used in Chapter 4 for all of the generalized coordinates described in this section is set forth below.

Upper torso element, $i = 1$: $x_1, y_1, z_1, \psi_1, \theta_1, \varphi_1$

Remaining torso elements (including leg elements), $2 \leq i \leq n$:

$\psi_i, \theta_i, \varphi_i$

Head: $\psi_h, \theta_h, \varphi_h$

Neck-head: x, y, z

3.3 THE BASIC JOINT MODEL

A "joint," in a loose sense, is a complicated system of muscle, tendon, bone, cartilage, and ligaments which allows relative movement between body "segments." Internal forces and moments affect the relative movement in a very complex manner. Moment components at opposite ends of a body segment are sometimes affected by the same muscle so that movement at one joint is not always strictly independent from movement at a second joint. Further, at a given joint moments resisting (or assisting) simultaneous rotation about more than one axis are in general interdependent to some extent (21, 24). The effect of these complications, while perhaps not negligible, is assumed to be small, however, and will not be considered in this model. Joints will be represented in their totality with limited explicit consideration of their structural elements.

All joints in this mathematical model are ball-and-socket joints with three superimposed moment characteristics. These are discussed qualitatively in Sections 3.3.1 - 3.3.3 below and in detail in Chapter 4. The moments discussed in Sections 3.3.1 and 3.3.2 result from Kelvin elements, i.e., torsional springs and dampers in parallel. The spring and viscous damping moment components are, accordingly, additive. Spring moments and damping moments are assumed to be proportional to a deformation and a deformation rate, respectively, but with non-linear spring and damping coefficients that are second-order polynomials in the deformation or deformation rate. Equivalently, then, the moments may be assumed to have linear, quadratic, and cubic components, each with a constant coefficient. Coulomb friction damping has not been included since Johns and Wright (25) have shown that its contribution is negligible, at least in an in vivo study of the human metacarpo-phalangeal (finger) joint. It may be expected that inclusion of such a moment component would give rise to serious numerical integration difficulties, as has been shown by Robbins, Bennett, and Roberts (15).

Three angles are necessary for describing the relative orientation of body elements connected at a joint. Relative Euler angles are suitable, but they have no general anatomical significance. Therefore, three angular coordinates were selected instead which can be interpreted easily in terms of angular deformation of a flexible body. The first is the angle, R, between the longitudinal axes of the body elements. (See Figure 5.) Basically, it is the amount of relative bending between the adjoining elements, and it will sometimes be referred to as a "generalized pitching angle." The second is the "heading angle", $\textcircled{w}$, which

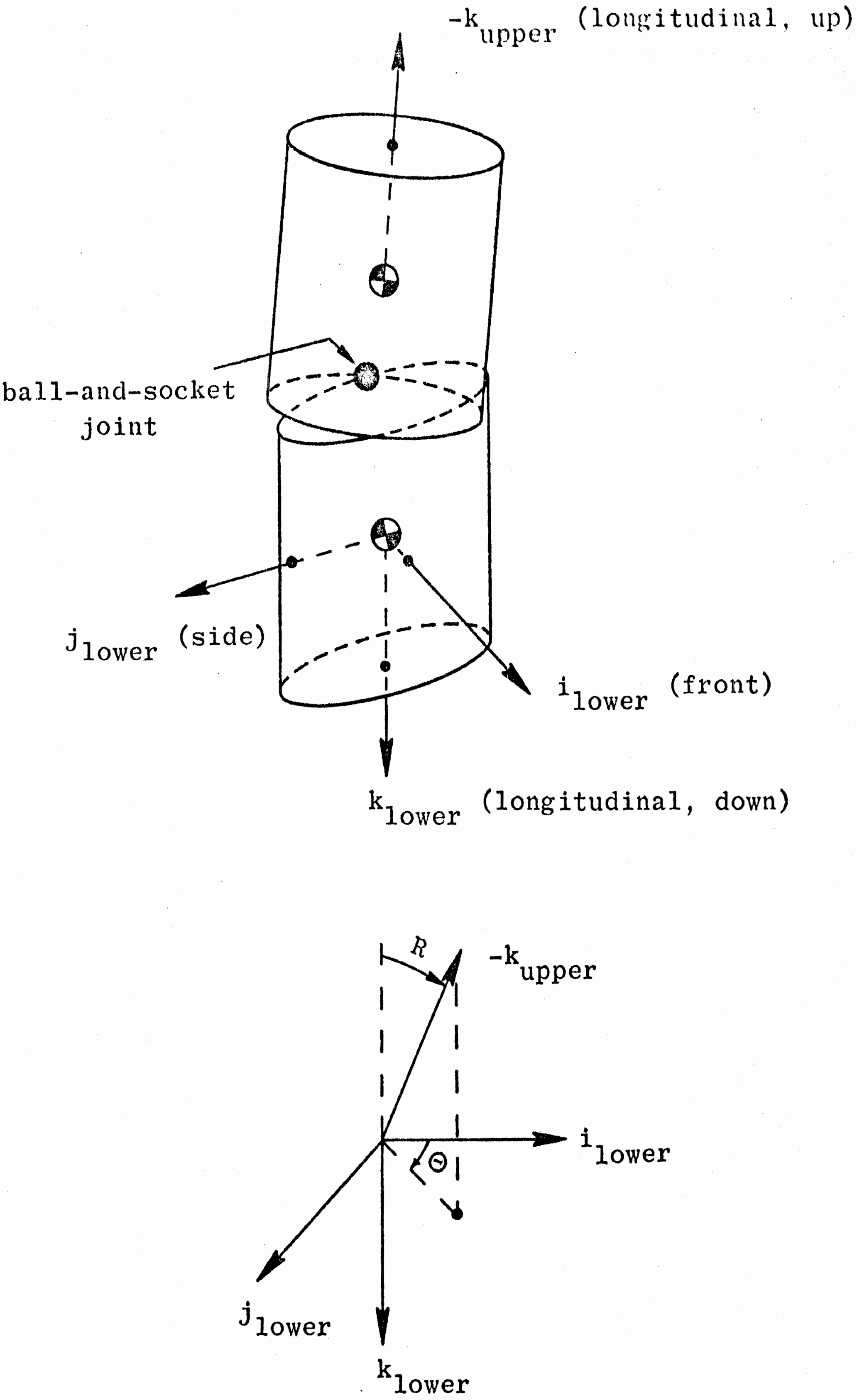
$-k_{upper}$ (longitudinal, up)
ball-and-socket joint
j_{lower} (side)
i_{lower} (front)
k_{lower} (longitudinal, down)
R
$-k_{upper}$
i_{lower}
Θ
j_{lower}
k_{lower}

Figure 5. The "generalized pitching angle" and the "heading angle" for bending at a typical torso joint.

describes the angular position relative to the "front" of the "lower" body element at which bending occurs.* The third is basically the amount of relative twisting between the elements and is defined as the relative yaw angle of the "lower" element with respect to the "upper." These definitions hold strictly only for torso joints. Neck joint angles are determined very similarly, as explained completely in Chapter 4.

3.3.1 Joint Stop Moments

Each ball-and-socket joint is first considered to have some range of free or almost free motion. The limits of this range correspond to a "hard" anatomical resistance to further relative angular motion. For example, the various investigators who have modeled two-dimensional crash victims having pin-joint necks have defined this range for head motion by "stops" at approximately sixty or seventy degrees forward (flexion) and about the same backward (extension).

In three dimensions the situation is, of course, more complex. The following reasoning has led to definition of a "free" range for the three-dimensional joint. First, generalized pitching stop angles in forward and backward directions should be the same as in a two-dimensional model. Also, for the three-dimensional joint, motion must be allowed directly to either side, and, because of sagittal symmetry of the human body, the corresponding stop angle values should be identical.

---

*Thus, if r, θ, and ϕ are spherical coordinates of a point with respect to the body axes of the "lower" element, then the negative longitudinal coordinate axis of the "upper" element is the unit vector $\hat{r}$, the bending angle R is π minus the azimuthal angle ϕ - always positive - and the heading angle Θ is the circumferential angle θ.

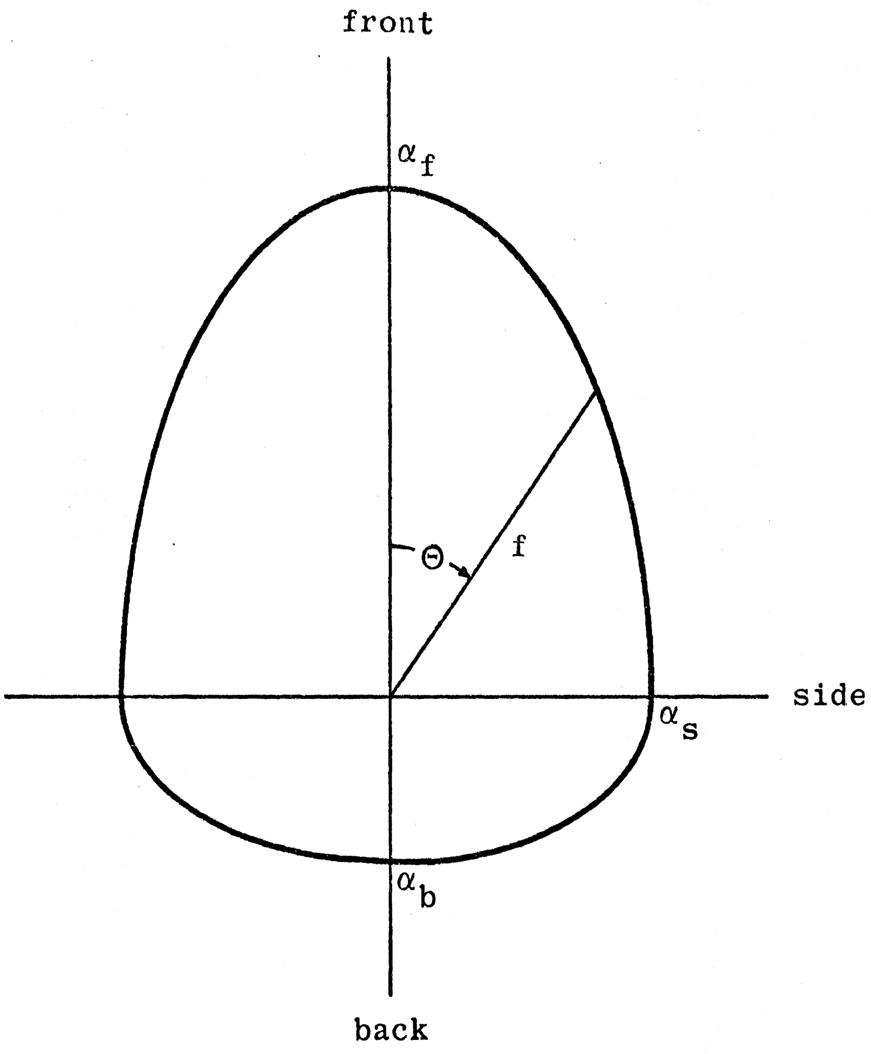
front
α_f
Θ
f
side
α_s
α_b
back

Figure 6. Stop angle "ellipse" for a ball-and-socket joint.

Motion toward intermediate positions is also possible, and stop angle values there must connect the forward, backward, right, and left stop angles as continuous functions of heading angle Θ and with sagittal symmetry.

Figure 6 illustrates the general stop angle function selected for use in this study. The radius of this diagram represents the stop angle, f, as a function of Θ. Halves of two ellipses have been selected as reasonable functions for joining the front, back, and side stops ($f = \alpha_f, \alpha_b$, and α_s), although experimental functions could be used if they become available. Note that there is slope continuity and that fore-aft symmetry is not required. The interior of this "ellipse" represents the range of free motion (with respect to generalized pitching joint stop moment) for the joint. The origin of the diagram corresponds to a generalized pitching angle of R equal to zero. The joint stop moment will be zero unless R is greater than $f(\Theta)$.

Relative twisting between elements is also restricted by a stop angle. The corresponding moment is zero unless the absolute value of the relative yaw angle at a joint exceeds the stop angle constant for that joint.

3.3.2 Elastic Moments

In the absence of muscle tension forces (Section 3.3.3), what will be called "elastic" forces are the only forces which act before stop angle forces come into play. They represent resistance to free motion inside the stop angle "ellipse." This joint feature is interpreted as representing, mainly, spinal stiffness against bending away from an equilibrium configuration. It is assumed that the configuration at the onset of the crash, time equal to zero, defines the equilibrium. Only slight modification would be required in the analysis to allow for a pre-determined anatomical equilibrium configuration, which will differ slightly in general from the initial posture of the vehicle occupant.

Other authors (11, 15, 17, 18) have included a similar feature in their joint models. All have in common that the initial configuration is taken as the equilibrium configuration. While the analytical approach is likewise almost identical in the two-dimensional models of McHenry and Naab (11) and Robbins, Bennett, and Roberts (15), it is quite dissimilar in the three-dimensional models given by Young (17) and Robbins, Bennett, and Roberts (18), and by this author in Chapter 4. Young determines what this author has called R, the generalized pitching angle. The elastic moment is then determined on the basis of a deformation $\delta = R(t) - R(0)$. This definition for deformation does not seem to take into account that direction and magnitude of the elastic moment must depend on the "headings" of the initial and final configurations. For example, suppose that initially R is R(0) = 5° forward and that finally R is R(t) = 5° to the side. Then the spine is obviously in a deformed configuration, yet the predicted deformation and moment are both zero. It is felt, therefore, that this model has validity only for two-dimensional situations. Robbins, *et al.*, define three separate deformations - based on relative yaw, relative pitch, and relative roll. The combined associated elastic moments do tend to restore the initial three-dimensional configuration. As has been mentioned, however, there is no unique definition of valid Euler angles. Therefore, the path in space of the oscillation about equilibrium will depend on which definition is used if moments are based directly on change in relative Euler angle.

The model used in this investigation attempts to overcome these difficulties. The direction cosines of one longitudinal axis at a joint with respect to the rotating frame of the adjoining element are determined both at $t = 0$ and at time t. The bending deformation is then simply the angle between the lines determined by these sets of direction cosines. The associated bending moment and a twisting moment based on the difference between initial and final relative yaw angles then tend to restore the initial relative orientation of the body elements.*

3.3.3 Muscle Tension Moments

In most crash situations a vehicle occupant is aware that a collision is impending. In such a case it is natural for him to involuntarily tighten his muscles in anticipation of the impact. This may quite conceivably have a significant effect on the crash kinematics of the system. Analytical representation of the effect would seem to be of obvious value.

Other investigators have attempted to model muscular restraint in body joints by adjustable values of constant friction (11, 15). This is a reasonable joint property if simulation of an anthropomorphic dummy is the goal. The goal, however, is assumed to be simulation of the living human body. Is constant joint friction the most reasonable model for muscle tension in the human body?

Recent experimental work done by Moffatt, Harris, and Haslam (24) involving the knee joint indicates that this property is properly represented by a Maxwell element, i.e., a spring and damper in series, with spring and damping coefficients that are simple functions of the voluntary static knee moment, M. Equations (3.3.3) and (3.3.4) give these coefficients as linear functions of the absolute value of M, i.e., of the "tightness" of the muscles.

---

*The Young model (17) does not provide any resistance to twisting at any ball-and-socket joint.

$$c = a_1|M| \tag{3.3.3}$$

$$k = a_2 + a_3|M| \tag{3.3.4}$$

The values of the constants a_1, a_2, and a_3 are joint properties and depend on the person involved. It is clear that when the muscles are completely relaxed (M = 0) the Maxwell element has no effect on motion at the joint since c is then zero.

The tests of Moffatt, Harris, and Haslam involved forced sinusoidal motion, with amplitude up to 12°, about an initial value of the joint angle. They state that in the tests performed there was no discernable dependence of the model coefficients upon joint angle and, also, no systematic dependence upon test amplitude.

The analytical development in Section 4.8 of the generalized forces for muscle tension allows for inclusion in the computer model of bending and twisting muscle tension at each torso and neck joint. Muscle tension resistance to stretching of the neck is also modeled.

CHAPTER 4

THE DIFFERENTIAL EQUATIONS OF MOTION

The vehicle occupant model described in Chapter 3 has N = 12 + 3(n - 1) degrees of freedom, where n is the number of torso masses. Equivalently, if two torso masses are thought of as representing upper and lower leg elements, the system has N' = 18 + 3(n' - 1) degrees of freedom, where n' is the number of torso elements. Use of a hinge joint for the knee would reduce N' by two.

The N (or N') differential equations of motion are developed in this chapter for the free motion problem. A certain class of forced motion problems can be studied by a simple modification of the system of free motion equations, and this procedure is explained in Chapter 7.

4.1 LAGRANGE'S EQUATIONS

The standard Lagrange formulation is the only practicable one for determining the kinetics involved in all but the simplest crash simulations. The Lagrange equations may be written as

$$\frac{d}{dt}\frac{\partial T}{\partial \dot{q}_k} - \frac{\partial T}{\partial q_k} + \frac{\partial V}{\partial q_k} + \frac{\partial D}{\partial \dot{q}_k} = Q_k \ , \qquad (4.1.1)$$

$$k = 1, 2, \cdots, N .$$

Here, T is the total kinetic energy of the system, V is the total potential energy, and D is one-half the rate of energy dissipation due to velocity-dependent damping. The generalized forces Q_k acting on the system represent all forces not arising from a potential, with the exception of velocity-dependent damping. The q_k's and $\dot{q}_k$'s are the generalized coordinates and velocities. The motion is entirely defined by this set of N second-order, ordinary differential equations together with initial conditions for each of the N generalized coordinates and N generalized velocities.

T, V, and D must be written out as functions of the q's and $\dot{q}$'s. (They are allowed to be explicit functions of t as well.) Since these expressions are extremely lengthy, they are not completely set down at any place in this chapter. Rather, additive components of each are dealt with separately. The total kinetic energy is divided into torso and head parts and is further divided into translational and rotational components. The potential energy and dissipation functions are also first divided into torso and head-neck parts. Further division separates the component properties of the joints discussed in Chapter 3. Muscle tension contributions are determined as components of the generalized forces, Q_k.

4.2 THE ROTATION MATRIX

The Euler angle coordinates defined in Section 3.2 make possible the definition of the rotation matrix which takes the inertial frame into the instantaneous orientation of a rotating frame. This matrix may be thought of as, more precisely, a transformation matrix since it defines the transformation between the two frames. The elements of its successive rows are the direction cosines of the inertial basis with respect to i_i, j_i, and k_i of the rotating frame. That is,

$$\begin{Bmatrix} i_i \\ j_i \\ k_i \end{Bmatrix} = \begin{bmatrix} a_{11,i} & a_{12,i} & a_{13,i} \\ a_{21,i} & a_{22,i} & a_{23,i} \\ a_{31,i} & a_{32,i} & a_{33,i} \end{bmatrix} \begin{Bmatrix} i \\ j \\ k \end{Bmatrix} , \qquad (4.2.1)$$

or with the notation of Section 3.2,

$$e_i = \left[A_i\right] e \quad . \qquad (4.2.2)$$

The rotation matrix $[A_i]$ is clearly orthornormal because of the relations existing between direction cosines.

The rotations for ψ_i, θ_i, and ϕ_i illustrated by Figure 4 correspond to the transformations of equations (4.2.3).

$$e^{*} = \begin{bmatrix} \cos\psi_i & \sin\psi_i & 0 \\ -\sin\psi_i & \cos\psi_i & 0 \\ 0 & 0 & 1 \end{bmatrix} e \qquad (4.2.3a)$$

$$e^{**} = \begin{bmatrix} \cos\theta_i & 0 & -\sin\theta_i \\ 0 & 1 & 0 \\ \sin\theta_i & 0 & \cos\theta_i \end{bmatrix} e^{*} \qquad (4.2.3b)$$

$$e_i = \begin{bmatrix} 1 & 0 & 0 \\ 0 & \cos\varphi_i & \sin\varphi_i \\ 0 & -\sin\varphi_i & \cos\varphi_i \end{bmatrix} e^{**} \qquad (4.2.3c)$$

Combining the above, we obtain

$$e_i = [\Phi_i][\Theta_i][\Psi_i]\, e \quad , \qquad (4.2.4)$$

or

$$[A_i] = [\Phi_i][\Theta_i][\Psi_i] \quad , \qquad (4.2.5)$$

which becomes

$$[A_i] = \begin{bmatrix} \cos\psi_i \cos\theta_i & \sin\psi_i \cos\theta_i & -\sin\theta_i \\ \cos\psi_i \sin\theta_i \sin\varphi_i - \sin\psi_i \cos\varphi_i & \sin\psi_i \sin\theta_i \sin\varphi_i + \cos\psi_i \cos\varphi_i & \cos\theta_i \sin\varphi_i \\ \cos\psi_i \sin\theta_i \cos\varphi_i + \sin\psi_i \sin\varphi_i & \sin\psi_i \sin\theta_i \cos\varphi_i - \cos\psi_i \sin\varphi_i & \cos\theta_i \cos\varphi_i \end{bmatrix} . \qquad (4.2.6)$$

The $a_{jk,i}$ are thus determined.

4.3 THE ANGULAR VELOCITY VECTOR

The angular velocity vector for rotations about a set of body axes is

$$\vec{\omega}_i = \alpha_i i_i + \beta_i j_i + \gamma_i k_i \quad . \qquad (4.3.1)$$

Resolved into components along the k, j^*, and i^{**} axes (see Figure 4), $\vec{\omega}_i$ is

$$\begin{aligned}\vec{\omega}_i &= \dot{\psi}_i k + \dot{\theta}_i j^* + \dot{\varphi}_i i^{**} \\ &= \dot{\psi}_i k + \dot{\theta}_i j^{**} + \dot{\varphi}_i i_i \quad .\end{aligned} \tag{4.3.2}$$

Since both $[A_i]$ and $[\Phi_i]$ are orthogonal, their inverses are identical to their transposes. Therefore, by multiplying the third equation of (4.2.3) by $[\Phi_i]^T$, we obtain

$$j^{**} = \cos\varphi_i \, j_i - \sin\varphi_i \, k_i \quad , \tag{4.3.3}$$

and similarly (4.2.2) and (4.2.6) yield

$$k = -\sin\theta_i \, i_i + \cos\theta_i \sin\varphi_i \, j_i + \cos\theta_i \cos\varphi_i \, k_i \, . \tag{4.3.4}$$

Equation (4.3.2) therefore becomes

$$\begin{aligned}\vec{\omega}_i = {} & (\dot{\varphi}_i - \dot{\psi}_i \sin\theta_i) i_i + (\dot{\psi}_i \cos\theta_i \sin\varphi_i + \dot{\theta}_i \cos\varphi_i) j_i \\ & + (\dot{\psi}_i \cos\theta_i \cos\varphi_i - \dot{\theta}_i \sin\varphi_i) k_i \, .\end{aligned} \tag{4.3.5}$$

Comparison of (4.3.5) with (4.3.1) then shows that

$$\begin{aligned}\alpha_i &= \dot{\varphi}_i - \dot{\psi}_i \sin\theta_i \\ \beta_i &= \dot{\psi}_i \cos\theta_i \sin\varphi_i + \dot{\theta}_i \cos\varphi_i \\ \gamma_i &= \dot{\psi}_i \cos\theta_i \cos\varphi_i - \dot{\theta}_i \sin\varphi_i \quad .\end{aligned} \tag{4.3.6}$$

4.4 TORSO KINETIC ENERGY

An n-mass torso has a kinetic energy of

$$T_t = \sum_{i=1}^{n} \Big[\tfrac{1}{2} m_i \left(\dot{x}_i^2 + \dot{y}_i^2 + \dot{z}_i^2 \right) + \tfrac{1}{2} I_i \alpha_i^2 + \tfrac{1}{2} J_i \beta_i^2 + \tfrac{1}{2} K_i \gamma_i^2 \Big] , \tag{4.4.1}$$

where (x_i, y_i, z_i) are the center-of-gravity coordinates for mass m_i, I_i, J_i, and K_i are the principal moments of inertia corresponding to the i_i, j_i, and k_i axes respectively, and α_i, β_i, and γ_i are the angular velocity components in the rotating frame, given by equations (4.3.6).

Figure 7 shows a typical torso element. The constant spinal length associated with torso element i is l_i. The center of mass is assumed to lie a distance t_i forward of the lower joint associated with element i and at $l_i/2$ upward from the lower joint. The joints and the center of mass lie on the sagittal plane.

The uppermost torso element will be labeled by i = 1 and the lowermost by i = n. Since an inextensible spine model has been assumed, it is possible to eliminate all cartesian coordinates except (x_1, y_1, z_1), which will serve as generalized coordinates, from equation (4.4.1). n-1 vector constraint relations may be obtained by considering closed loops containing the origin of the inertial frame, one or more joints, and two centers of mass. This is illustrated for masses 1 and 2 in Figure 8, and results are given by equations (4.4.2).

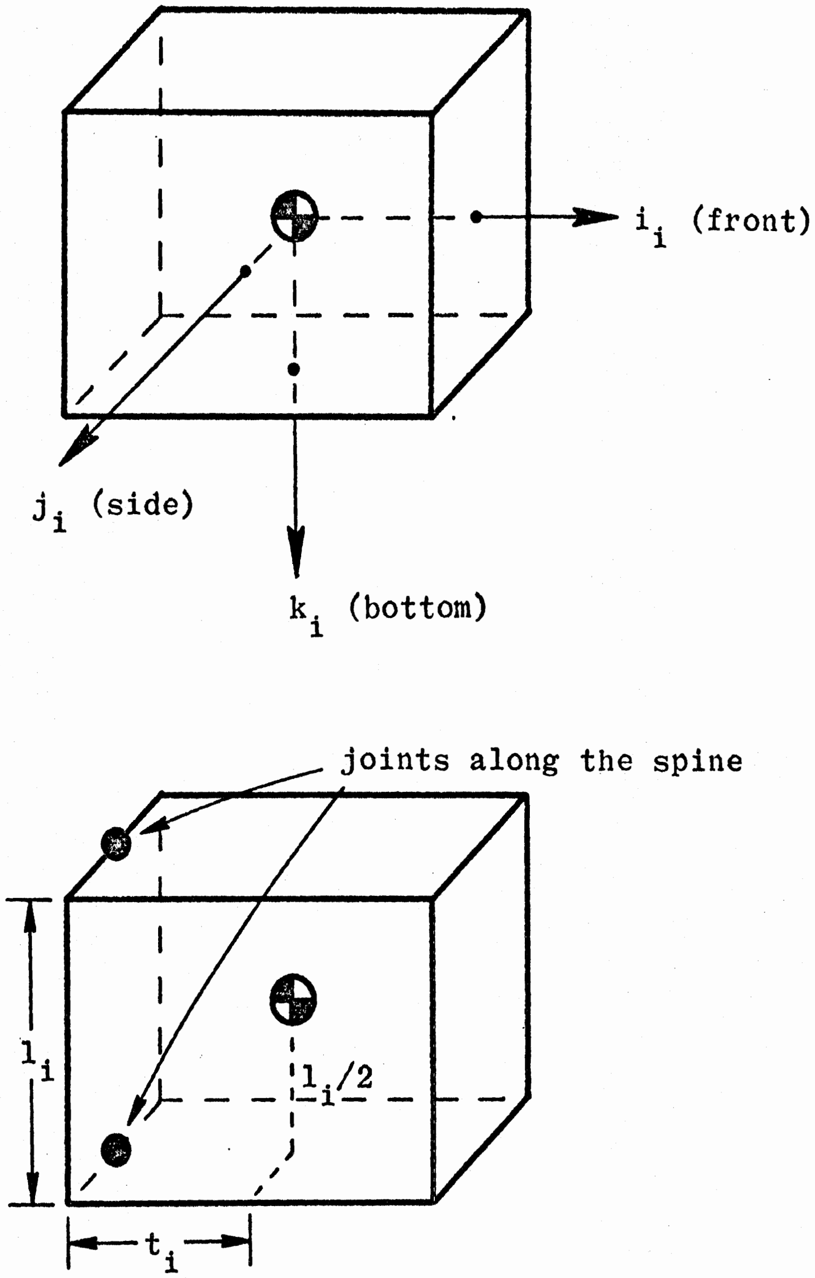
i_i (front)
j_i (side)
k_i (bottom)
joints along the spine
l_i
$l_i/2$
t_i

Figure 7. Illustration of the relative positions of spinal joints and the center of mass for torso element i.

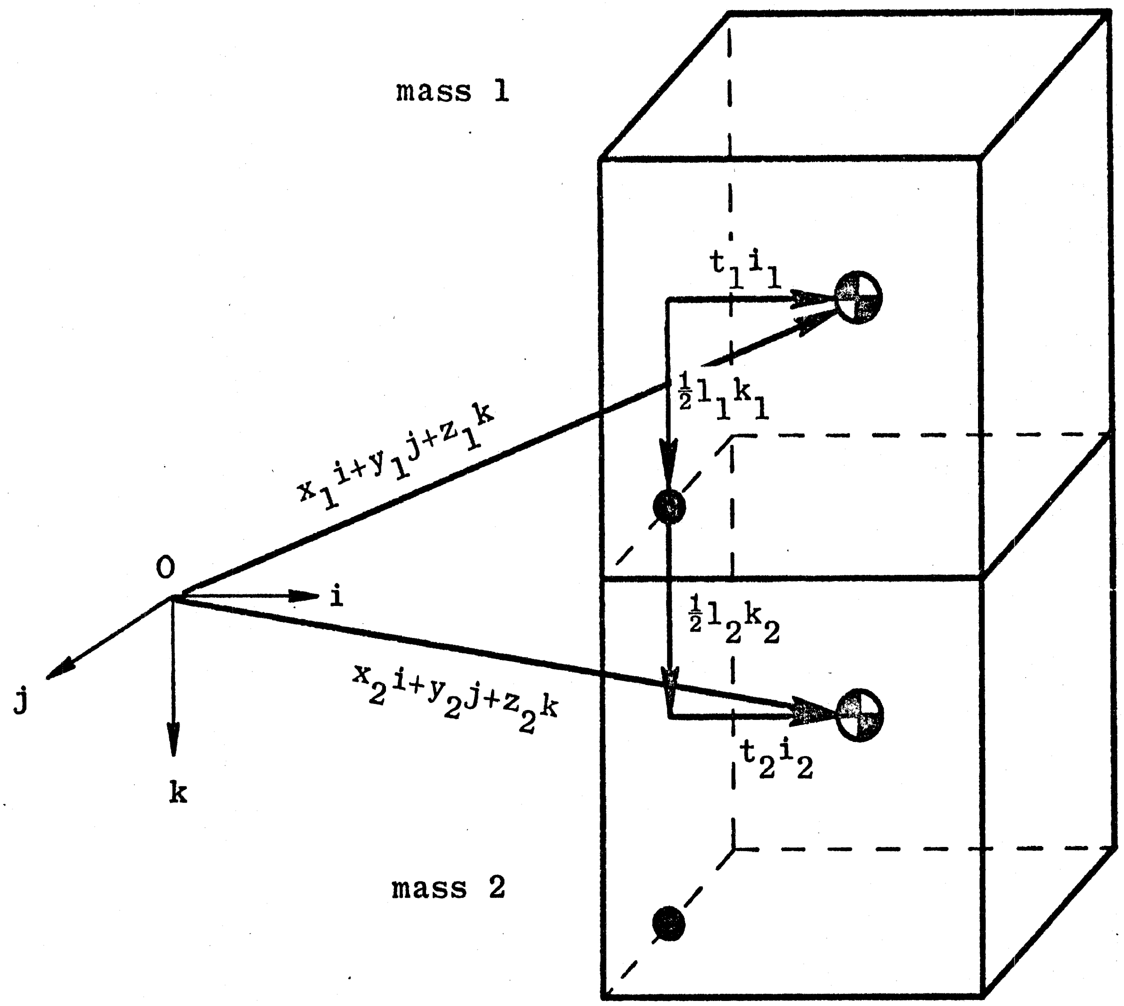
mass 1
$t_1 i_1$
$\frac{1}{2} l_1 k_1$
$x_1 i + y_1 j + z_1 k$
O
i
j
k
$\frac{1}{2} l_2 k_2$
$x_2 i + y_2 j + z_2 k$
$t_2 i_2$
mass 2

Figure 8. Vector constraint loop for elimination of (x_2, y_2, z_2).

$$\begin{aligned}
& x_1 i + y_1 j + z_1 k - t_1 i_1 + \frac{l_1}{2} k_1 + \frac{l_2}{2} k_2 + t_2 i_2 \\
& \qquad = x_2 i + y_2 j + z_2 k \\
& x_1 i + y_1 j + z_1 k - t_1 i_1 + \frac{l_1}{2} k_1 + l_2 k_2 + \frac{l_3}{2} k_3 + t_3 i_3 \\
& \qquad = x_3 i + y_3 j + z_3 k \\
& \cdot \quad \cdot \quad \cdot \quad \cdot \quad \cdot \quad \cdot \quad = \quad \cdot \quad \cdot \quad \cdot \qquad (4.4.2) \\
& x_1 i + y_1 j + z_1 k - t_1 i_1 + \frac{l_1}{2} k_1 + l_2 k_2 + \cdots + l_{n-1} k_{n-1} \\
& \qquad + \frac{l_n}{2} k_n + t_n i_n = x_n i + y_n j + z_n k
\end{aligned}$$

Each of the vector equations (4.4.2) yields three scalar equations after the body axis unit vectors are eliminated by (4.2.1). These 3(n-1) constraints are expressed in equations (4.4.3). These equations may be thought of as representing results for first and second time derivatives as well since x_1, y_1, z_1, and the $a_{ij,k}$'s occur linearly. Determination of the $\dot{a}_{ij,k}$'s and $\ddot{a}_{ij,k}$'s is somewhat tedious. They

$$\begin{aligned}
x_2 &= x_1 - t_1 a_{11,1} + \frac{l_1}{2} a_{31,1} + \frac{l_2}{2} a_{31,2} + t_2 a_{11,2} \\
y_2 &= y_1 - t_1 a_{12,1} + \frac{l_1}{2} a_{32,1} + \frac{l_2}{2} a_{32,2} + t_2 a_{12,2} \\
z_2 &= z_1 - t_1 a_{13,1} + \frac{l_1}{2} a_{33,1} + \frac{l_2}{2} a_{33,2} + t_2 a_{13,2} \qquad \begin{array}{c}(4.4.3)\\ \text{(continued)}\end{array} \\
x_3 &= x_1 - t_1 a_{11,1} + \frac{l_1}{2} a_{31,1} + l_2 a_{31,2} + \frac{l_3}{2} a_{31,3} + t_3 a_{11,3} \\
y_3 &= y_1 - t_1 a_{12,1} + \frac{l_1}{2} a_{32,1} + l_2 a_{32,2} + \frac{l_3}{2} a_{32,3} + t_3 a_{12,3}
\end{aligned}$$

$$z_3 = z_1 - t_1 a_{13,1} + \frac{l_1}{2} a_{33,1} + l_2 a_{33,2} + \frac{l_3}{2} a_{33,3} + t_3 a_{13,3}$$

$$\cdot = \cdot \quad \cdot \quad \cdot \quad \cdot \quad \cdot \quad \cdot \quad \cdot \quad \cdot \quad \cdot$$

$$\begin{aligned} x_n = {} & x_1 - t_1 a_{11,1} + \frac{l_1}{2} a_{31,1} + l_2 a_{31,2} + \cdots + l_{n-1} a_{31,n-1} \\ & + \frac{l_n}{2} a_{31,n} + t_n a_{11,n} \qquad \text{(4.4.3) (concluded)} \\ y_n = {} & y_1 - t_1 a_{12,1} + \frac{l_1}{2} a_{32,1} + l_2 a_{32,2} + \cdots + l_{n-1} a_{32,n-1} \\ & + \frac{l_n}{2} a_{32,n} + t_n a_{12,n} \\ z_n = {} & z_1 - t_1 a_{13,1} + \frac{l_1}{2} a_{33,1} + l_2 a_{33,2} + \cdots + l_{n-1} a_{33,n-1} \\ & + \frac{l_n}{2} a_{33,n} + t_n a_{13,n} \end{aligned}$$

appear in Appendix A. Appendix A also contains $\dot{\alpha}_i$, $\dot{\beta}_i$, $\dot{\gamma}_i$, and the results for all partial derivatives of α_i, β_i, γ_i, and of the $\dot{a}_{ij,k}$'s which derive from the kinetic energy terms of the Lagrange equations.

4.4.1 Translational Terms in the Equations of Motion

Substitution of (4.4.1) into the Lagrange equations (4.1.1) will obviously lead to terms of the form

$$m_i \dot{x}_i \left[\frac{d}{dt} \frac{\partial \dot{x}_i}{\partial \dot{q}_k} - \frac{\partial \dot{x}_i}{\partial q_k} \right] + m_i \ddot{x}_i \frac{\partial \dot{x}_i}{\partial \dot{q}_k}$$

and similar terms for y_i and z_i. It is easily shown that the first term of the above expression is identically zero. Goldstein (26) shows (pp. 16, 17) that

$$\frac{\partial \dot{\vec{r}}}{\partial \dot{q}} = \frac{\partial \vec{r}}{\partial q} \quad , \tag{4.4.4}$$

where $\vec{r}$ is the inertial position vector of any particle in a system and q is any generalized coordinate of the system. If equation (4.4.4) is differentiated with respect to time, with the order of differentiation interchanged on the right-hand side, we obtain

$$\frac{d}{dt}\frac{\partial \dot{\vec{r}}}{\partial \dot{q}} = \frac{\partial \dot{\vec{r}}}{\partial q} \quad . \tag{4.4.5}$$

Since $\vec{r}$ may represent the position vector for the center of mass of any of the torso elements, we have

$$\frac{d}{dt}\frac{\partial(\dot{x}_i, \dot{y}_i, \dot{z}_i)}{\partial \dot{q}_k} - \frac{\partial(\dot{x}_i, \dot{y}_i, \dot{z}_i)}{\partial q_k} = 0, \tag{4.4.6}$$

and the only non-zero translational terms are

$$m_i(\ddot{x}_i, \ddot{y}_i, \ddot{z}_i)\frac{\partial(\dot{x}_i, \dot{y}_i, \dot{z}_i)}{\partial \dot{q}_k} \quad .$$

(There is no similar cancellation that can be applied to the rotational kinetic energy terms.)

These terms are determined below for x_i from equations (4.4.3). The same results hold for y_i and z_i as long as x is replaced by y or z and second subscripts on the a's are replaced by 2 or 3, respectively. Derivatives that are obviously zero, for example

$$\frac{\partial \dot{y}_2}{\partial \dot{x}_1} \quad ,$$

are not written out at all.

Let

$$b_{ik} = m_i \ddot{x}_i \frac{\partial \dot{x}_i}{\partial \dot{q}_k} \quad . \tag{4.4.7}$$

Then

$$\begin{array}{ll}
q_k = x_1, \ i \geq 1: & b_{ik} = m_i \ddot{x}_i \, . \\[2ex]
q_k = (\psi_1, \theta_1, \varphi_1), \ i \geq 2: & b_{ik} = m_i \ddot{x}_i \Big(-t_1 \dfrac{\partial \dot{a}_{11,1}}{\partial \dot{q}_k} \\
 & \qquad + \dfrac{\ell_1}{2} \dfrac{\partial \dot{a}_{31,1}}{\partial \dot{q}_k} \Big) \\[2ex]
q_k = (\psi_r, \theta_r, \varphi_r), & b_{ik} = m_i \ddot{x}_i \Big(\ell_r \dfrac{\partial \dot{a}_{31,r}}{\partial \dot{q}_k} \Big) \\
\qquad i \geq 3, \ 1 < r < i: & \\[2ex]
q_k = (\psi_i, \theta_i, \varphi_i), & b_{ik} = m_i \ddot{x}_i \Big(\dfrac{\ell_i}{2} \dfrac{\partial \dot{a}_{31,i}}{\partial \dot{q}_k} \\
\qquad i \geq 2: & \qquad + t_i \dfrac{\partial \dot{a}_{11,i}}{\partial \dot{q}_k} \Big)
\end{array} \tag{4.4.8}$$

4.4.2 Rotational Terms in the Equations of Motion

The rotational terms for α_i have the form

$$I_i\left[\dot{\alpha}_i \frac{\partial \alpha_i}{\partial \dot{q}_k} + \alpha_i \frac{d}{dt}\frac{\partial \alpha_i}{\partial \dot{q}_k} - \alpha_i \frac{\partial \alpha_i}{\partial q_k}\right] .$$

The terms for β_i and γ_i, with J_i and K_i, are similar.

4.5 HEAD KINETIC ENERGY

The total kinetic energy of the head is

$$\begin{aligned} T_h &= \frac{1}{2} m_h \left(\dot{x}_h^2 + \dot{y}_h^2 + \dot{z}_h^2\right) \\ &\quad + \frac{1}{2} I_h \alpha_h^2 + \frac{1}{2} J_h \beta_h^2 + \frac{1}{2} K_h \gamma_h^2 . \end{aligned} \tag{4.5.1}$$

The subscript "h" indicates "head," and the quantities in this expression are defined analogously to those in equation (4.4.1).

Figure 9 illustrates the relation between the head, neck, and upper torso element portions of the kinetic linkage. The generalized coordinates associated with the neck element were defined in Section 3.2. In terms of l, Θ, and R they are

$$\begin{aligned} x &= l \sin R \cos \Theta \\ y &= l \sin R \sin \Theta \\ z &= -l \cos R \end{aligned} \tag{4.5.2}$$

,

and the velocities are

$$\begin{aligned} \dot{x} &= \dot{l} \sin R \cos \Theta + l \left(\dot{R} \cos R \cos \Theta - \dot{\Theta} \sin R \sin \Theta\right) \\ \dot{y} &= \dot{l} \sin R \sin \Theta + l \left(\dot{R} \cos R \sin \Theta + \dot{\Theta} \sin R \cos \Theta\right) \\ \dot{z} &= -\dot{l} \cos R + l \dot{R} \sin R \end{aligned} \tag{4.5.3}$$

.

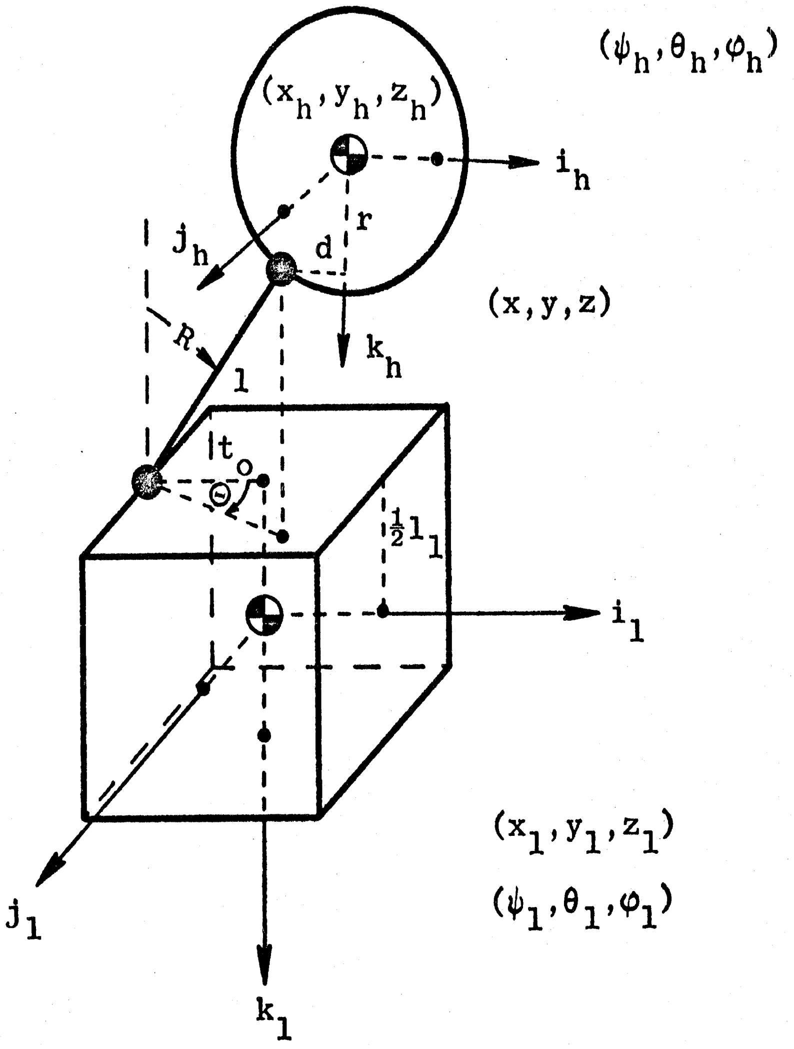

$(\psi_h, \theta_h, \varphi_h)$
(x_h, y_h, z_h)
i_h
j_h
r
d
(x, y, z)
k_h
R
l
t_o
Θ
$\frac{1}{2}l_1$
i_1
(x_1, y_1, z_1)
$(\psi_1, \theta_1, \varphi_1)$
j_1
k_1

Figure 9. The head-neck-torso linkage.

It can be seen from Figure 9 that the following constraint relation holds:

$$\begin{aligned} & x_1 i + y_1 j + z_1 k - t_0 i_1 - \frac{l_1}{2} k_1 \\ & \quad + \vec{l}(t) + d\, i_h - r\, k_h = x_h i + y_h j + z_h k . \end{aligned} \tag{4.5.4}$$

Where $\vec{l}$ is directed from torso to head, it is also clear that

$$\vec{l}(t) = x\, i_1 + y\, j_1 + z\, k_1 \quad . \tag{4.5.5}$$

Equation (4.5.5) is used to eliminate $\vec{l}$ in equation (4.5.4). Also, since equation (4.2.1) applies to the rotating head frame as well as to the torso element frames, all of the unit vectors i_1, j_1, k_1, i_h, j_h, and k_h may be eliminated from (4.5.4). Equation (4.5.4) then becomes

$$\begin{aligned} & x_1 i + y_1 j + z_1 k + (x - t_0)(a_{11,1} i + a_{12,1} j + a_{13,1} k) \\ & \quad + y\,(a_{21,1} i + a_{22,1} j + a_{23,1} k) \\ & \quad - \left(-z + \frac{l_1}{2}\right)(a_{31,1} i + a_{32,1} j + a_{33,1} k) \\ & \quad + d\,(a_{11,h} i + a_{12,h} j + a_{13,h} k) \\ & \quad - r\,(a_{31,h} i + a_{32,h} j + a_{33,h} k) \\ & \qquad = x_h i + y_h j + z_h k \quad . \end{aligned} \tag{4.5.6}$$

Therefore, x_h is

$$\begin{aligned} x_h &= x_1 + (x - t_0)\, a_{11,1} + y\, a_{21,1} \\ &\quad - \left(-z + \frac{\ell_1}{2}\right) a_{31,1} + d\, a_{11,h} - r\, a_{31,h} \; . \end{aligned} \tag{4.5.7}$$

The velocity and acceleration are

$$\begin{aligned} \dot{x}_h &= \dot{x}_1 + \dot{x}\, a_{11,1} + (x - t_0)\, \dot{a}_{11,1} + \dot{y}\, a_{21,1} \\ &\quad + y\, \dot{a}_{21,1} - (-\dot{z})\, a_{31,1} - \left(-z + \frac{\ell_1}{2}\right) \dot{a}_{31,1} \\ &\quad + d\, \dot{a}_{11,h} - r\, \dot{a}_{31,h} \end{aligned} \tag{4.5.8}$$

and

$$\begin{aligned} \ddot{x}_h &= \ddot{x}_1 + \ddot{x}\, a_{11,1} + 2\dot{x}\, \dot{a}_{11,1} + (x - t_0)\, \ddot{a}_{11,1} \\ &\quad + \ddot{y}\, a_{21,1} + 2\dot{y}\, \dot{a}_{21,1} + y\, \ddot{a}_{21,1} \\ &\quad - (-\ddot{z})\, a_{31,1} - 2(-\dot{z})\, \dot{a}_{31,1} \\ &\quad - \left(-z + \frac{\ell_1}{2}\right) \ddot{a}_{31,1} + d\, \ddot{a}_{11,h} - r\, \ddot{a}_{31,h} \; . \end{aligned} \tag{4.5.9}$$

Similar results hold for y_h, z_h, and their derivatives if $(x_1, \dot{x}_1, \ddot{x}_1)$ are replaced by $(y_1, \dot{y}_1, \ddot{y}_1)$ or $(z_1, \dot{z}_1, \ddot{z}_1)$ and if the second subscripts on all a's are replaced by 2 or 3, respectively. These results then allow $\dot{x}_h$, $\dot{y}_h$, $\dot{z}_h$, $\ddot{x}_h$, $\ddot{y}_h$, and $\ddot{z}_h$ to be eliminated from the differential equations of motion.

4.5.1 Translational Terms in the Equations of Motion

It was shown in Section 4.4.1 that only one type of term remains uncancelled as a contribution of the translational kinetic energy to the equations of motion. For the head this is

$$m_k \left(\ddot{x}_k \frac{\partial \dot{x}_k}{\partial \dot{q}_k} + \ddot{y}_k \frac{\partial \dot{y}_k}{\partial \dot{q}_k} + \ddot{z}_k \frac{\partial \dot{z}_k}{\partial \dot{q}_k} \right).$$

The partial derivatives in this expression, and also the ones appearing in the rotational terms, may be found in Appendix A.

4.5.2 Rotational Terms in the Equations of Motion

The rotational terms for the head have exactly the same form as the torso rotational terms. It is necessary only to replace all "i" subscripts by "h" in the results of Section 4.4.2.

4.6 TORSO POTENTIAL ENERGY AND DISSIPATION FUNCTIONS AND CONTRIBUTIONS TO THE EQUATIONS OF MOTION

In this section and in Section 4.7 many types of contributions to the total potential energy and dissipation functions are dealt with. Subscripts could be provided to explicitly designate the various components, for example, "$V_{gravity}$" or "V_g." This is not done, however, as only one type of contribution is discussed within any sub-section; use of simply "V" or "D" can lead to no confusion regarding the component being considered. Similarly, spring and damping coefficients will be simply "k" and "c."

4.6.1 Torso Gravitational Terms

The effect of gravity in a crash situation is not significant. It is easily included, however, in the equations of motion.

The torso potential energy due to gravity is

$$V = -g \sum_{i=1}^{n} m_i z_i \quad .. \qquad (4.6.1)$$

The non-zero contributions to the equations of motion are

$$\frac{\partial V}{\partial z_1} = -g \sum_{i=1}^{m} m_i \tag{4.6.2}$$

and

$$\frac{\partial V}{\partial q_k} = -g \sum_{i=1}^{m} m_i \frac{\partial z_i}{\partial q_k} \quad , \tag{4.6.3}$$

where:

$$\begin{array}{ll} q_k = (\psi_1, \theta_1, \phi_1): & \dfrac{\partial z_i}{\partial q_k} = -t_1 \dfrac{\partial a_{13,1}}{\partial q_k} + \dfrac{l_1}{2} \dfrac{\partial a_{33,1}}{\partial q_k} \\ \quad i \geq 2 & \\ q_k = (\psi_r, \theta_r, \phi_r): & \dfrac{\partial z_i}{\partial q_k} = l_r \dfrac{\partial a_{33,r}}{\partial q_k} \\ \quad i \geq 3, \ 1 < r < i & \\ q_k = (\psi_i, \theta_i, \phi_i): & \dfrac{\partial z_i}{\partial q_k} = \dfrac{l_i}{2} \dfrac{\partial a_{33,i}}{\partial q_k} + t_i \dfrac{\partial a_{13,i}}{\partial q_k} \\ \quad i \geq 2 & \end{array} \tag{4.6.4}$$

The partial derivatives of the a's are in Appendix A.

4.6.2 Torso Joint Stop Terms for Bending

The generalized pitching angle between torso elements i and i + 1, as defined in Section 3.3, is

$$R_i = \cos^{-1}\left(\mathbf{k}_i \cdot \mathbf{k}_{i+1}\right) \quad . \tag{4.6.5}$$

After eliminating k_i and k_{i+1} by equation (4.2.1) and carrying out the dot product we obtain

$$R_i = \cos^{-1}\left(a_{31,i}\, a_{31,i+1} + a_{32,i}\, a_{32,i+1} + a_{33,i}\, a_{33,i+1}\right) . \tag{4.6.6}$$

The heading angle described in Section 3.3 is shown in Figures 10 and 11. The vector $\vec{v}$ is directed from the center of mass of element i + 1 to the center of mass of element i. Reference to Figure 8 shows that this vector can be determined from the following vector constraint:

$$\vec{v} - t_i i_i + \frac{l_i}{2} k_i + \frac{l_{i+1}}{2} k_{i+1} + t_{i+1} i_{i+1} = \vec{0} . \tag{4.6.7}$$

Also, it is clear from Figure 11 that

$$\Theta_i = \tan^{-1} \frac{\vec{v} \cdot j_{i+1}}{\vec{v} \cdot i_{i+1}} . \tag{4.6.8}$$

Elimination of $\vec{v}$ in equation (4.6.8) by (4.6.7) yields

$$\Theta_i = \tan^{-1} \frac{\left(t_i i_i - \frac{l_i}{2} k_i\right) \cdot j_{i+1}}{-t_{i+1} + \left(t_i i_i - \frac{l_i}{2} k_i\right) \cdot i_{i+1}} . \tag{4.6.9}$$

After the unit vectors in (4.6.9) are eliminated by (4.2.1) and the dot products carried out, this becomes

$$\Theta_i = \tan^{-1} \frac{n_i}{d_i} , \tag{4.6.10}$$

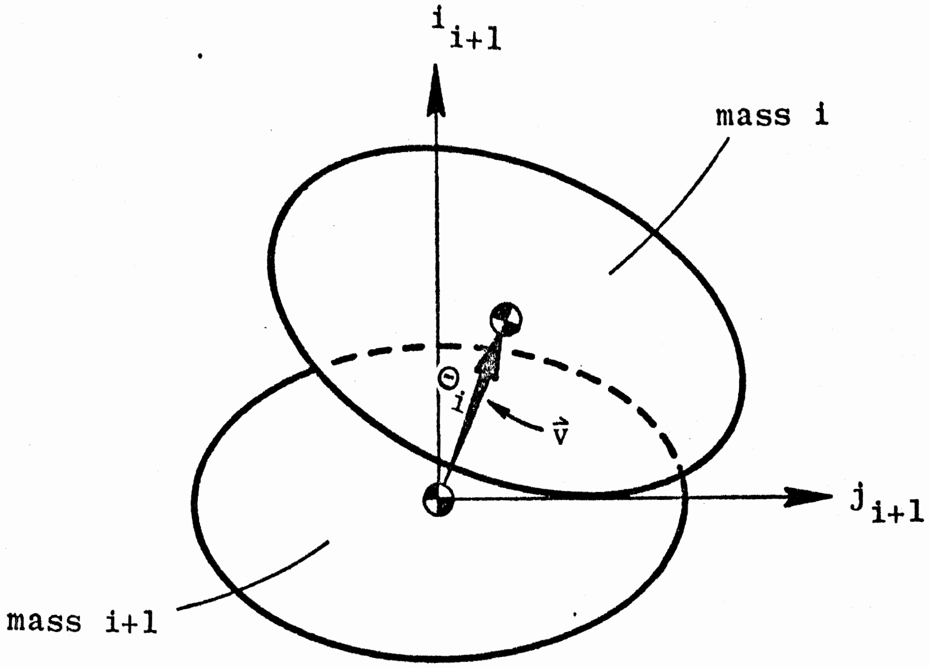
i_{i+1}
mass i
Θ_i
$\vec{v}$
j_{i+1}
mass i+1

Figure 10. View along k_{i+1}, showing heading angle Θ_i.

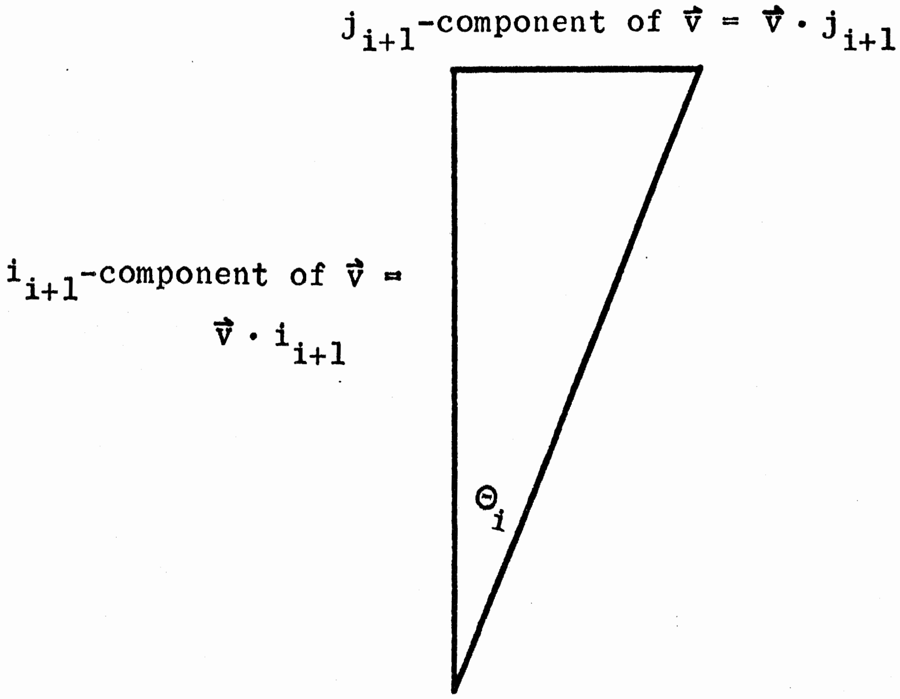
j_{i+1}-component of $\vec{v} = \vec{v} \cdot j_{i+1}$
i_{i+1}-component of $\vec{v}$ =
$\vec{v} \cdot i_{i+1}$
Θ_i

Figure 11. Heading angle Θ_i as the angle between i_{i+1} and the projection of $\vec{v}$ on the i_{i+1}-j_{i+1} plane.

where

$$\begin{aligned} m_i = {} & t_i\left(a_{11,i}\, a_{21,i+1} + a_{12,i}\, a_{22,i+1} + a_{13,i}\, a_{23,i+1}\right) \\ & - \frac{\ell_i}{2}\left(a_{31,i}\, a_{21,i+1} + a_{32,i}\, a_{22,i+1} + a_{33,i}\, a_{23,i+1}\right) \end{aligned} \tag{4.6.11}$$

and

$$\begin{aligned} d_i = {} & -t_{i+1} + t_i\left(a_{11,i}\, a_{11,i+1} + a_{12,i}\, a_{12,i+1} + a_{13,i}\, a_{13,i+1}\right) \\ & - \frac{\ell_i}{2}\left(a_{31,i}\, a_{11,i+1} + a_{32,i}\, a_{12,i+1} + a_{33,i}\, a_{13,i+1}\right). \end{aligned} \tag{4.6.12}$$

The joint stop angle "ellipse" may now be defined. With reference to Figure 12 consider that angles x and y are measured to the (right) "side" and the "front," respectively. Then,

$$\begin{aligned} x &= f_i(\Theta_i) \sin \Theta_i \\ y &= f_i(\Theta_i) \cos \Theta_i \quad . \end{aligned} \tag{4.6.13}$$

Consider, first, the front half-ellipse.

$|\Theta_i| \le \frac{\pi}{2}$:

$$\left(\frac{x}{\alpha_{s,i}}\right)^2 + \left(\frac{y}{\alpha_{f,i}}\right)^2 = 1 \tag{4.6.14}$$

Elimination of x and y by (4.6.13) gives

$$f_i^2\left[\left(\frac{\sin \Theta_i}{\alpha_{s,i}}\right)^2 + \left(\frac{\cos \Theta_i}{\alpha_{f,i}}\right)^2\right] = 1 \ , \tag{4.6.15}$$

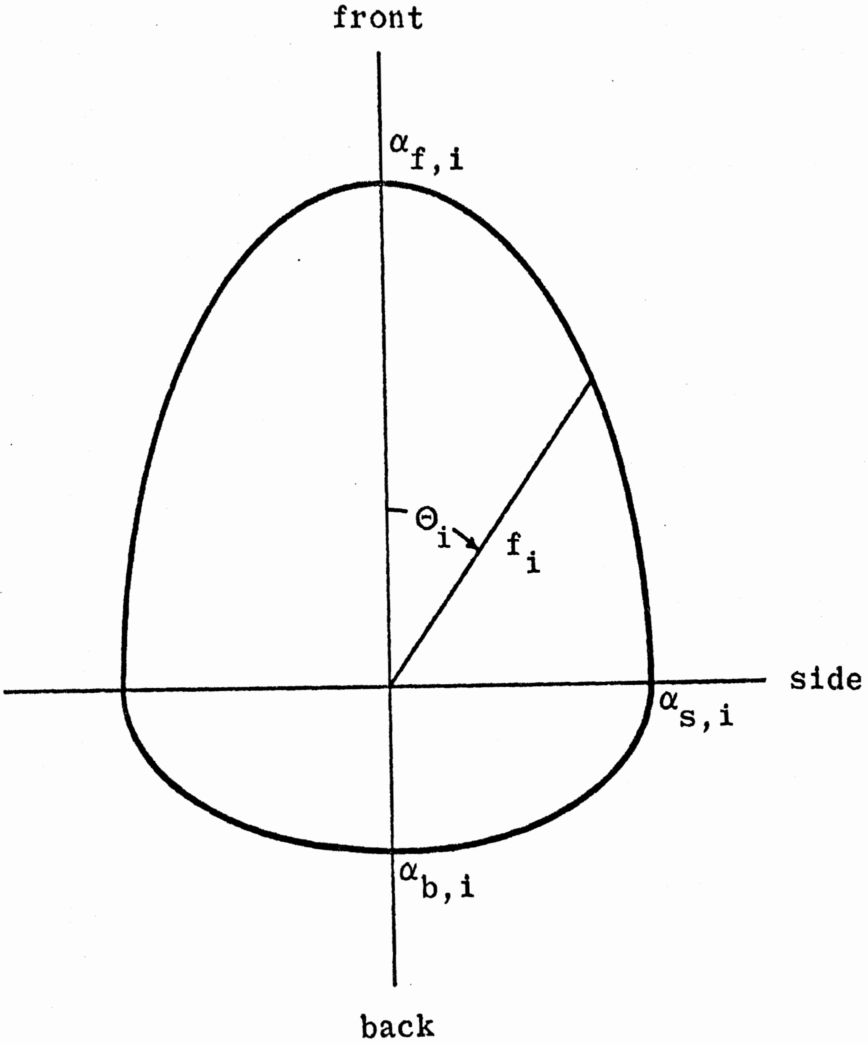
front
$\alpha_{f,i}$
Θ_i
f_i
side
$\alpha_{s,i}$
$\alpha_{b,i}$
back

Figure 12. Stop angle "ellipse."

or

$$f_i = \alpha_{s,i}\,\alpha_{f,i} \Big/ \sqrt{(\alpha_{f,i} \sin\Theta_i)^2 + (\alpha_{s,i} \cos\Theta_i)^2}\,. \qquad (4.6.16)$$

Also,

$$f_i'(\Theta_i) = -\alpha_{s,i}\,\alpha_{f,i}\,(\alpha_{f,i}^2 - \alpha_{s,i}^2) \sin\Theta_i \cos\Theta_i \Big/ \left[(\alpha_{f,i} \sin\Theta_i)^2 + (\alpha_{s,i} \cos\Theta_i)^2\right]^{3/2}. \qquad (4.6.17)$$

$$(f_i = f_i' = 0 \text{ if } \alpha_{s,i} = \alpha_{f,i} = 0.)$$

$|\Theta_i| > \frac{\pi}{2}$:

It is clear that similar results will hold for the back half-ellipse. It is necessary only to replace the subscript "f" (front) by the subscript "b" (back) in equations (4.6.16) and (4.6.17).

Joint stop moments may now be determined. Spring and damping components will both be zero unless R_i is greater than $f_i(\Theta_i)$. In the following, "M_i" may indicate either a spring or damping moment component. The context of its use will always make clear its meaning. Moments will be assumed to have linear, quadratic, and cubic terms, and all spring and damping rates may be assumed to have Θ_i-dependence.

The spring moment component is

$$M_i = -\sum_{j=1}^{3} k_{i,j}(\Theta_i)\left[R_i - f_i(\Theta_i)\right]^j, \qquad R_i > f_i, \qquad (4.6.18)$$

or

$$\dot{M}_i = 0 , \quad R_i \leq f_i \quad . \tag{4.6.19}$$

Then,

$$V = -\int_0^{R_i - f_i} M_i \, \partial(R_i - f_i) \quad , \tag{4.6.20}$$

or

$$V = \sum_{j=1}^{3} k_{i,j} \frac{(R_i - f_i)^{j+1}}{j+1} \quad . \tag{4.6.21}$$

Hence, from (4.6.18) and (4.6.21),

$$\begin{aligned} \frac{\partial V}{\partial q_k} = & -M_i \left(\frac{\partial R_i}{\partial q_k} - f_i'(\Theta_i) \frac{\partial \Theta_i}{\partial q_k} \right) \\ & + \sum_{j=1}^{3} \frac{(R_i - f_i)^{j+1}}{j+1} k_{i,j}'(\Theta_i) \frac{\partial \Theta_i}{\partial q_k} \end{aligned} \tag{4.6.22}$$

for $R_i > f_i$.

The partial derivatives of R_i and Θ_i in (4.6.22) will now be determined.

Define Arg as the argument in equation (4.6.6), i.e.,

$$Arg = a_{31,i} a_{31,i+1} + a_{32,i} a_{32,i+1} + a_{33,i} a_{33,i+1} \quad . \tag{4.6.23}$$

Then,

$$\frac{\partial R_i}{\partial q_k} = \frac{\partial \cos^{-1} Arg}{\partial q_k} \quad . \tag{4.6.24}$$

This becomes

$$\frac{\partial R_i}{\partial q_k} = -\frac{1}{\sqrt{1 - Arg^2}} \frac{\partial Arg}{\partial q_k} \quad , \tag{4.6.25}$$

or, since Arg = $\cos R_i$,

$$\frac{\partial R_i}{\partial q_k} = -\frac{1}{\sin R_i} \frac{\partial Arg}{\partial q_k} \quad . \tag{4.6.26}$$

(Note that a division by zero when $R_i = 0$ is never a difficulty. The potential energy contribution to the equations of motion can be set directly equal to zero in this case since, by (4.6.19), the moment will be zero.) By equation (4.6.23) we have

$q_k = (\psi_i, \theta_i, \varphi_i)$:

$$\frac{\partial Arg}{\partial q_k} = \frac{\partial a_{31,i}}{\partial q_k} a_{31,i+1} + \frac{\partial a_{32,i}}{\partial q_k} a_{32,i+1} + \frac{\partial a_{33,i}}{\partial q_k} a_{33,i+1} \quad . \tag{4.6.27}$$

$q_k = (\psi_{i+1}, \theta_{i+1}, \varphi_{i+1})$:

$$\frac{\partial Arg}{\partial q_k} = a_{31,i}\frac{\partial a_{31,i+1}}{\partial q_k} + a_{32,i}\frac{\partial a_{32,i+1}}{\partial q_k} + a_{33,i}\frac{\partial a_{33,i+1}}{\partial q_k} \quad . \tag{4.6.28}$$

Also, from equations (4.6.10) to (4.6.12) we get

$q_k = (\psi_i, \theta_i, \varphi_i)$:

$$\begin{aligned}\frac{\partial \Theta_i}{\partial q_k} = \frac{1}{n_i^2 + d_i^2}\Bigg\{ & d_i\Bigg[t_i\Big(\frac{\partial a_{11,i}}{\partial q_k}a_{21,i+1} \\ & + \frac{\partial a_{12,i}}{\partial q_k}a_{22,i+1} + \frac{\partial a_{13,i}}{\partial q_k}a_{23,i+1}\Big) \\ & - \frac{\ell_i}{2}\Big(\frac{\partial a_{31,i}}{\partial q_k}a_{21,i+1} + \frac{\partial a_{32,i}}{\partial q_k}a_{22,i+1} \\ & + \frac{\partial a_{33,i}}{\partial q_k}a_{23,i+1}\Big)\Bigg] \\ & - n_i\Bigg[t_i\Big(\frac{\partial a_{11,i}}{\partial q_k}a_{11,i+1} + \frac{\partial a_{12,i}}{\partial q_k}a_{12,i+1} \\ & + \frac{\partial a_{13,i}}{\partial q_k}a_{13,i+1}\Big) - \frac{\ell_i}{2}\Big(\frac{\partial a_{31,i}}{\partial q_k}a_{11,i+1}\end{aligned} \tag{4.6.29}$$

$$+ \frac{\partial a_{32,i}}{\partial q_k} a_{12,i+1} + \frac{\partial a_{33,i}}{\partial q_k} a_{13,i+1}\Big)\Big]\Big\} .$$

The results for $q_k = (\psi_{i+1}, \theta_{i+1}, \varphi_{i+1})$ are different from (4.6.29) only in that the a's with i + 1 as a third subscript, instead of i, are differentiated with respect to q_k. Θ_i is not a function of any other generalized coordinates.

The contribution from damping to the total joint stop moment is*

$$M_i = -\sum_{j=1}^{3} c_{i,j} |\dot{R}_i|^j \operatorname{sgn} \dot{R}_i \quad , \qquad R_i > f_i \; . \tag{4.6.30}$$

(And $M_i = 0$ if $R_i \leq f_i$.)

The Rayleigh dissipation function is then

$$D = -\int_0^{\dot{R}} M_i \, \partial \dot{R}_i \quad , \tag{4.6.31}$$

which is

$$D = \sum_{j=1}^{3} c_{i,j} \frac{|\dot{R}_i|^{j+1}}{j+1} \quad . \tag{4.6.32}$$

---

*All damping coefficients $c_{i,j}$ for joint stop damping moments are constant only for deformation greater than a specified amount and increase linearly from zero to their constant values. That is, where $C_{i,j}$ are the constant values, δ is a deformation, and Δ is the specified deformation after which $c_{i,j} = C_{i,j}$, the coefficient values for $\delta \leq \Delta$ are $c_{i,j} = \delta C_{i,j}/\Delta$. This definition for joint stop damping coefficients is necessary because the numerical integration balks at the discontinuous moments at $\delta = (0^-, 0^+)$ resulting from constant coefficient values. A "ramp" length of $\Delta = 5°$ has been used.

Therefore, since $\partial|\theta|/\partial q = (\partial\theta/\partial q)\mathrm{sgn}\theta$,

$$\frac{\partial D}{\partial q_k} = -M_i \frac{\partial \dot{R}_i}{\partial \dot{q}_k} , \tag{4.6.33}$$

for $R_i > f_i$.

The velocity $\dot{R}_i$ is determined from (4.6.6) as

$$\begin{aligned} \dot{R}_i = -\frac{1}{\sin R_i}\Big(&\dot{a}_{31,i}\, a_{31,i+1} + a_{31,i}\, \dot{a}_{31,i+1} \\ &+ \dot{a}_{32,i}\, a_{32,i+1} + a_{32,i}\, \dot{a}_{32,i+1} \\ &+ \dot{a}_{33,i}\, a_{33,i+1} + a_{33,i}\, \dot{a}_{33,i+1}\Big) . \end{aligned} \tag{4.6.34}$$

An important observation is made here. The partial derivatives in (4.6.33) could now be obtained by differentiation of (4.6.34). It could then be shown by writing out $\partial R_i/\partial q_k$ and $\partial \dot{R}_i/\partial \dot{q}_k$ that they are equal. The necessity of this equality can be demonstrated in a general manner, however. Suppose that F is any function of the generalized coordinates alone. We then have equations (4.6.35):

$$\begin{aligned} F &= F(q) \\ \dot{F} &= \sum_{i=1}^{N} \frac{\partial F}{\partial q_i}\, \dot{q}_i \quad . \end{aligned} \tag{4.6.35}$$

Upon differentiation of the second of (4.6.35), we obtain

$$\frac{\partial \dot{F}}{\partial \dot{q}_{jk}} = \frac{\partial F}{\partial q_{jk}} \quad . \tag{4.6.36}$$

In particular for F = R_i we have

$$\frac{\partial \dot{R}_i}{\partial \dot{q}_{jk}} = \frac{\partial R_i}{\partial q_{jk}} \quad . \tag{4.6.37}$$

The general result (4.6.36) will be used several times in the rest of this chapter where damping contributions are determined.

The damping coefficients $c_{i,j}$ may be taken as functions of Θ_i and R_i without changing the form of the result (4.6.33). The spring rates $k_{i,j} = k_{i,j}(\Theta_i)$ could also be taken as functions of R_i by simply adding terms involving

$$\frac{\partial k_{i,j}(\Theta_i, R_i)}{\partial R_i} \; \frac{\partial R_i}{\partial q_{jk}}$$

to the right-hand side of (4.6.22). In this investigation, however, all spring and damping coefficients will be assumed to be constants since no experimental results are available for the dependence on Θ_i and R_i. Hence, the summed term in (4.6.22) is equal to zero.

4.6.3 Torso Joint Stop Terms for Twisting

It was noted in Section 3.3 that the amount of "twist" at a joint will be represented by the relative yaw angle of one body element with respect to the other. The relative Euler angles which take e_i into e_{i+1}

will now be determined. The pitch and roll angles are determined for output but are never used directly.

Call the relative angles ψ'_{i+1}, θ'_{i+1}, and φ'_{i+1}. Then,

$$\ell_{i+1} = \left[A'_{i+1}\right] \ell_i \tag{4.6.38}$$

in the notation of Section 4.2. Since

$$\ell_i = \left[A_i\right] \ell \quad , \tag{4.6.39}$$

we have

$$\ell_{i+1} = \left[A'_{i+1}\right]\left[A_i\right] \ell \quad . \tag{4.6.40}$$

But also,

$$\ell_{i+1} = \left[A_{i+1}\right] \ell \quad , \tag{4.6.41}$$

so

$$\left[A_{i+1}\right] = \left[A'_{i+1}\right]\left[A_i\right] \quad . \tag{4.6.42}$$

Since $[A_i]$ is orthogonal, $[A]^{-1} = [A]^T$, and

$$\left[A'_{i+1}\right] = \left[A_{i+1}\right]\left[A_i\right]^T \equiv \left[B\right] \quad . \tag{4.6.43}$$

Let (4.6.43) define the matrix [B]. By (4.6.43) and (4.2.6), then, we have

$$\tan^{-1}\frac{b_{12}}{b_{11}} = \tan^{-1}\frac{\sin\psi'_{i+1}\cos\theta'_{i+1}}{\cos\psi'_{i+1}\cos\theta'_{i+1}} = \psi'_{i+1}\,, \tag{4.6.44}$$

or, obtaining b_{12} and b_{11} from the matrix product in (4.6.43),

$$\psi'_{i+1} = \tan^{-1}\frac{a_{11,i+1}a_{21,i} + a_{12,i+1}a_{22,i} + a_{13,i+1}a_{23,i}}{a_{11,i+1}a_{11,i} + a_{12,i+1}a_{12,i} + a_{13,i+1}a_{13,i}}\,. \tag{4.6.45}$$

This is the relative yaw, or "twist," angle. Similarly, by considering $-b_{13}|\cos\varphi'_{i+1}|/b_{33}\ \mathrm{sgn}(\cos\varphi'_{i+1})$ and b_{23}/b_{33}, respectively, we obtain

$$\theta'_{i+1} = \tan^{-1}\frac{-(a_{11,i+1}a_{31,i} + a_{12,i+1}a_{32,i} + a_{13,i+1}a_{33,i})\,|\cos\varphi'_{i+1}|}{(a_{31,i+1}a_{31,i} + a_{32,i+1}a_{32,i} + a_{33,i+1}a_{33,i})\,\mathrm{sgn}(\cos\varphi'_{i+1})} \tag{4.6.46}$$

and

$$\varphi'_{i+1} = \tan^{-1}\frac{a_{21,i+1}a_{31,i} + a_{22,i+1}a_{32,i} + a_{23,i+1}a_{33,i}}{a_{31,i+1}a_{31,i} + a_{32,i+1}a_{32,i} + a_{33,i+1}a_{33,i}}\,. \tag{4.6.47}$$

Where f_i is now a constant (symmetric) joint stop angle for twisting at joint i, the spring moment for twisting is

$$M_i = -\sum_{j=1}^{3} k_{i,j}\left[|\psi'_{i+1}| - f_i\right]^j \mathrm{sgn}\,\psi'_{i+1} \tag{4.6.48}$$

for $|\psi'_{i+1}| > f_i$, and $M_i = 0$ otherwise. Also, in the same manner as for the bending moment, we obtain

$$\frac{\partial V}{\partial q_k} = -M_i\frac{\partial\psi'_{i+1}}{\partial q_k}\,, \qquad |\psi'_{i+1}| > f_i\,. \tag{4.6.49}$$

The damping moment is similarly

$$M_i = -\sum_{j=1}^{3} c_{i,j} \left| \dot{\psi}'_{i+1} \right|^j \operatorname{sgn} \dot{\psi}'_{i+1} \quad , \tag{4.6.50}$$

and

$$\frac{\partial D}{\partial \dot{q}_k} = -M_i \frac{\partial \dot{\psi}'_{i+1}}{\partial \dot{q}_k} \quad , \qquad \left| \dot{\psi}'_{i+1} \right| > f_i \; . \tag{4.6.51}$$

Let the numerator and denominator of (4.6.45) be called n_i and d_i. Then, the velocity in (4.6.50) is

$$\begin{aligned} \dot{\psi}'_{i+1} = \frac{1}{n_i^2 + d_i^2} \Big[& d_i \big(\dot{a}_{21,i} a_{11,i+1} + \dot{a}_{22,i} a_{12,i+1} \\ & + \dot{a}_{23,i} a_{13,i+1} + a_{21,i} \dot{a}_{11,i+1} + a_{22,i} \dot{a}_{12,i+1} \\ & + a_{23,i} \dot{a}_{13,i+1} \big) - n_i \big(\dot{a}_{11,i} a_{11,i+1} \\ & + \dot{a}_{12,i} a_{12,i+1} + \dot{a}_{13,i} a_{13,i+1} + a_{11,i} \dot{a}_{11,i+1} \\ & + a_{12,i} \dot{a}_{12,i+1} + a_{13,i} \dot{a}_{13,i+1} \big) \Big] \; . \end{aligned} \tag{4.6.52}$$

Also, for $q_k = (\psi_i, \theta_i, \phi_i)$, we have

$$\begin{aligned} \frac{\partial \dot{\psi}'_{i+1}}{\partial q_k} = \frac{1}{n_i^2 + d_i^2} \Big[& d_i \Big(\frac{\partial a_{21,i}}{\partial q_k} a_{11,i+1} \\ & + \frac{\partial a_{22,i}}{\partial q_k} a_{12,i+1} + \frac{\partial a_{23,i}}{\partial q_k} a_{13,i+1} \Big) \end{aligned} \tag{4.6.53}$$

(continued)

$$-n_i\left(\frac{\partial a_{11,i}}{\partial q_k}a_{11,i+1}+\frac{\partial a_{12,i}}{\partial q_k}a_{12,i+1}+\frac{\partial a_{13,i}}{\partial q_k}a_{13,i+1}\right)\Big] \tag{4.6.53}$$

(concluded)

The results (4.6.53) hold for $q_k = (\psi_{i+1}, \theta_{i+1}, \varphi_{i+1})$ as well if the a's for i + 1, instead of i, are differentiated. By equation (4.6.36),

$$\frac{\partial \dot{\psi}'_{i+1}}{\partial \dot{q}_k} = \frac{\partial \psi'_{i+1}}{\partial q_k} . \tag{4.6.54}$$

4.6.4 Torso Elastic Terms for Bending

The term "elastic" is properly applied only to joint moment characteristics which tend to restore a state of zero deformation. Velocity-dependent damping is not such a characteristic, but it will be discussed along with spring-type elastic moments wherever their values are based upon the same angle.

The same non-linear form as used for joint stop moments is assumed for elastic moments, i.e., they contain linear, quadratic, and cubic terms. The elastic spring moment is

$$M_i = -\sum_{j=1}^{3} k_{i,j} S_i^j , \tag{4.6.55}$$

where S_i, as explained in Section 3.3.2, is the angular difference in the positions of k_i, with respect to e_{i+1}, at times zero and t. The contribution of (4.6.55) to the equations of motion is

$$\frac{\partial V}{\partial q_k} = -M_i \frac{\partial S_i}{\partial q_k} \quad . \tag{4.6.56}$$

The angle S_i will now be determined. At t = 0 the position of k_i with respect to the basis $(i, j, k)_{i+1}$ is the initial position of interest for obtaining S_i. At time t the basis has rotated in space, and so has the vector k_i, although not in the same manner. If now the basis at t is rotated back to its initial position $(i^o, j^o, k^o)_{i+1}$ and the vector k_i along with it, k_i becomes a vector k_i'. Then, S_i is the angle between k_i^o and k_i':

$$S_i = \cos^{-1}(k_i^o \cdot k_i') \quad . \tag{4.6.57}$$

It remains to determine k_i'.

Now, k_i' has the same orientation with respect to e_{i+1}^o as does k_i with respect to e_{i+1}. Therefore, the components in the two systems are equal:

$$\begin{aligned} k_i' \cdot i_{i+1}^o &= k_i \cdot i_{i+1} \\ k_i' \cdot j_{i+1}^o &= k_i \cdot j_{i+1} \\ k_i' \cdot k_{i+1}^o &= k_i \cdot k_{i+1} \quad . \end{aligned} \tag{4.6.58}$$

Resolved along the e^0_{i+1}-axes, k'_i is

$$
\begin{aligned}
k'_i = (k'_i \cdot i^0_{i+1})\, i^0_{i+1} + (k'_i \cdot j^0_{i+1})\, j^0_{i+1} \\
+ (k'_i \cdot k^0_{i+1})\, k^0_{i+1}
\end{aligned}
\tag{4.6.59}
$$

or by (4.6.58),

$$
\begin{aligned}
k'_i = (k_i \cdot i_{i+1})\, i^0_{i+1} + (k_i \cdot j_{i+1})\, j^0_{i+1} \\
+ (k_i \cdot k_{i+1})\, k^0_{i+1} \quad .
\end{aligned}
\tag{4.6.60}
$$

Therefore,

$$
\begin{aligned}
k^0_i \cdot k'_i = {} & (k_i \cdot i_{i+1})(i^0_{i+1} \cdot k^0_i) \\
& + (k_i \cdot j_{i+1})(j^0_{i+1} \cdot k^0_i) + (k_i \cdot k_{i+1})(k^0_{i+1} \cdot k^0_i)
\end{aligned}
\tag{4.6.61}
$$

where

$$
\begin{aligned}
i^0_{i+1} \cdot k^0_i &= a^0_{31,i}\, a^0_{11,i+1} + a^0_{32,i}\, a^0_{12,i+1} + a^0_{33,i}\, a^0_{13,i+1} \\
j^0_{i+1} \cdot k^0_i &= a^0_{31,i}\, a^0_{21,i+1} + a^0_{32,i}\, a^0_{22,i+1} + a^0_{33,i}\, a^0_{23,i+1} \\
k^0_{i+1} \cdot k^0_i &= a^0_{31,i}\, a^0_{31,i+1} + a^0_{32,i}\, a^0_{32,i+1} + a^0_{33,i}\, a^0_{33,i+1}
\end{aligned}
\tag{4.6.62}
$$

and the other factors are of the same form as (4.6.62) except without superscripts. S_i is thus determined.

The partial derivatives of S_i, for (4.6.56), are next determined. Define factors c_1, c_2, and c_3 implicitly by

$$k_i^o \cdot k_i' = c_1 (i_{i+1}^o \cdot k_i^o) + c_2 (j_{i+1}^o \cdot k_i^o) + c_3 (k_{i+1}^o \cdot k_i^o) \quad . \tag{4.6.63}$$

(Compare with (4.6.61).) Then, for $q_k = (\psi_i, \theta_i, \varphi_i)$, we obtain

$$\frac{\partial (k_i^o \cdot k_i')}{\partial q_k} = \frac{\partial c_1}{\partial q_k} (i_{i+1}^o \cdot k_i^o) + \frac{\partial c_2}{\partial q_k} (j_{i+1}^o \cdot k_i^o) + \frac{\partial c_3}{\partial q_k} (k_{i+1}^o \cdot k_i^o), \tag{4.6.64}$$

where

$$\frac{\partial c_j}{\partial q_k} = \frac{\partial a_{31,i}}{\partial q_k} a_{j1,i+1} + \frac{\partial a_{32,i}}{\partial q_k} a_{j2,i+1} + \frac{\partial a_{33,i}}{\partial q_k} a_{j3,i+1} \quad . \tag{4.6.65}$$

The result (4.6.64) holds also for $q_k = (\psi_{i+1}, \theta_{i+1}, \varphi_{i+1})$, but for this case the equation (4.6.65) must be modified so that the a's for i + 1, instead of i, are differentiated. Then,

$$\frac{\partial S_i}{\partial q_k} = - \frac{1}{\sin S_i} \frac{\partial (k_i^o \cdot k_i')}{\partial q_k} \quad , \tag{4.6.66}$$

and (4.6.56) is completely determined. Whenever S_i is zero (e.g., at t = 0), the result (4.6.66) need not be calculated, for M_i is then zero.

The associated damping moment is

$$M_i = -\sum_{j=1}^{3} c_{i,j} |\dot{S}_i|^j \operatorname{sgn} \dot{S}_i \quad , \tag{4.6.67}$$

and

$$\frac{\partial D}{\partial \dot{q}_k} = -M_i \frac{\partial \dot{S}_i}{\partial \dot{q}_k} \quad , \tag{4.6.68}$$

where

$$\frac{\partial \dot{S}_i}{\partial \dot{q}_k} = \frac{\partial S_i}{\partial q_k} \tag{4.6.69}$$

and

$$\begin{aligned}
\dot{S}_i &= -\frac{1}{\sin S_i} \frac{d}{dt}\left(k_i^{\circ} \cdot k_i'\right) \\
&= -\frac{1}{\sin S_i}\Big[\left(i_{i+1}^{\circ} \cdot k_i^{\circ}\right)\big(a_{31,i}\,\dot{a}_{11,i+1} + a_{32,i}\,\dot{a}_{12,i+1} \\
&\quad + a_{33,i}\,\dot{a}_{13,i+1} + \dot{a}_{31,i}\,a_{11,i+1} + \dot{a}_{32,i}\,a_{12,i+1} \\
&\quad + \dot{a}_{33,i}\,a_{13,i+1}\big) + \left(j_{i+1}^{\circ} \cdot k_i^{\circ}\right)\big(a_{31,i}\,\dot{a}_{21,i+1} \\
&\quad + a_{32,i}\,\dot{a}_{22,i+1} + a_{33,i}\,\dot{a}_{23,i+1} + \dot{a}_{31,i}\,a_{21,i+1} \\
&\quad + \dot{a}_{32,i}\,a_{22,i+1} + \dot{a}_{33,i}\,a_{23,i+1}\big) \\
&\quad + \left(k_{i+1}^{\circ} \cdot k_i^{\circ}\right)\big(a_{31,i}\,\dot{a}_{31,i+1} + a_{32,i}\,\dot{a}_{32,i+1} \\
&\quad + a_{33,i}\,\dot{a}_{33,i+1} + \dot{a}_{31,i}\,a_{31,i+1} \\
&\quad + \dot{a}_{32,i}\,a_{32,i+1} + \dot{a}_{33,i}\,a_{33,i+1}\big)\Big] \quad .
\end{aligned} \tag{4.6.70}$$

4.6.5 Torso Elastic Terms for Twisting

Let the initial twist angle be $\psi^0_{i+1} = \psi'_{i+1}(0)$. Then the elastic spring moment is

$$M_i = -\sum_{j=1}^{3} k_{i,j} \left| \psi'_{i+1} - \psi^0_{i+1} \right|^j \operatorname{sgn}\left(\psi'_{i+1} - \psi^0_{i+1}\right). \tag{4.6.71}$$

The contribution to the equations of motion is

$$\frac{\partial V}{\partial q_{f_k}} = -M_i \frac{\partial \psi'_{i+1}}{\partial q_{f_k}} \quad , \tag{4.6.72}$$

where the derivative on the right-hand side is given by equation (4.6.53).

The corresponding damping moment is

$$M_i = -\sum_{j=1}^{3} c_{i,j} \left| \dot{\psi}'_{i+1} \right|^j \operatorname{sgn} \dot{\psi}'_{i+1} \quad , \tag{4.6.73}$$

and

$$\frac{\partial D}{\partial \dot{q}_{f_k}} = -M_i \frac{\partial \dot{\psi}'_{i+1}}{\partial \dot{q}_{f_k}} \quad , \tag{4.6.74}$$

where

$$\frac{\partial \dot{\psi}'_{i+1}}{\partial \dot{q}_{f_k}} = \frac{\partial \psi'_{i+1}}{\partial q_{f_k}} \quad . \tag{4.6.75}$$

4.7 NECK-LINKAGE POTENTIAL ENERGY AND DISSIPATION FUNCTIONS AND CONTRIBUTIONS TO THE EQUATIONS OF MOTION

4.7.1 Head Gravitational Terms

The gravitational potential energy for the head is

$$V = -m_h g z_h \quad . \tag{4.7.1}$$

z_h has already been determined from (4.5.6). Hence,

$$\begin{aligned} V = -m_h g \Big[& z_1 + (x - t_0) a_{13,1} + y a_{23,1} \\ & - \left(-z + \frac{l_1}{2}\right) a_{33,1} + d a_{13,h} - r a_{33,h} \Big] . \end{aligned} \tag{4.7.2}$$

Therefore,

$$\begin{aligned} \frac{\partial V}{\partial z_1} &= -m_h g \\ \frac{\partial V}{\partial x} &= -m_h g a_{13,1} \\ \frac{\partial V}{\partial y} &= -m_h g a_{23,1} \\ \frac{\partial V}{\partial z} &= -m_h g a_{33,1} \quad . \end{aligned} \tag{4.7.3}$$

Also,

$$q_k = (\psi_1, \theta_1, \varphi_1):$$

$$\frac{\partial V}{\partial q_k} = -m_h g\Big[(x - t_0)\frac{\partial a_{13,1}}{\partial q_k} + y\frac{\partial a_{23,1}}{\partial q_k} - \left(-z + \frac{l_1}{2}\right)\frac{\partial a_{33,1}}{\partial q_k}\Big] \qquad (4.7.4)$$

and

$$q_k = (\psi_h, \theta_h, \varphi_h):$$

$$\frac{\partial V}{\partial q_k} = -m_h g\left[d\frac{\partial a_{13,h}}{\partial q_k} - r\frac{\partial a_{33,h}}{\partial q_k}\right]. \qquad (4.7.5)$$

4.7.2 Neck-Torso Joint Stop Terms for Bending

The equations of motion contributions associated with the neck-torso joint are most simply expressed in terms of 1, Θ, and R. (See Figure 9.) For this reason, and for output, these quantities and time derivatives are determined below. The results (4.7.6) and (4.7.7) can be thought of as the inverse of (4.5.2) and (4.5.3).

Figure 13 shows the relationship of the various neck-torso coordinates. The results (4.7.6) are obvious.

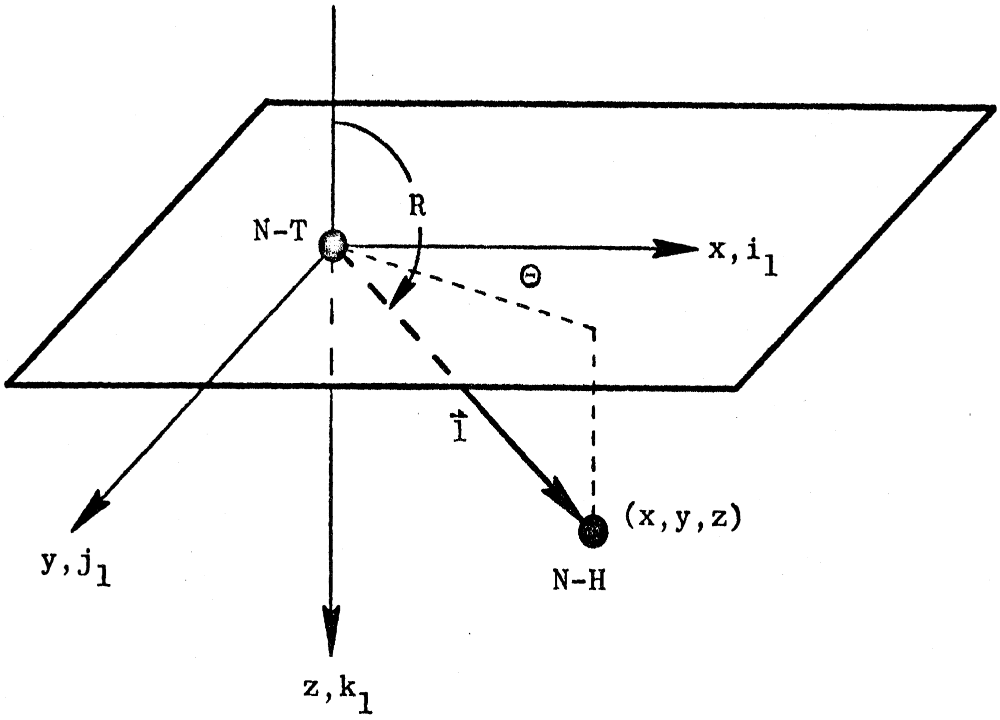
R
N-T
x, i1
Θ
l⃗
(x, y, z)
N-H
y, j1
z, k1

Figure 13. Neck-torso joint coordinates.

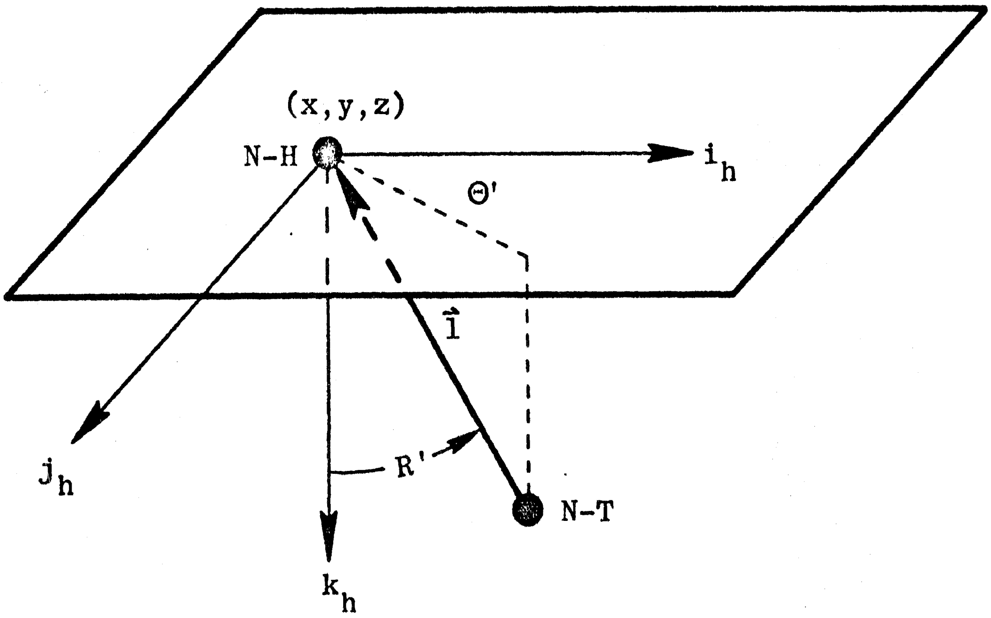
(x, y, z)
N-H
ih
Θ'
l⃗
jh
R'
N-T
kh

Figure 14. Neck-head joint coordinates.

$$\begin{aligned} \ell &= \sqrt{x^2 + y^2 + z^2} \\ \Theta &= \tan^{-1}(y/x) \qquad\qquad (4.7.6) \\ R &= \tan^{-1}\left[\sqrt{x^2+y^2}/(-z)\right] \quad , \quad R < \pi \end{aligned}$$

From (4.7.6) we obtain

$$\begin{aligned} \dot{\ell} &= \frac{x\dot{x} + y\dot{y} + z\dot{z}}{\ell} \\ \dot{\Theta} &= \frac{x\dot{y} - y\dot{x}}{x^2 + y^2} \qquad\qquad (4.7.7) \\ \dot{R} &= \frac{1}{\ell^2}\left[\frac{-z(x\dot{x} + y\dot{y}) + \dot{z}(x^2+y^2)}{\sqrt{x^2+y^2}}\right] \quad . \end{aligned}$$

The accelerations found from (4.7.7) are, after simplification,

$$\begin{aligned} \ddot{\ell} &= \frac{(x\ddot{x} + \dot{x}^2 + y\ddot{y} + \dot{y}^2 + z\ddot{z} + \dot{z}^2) - \dot{\ell}^2}{\ell} \\ \ddot{\Theta} &= \frac{(x\ddot{y} - y\ddot{x}) - 2(x\dot{x} + y\dot{y})\dot{\Theta}}{x^2 + y^2} \qquad\qquad (4.7.8) \\ \ddot{R} &= -\frac{2\dot{\ell}\dot{R}}{\ell} + \frac{1}{\ell^2(x^2+y^2)^{3/2}}\Big\{(x^2+y^2)\big[\ddot{z}(x^2+y^2) \\ &\quad - z(x\ddot{x} + y\ddot{y})\big] - z(y\dot{x} - x\dot{y})^2\Big\} \quad . \end{aligned}$$

Where α_s, α_f, and α_b are the "side," "front," and "back" stop angles for the neck-torso joint, Θ is the heading angle, and f is the joint stop angle as a function of Θ, the stop angle ellipse results (4.6.16) and

(4.6.17) for the torso hold also for the neck-torso joint. Then, with the obvious necessary changes in notation - for example, R replacing R_i - the results for torso bending joint stop moments and the general form of their contributions to the equations of motion represent equally well the corresponding neck-torso joint quantities.

Spring and damping results are hence given by equations (4.6.18) to (4.6.22), (4.6.30) to (4.6.33), and (4.6.37). It is necessary, however, to calculate the partial derivatives of R and Θ anew since they have different form from R_i and Θ_i. The non-zero derivatives are given by equations (4.7.9).

$$\frac{\partial R}{\partial x} = -\frac{xz}{\ell^2\sqrt{x^2+y^2}}$$

$$\frac{\partial R}{\partial y} = -\frac{yz}{\ell^2\sqrt{x^2+y^2}}$$

$$\frac{\partial R}{\partial z} = \frac{\sqrt{x^2+y^2}}{\ell^2} \tag{4.7.9}$$

$$\frac{\partial \Theta}{\partial x} = -\frac{y}{x^2+y^2}$$

$$\frac{\partial \Theta}{\partial y} = \frac{x}{x^2+y^2}$$

4.7.3 Neck-Head Joint Stop Terms for Bending

Coordinates R' and Θ' for the neck-head joint will be defined similarly to R and Θ. However, whereas R and Θ are defined in terms of $\vec{l}$ and the first torso element basis, the neck-head coordinates R' and Θ'

are naturally defined in terms of $\vec{l}$ and the head basis. Figure 14 illustrates the relationship of the neck-head coordinates.

Where $\hat{l}$ is the unit vector for $\vec{l}$, R' is

$$R' = \cos^{-1}\left(-k_h \cdot \hat{l}\right) \,, \tag{4.7.10}$$

or by (4.5.5),

$$R' = \cos^{-1}\left(-k_h \cdot \frac{x i_1 + y j_1 + z k_1}{l}\right) . \tag{4.7.11}$$

Eliminating the unit base vectors by (4.2.1) and then performing the dot product we obtain

$$\begin{aligned} R' = \cos^{-1}\Big(-\frac{1}{l}\Big[& x\left(a_{11,1}a_{31,h} + a_{12,1}a_{32,h}\right. \\ & \left. + a_{13,1}a_{33,h}\right) + y\left(a_{21,1}a_{31,h} + a_{22,1}a_{32,h}\right. \\ & \left. + a_{23,1}a_{33,h}\right) + z\left(a_{31,1}a_{31,h} + a_{32,1}a_{32,h}\right. \\ & \left. + a_{33,1}a_{33,h}\right)\Big]\Big) \quad . \end{aligned} \tag{4.7.12}$$

It can be seen from Figure 14 that the heading angle Θ' is

$$\Theta' = \tan^{-1}\frac{(-\vec{l}\cdot j_h)}{(-\vec{l}\cdot i_h)} \quad . \tag{4.7.13}$$

By (4.5.5) and (4.2.1), this becomes

$$\textcircled{\scriptsize H}' = \tan^{-1}\frac{n}{d} \quad , \tag{4.7.14}$$

where

$$\begin{aligned} n = -\Big[& x\left(a_{11,1}a_{21,k} + a_{12,1}a_{22,k} + a_{13,1}a_{23,k}\right) \\ & + y\left(a_{21,1}a_{21,k} + a_{22,1}a_{22,k} + a_{23,1}a_{23,k}\right) \\ & + z\left(a_{31,1}a_{21,k} + a_{32,1}a_{22,k} + a_{33,1}a_{23,k}\right)\Big] \end{aligned} \tag{4.7.15}$$

and

$$\begin{aligned} d = -\Big[& x\left(a_{11,1}a_{11,k} + a_{12,1}a_{12,k} + a_{13,1}a_{13,k}\right) \\ & + y\left(a_{21,1}a_{11,k} + a_{22,1}a_{12,k} + a_{23,1}a_{13,k}\right) \\ & + z\left(a_{31,1}a_{11,k} + a_{32,1}a_{12,k} + a_{33,1}a_{13,k}\right)\Big] . \end{aligned} \tag{4.7.16}$$

Now let the three expressions in parentheses in equation (4.7.12) be called P_{31}, P_{32}, and P_{33}, or in general, define P_{ij} by

$$P_{ij} = \sum_{m=1}^{3} a_{im,k}\, a_{jm,1} \quad . \tag{4.7.17}$$

It follows that

$$\dot{P}_{ij} = \sum_{m=1}^{3} \left(a_{im,k}\, \dot{a}_{jm,1} + \dot{a}_{im,k}\, a_{jm,1}\right) . \tag{4.7.18}$$

The time derivative of (4.7.12) is therefore

$$\dot{R}' = \frac{1}{\sin R'}\Big\{ -\frac{\dot{\ell}}{\ell^2}(-\ell\cos R') + \frac{1}{\ell}\Big[\dot{x}P_{31} + \dot{y}P_{32} + \dot{z}P_{33} + x\dot{P}_{31} + y\dot{P}_{32} + z\dot{P}_{33}\Big]\Big\} . \tag{4.7.19}$$

Again, joint stop angle ellipse results obtained previously, in Section 4.6.2, apply for the neck-head joint, and non-linear spring and damping results given by equations (4.6.18) to (4.6.22), (4.6.30) to (4.6.33), and (4.6.37) are applicable in form. The required (non-zero) derivatives of R' and Θ' are as follows.

$$\begin{aligned} \frac{\partial R'}{\partial x} &= \frac{1}{\sin R'}\left[\frac{x\cos R'}{\ell^2} + \frac{P_{31}}{\ell}\right] \\ \frac{\partial R'}{\partial y} &= \frac{1}{\sin R'}\left[\frac{y\cos R'}{\ell^2} + \frac{P_{32}}{\ell}\right] \\ \frac{\partial R'}{\partial z} &= \frac{1}{\sin R'}\left[\frac{z\cos R'}{\ell^2} + \frac{P_{33}}{\ell}\right] \end{aligned} \tag{4.7.20}$$

Also,

$$q_k = (\psi_1, \theta_1, \varphi_1):$$

$$\frac{\partial R'}{\partial q_k} = \frac{1}{\ell\sin R'}\Big[x\Big(\frac{\partial a_{11,1}}{\partial q_k}a_{31,k} + \frac{\partial a_{12,1}}{\partial q_k}a_{32,k} + \frac{\partial a_{13,1}}{\partial q_k}a_{33,k}\Big) + y\Big(\frac{\partial a_{21,1}}{\partial q_k}a_{31,k} \tag{4.7.21}$$

(continued)

$$+ \frac{\partial a_{22,1}}{\partial q_k} a_{32,k} + \frac{\partial a_{23,1}}{\partial q_k} a_{33,k} \Big)$$

$$+ z \left(\frac{\partial a_{31,1}}{\partial q_k} a_{31,k} + \frac{\partial a_{32,1}}{\partial q_k} a_{32,k} \right. \qquad \begin{matrix} (4.7.21) \\ \text{(concluded)} \end{matrix}$$

$$\left. + \frac{\partial a_{33,1}}{\partial q_k} a_{33,k} \right) \Big]$$

and

$q_k = (\psi_k, \theta_k, \varphi_k)$:

$$\frac{\partial R'}{\partial q_k} = \frac{1}{l \sin R'} \left[x \left(a_{11,1} \frac{\partial a_{31,k}}{\partial q_k} + a_{12,1} \frac{\partial a_{32,k}}{\partial q_k} \right. \right.$$

$$\left. + a_{13,1} \frac{\partial a_{33,k}}{\partial q_k} \right) + y \left(a_{21,1} \frac{\partial a_{31,k}}{\partial q_k} \right.$$

$$\left. + a_{22,1} \frac{\partial a_{32,k}}{\partial q_k} + a_{23,1} \frac{\partial a_{33,k}}{\partial q_k} \right) \qquad (4.7.22)$$

$$+ z \left(a_{31,1} \frac{\partial a_{31,k}}{\partial q_k} + a_{32,1} \frac{\partial a_{32,k}}{\partial q_k} \right.$$

$$\left. \left. + a_{33,1} \frac{\partial a_{33,k}}{\partial q_k} \right) \right] .$$

In terms of P_{ij} from (4.7.17), it is seen that (4.7.15) and (4.7.16) may be written

$$n = -\left(x P_{21} + y P_{22} + z P_{23}\right)$$
$$d = -\left(x P_{11} + y P_{12} + z P_{13}\right) \quad . \qquad (4.7.23)$$

Then, equation (4.7.14) gives

$$\frac{\partial \Theta'}{\partial q_k} = \frac{1}{n^2+d^2}\left[d \frac{\partial n}{\partial q_k} - n \frac{\partial d}{\partial q_k}\right] , \qquad (4.7.24)$$

and therefore

$$\frac{\partial \Theta'}{\partial x} = \frac{-1}{n^2+d^2}\left(d P_{21} - n P_{11}\right)$$
$$\frac{\partial \Theta'}{\partial y} = \frac{-1}{n^2+d^2}\left(d P_{22} - n P_{12}\right) \qquad (4.7.25)$$
$$\frac{\partial \Theta'}{\partial z} = \frac{-1}{n^2+d^2}\left(d P_{23} - n P_{13}\right) \quad .$$

Also, differentiation of (4.7.15) and (4.7.16) completes the determination of $\partial \Theta'/\partial q_k$ for $q_k = (\psi_1, \theta_1, \varphi_1, \psi_h, \theta_h, \varphi_h)$. We obtain

$q_k = (\psi_1, \theta_1, \varphi_1)$:

$$\frac{\partial n}{\partial q_k} = -\left[x\left(\frac{\partial a_{11,1}}{\partial q_k} a_{21,h} + \frac{\partial a_{12,1}}{\partial q_k} a_{22,h}\right.\right.$$
$$\left. + \frac{\partial a_{13,1}}{\partial q_k} a_{23,h}\right) + y\left(\frac{\partial a_{21,1}}{\partial q_k} a_{21,h}\right. \qquad \begin{array}{c}(4.7.26)\\ \text{(continued)}\end{array}$$

$$+ \frac{\partial a_{22,1}}{\partial q_k} a_{22,k} + \frac{\partial a_{23,1}}{\partial q_k} a_{23,k}\Big)$$

$$+ z\Big(\frac{\partial a_{31,1}}{\partial q_k} a_{21,k} + \frac{\partial a_{32,1}}{\partial q_k} a_{22,k} \qquad \text{(4.7.26) (concluded)}$$

$$+ \frac{\partial a_{33,1}}{\partial q_k} a_{23,k}\Big)\Big]$$

and

$$q_k = (\psi_k, \theta_k, \phi_k):$$

$$\frac{\partial m}{\partial q_k} = -\Big[x\Big(a_{11,1} \frac{\partial a_{21,k}}{\partial q_k} + a_{12,1} \frac{\partial a_{22,k}}{\partial q_k}$$

$$+ a_{13,1} \frac{\partial a_{23,k}}{\partial q_k}\Big) + y\Big(a_{21,1} \frac{\partial a_{21,k}}{\partial q_k}$$

$$+ a_{22,1} \frac{\partial a_{22,k}}{\partial q_k} + a_{23,1} \frac{\partial a_{23,k}}{\partial q_k}\Big) \qquad (4.7.27)$$

$$+ z\Big(a_{31,1} \frac{\partial a_{21,k}}{\partial q_k} + a_{32,1} \frac{\partial a_{22,k}}{\partial q_k}$$

$$+ a_{33,1} \frac{\partial a_{23,k}}{\partial q_k}\Big)\Big] \quad .$$

The results for $\partial d/\partial q_k$ are the same as the right-hand sides of equations

(4.7.26) and (4.7.27) except that each $a_{2j,h}$ must be replaced by $a_{1j,h}$.

4.7.4 Head-Torso Joint Stop Terms for Twisting

Terms for the equations of motion resulting from twisting of the neck will not be obtained from moments at the neck-head and neck-torso joints, but instead from the composite twisting of the head with respect to the torso. This twisting angle will be of exactly the same form as torso twisting angles given by equation (4.6.45). The head element corresponds to torso element i + 1, and the first torso element (i = 1) corresponds to torso element i. Hence, the relative angle defining twisting of the head with respect to the torso is

$$\psi^h = \tan^{-1} \frac{a_{11,h} a_{21,1} + a_{12,h} a_{22,1} + a_{13,h} a_{23,1}}{a_{11,1} a_{11,h} + a_{12,1} a_{12,h} + a_{13,1} a_{13,h}} , \qquad (4.7.28)$$

or in terms of the notation of Section 4.7.3,

$$\psi^h = \tan^{-1} \frac{P_{12}}{P_{11}} \quad . \qquad (4.7.29)$$

The corresponding velocity is then

$$\dot{\psi}_h = \frac{1}{P_{11}^2 + P_{12}^2} \left(P_{11} \dot{P}_{12} - P_{12} \dot{P}_{11} \right) \quad . \qquad (4.7.30)$$

The results for torso joint stop twisting moments and associated terms for the equations of motion have been determined in Section 4.6.3. With the obvious changes in notation those results - equations (4.6.48) to (4.6.51) - apply also for twisting of the neck. The only non-zero partial derivatives of ψ^h are given below.

$q_k = (\psi_1, \theta_1, \varphi_1)$:

$$\begin{aligned}\frac{\partial \psi^h}{\partial q_k} = \frac{1}{P_{11}^2 + P_{12}^2}\Bigg[& P_{11}\Bigg(\frac{\partial a_{21,1}}{\partial q_k} a_{11,h} \\ & + \frac{\partial a_{22,1}}{\partial q_k} a_{12,h} + \frac{\partial a_{23,1}}{\partial q_k} a_{13,h}\Bigg) \\ & - P_{12}\Bigg(\frac{\partial a_{11,1}}{\partial q_k} a_{11,h} + \frac{\partial a_{12,1}}{\partial q_k} a_{12,h} \\ & + \frac{\partial a_{13,1}}{\partial q_k} a_{13,h}\Bigg)\Bigg]\end{aligned} \tag{4.7.31}$$

$q_k = (\psi_h, \theta_h, \varphi_h)$:

$$\begin{aligned}\frac{\partial \psi^h}{\partial q_k} = \frac{1}{P_{11}^2 + P_{12}^2}\Bigg[& P_{11}\Bigg(a_{21,1} \frac{\partial a_{11,h}}{\partial q_k} \\ & + a_{22,1} \frac{\partial a_{12,h}}{\partial q_k} + a_{23,1} \frac{\partial a_{13,h}}{\partial q_k}\Bigg) \\ & - P_{12}\Bigg(a_{11,1} \frac{\partial a_{11,h}}{\partial q_k} + a_{12,1} \frac{\partial a_{12,h}}{\partial q_k} \\ & + a_{13,1} \frac{\partial a_{13,h}}{\partial q_k}\Bigg)\Bigg]\end{aligned} \tag{4.7.32}$$

4.7.5 Neck-Torso Elastic Terms for Bending

Assume a neck-torso elastic spring moment of the same form as the torso moment of Section 4.6.4.

$$M = -\sum_{j=1}^{3} k_j S^j \tag{4.7.33}$$

S is defined quite analogously to S_i:

$$S = \cos^{-1}(\hat{\ell}^o \cdot \hat{\ell}') \quad . \tag{4.7.34}$$

The initial components of $\hat{l}$ in e_1 define $\hat{l}^o$, which corresponds directly to k_i^o. $\hat{l}'$ is defined similarly to k_i' in the torso analysis, i.e., it is obtained by rotating $(i, j, k)_1$ to $(i^o, j^o, k^o)_1$. The results for S_i obtained for torso joints apply here if the following identifications are made:

$$(i, j, k)_{i+1} \longrightarrow (i, j, k)_1$$

$$(i^o, j^o, k^o)_{i+1} \longrightarrow (i^o, j^o, k^o)_1$$

$$k_i \longrightarrow \hat{\ell}$$

$$k_i' \longrightarrow \hat{\ell}'$$

$$k_i^o \longrightarrow \hat{\ell}^o$$

Thus, from (4.6.61), we obtain

$$\hat{\ell}^{\circ}\cdot\hat{\ell}' = (\hat{\ell}\cdot i_1)(i_1^{\circ}\cdot\hat{\ell}^{\circ}) + (\hat{\ell}\cdot j_1)(j_1^{\circ}\cdot\hat{\ell}^{\circ}) + (\hat{\ell}\cdot k_1)(k_1^{\circ}\cdot\hat{\ell}^{\circ}) \quad . \tag{4.7.35}$$

Eliminating the unit vectors $\hat{l}$ and $\hat{l}^{o}$ by $\hat{l} = \vec{l}/l$ with equation (4.5.5) and carrying out the dot products, we get

$$\hat{\ell}^{\circ}\cdot\hat{\ell}' = \frac{1}{\ell\ell^{\circ}}(xx^{\circ} + yy^{\circ} + zz^{\circ}) \quad . \tag{4.7.36}$$

S is therefore completely determined by (4.7.34) with (4.7.36).

Let the argument of S be called Arg, i.e.,

$$Arg = \frac{1}{\ell\ell^{\circ}}(xx^{\circ} + yy^{\circ} + zz^{\circ}) \quad . \tag{4.7.37}$$

The partial derivatives of S are

$$\frac{\partial S}{\partial q_k} = -\frac{1}{\sin S}\frac{\partial Arg}{\partial q_k} \quad , \tag{4.7.38}$$

where the only non-zero partial derivatives of Arg are

$$\begin{aligned}
\frac{\partial Arg}{\partial x} &= \frac{1}{\ell\ell^{\circ}}\left[x^{\circ} - \frac{(xx^{\circ} + yy^{\circ} + zz^{\circ})\,x}{\ell^{2}}\right] \\
\frac{\partial Arg}{\partial y} &= \frac{1}{\ell\ell^{\circ}}\left[y^{\circ} - \frac{(xx^{\circ} + yy^{\circ} + zz^{\circ})\,y}{\ell^{2}}\right] \\
\frac{\partial Arg}{\partial z} &= \frac{1}{\ell\ell^{\circ}}\left[z^{\circ} - \frac{(xx^{\circ} + yy^{\circ} + zz^{\circ})\,z}{\ell^{2}}\right] .
\end{aligned} \tag{4.7.39}$$

Equation (4.7.6), which gives l as a function of x, y, and z, has been used with (4.7.37) to obtain equations (4.7.39).

The terms $\partial V/\partial q_k$ have thus been determined:

$$\frac{\partial V}{\partial q_k} = -M \frac{\partial S}{\partial q_k} \quad . \tag{4.7.40}$$

Equations (4.6.67) to (4.6.69), with $\dot{S}_i$ replaced by $\dot{S}$, represent the associated damping contributions to the total neck-torso joint moment and to the equations of motion. Only $\dot{S}$ must yet be determined. From (4.7.34) and (4.7.36), $\dot{S}$ may be obtained as follows:

$$\dot{S} = -\frac{1}{\sin S}\left[\frac{\dot{x}x^\circ + \dot{y}y^\circ + \dot{z}z^\circ}{\ell \ell^\circ} - \frac{\dot{\ell}\, Arg}{\ell}\right] . \tag{4.7.41}$$

4.7.6 Neck-Head Elastic Terms for Bending

Let the angle of deformation for the neck-head joint be called S'. It corresponds directly to S of Section 4.7.5 if the following identifications are made:

$$(i,j,k)_1 \longrightarrow (i,j,k)_h$$

$$(i^\circ,j^\circ,k^\circ)_1 \longrightarrow (i^\circ,j^\circ,k^\circ)_h$$

$$\hat{\ell} \longrightarrow \hat{\ell}$$

$$\hat{\ell}' \longrightarrow \hat{\ell}''$$

$$\hat{\ell}^\circ \longrightarrow \hat{\ell}^\circ$$

S' is then

$$S' = \cos^{-1}(\hat{\ell}^{\circ} \cdot \hat{\ell}'') \tag{4.7.42}$$

and

$$\begin{aligned}\hat{\ell}^{\circ} \cdot \hat{\ell}'' = {} & (\hat{\ell} \cdot i_{k})(i_{k}^{\circ} \cdot \hat{\ell}^{\circ}) + (\hat{\ell} \cdot j_{k})(j_{k}^{\circ} \cdot \hat{\ell}^{\circ}) \\ & + (\hat{\ell} \cdot k_{k})(k_{k}^{\circ} \cdot \hat{\ell}^{\circ}) \, .\end{aligned} \tag{4.7.43}$$

Elimination of $\hat{l}$ and the unit base vectors in the time dependent factors of (4.7.43) yields

$$\begin{aligned}\hat{\ell} \cdot i_{k} &= \frac{1}{\ell}(x P_{11} + y P_{12} + z P_{13}) \\ \hat{\ell} \cdot j_{k} &= \frac{1}{\ell}(x P_{21} + y P_{22} + z P_{23}) \\ \hat{\ell} \cdot k_{k} &= \frac{1}{\ell}(x P_{31} + y P_{32} + z P_{33}) \, .\end{aligned} \tag{4.7.44}$$

The remaining factors in (4.7.43) are clearly constants equal to the values of the right-hand sides of (4.7.44) at t = 0. Let c_1, c_2, and c_3 (time dependent) be defined as the right-hand sides of (4.7.44), and let c_1^0, c_2^0, and c_3^0 be their values at t = 0. Then,

$$c_i = \frac{1}{\ell}(x P_{i1} + y P_{i2} + z P_{i3}) \tag{4.7.45}$$

and

$$\hat{\ell}^{\circ} \cdot \hat{\ell}'' = c_1 c_1^{\circ} + c_2 c_2^{\circ} + c_3 c_3^{\circ} \, . \tag{4.7.46}$$

Where Arg, now, is defined by the right-hand side of (4.7.46), S' is

$$S' = \cos^{-1}(\text{Arg}) \quad , \tag{4.7.47}$$

and its partial derivatives are

$$\frac{\partial S'}{\partial q_k} = -\frac{1}{\sin S'}\frac{\partial \text{Arg}}{\partial q_k} \quad , \tag{4.7.48}$$

or

$$\frac{\partial S'}{\partial q_k} = -\frac{1}{\sin S'}\left[c_1^0\frac{\partial c_1}{\partial q_k} + c_2^0\frac{\partial c_2}{\partial q_k} + c_3^0\frac{\partial c_3}{\partial q_k}\right] \quad . \tag{4.7.49}$$

The partial derivatives appearing in (4.7.49), for $q_k = (x, y, z)$, are found to be

$$\begin{aligned} \frac{\partial c_i}{\partial x} &= -\frac{x c_i}{\ell^2} + \frac{1}{\ell} P_{i1} \\ \frac{\partial c_i}{\partial y} &= -\frac{y c_i}{\ell^2} + \frac{1}{\ell} P_{i2} \\ \frac{\partial c_i}{\partial z} &= -\frac{z c_i}{\ell^2} + \frac{1}{\ell} P_{i3} \quad . \end{aligned} \tag{4.7.50}$$

The other non-zero derivatives are for $q_k = (\psi_1, \theta_1, \phi_1, \psi_h, \theta_h, \phi_h)$. For these six generalized coordinates equation (4.7.45) gives

$$\frac{\partial c_i}{\partial q_k} = \frac{1}{\ell}\left(x\frac{\partial P_{i1}}{\partial q_k} + y\frac{\partial P_{i2}}{\partial q_k} + z\frac{\partial P_{i3}}{\partial q_k}\right). \qquad (4.7.51)$$

The partial derivatives appearing in (4.7.51) may be found from equation (4.7.17), which defines P_{ij}.

$q_k = (\psi_1, \theta_1, \varphi_1)$:

$$\frac{\partial P_{ij}}{\partial q_k} = \sum_{m=1}^{3} a_{im,k}\frac{\partial a_{jm,1}}{\partial q_k} \qquad (4.7.52)$$

$q_k = (\psi_k, \theta_k, \varphi_k)$:

$$\frac{\partial P_{ij}}{\partial q_k} = \sum_{m=1}^{3} \frac{\partial a_{im,k}}{\partial q_k} a_{jm,1} \qquad (4.7.53)$$

$\partial S'/\partial q_k$ is thus entirely determined, and

$$\frac{\partial V}{\partial q_k} = -M\frac{\partial S'}{\partial q_k} \quad . \qquad (4.7.54)$$

Again, damping terms are represented in form by equations (4.6.67) to (4.6.69), but $\dot{S}'$ must still be determined. From (4.7.42) and (4.7.46), $\dot{S}'$ is found as

$$\dot{S}' = -\frac{1}{\sin S'}\left[\dot{c}_1 c_1^\circ + \dot{c}_2 c_2^\circ + \dot{c}_3 c_3^\circ\right]. \qquad (4.7.55)$$

Here, from (4.7.45),

$$\dot{c}_i = \frac{1}{\ell}\left(x\,\dot{P}_{i1} + y\,\dot{P}_{i2} + z\,\dot{P}_{i3} + \dot{x}\,P_{i1} + \dot{y}\,P_{i2} + \dot{z}\,P_{i3} - c_i\,\dot{\ell}\right). \tag{4.7.56}$$

The factors $\dot{P}_{ij}$ are already known from equation (4.7.18).

4.7.7 Head-Torso Elastic Terms for Twisting

The composite "head-torso joint" (H-T) for twisting will have attributed to it elastic twisting moments of the same form as (4.6.71) and (4.6.73). ψ^h corresponds to ψ'_{i+1} and $\psi^{h,o} = \psi^h(0)$ corresponds to ψ^o_{i+1}. The contributions to the equations of motion are represented by equations (4.6.72) and (4.6.74). ψ^h and all required derivatives have already been determined in Section 4.7.4.

4.7.8 Neck Stretching Terms

Resistance to lengthening or shortening of the neck will be in the form of a non-linear Kelvin element. The spring tends to restore the neck length l to an equilibrium value, l_{eq}. Linear, quadratic, and cubic terms are assumed for both the spring and dissipative forces. These forces are additive, of course, and they are expressed as the two components of the total force given by equation (4.7.57).

$$F = -\sum_{j=1}^{3} k_j\,|\ell - \ell_{eq}|^j \,\mathrm{sgn}(\ell - \ell_{eq}) - \sum_{j=1}^{3} c_j\,|\dot{\ell}|^j \,\mathrm{sgn}\,\dot{\ell} \tag{4.7.57}$$

The terms required for the equations of motion are then

$$\frac{\partial V}{\partial q_k} + \frac{\partial D}{\partial \dot{q}_k} = -F\frac{\partial \ell}{\partial q_k} \qquad (4.7.58)$$

since, by (4.6.36), $\partial \dot{l}/\partial \dot{q}_k = \partial l/\partial q_k$. Here, from (4.7.6),

$$\frac{\partial \ell}{\partial q_k} = \frac{q_k}{\ell} \qquad (4.7.59)$$

for $q_k = (x, y, z)$, and all other partial derivatives of l are zero.

4.8 MUSCLE TENSION

The inclusion of muscle tension as a bio-dynamic property of a model for the living human body was discussed in Section 3.3.3. The effect of the crash victim's tensing his muscles, voluntarily or involuntarily, is to be introduced through Maxwell elements at each joint. The coefficients k and c of the series spring and damping components are to be functions of the parameter M, which indicates the degree of tensing of the muscles; these coefficients are expressed in equations (3.3.3) and (3.3.4). It will be assumed in this investigation that the crash victim has anticipated the impact and is "pre-tensed;" M will be constant for $t \geq 0$. With only small change in the computer program logic it would be possible to allow a reaction time t_r, before which M would be zero and after which M would take on a constant value.*

---

*The neuromuscular time constant is between 100 and 200 msec. (22, 27)

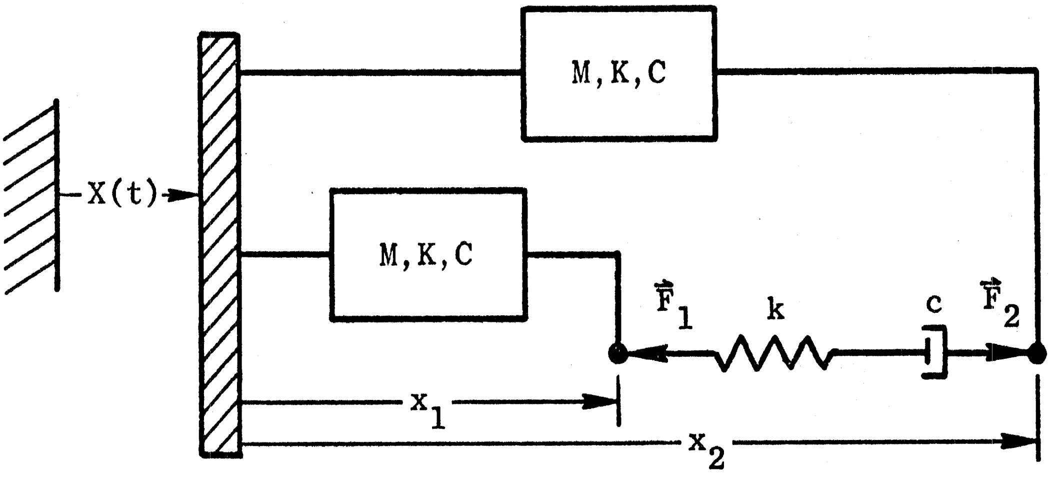
M,K,C
X(t)
M,K,C
$\vec{F}_1$
k
c
$\vec{F}_2$
x_1
x_2

Figure 15. A linear Maxwell element forced by x(t), $x = x_2 - x_1$.

Determination of the generalized forces attributable to non-zero muscle tension involves, first, the solution of a forced motion problem for a Maxwell element. Although all but one Maxwell element to be included in the vehicle occupant model will be "angular" rather than "linear," the problem formulated below is in terms of a linear element. The only reason for this is to make as clear as possible the figure used for illustration of the problem, Figure 15. The general form of the solution for this problem obviously applies also to the torsional Maxwell elements.

In Figure 15, x_1 and x_2 are the coordinates of two points with respect to some moving base. Each point is considered to be connected to the base by some "black box" element involving masses, springs, and dampers. The Maxwell element is "forced" in the sense that the coordinates of its endpoints are functions of time resulting in part from the motion of an external system, represented here by the base motion, X(t), and the "black boxes." Through coupling, the external motion is in turn determined in part by the Maxwell element. The problem is to determine the tensile force in the Maxwell element as a function of $x_1(t)$ and $x_2(t)$.

F_1 and F_2 are the generalized forces which result from the Maxwell element. Where $\hat{e}$ is a unit vector to the right in Figure 15, we have

$$\vec{F}_2 = -\vec{F}_1 = F\hat{e} . \tag{4.8.1}$$

Equation (4.8.1) defines the force F. Let δ_1 be the deformation of the spring element and let $\dot{\delta}_2$ be the deformation rate of the damper. Then,

$$F = -k\delta_1 = -c\dot{\delta}_2 . \tag{4.8.2}$$

Now, with x defined as

$$x = x_2 - x_1 \ , \tag{4.8.3}$$

we may write

$$\dot{x} = \dot{\delta}_1 + \dot{\delta}_2 \ . \tag{4.8.4}$$

By equations (4.8.2), this becomes

$$\dot{x} = -\frac{\dot{F}}{k} - \frac{F}{c} \ , \tag{4.8.5}$$

or

$$\dot{F} + \frac{k}{c} F = -k\dot{x} \ . \tag{4.8.6}$$

Two basically different approaches might be taken for obtaining the solution F(t) of equation (4.8.6). First, the problem could be reduced to quadrature. This approach is presented in Appendix B, but, while it could have been utilized with some difficulty, a more workable method is available. The difficulty with the method of solution by quadrature, in the context of this investigation, is that it clashes with the "back-stepping" capability of the rather sophisticated integration algorithm (Chapter 5) that was used to solve the equations of motion. (Equation (4.8.6) is, of course, coupled to the equations of motion through $\dot{x}$.) This first method could be used without difficulty in conjunction with a simpler integration procedure. The method used, and one perhaps more efficient even if the above described difficulty does not exist, is to treat (4.8.6) as an additional "equation of motion." There is no difficulty involved in integrating it as a part of a general system of coupled differential equations. The differential equations governing a simple dynamic system are determined in Appendix C as an illustration of this procedure.

The initial value F(0) is an input quantity for the computer program, as are all initial values. In practice, however, since the body elements are generally assumed not to be in relative motion at t = 0, the deformation rate $\dot{\delta}_2(0)$ is zero; equation (4.8.2) therefore indicates that F(0) should be selected as zero.

The muscle tension force (or moment) F associated with coordinate x having been found, it is now a simple matter to obtain its contribution to the equations of motion. The corresponding generalized forces for q_k for equations (4.1.1) are simply

$$Q_k = F \frac{\partial x}{\partial q_k} \quad . \tag{4.8.7}$$

4.8.1 Muscle Tension Moments

Let R represent any of the generalized pitching angles and let ψ be any of the twist angles, with associated muscle tension moments of M_R and M_ψ. Then,

$$Q_k^{(R)} = M_R \frac{\partial R}{\partial q_k} \tag{4.8.8}$$

and

$$Q_k^{(\psi)} = M_\psi \frac{\partial \psi}{\partial q_k} \quad . \qquad (4.8.9)$$

4.8.2 Muscle Tension Forces

The only linear muscle tension element in this vehicle occupant model is the neck length. Its effect enters the equations of motion in basically the same way as do moment effects at joints, but a modification is imposed. Because of opposing sets of muscles, muscle tension resistance at joints may be in the form of negative or positive moments. A muscle tension force F_ℓ, however, may be negative only, i.e., it can resist lengthening of l but cannot assist it. Accordingly, computer program logic is provided to keep muscle tension for the neck length either negative or zero. The muscle tension force is governed by

$$\dot{F} + \frac{k}{c} F = -k\dot{\ell} \qquad (4.8.10)$$

and the generalized forces are

$$Q_k = F \frac{\partial \ell}{\partial q_k} \quad , \qquad (4.8.11)$$

but if F becomes greater than zero, it is set to zero until such time as $\dot{l}$ changes from a negative value to a positive value.

CHAPTER 5

THE NUMERICAL SOLUTION

The Lagrange equations of motion as given by (4.1.1) can now be considered to have been determined in the form

$$\left[\sum_{i=1}^{N} G_{ki}\ddot{q}_i + H_k\right] - \frac{\partial T}{\partial q_k} + \frac{\partial V}{\partial q_k} + \frac{\partial D}{\partial \dot{q}_k} = Q_k , \qquad (5.1)$$

$$k = 1, 2, \cdots, N.$$

The quantity G_{ki} is the coefficient of $\ddot{q}_i$ which occurs in the first term,

$$\frac{d}{dt}\frac{\partial T}{\partial \dot{q}_k} ,$$

of the q_k-equation. The quantity H_k is that part of the first term which does not contain any $\ddot{q}_i$. After transposing terms in equations (5.1), we have a system of N non-linear differential equations of the following form:

$$[G]\{\ddot{q}\} = \{f\} . \qquad (5.2)$$

$\{\ddot{q}\}$ and $\{f\}$ are vectors of length N and [G] is a symmetric matrix of size NxN.

Once the system (5.2) has been set up, two major steps are involved in obtaining the solution for the motion.

Each time that the integration algorithm requires values for the generalized accelerations, $\ddot{q}_i$, it is necessary to "invert" the system of equations (5.2). A subroutine, DGELG, in the IBM 360 Scientific Subroutine Package (SSP) is used for this purpose. DGELG solves a system of general simultaneous linear algebraic equations by means of Gauss elimination with complete pivoting. This method results in an upper-diagonalized system of equations, which yields $\ddot{q}_N$ immediately. The remaining $\ddot{q}_i$ are then found by successive back substitutions.

Integration of the generalized velocities, $\dot{q}_i$, and the generalized accelerations, $\ddot{q}_i$, is accomplished by means of a slightly altered version of the SSP subroutine DHPCG. This subroutine uses Hamming's predictor-corrector method with modifier for the solution of a general system of first-order ordinary differential equations with given initial values. (The accelerations may be thought of as first derivatives of the $\dot{q}$'s instead of second derivatives of the q's.) This is a stable fourth-order integration procedure that has two significant advantages over many other methods of the same order of accuracy. First, only two evaluations of the derivatives are necessary, in general, for each integration time step, as compared with four required by Runge-Kutta methods. Second, it is possible with this procedure to "automatically" make the integration step size larger or smaller depending on whether the motion is locally smooth or violent. This is done on the basis of an estimate for the local truncation error, which will already have been calculated for purpose of defining the modifier. As many as ten halvings of the initially prescribed maximum allowable time step size are possible. If truncation error is still greater than an upper bound prescribed by the user, then the integration is terminated. The predictor-corrector method itself is not self-starting, i.e., functional values at more than a single previous point are required in order to get values ahead. A fourth-order Runge-Kutta starter is therefore used.

The side impact crash simulation of Section 10.2 was repeated several times for the purpose of determining a maximum size for the upper bound on local truncation error which would result in convergence of the integration to within 0.1 degrees for all Euler angle values (at the end of the crash). The side impact simulation was selected as the standard because it is the most general of the model verification exercises of Chapter 10 and because it is only slightly less violent (in terms of acceleration values) than the most violent crash simulation studied (frontal impact, Section 10.1).

The entire computer program written for this investigation is approximately 4100 Fortran lines in length.

CHAPTER 6

PRELIMINARY TEST RUNS OF THE COMPUTER MODEL

A series of preliminary exercises for the computer model was carried out for several purposes: 1) to verify the analysis presented in Chapter 4; 2) to verify the implementation of that analysis in the computer program; and 3) wherever verification failed, to provide clues for debugging. These tests were concerned with the mathematical model only as a dynamic system and not as a model for the human body. Several of the tests involved only the torso portion of the model since the torso model was fully developed before analysis for the head-neck portion was even begun. Most of these exercises were for free motion problems; verification for forced motion is discussed in Chapter 7.

The analytical detail of several of the free motion tests is given in Appendix D. For those tests the procedure was always to obtain the solution for a problem that could be solved completely (or almost completely) by hand and then to compare the exact solution with results obtained by exercising the computer model. Exact analytical solutions could be found only for a limited range of problems. In general these are symmetric and two-dimensional. The problems solved involve, independently, most of the joint properties. Excellent agreement between exact and computer solutions was achieved.

While this agreement is encouraging, the tests referred to have one weakness. It is probably not of consequence that an explicit solution could not be obtained for a problem involving several superimposed joint properties. Since the associated joint moments are additive, it can be expected that independent verification of each will imply a valid composite. A more serious weakness of the series of tests is that they are all one- and two-dimensional problems. While the collective tests bring into play most of the generalized coordinates, only limited mixing occurs, i.e., "cross terms" are not fully tested. A completely general three-dimensional problem would, of course, test all terms in the equations of motion, but, needless to say, the motion cannot be found as an explicit function of time so there is nothing against which to compare the computer model results. There is a solution to this dilemma. Since we are dealing with a free motion problem, all components of the linear and angular momentum vectors should be conserved, and also total energy should be conserved if dissipated energy is accounted for. These quantities are determined at the end of the integration interval and compared against their values at t = 0.

Calculation of the i-, j-, and k-components of linear momentum for the system is straightforward. Determination of kinetic energy and potential energy is also clear. The total energy dissipated over the integration interval was obtained by storing values of the energy dissipation rate as a function of time and then integrating over the entire interval. Determination of the components of angular momentum is not as obvious. Detail of the angular momentum analysis is presented below.

The angular momentum vector with respect to the origin of the inertial frame is

$$\vec{L}_o = \sum_{i=1}^{N''} \left\{ M^{(i)} \left(\vec{R}^{(i)} \times \dot{\vec{R}}^{(i)} \right) + \overline{I}^{(i)} \cdot \vec{\omega}^{(i)} \right\} \quad . \tag{6.1}$$

Here, N" is the number of body elements, $M^{(i)}$ is the mass of body element i, $\vec{R}^{(i)}$ is the position vector of the center of mass of element i,

$\overline{I}^{(i)}$ is the inertia tensor for element i (components defined in the rotating coordinate frame e_i), and $\vec{\omega}^{(i)}$ is the angular velocity vector for element i. Let the $\dot{\vec{R}}$ and $\vec{\omega}$ terms of (6.1) be called $\vec{L}^{(v)}$ and $\vec{L}^{(\omega)}$ so that (6.1) becomes

$$\vec{L}_0 = \vec{L}^{(v)} + \vec{L}^{(\omega)} . \tag{6.2}$$

Now,

$$\vec{R}^{(i)} = x_i i + y_i j + z_i k \tag{6.3}$$

and

$$\dot{\vec{R}}^{(i)} = \dot{x}_i i + \dot{y}_i j + \dot{z}_i k . \tag{6.4}$$

After carrying out the cross products for $\vec{L}^{(v)}$ and separating the result into i, j, and k components, we have

$$\begin{aligned} L_x^{(v)} &= \sum_{i=1}^{N''} M^{(i)} (\dot{z}_i y_i - \dot{y}_i z_i) \\ L_y^{(v)} &= \sum_{i=1}^{N''} M^{(i)} (\dot{x}_i z_i - \dot{z}_i x_i) \\ L_z^{(v)} &= \sum_{i=1}^{N''} M^{(i)} (\dot{y}_i x_i - \dot{x}_i y_i) . \end{aligned} \tag{6.5}$$

Since the inertial components of $\vec{L}_0$ are sought, it is necessary to transform the components of the inertia tensor to inertial reference. The transformation from system e_i to e is

$$I_{j\ell,i} = \sum_{p=1}^{3} \sum_{k=1}^{3} a_{pj,i} \, a_{k\ell,i} \, I_{pk}^{(i)} \quad . \tag{6.6}$$

Since $\overline{I}^{(i)}$ is diagonalized in the rotating frame, i.e.,

$$I_{pk}^{(i)} = I_{pp}^{(i)} \, \delta_{pk} \quad , \tag{6.7}$$

equation (6.6) becomes

$$I_{j\ell,i} = \sum_{k=1}^{3} a_{kj,i} \, a_{k\ell,i} \, I_{kk}^{(i)} \quad . \tag{6.8}$$

$\vec{\omega}^{(i)}$ must also be transformed. In e_i it is

$$\vec{\omega}^{(i)} = \alpha_i \, i_i + \beta_i \, j_i + \gamma_i \, k_i \quad . \tag{6.9}$$

Elimination of (i_i, j_i, k_i) by (4.2.1) gives

$$\vec{\omega}^{(i)} = \omega_x^{(i)} \, i + \omega_y^{(i)} \, j + \omega_z^{(i)} \, k \quad , \tag{6.10}$$

where

$$\begin{aligned} \omega_x^{(i)} &= \left(\alpha_i \, a_{11,i} + \beta_i \, a_{21,i} + \gamma_i \, a_{31,i}\right) \\ \omega_y^{(i)} &= \left(\alpha_i \, a_{12,i} + \beta_i \, a_{22,i} + \gamma_i \, a_{32,i}\right) \\ \omega_z^{(i)} &= \left(\alpha_i \, a_{13,i} + \beta_i \, a_{23,i} + \gamma_i \, a_{33,i}\right) \quad . \end{aligned} \tag{6.11}$$

Hence,

$$\overline{I}^{(i)} \cdot \vec{\omega}^{(i)} = \left(I_{11,i}\,\omega_x^{(i)} + I_{12,i}\,\omega_y^{(i)} + I_{13,i}\,\omega_z^{(i)}\right) i + \left(I_{21,i}\,\omega_x^{(i)} + I_{22,i}\,\omega_y^{(i)} + I_{23,i}\,\omega_z^{(i)}\right) j + \left(I_{31,i}\,\omega_x^{(i)} + I_{32,i}\,\omega_y^{(i)} + I_{33,i}\,\omega_z^{(i)}\right) k, \quad (6.12)$$

where the inertia tensor and angular velocity components are as given by (6.8) and (6.11). $\vec{L}^{(\omega)}$ is then obtained by summing (6.12) over i, and we have

$$\begin{aligned} L_x^{(\omega)} &= \sum_{i=1}^{N''} \left(I_{11,i}\,\omega_x^{(i)} + I_{12,i}\,\omega_y^{(i)} + I_{13,i}\,\omega_z^{(i)}\right) \\ L_y^{(\omega)} &= \sum_{i=1}^{N''} \left(I_{21,i}\,\omega_x^{(i)} + I_{22,i}\,\omega_y^{(i)} + I_{23,i}\,\omega_z^{(i)}\right) \qquad (6.13) \\ L_z^{(\omega)} &= \sum_{i=1}^{N''} \left(I_{31,i}\,\omega_x^{(i)} + I_{32,i}\,\omega_y^{(i)} + I_{33,i}\,\omega_z^{(i)}\right) . \end{aligned}$$

Then, conservation of angular momentum requires that

$$\begin{aligned} L_x &= L_x^{(N)} + L_x^{(\omega)} = \mathrm{Const}_1 \\ L_y &= L_y^{(N)} + L_y^{(\omega)} = \mathrm{Const}_2 \qquad (6.14) \\ L_z &= L_z^{(N)} + L_z^{(\omega)} = \mathrm{Const}_3 \quad . \end{aligned}$$

Now, suppose that linear and angular momenta and total energy are shown to be "nearly" conserved, over the integration interval, for a computer model solution. Then it may reasonably be assumed that both the analysis and the numerical solution for the free motion problem are good. In order to quantify how nearly the momenta and energy are conserved, non-dimensional quantities are defined as described below and are determined and printed out by the output subroutine along with the values of the various conserved quantities.

Let E_0 be the total energy at $t = 0$. Let E be the sum of the kinetic and potential energies at the end of the integration interval. Let DISS be the total energy dissipated over the integration interval. Then, define

$$\epsilon_E = \frac{|E + \mathrm{DISS} - E_0|}{E_0} \quad . \tag{6.15}$$

The numerator represents the amount of energy "created" or "lost" during the integration. If this amount is very small compared with E_0, i.e., if $\epsilon_E \ll 1$, then total energy will be said to be conserved.

Let (P_x, P_y, P_z) and (L_x, L_y, L_z) be the components of the linear and angular momenta for the system. A non-dimensional ϵ is calculated for each of these six components, and all are defined analogously to ϵ_{P_x}, as below:

$$\epsilon_{P_x} = \frac{|P_x - P_x(0)|}{\sum_{i=1}^{N''} |P_{x_i}|} \quad . \tag{6.16}$$

Some comments should be made regarding this definition. First, whereas $E_0 = 0$ guarantees a trivial zero-motion problem, $P_X(0) = 0$ does not necessarily indicate a trivial problem. As an example, the system might initially contain potential energy but no kinetic energy so that when "released" at t = 0 transfer of energy would begin to take place. Accordingly, $|P_X(0)|$ is not a suitable denominator for ϵ_{P_X}. One reasonable definition for the denominator would be the maximum value of $|P_X|$ occurring in the integration interval. But a definition probably as good as any is the one used in (6.16), i.e., the sum of the absolute values of the contributions to P_X from all of the masses. The linear and angular momentum components are conserved if their ϵ's are much less than 1.

Incorporation of the foregoing into the computer program makes possible the valuation of results for a completely general, three-dimensional, free motion problem. A test exercise selected for the torso, with no head, involved winding up the linkage at t = 0 in an arbitrary manner through all of the angular degrees of freedom. Muscle tension parameters were all zero, but all other joint properties were "on." The integration interval (in seconds) was [0, 0.1], and angular acceleration values were comparable to values in a crash situation. All of the ϵ's had values in the approximate range 0.0001 to 0.00001. It was discovered, as expected, that these values could be made smaller as desired by either reducing the maximum allowed integration time step or by prescribing a smaller maximum allowed local truncation error for the integration.

The necessary energy and angular momentum quantities are not determined in the computer program for the head-neck portion of the model, so a corresponding valuation could not be made for the complete occupant model. The linear momentum components are determined, however, and the resulting ϵ's for the three-dimensional test exercise were still in the range 0.0001 to 0.00001. It may be inferred, in consequence, that energy and angular momentum would also be found to be conserved if they were calculated since the equations of motion are highly coupled.

One last note is made here regarding the energy and momentum checks. Since both energy and the momenta are highly dependent on generalized velocities, the ϵ's are largely a reflection of how good the velocity values are. Values for the generalized coordinates themselves will, in general, be more accurate still than the velocity values; they are obtained by integrating the generalized velocities, and it is known that error is in general reduced by successive numerical integrations. Conversely, the generalized acceleration values from which the velocities are obtained are not as accurate.

CHAPTER 7

FORCED MOTION

It was made clear in Chapter 1 that this study is not concerned with modeling a vehicle interior for interaction with the crash victim model. It is nonetheless desirable to investigate forced motion response of the model. Short of determining generalized forces associated with vehicle interior/crash victim interaction, whatever form of excitation is provided will be somewhat arbitrary. A reasonably general displacement excitation has been allowed for because it is easily implemented in the computer model and because this feature may be used other than as a means of investigating forced response.

7.1 THE FORCING FEATURE

Consider the system of free motion equations (5.2), i.e., N equations of the form

$$\sum_{i=1}^{N} G_{ki}(q)\,\ddot{q}_i = f_k(q,\dot{q}) \; . \tag{7.1.1}$$

There is one equation for each generalized coordinate q_k. The coefficients G_{ki} are functions of the generalized coordinates while the f_k are functions of the generalized velocities as well.

Suppose that some q_j is not a degree of freedom but instead is forced as a function of time. Then the Lagrange equation for q_j has no significance, and all q_j, $\dot{q}_j$, and $\ddot{q}_j$ appearing in any of the remaining N-1 equations have known values and serve as an excitation to the remaining N-1 degrees of freedom. The procedure is clear. When q_j, $\dot{q}_j$, and $\ddot{q}_j$ are prescribed: 1) the Lagrange equation for q_j is disregarded; 2) all q_j and $\dot{q}_j$ appearing in all G_{ki} and f_k must be given their prescribed values for each value of t during the integration; and 3) all $G_{kj}\,\ddot{q}_j$ must be transposed so as to become parts of the f_k.

This procedure is illustrated by the following two-degree-of-freedom problem. Consider the system shown in Figure 16.

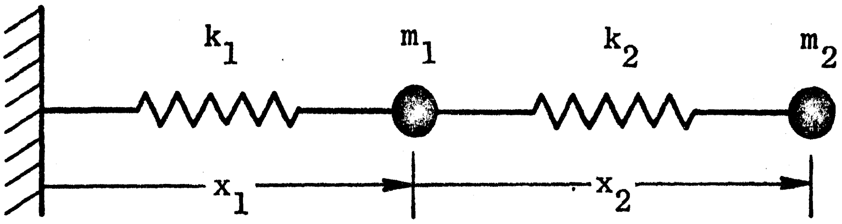

Figure 16. A free system to be forced by $x_1(t)$.

The Lagrange equations for the free system are

$$x_1: \qquad (m_1+m_2)\ddot{x}_1 + m_2\ddot{x}_2 = -k_1(x_1-\ell_1) \tag{7.1.2}$$

$$x_2: \qquad m_2\ddot{x}_1 + m_2\ddot{x}_2 = -k_2(x_2-\ell_2), \tag{7.1.3}$$

where l_1 and l_2 are equilibrium lengths for k_1 and k_2. Suppose that x_1 is prescribed as a function of t. Then (7.1.2) is disregarded and (7.1.3) becomes

$$m_2\ddot{x}_2 = -k_2(x_2-\ell_2) - m_2\ddot{x}_1(t) \quad . \tag{7.1.4}$$

This same equation results, of course, if the forced, one-degree-of-freedom problem is solved directly, i.e., if k_1 and m_1 are not included in the system.

7.2 USES OF THE FORCING FEATURE

7.2.1 Excitation

With from one to N-1 sets of values $(q_j, \dot{q}_j, \ddot{q}_j)$ prescribed as tabular or functional time histories there is considerable flexibility for studying forced response of the vehicle occupant model.* However, this is not the only importance of the forcing feature.

7.2.2 Elimination of Non-participating Degrees of Freedom

It can often be seen by symmetry that "special case" exercises of the three-dimensional vehicle occupant model will show activity in only some of the generalized coordinates. The case of greatest interest is when the model is exercised in a plane, i.e., as a two-dimensional vehicle occupant. Suppose, for example, that motion is in the i-k plane. Then, there are only n + 5 active generalized coordinates: x_1, z_1, x, z, and all pitching angles. The remaining 2n + 4 generalized coordinates (with their velocities and accelerations) may be set identically to zero in the excitation subroutine.

The value in being able to do this is a savings in computation time. Each coordinate eliminated in the manner described in Section 7.1 clearly reduces the order of the coefficient matrix [G] by one. As was noted in Chapter 2 the number of multiplication operations required for the inversion of an algebraic system of order N is nearly proportional to N^3.

---

*The computer program is dimensioned for a maximum of six sets of prescribed time histories, i.e., up to six degrees of freedom can be forced. Allowing for up to N-1 could be done very simply by dimensioning for a higher number. Also, it is noted here that tabular time histories are made continuous by linear interpolation.

In terms of the planar exercise this means, for example, that the cost for inversion can be reduced to

$$\frac{(n+5)^3}{(3n+9)^3}$$

of what it would be if none of the non-participating coordinates were eliminated. For n equal to 3, for example, this is about 0.088, i.e., there is a savings in inversion cost of about 91%. Inversion does not represent the major cost in operation of the full, three-dimensional model, but it is quite significant. (Determination of {f} and [G] is more costly.)

7.2.3 Constraining the Mathematical Model

It is possible to use a modified and expanded version of the forcing capability as a means of imposing constraints on the mathematical model. This application has not been made, nor has it been provided for in the excitation subroutine, but the required revisions are not extensive.

Probably the most important potential application would be the reduction of any ball-and-socket joint to a hinge joint. Such a joint might be more appropriate for the knee, for example, although it can be adequately modeled by using a degenerate stop angle "ellipse" (side stop angle equal to zero), a twisting stop angle of zero, and sufficiently large joint stop stiffnesses. The reduction to a hinge joint cannot be accomplished with the forcing feature as it was described in Section 7.1 because the knee angle for the hinged knee is a relative Euler angle

($-\Theta'_{i+1}$, for the i^{th} joint), which is not a generalized coordinate. Elimination of two of the equations of motion cannot, therefore, bring about the desired result; it is necessary to eliminate the three equations for the lower leg angles (ψ_{i+1}, θ_{i+1}, φ_{i+1}) and replace them by an equation for the knee angle.

An alternative approach to reducing a ball-and-socket joint to a hinge would be to add two constraint relations (and associated constraint force terms) to the system of equations, retaining all generalized coordinates. The cost disadvantage of this method was pointed out in Chapter 2.

7.3 VERIFICATION FOR SIMPLE FORCED MOTION PROBLEMS

One check made on the forcing feature of the computer model was simply to eliminate non-participating degrees of freedom for planar problems, as explained in Section 7.2.2. Numerical results were observed to be unchanged (while computation time was reduced).

Various of the free motion verifications discussed in Appendix D involve selecting very large masses and moments of inertia for some of the elements of the dynamic system. The purpose is to provide an anchor for the remaining part of the system so that approximate agreement with exact solutions for simpler systems can be demonstrated. The anchors for the free motion problems are, of course, not entirely unaffected by motion of the less massive elements in the system. Some of the exercises discussed in Appendix D were repeated in order to further test the forcing feature. It was possible to demonstrate exact agreement with true solutions by forcing what had been anchor elements to remain fixed in space; effectively, the anchors are thus attributed with infinite -

not merely "large" - masses and moments of inertia.

Finally, a sinusoidally forced spring-mass system was solved with the computer model, and the results were shown to agree with the analytical time-dependent solution. The spring portion of the neck length Kelvin element and the head mass constituted the one-degree-of-freedom system, and the first torso mass was excited by $z_1 = A(1 - \sin \omega t)$.

CHAPTER 8

PRELIMINARIES FOR CRASH SIMULATIONS

The analytical and computer development having been completed - and the model verified as a dynamic system - it was next of interest to exercise the model as a vehicle occupant in a crash situation. Several such exercises are described and discussed in Chapter 10. Common to all of those crash simulations is the set of parameter values which describe the crash victim. Selection of those values is discussed in this chapter, in Section 8.1. In Section 8.2 is discussed a necessary consideration for selection of certain of the initial conditions.

8.1 SELECTION OF VEHICLE OCCUPANT PARAMETER VALUES

8.1.1 Body Parameters

Some of the crash simulations of Chapter 10 are intended to be compared with results obtained from the three-dimensional model of Robbins, Bennett, and Roberts (18), hereafter referred to as the "HSRI 3-D" model. Vehicle occupant parameter values are therefore selected to be in accord with HSRI 3-D values to the extent allowed by the differences in the analytical models. The HSRI values given here are for a 50th-percentile man.

The only torso investigated in this study has been one of three masses although the computer program can be dimensioned for n. It has been commented earlier that the third torso element should probably be thought of as the pelvic mass. Comparison of the three-mass torso length with the HSRI model (one-mass torso, with legs) indicates a choice of l_3 = 6.5 in. The overall HSRI torso length is 23 in., so

$l_1 + l_2 = 16.5$ in. Then, the lengths l_1 and l_2 are proportioned equivalently to corresponding HSRI 2-D values (15): $l_1/l_2 = 12.59/5.75 = 2.19$. Hence, $l_1 = 11.33$ in. and $l_2 = 5.17$ in.*

It is desired to place the torso joints along the spine. The HSRI torso thickness indicates the choices $t_0 = t_1 = t_2 = t_3 = 4.6$ in. to be reasonable.

For the purpose of determining mass and moment of inertia values the approximation is made that the torso has uniform cross section dimensions along its length and that the mass density is constant. Then, where W is the total torso weight, 90.4 lb., we have $(W_1 + W_2)/(l_1 + l_2) = W/(l_1 + l_2 + l_3)$. Also, $W_1/W_2 = l_1/l_2 = 2.19$. It follows from this that $W_1 = 44.5$ lb., $W_2 = 20.3$ lb., and $W_3 = 25.6$ lb. The corresponding masses, in slugs, are 1.383, 0.630, and 0.795.

Torso moments of inertia are approximated as values for right elliptical cylinders of heights equal to l_1, l_2, and l_3 and semi-major and semi-minor axes a and b of 6.5 in. and 4.5 in. These values for a and b are assumed from HSRI dimensions. Where the minor axes are fore-aft for each of the torso elements, the moments of inertia are then

$$\begin{aligned} I_i &= \frac{m_i}{12}\left(3a^2 + l_i^2\right) \\ J_i &= \frac{m_i}{12}\left(3b^2 + l_i^2\right) \qquad (8.1.1) \\ K_i &= \frac{m_i}{4}\left(a^2 + b^2\right) \quad . \end{aligned}$$

---

*Length values given here in inches are converted to feet for input to the computer program.

These equations give values in [lb-in-sec^2] of I_{1-3} = (2.45, 0.673, 0.932), J_{1-3} = (1.81, 0.383, 0.568), and K_{1-3} = (1.80, 0.822, 1.035). If the three elliptical cylinders are considered to be joined rigidly into one cylinder, the values I = 15.34, J = 13.8, K = 4.39 result. These are reasonably close to the HSRI 3-D values of 12.78, 11.5, and 3.65, so it is assumed that the values found for I_i, J_i, and K_i are not unreasonable for use in investigations comparing the vehicle occupant models.

The HSRI head weight of 15.8 lb has been adopted; this is 0.490 slugs. Values of 6 in. and 2.125 in. are approximate values for the head quantities r and d (Figure 9). The equilibrium neck length l_{eq} is arbitrarily taken as 4 inches.

The head moments of inertia, I_h, J_h, K_h, are, respectively, 0.3672, 0.4420, and 0.2210 lb-in-sec^2. These are the same as HSRI values and were obtained by assuming the head element to be an ellipsoid with uniform mass distribution. The semi-axis lengths for the x-, y-, and z-principal axis directions are a = 4.25, b= 3.00, and c = 6.00 inches, and ellipsoid equations replace (8.1.1); for example, $I_h = m_h(b^2 + c^2)/5$.*

8.1.2 Joint Parameters

According to von Gierke (28) the undamped natural frequency for head motion caused by z-excitation of the upper torso is about f_0 = 30

---

*The values for head mass and head moments of inertia given here are possibly as much as fifty percent greater than proper values for a 50th-percentile male (4, 22). The HSRI values were selected to agree with values determined for an anthropomorphic dummy.

Hz. Consequently, the first-order spring rate* for the neck length can be approximated by

$$k = 4\pi^2 f_0^2 m_h = 17,400 \text{ lb/ft}. \qquad (8.1.2)$$

A spring rate value of the same order of magnitude can be estimated in a completely different manner. Consider the intervertebral discs in the cervical spine to represent seven identical springs, k', in series. The composite spring rate is then k = k'/7. The stiffness k' can be approximated from data available in the literature. Orne and Liu (29) give 6600 lb/in^2 as an estimated value for Young's modulus, E, for disc material. McKenzie and Williams (30) give radiographically determined values for cervical disc areas, the average area being $A = 0.483 \text{ in}^2$. McKenzie and Williams also give values for the vertebral body heights, the average of which is 0.578 inches. No disc thicknesses are given, but examination of x-rays (for example, see reference (21)) indicates them to be about one-third of the vertebral heights, i.e., h = 0.193 inches. Then, the axial stiffness for a single disc is k' = AE/h = 16,500 lb/in. Hence, the composite neck stiffness is k = 2360 lb/in, or 28,300 lb/ft. This is about 63% larger than the previously determined value. If experimental stiffness values for the thoracic discs obtained by Markolf and Steidel (31) - 11,000 to 21,000 lb/in - are assumed to approximate cervical disc stiffnesses, then we obtain k = 20,600 lb/ft, which is somewhat closer to the result of equation (8.1.2).

---

*There is enough uncertainty at this stage of the investigation regarding proper choice of values for even first-order spring and damping coefficients that second- and third-order terms will be assumed zero, i.e., moments (and forces) will be linear functions of deformations and deformation rates. Non-linearity can still be introduced on the basis of any subsequent experimental determination of non-linear moment curves or by empirical adjustment to experimental crash dynamics.

For a simple mass-spring-damper model for the human body with spinal column, von Gierke (28) gives a range of 0.221 to 0.266 for the damping ratio for the composite spinal column damper. A value of 0.224 has been assumed reasonable in this study for the cervical spine. Hence,

$$\gamma = 0.224 = \frac{c}{2\sqrt{k m_h}} , \tag{8.1.3}$$

where the denominator is the critical damping value. k and m_h have been determined, so c can be found as

$$c = 41.4 \ \mathrm{lb}/(\mathrm{ft}/\mathrm{sec}) . \tag{8.1.4}$$

First-order spring and damping coefficients for bending and twisting at the neck do not have a direct correspondence to HSRI 3-D neck quantities because of the differences in the analytical models. But as nearly as correspondences between the models can be made, the following values are indicated. Joint stop spring and damping coefficients for bending at N-T are 189 ft.lb/deg and 0.00291 ft.lb/(deg/sec). The respective values for N-H are taken as 378 and 0.00582. For joint stop twisting (H-T) the values are 160 and 0.00291.* The respective elastic k and c values are 0.873, 0., 1.746, 0., 0.873, and 0.

---

*Joint stop damping coefficients given here are felt by this author to be too small. The HSRI 3-D values are completely arbitrary. Better values, although still arbitrary, could probably be obtained by making estimates on the basis of critical damping, with damping ratios of 1 or greater.

First-order spring and damping coefficients for bending at the torso joints are suggested by HSRI 2-D values. At both joints the joint stop coefficients are, respectively, 333 ft.lb/deg and 0. ft.lb/(deg/sec). For twisting the joint stop coefficients used are similar to neck values: 160 and 0.00582. The elastic coefficients are all zero.

Values were obtained for a volunteer for the front, back, and side stop angles for generalized pitching at the two centers of rotation for the neck (N-T and N-H) discussed in Section 3.1. The value for twisting was also obtained. These are rough values since a hand-held protractor was used. Head movements were made voluntarily by the subject.

	N-T	N-H
Front (flexion)	60°	10°
Back (extension)	15°	30°
Side (lateral flexion)	25°	25°

Twisting, H-T: 60°

Tarrière and Sapin (22) give average values for maximum voluntary flexion and extension as: a) 65° and 70° at N-T; and b) 20° and 30° at N-H. These values are in basically good agreement with those given above except for the 70° extension value at N-T. This value seems rather large in view of the fact that the 30° extension range at N-H implies a total voluntary extension of 100°. On the otherhand the value of 15° given in the table seems small since it implies a total voluntary extension of 45°. (About 70° is regarded as normal total voluntary extension of the neck.) The value of 15° is used in this investigation.

Joint stop angle values are needed also for the torso joints. Definition of joints for the thoracic and lumbar sprines is considerably more arbitrary than definition of joints in the neck linkage, and the joint stop angle values are less easily obtained. Again with the aid of a volunteer, extreme ranges of voluntary bending and twisting were determined approximately. However, only the ranges for the torso as a whole could be measured in any reasonable manner. It therefore becomes necessary to find a method of distributing the values over the length of the torso, i.e., to the n-1 torso joints. There seems to be no "unique" reasonable method, but there possibly is a "best" way.

Figure 17 shows the torso in a position of extreme forward bending. The pelvic mass is considered to be unrotated, and the angle θ to the tangent at N-T is the value measured for forward bending. The approximation is made that in the extreme bending position the spine has constant curvature. Also, the chord lengths in the figure are approximated by l_1 and l_2. The joint stop angles θ_1 and θ_2 are to be determined. Constant curvature implies that

$$2\theta_2 + 2\varphi_1 = \theta \quad . \tag{8.1.5}$$

Since

$$\theta_1 = \theta_2 + \varphi_1 \quad , \tag{8.1.6}$$

we obtain

$$\theta_1 = \frac{\theta}{2} \quad . \tag{8.1.7}$$

To find θ_2, note first that

$$\varphi_2 = \theta_2 \quad . \tag{8.1.8}$$

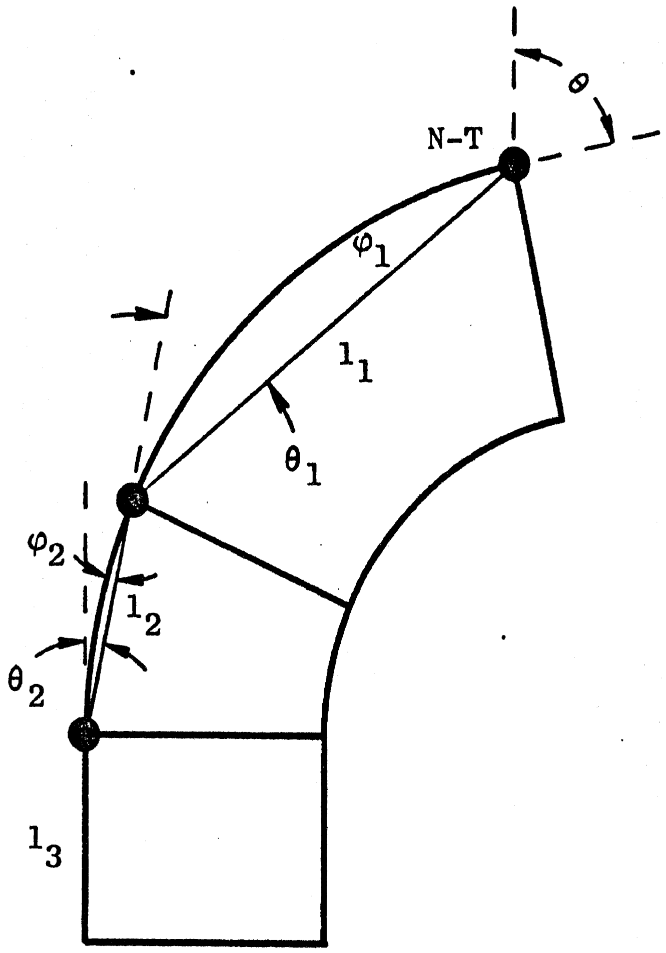
N-T
θ
φ_1
l_1
θ_1
φ_2
l_2
θ_2
l_3

Figure 17. Extreme voluntary forward bending of torso.

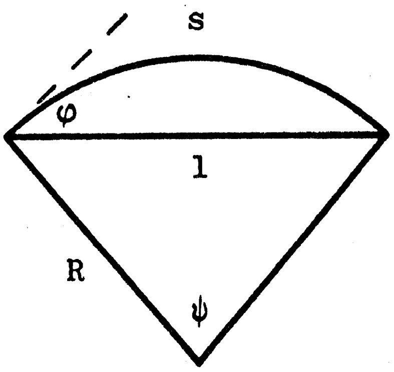

Figure 18. A sector.

Also, where ψ_2 is the central angle for the chord l_2 (refer to Figure 18), we have that

$$\psi_2 = 2\varphi_2 = 2 \sin^{-1}\frac{\ell_2}{2R_2} \quad . \tag{8.1.9}$$

Eliminating φ_2 in (8.1.9) and solving for R_2 we have

$$R_2 = \frac{\ell_2}{2 \sin\theta_2} \quad . \tag{8.1.10}$$

Similarly,

$$R_1 = \frac{\ell_1}{2 \sin\varphi_1} \quad . \tag{8.1.11}$$

Since constant curvature has been assumed, R_1 equals R_2, and therefore (8.1.10) and (8.1.11) give (8.1.12). Equation (8.1.13) derives from (8.1.6) and (8.1.7).

$$\ell_2 \sin\varphi_1 = \ell_1 \sin\theta_2 \tag{8.1.12}$$

$$\varphi_1 = \frac{\theta}{2} - \theta_2 \tag{8.1.13}$$

These two equations can be solved for θ_2 and φ_1. Only θ_2 is of particular interest. The result is

$$\theta_2 = \tan^{-1}\left[\frac{\ell_2 \sin\frac{\theta}{2}}{\ell_1 + \ell_2 \cos\frac{\theta}{2}}\right] \quad . \tag{8.1.14}$$

The forward stop angles θ_1 and θ_2 have thus been determined as functions of θ. It will be assumed that the same results, (8.1.7) and (8.1.14), apply for backward bending by amount $\theta > 0$ and also for bending to the side.

Next, consider twisting, and let θ be the measured extreme value. Twist per unit length along the torso will be assumed constant and equal to

$$\bar{\theta} = \frac{\theta}{\ell_1 + \ell_2 + \ell_3} \quad . \tag{8.1.15}$$

The distribution of twisting stop angles is then taken as

$$\theta_1 = \int_{-\ell_2/2}^{\ell_1} \bar{\theta} \, d\ell \tag{8.1.16}$$

$$\theta_2 = \int_{-\ell_3}^{\ell_2/2} \bar{\theta} \, d\ell \quad . \tag{8.1.17}$$

Three or more joints would lead to additional stop angles of the form

$$\theta_i = \int_{-\ell_{i+1}/2}^{\ell_i/2} \bar{\theta} \, d\ell \quad . \tag{8.1.18}$$

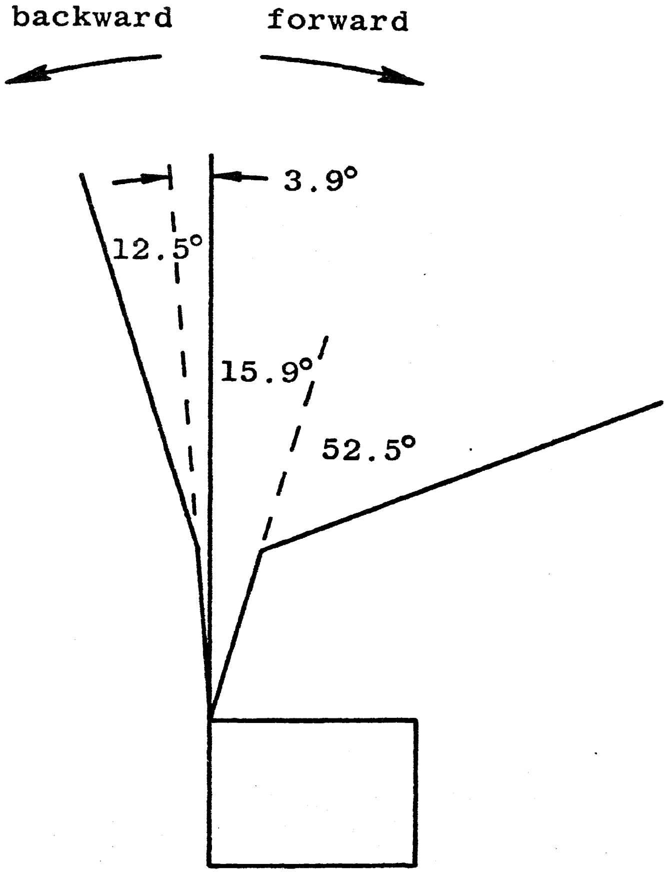
backward
forward
3.9°
12.5°
15.9°
52.5°

Figure 19. Extreme voluntary fore-aft bending of torso.

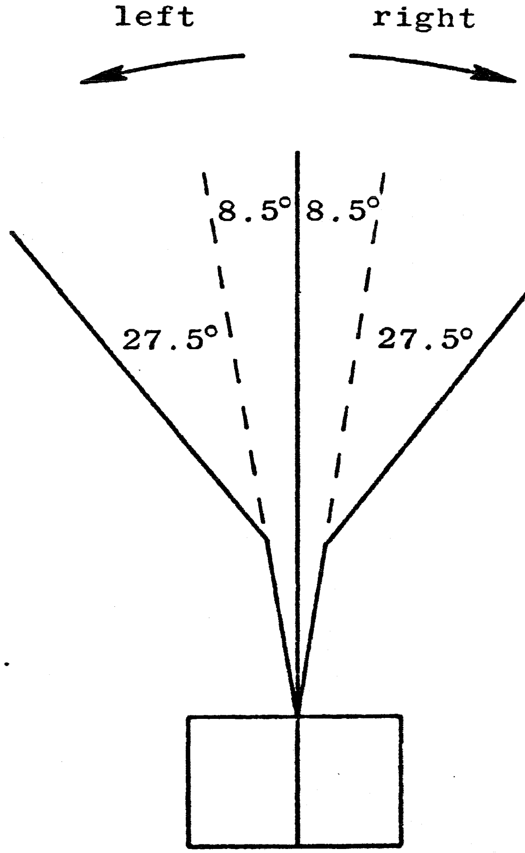
left
right
8.5°
8.5°
27.5°
27.5°

Figure 20. Extreme voluntary lateral bending of torso.

The techniques illustrated here clearly must give results that are more and more meaningful as the number of joints is increased, but the results obtained for the three-mass torso do not seem unreasonable. The values of θ measured for forward, backward, and sideward bending and for twisting, respectively, were 105°, 25°, 55° and 50°. The joint stop angles determined as in the foregoing analysis are given below.

	Joint 1	Joint 2
Front	52.5°	15.9°
Back	12.5°	3.9°
Side	27.5°	8.5°
Twisting	30.3°	19.7°

The extreme positions for bending are illustrated in Figures 19 and 20. The rectangles represent the pelvic element.

8.2 NECK INITIAL CONDITIONS

Reasonable initial conditions can easily be specified for a vehicle occupant who, at impact, is in a normal sitting position and is facing straight ahead. Supposing that the vehicle is initially headed parallel to the inertial x-axis, we would ordinarily have initial Euler angle values for the head and the first torso element of the order of zero. The neck coordinates would have typical values of $l(0) = l_{eq}$, $\Theta(0) = 0°$, and $R(0) = 10°$ to $15°$.

In less normal initial situations, however, proper choice of initial values for (l, Θ, R) can be uncertain. The desired orientation of the head and of the first torso element can always be set up with little difficulty, and $l(0)$ can always reasonably be given the value l_{eq}, but $\Theta(0)$ and $R(0)$ must be selected with care. Strictly, these initial values are independent and arbitrary, but anatomical restrictions must be considered. Initial R- and R'-deformations of the joint stop "ellipses" cannot be justified. The ellipses represent "hard" stops and are the limit for voluntary relative motion at the joints; deformation can be allowed only after impact. However, with given values for $(\psi, \theta, \varphi)_1$, $(\psi, \theta, \varphi)_h$, and l at $t = 0$, an arbitrary selection of values for $\Theta(0)$ and $R(0)$ is very likely to result in deformation at one or both pitching stops.

A short computer program was therefore written to aid in selecting reasonable initial values. It can be run before the main computer program whenever there is uncertainty about the selection of initial values. The program accepts as input: the front, back, and side stop angle values for both ellipses; the initial Euler angle values for both the head and the first torso element; $l(0)$; and $\Theta(0)$, for which a reasonable value can be estimated from consideration of the desired initial situation. The computer program then determines the stop angle $f(\Theta(0))$ for the N-T joint. For each of a set of R values $0 \leq R \leq f(\Theta(0))$ the quantities Θ', R', and $f_1(\Theta')$ are next determined, f_1 being the joint stop angle for N-H. If the set of resulting R' and f_1 values contains a subset for which $R' > f_1$, then the doubt about reasonable choice of initial values is justified. (It may have been warranted even if such a sub-set does not result since unallowable situations at N-T have already been eliminated.) The complementary sub-set $R' < f_1$ then indicates the limits of the allowable range of values for $R(0)$, and any value within the range may be selected.

CHAPTER 9

THE PHILOSOPHY OF MODEL VERIFICATION

All investigators to date in mathematical modeling of crash victims have had to contend with a serious lack of pertinent experimental data. First, development and use of the model are hampered by unavailability of bioparameter values. Second, verification that the model is a good representation of the human body is made extremely difficult by the lack of experimental crash kinematics for living human subjects. What little experimental work has been done in these areas applies primarily to the range of voluntary movement of body parts and to non-severe crash situations. The mathematical modeler must accept that these difficulties can never be entirely overcome. While the complexities of the experimental problems and a general shortage of good experimentalists are not small hindrances, the overriding difficulty would seem to be a complete lack of expendable subjects for laboratory testing.

There can be little doubt that the best alternative to use of human volunteers is use of cadavers. A limited amount of work involving cadavers and of possible value to the mathematical modeler has, in fact, been done (4). But it is obvious that use of anthropomorphic dummies is much more convenient in impact sled crash simulations, and it is in this direction that virtually all laboratory crash investigation programs have gone.

Unfortunately, present anthropomorphic dummies are less than perfect representations of the human body as a biomechanical system. The most serious defect is probably that joints have been designed with a large amount of Coulomb friction.* This is not at all characteristic of joints in the human, nor is it characteristic of joint representations used in most mathematical models. (It seems likely that mathematical models that do have Coulomb friction in the joints stand a better chance of agreeing with dummy test results, and there are perhaps some arguments for trying to reproduce the anthropomorphic dummy analytically.) A mathematical model might have the potential of surpassing the dummy - an engineering model - as an approximation of the living human, and in such case verification of the model by comparison with dummy test results would have meaning only to the extent that the dummy itself had been validated by comparison with human subjects.

Very little dynamic testing has been done for dummy-against-human verification. And, surprisingly, only a limited amount of model-against-dummy testing has been done; so far, model and dummy crash simulation studies have proceeded almost independently. It is worth noting that a special problem exists in verifying mathematical vehicle occupant models against human, cadaver, or dummy response: Complete mathematical crash simulation models include analytical representation of restraint systems and vehicle interiors as well as of the vehicle occupant, and therefore a "perfect" vehicle occupant model will respond differently from the equivalent human to a given vehicle excitation unless the restraint system and vehicle interior are themselves modeled "perfectly."

In any case the vehicle occupant model in the present investigation cannot be compared directly against human, cadaver, or dummy response for a laboratory crash since a vehicle has not been analytically simulated. The only apparent manner in which the model can be even partially verified is to compare it against another mathematical model. Strong arguments can be raised against such a practice (as common as it is, by necessity, in some engineering areas). The primary weakness of this approach is that the model against which comparison is made is manifestly only an imperfect representation of reality. Further, it is in most cases assumed to be the simpler model, and yet comparison of a "more complex" model with a "more simple" one presumedly indicates a degree of validity for the simpler model more than it validates the complex model.

---

*Recent improvements have been made in neck design in this regard (32).

Still, such a procedure is thought to be of value. For the case in point the simpler vehicle occupant model is the HSRI 3-D simulation (18), which is described in the literature review in Chapter 1. That model has been reasonably well verified, and its limitations are recognized. Comparison of the model under investigation with the HSRI 3-D model should at least indicate whether the gross response of the new model is reasonable. Further, it allows for studying the effects of adding torso and neck flexibility, muscle tension, etc. If departures from HSRI 3-D response can be explained reasonably in this context, then, to the degree that one agrees with the considerations that went into defining the vehicle occupant model, one may assume that the mathematical model can be "tuned" - by properly choosing bioparameter values - to more closely approximate the living human.

CHAPTER 10

VERIFICATION OF THE VEHICLE OCCUPANT MODEL

Because of lack of a vehicle interior the vehicle occupant model is reasonably compared against the HSRI 3-D simulation only for idealized crash situations. This restriction is not of consequence since desired degrees of crash severity can still be investigated.

Exercises of the vehicle occupant computer model will be described in this chapter along with description of the idealized crashes simulated with the HSRI 3-D computer model. The various crash situations were devised so as to allow the study of all of the important features of the analytical model. Results and discussion of results for each crash follow description of the crash. Reference to "VOM" will always indicate the "vehicle occupant model" developed in this investigation.

10.1 FRONTAL IMPACT

This test allows examination of the behavior of the neck and torso in sagittal-plane bending. The crash description is as follows: With uniform forward velocity v_0 at $t = 0$, the vehicle occupant is considered to be stopped instantaneously at the hip. This is accomplished for the HSRI 3-D model by enclosing the hip contact sphere inside a cube of hard contact surfaces while prescribing non-zero initial velocity conditions; the torso rebounds in a normal manner because the leg element is held between two hard contact planes. Stopping the hip instantaneously is necessary for this test because x-y-z motion at the hip cannot be forced for the vehicle occupant model; the only cartesian generalized coordinates are in the upper torso. Hip motion can be made almost zero, however, by assigning a large value for m_3 and by making sure that the

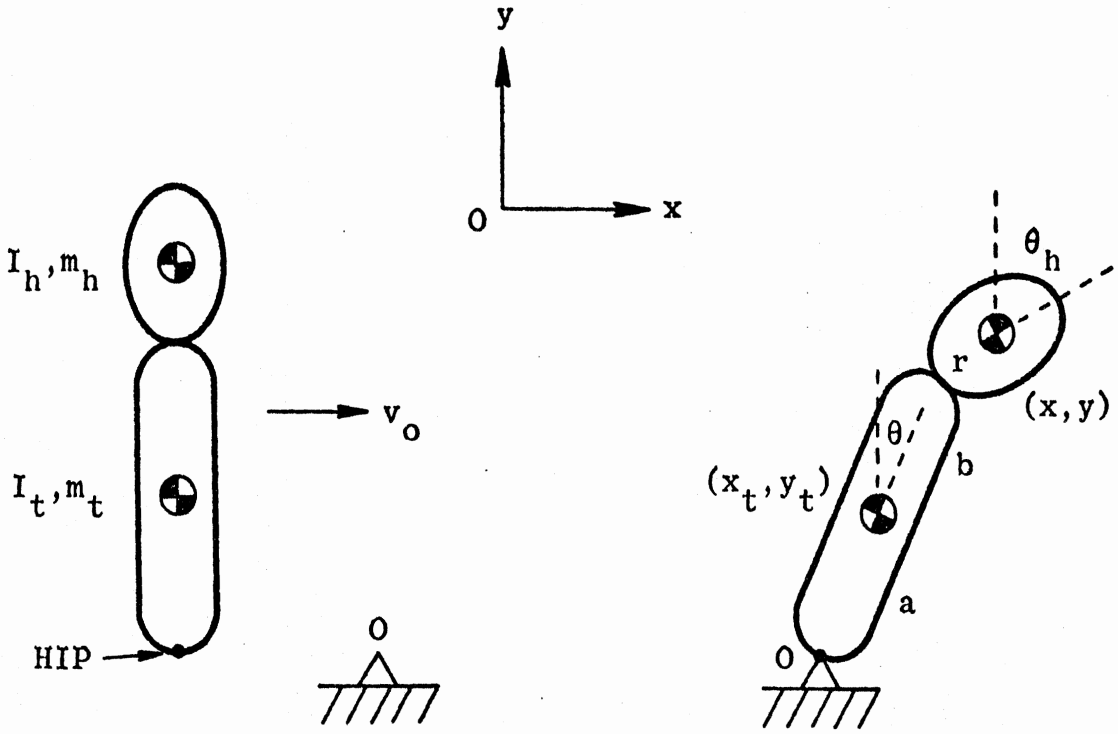

Figure 21. Frontal impact: before and after t = 0.

velocity of the third torso element is zero at t = 0 by use of velocity constraint relations.

This test, in effect, by-passes the "impact." That is, initial conditions (t = 0) are really for $t = +\epsilon$, which is immediately after impact. The following analysis determines the proper initial conditions as a function of the impact velocity, v_0. Figure 21 shows the head-torso system considered for the HSRI 3-D simulation. Except for pinning the hip, this is a four-degree-of-freedom problem. Pinning the hip eliminates the cartesian generalized coordinates, but their Lagrange equations may be retained if two Lagrange multipliers are introduced.

Let the generalized coordinates be x, y, θ, and θ_h. (See Figure 21.) The four Lagrange equations for the general four-degree-of-freeom, free motion case may be easily determined. We are concerned, however, only with the range $t = 0^-$ to $t = +\epsilon$, with ϵ approaching zero. Since θ, θ_h, and $\dot{y}$ are all zero for $t = 0$, all terms in the Lagrange equations that contain $\sin\theta$, $\sin\theta_h$, or $\dot{y}$ as a factor will be equal to zero. Similarly, cosine factors are equal to unity. With these considerations we obtain:

$$\begin{aligned}
\theta:&\quad (I_t + m_t b^2)\ddot{\theta} + m_t r b \ddot{\theta}_h - m_t b \ddot{x} = 0 \\
\theta_h:&\quad m_t r b \ddot{\theta} + (I_h + m_t r^2)\ddot{\theta}_h - m_t r \ddot{x} = 0 \\
x:&\quad - m_t b \ddot{\theta} - m_t r \ddot{\theta}_h + (m_h + m_t)\ddot{x} = 0 \\
y:&\quad (m_h + m_t)\ddot{y} + m_t(r \dot{\theta}_h^2 + b \dot{\theta}^2) = 0 .
\end{aligned} \tag{10.1.1}$$

Next, consider the constraint conditions that hold if the hip is pinned:

$$\begin{aligned}
\dot{x} &= r \dot{\theta}_h \cos\theta_h + (a+b)\dot{\theta}\cos\theta \\
\dot{y} &= - r \dot{\theta}_h \sin\theta_h - (a+b)\dot{\theta}\sin\theta \quad .
\end{aligned} \tag{10.1.2}$$

In terms of virtual displacements, the constraints are

$$\begin{aligned}
&\delta x - r\cos\theta_h\,\delta\theta_h - (a+b)\cos\theta\,\delta\theta = 0 \\
&\delta y + r\sin\theta_h\,\delta\theta_h + (a+b)\sin\theta\,\delta\theta = 0 \quad .
\end{aligned} \tag{10.1.3}$$

At t = 0, these reduce to

$$-(a+b)\,\delta\theta - r\,\delta\theta_h + \delta x = 0 \tag{10.1.4}$$

$$\delta y = 0 \quad . \tag{10.1.5}$$

We see that the Lagrange multiplier λ_y for the y-constraint will not contribute to the x-, θ-, or θ_h-equations, and therefore we need consider neither λ_y nor the y-equation itself. Let the Lagrange multiplier associated with constraint (10.1.4) be $\lambda = \lambda_x$. The coefficients of the virtual displacements are

$$\begin{aligned} a_\theta &= -(a+b) \\ a_{\theta_h} &= -r \\ a_x &= 1 \quad , \end{aligned} \tag{10.1.6}$$

so the associated generalized forces are

$$\begin{aligned} Q_\theta &= -(a+b)\lambda \\ Q_{\theta_h} &= -r\lambda \\ Q_x &= \lambda \quad . \end{aligned} \tag{10.1.7}$$

(See Goldstein (26), pp. 40-42.) At impact, the governing equations (10.1.1) must then become

$$\begin{aligned} \theta:&\ \left(I_t + m_t b^2\right)\ddot{\theta} + m_t r b \ddot{\theta}_h - m_t b \ddot{x} = -(a+b)\lambda \\ \theta_h:&\ m_t r b \ddot{\theta} + \left(I_h + m_t r^2\right)\ddot{\theta}_h - m_t r \ddot{x} = -r\lambda \\ x:&\ -m_t b \ddot{\theta} - m_t r \ddot{\theta}_h + \left(m_h + m_t\right)\ddot{x} = \lambda \quad . \end{aligned} \tag{10.1.8}$$

Since the hip is stopped instantaneously, λ is an infinite spike, a "delta function." The integral past t = 0 is finite, however, and will be defined as

$$J = \int_{0^-}^{\epsilon} \lambda \, dt \quad . \tag{10.1.9}$$

Consider next that

$$\dot{\theta}(0^-) = \dot{\theta}_h(0^-) = 0 \quad . \tag{10.1.10}$$

and

$$\dot{x}(0^-) = v_0 \quad . \tag{10.1.11}$$

Integration of the equations (10.1.8) from 0^- to ϵ gives

$$\begin{aligned} A_{11}\dot{\theta}(\epsilon) + A_{12}\dot{\theta}_h(\epsilon) + A_{13}\dot{x}(\epsilon) + (a+b)J &= -m_t b v_0 \\ A_{21}\dot{\theta}(\epsilon) + A_{22}\dot{\theta}_h(\epsilon) + A_{23}\dot{x}(\epsilon) + r J &= -m_t r v_0 \\ A_{31}\dot{\theta}(\epsilon) + A_{32}\dot{\theta}_h(\epsilon) + A_{33}\dot{x}(\epsilon) - J &= (m_h + m_t) v_0 , \end{aligned} \tag{10.1.12}$$

where the A_{ij} are the constant coefficients in equations (10.1.8). Equations (10.1.12) are three equations in four unknowns: $\dot{\theta}(\epsilon)$, $\dot{\theta}_h(\epsilon)$, $\dot{x}(\epsilon)$, and J. The required fourth equation is the constraint relation for $\dot{x}$, the first of equations (10.1.2). At t = ϵ, the constraint relation becomes

$$-(a+b)\dot{\theta}(\epsilon) - r\dot{\theta}_h(\epsilon) + \dot{x}(\epsilon) = 0 \quad . \tag{10.1.13}$$

Equations (10.1.12) and (10.1.13) may now be solved for the four unknowns. The values of $(-)\dot{\theta}(\epsilon)$, $(-)\dot{\theta}_h(\epsilon)$, and $\dot{x}_t(\epsilon) = a\dot{\theta}(\epsilon)$ are then the required initial conditions for the HSRI 3-D frontal impact run as a function of impact velocity v_0.

The four algebraic equations were solved with a short computer program. As a check on the results angular momentum with respect to point 0, the final hip position, was calculated for $t < 0$ and at $t = +\epsilon$:

$$\begin{aligned} L(t<0) &= m_t v_0 a + m_h v_0 (a+b+r) \\ L(\epsilon) &= (I_t + m_t a^2)\dot{\theta}(\epsilon) + I_h \dot{\theta}_h(\epsilon) \\ &\qquad + m_h \dot{x}(\epsilon)(a+b+r) \quad . \end{aligned} \tag{10.1.14}$$

Computer results for $L(t < 0)$ and $L(\epsilon)$ are found to be identical, and therefore angular momentum is conserved, as expected.

All necessary input for the HSRI 3-D run is now known. Compatible initial conditions for the vehicle occupant of this investigation must next be determined. Consider first the initial head pitching velocity. It is clear that its values for the idealized HSRI 3-D frontal impact will be non-zero and opposite in sign (positive) to the initial torso pitching velocity (negative) because of articulation at the simple ball-and-socket neck joint; the ball-and-socket connection is, in one sense, an element of infinite mechanical impedance since motion of the torso is transmitted immediately to the head. The extensible, two-joint neck, however, does not transmit motion to the head with zero time lag, so the initial head pitching velocity is set equal to its value before impact, i.e., zero. All torso element pitching velocities are given initial values equal to the initial value for the HSRI 3-D torso. The initial value for $\dot{z}_1$ is, of course, zero. The initial value for $\dot{x}_1$ is found from the constraint relation defining $\dot{x}_3$ (see equations (4.4.3)); $\dot{x}_3$ is set equal to zero so that approximate zero hip motion is effected, as explained earlier. We obtain

$$\dot{x}_1(0) = -\left(\frac{\ell_1}{2} + \ell_2 + \frac{\ell_3}{2}\right)\dot{\theta}(0) \quad . \qquad (10.1.15)$$

where $\dot{\theta}(0) = \dot{\theta}_1(0) = \dot{\theta}_2(0) = \dot{\theta}_3(0)$.

Compatible initial values for $\dot{l}$ and $\dot{R}$ are also required. These were obtained with a short computer program on the basis of the following analysis. We require that $\dot{x}_h(0) = v_0$ and $\dot{z}_h(0) = 0$. Since $\dot{\Theta}$ is identically zero for this problem and since $\Theta(0) = 0$, the relations (4.5.2) and (4.5.3) give the initial values for x, y, z, $\dot{x}$, $\dot{y}$, and $\dot{z}$ as functions of initial values for l, R, $\dot{l}$, and $\dot{R}$. If (4.5.2) and (4.5.3) are then substituted into (4.5.8), we obtain a constraint relation for $\dot{x}_h(0)$, which is set equal to v_0. Similarly, an expression is obtained for $\dot{z}_h(0)$, and it is set equal to zero. The results we then have are

$$\begin{aligned} &\dot{\ell}(0)\sin R(0) + \dot{R}(0)\,\ell(0)\cos R(0) \\ &\quad = v_0 - \dot{x}_1(0) + \left[\ell(0)\cos R(0) + \frac{\ell_1}{2}\right]\dot{\theta}(0) \end{aligned} \qquad (10.1.16a)$$

$$-\dot{\ell}(0)\cos R(0)+\dot{R}(0)\,\ell(0)\sin R(0)$$

$$=\left[\ell(0)\sin R(0)-t_0\right]\dot{\theta}(0) \quad . \qquad (10.1.16b)$$

Equations (10.1.16) determine $\dot{l}(0)$ and $\dot{R}(0)$ in terms of known quantities.

Finally, rebound of the torso after maximum forward pitching must be provided for. The frontal impact thus far described for the vehicle occupant computer model will produce continuous forward rotation about the (approximate) center of gravity of the massive third torso element. There is no leg element and hence no torso-leg joint (i.e., hip joint) to produce a resisting moment. It was decided that the most reasonable manner of accomplishing rebound is to force $\theta_2(t)$ with the torso pitching angle from the HSRI 3-D run, which does, of course, have rebound.

This particular verification run was made with joint stop angle stiffness values for N-T and N-H of about half those given in Chapter 8 in order to correspond to a smaller value used for the HSRI 3-D neck. All muscle tension parameters were set to zero and all elastic spring and damping coefficients were zero. The impact velocity for this test was v_0 = 15 mph. This is a low velocity crash, but it is quite violent since the hip is stopped instantaneously.

Figure 22 shows some of the dimensions used for the vehicle occupant. All values shown are constants except for the neck length, which is the equilibrium value l_{eq}. Results of the frontal impact test are shown in Figures 23 to 29. Various HSRI 3-D results (indicated by the subscript "HSRI") are also given for comparison.

The stick figures in Figure 23 are a time history of the head and torso pitching. The individual figures are to scale but the length d(= 0.177 ft) is left out for pictorial clarity.

Figures 24 to 28 break down the results illustrated by Figure 23. Pitching angles for the three torso elements are shown in Figure 24. Maximum pitching for the flexible torso occurs for the uppermost element, of course. Also, it is observed that rebound of that element lags behind θ_2, as it must since the only restoring moment for the first element is produced at the first torso joint.

Inertial head pitch angles are shown in Figure 25. Direct comparison of the inertial head angles has real meaning only if it is kept in mind that torso flexibility as well as neck linkage is reflected in the results. It may be seen that maximum head angle lags behind the beginning of upper torso rebound (Figure 24) by about 30 msec. Also, the head rotation for VOM does appear to follow a translational mode (Ewing, et al. (19)), there being a delay relative to rotation of the HSRI 3-D head with the simple neck model. The less immediate reaction to torso motion for VOM is made more clear by comparing the relative head pitch angle in Figure 26 with θ_1 in Figure 24. Also, Figure 26 clearly shows that the flexible, extensible neck results in a definite lag with respect to the HSRI 3-D motion for head angle with respect to the torso.

Figures 27 and 28 show the components at N-T and N-H of the total relative pitch angle θ^h in Figure 26. These relative angles, θ^{N-T} and θ^{N-H} (which equal R and R' in absolute value), cannot be defined as additive components of θ^h for general three-dimensional motion, but the frontal impact test is a planar problem. θ^{N-T} and θ^{N-H} are seen to stay in the vicinity of the extension stop angles for R and R' until about the time that upper torso rebound begins, after which potentially injurious flexion occurs at each joint.

The only viscoelastic components for the neck length in this test were the Kelvin spring and damper. Their net effect is the force F_ℓ, which is resolved into components F_x and F_z in e_1. These should be thought of as neck forces at N-T, where the neck angle is R (Figure 27). Both components reach maximum values at about the time that the neck angle R hits its flexion stop. Maximum neck length extension of 1.25 inches occurs at about t = 160 msec. Maximum compression of 0.54 inches occurs at 195 msec. The neck is compressed by about 0.28 inches almost immediately (10 msec) after impact as the torso passes under the head while pitching forward. The maximum extension of 1.25 inches does not seem unreasonable. Schulman, *et al*. (23), conducted a series of tests in which neck extension occurred as a result of "tailward" decelerations. Volunteers were strapped securely in a supine position to a sled with their heads in the direction of sled motion. With maximum sled decelerations of about 23 g and resultant torso deceleration of about 17 g, neck extensions of up to 2.4 inches were observed.

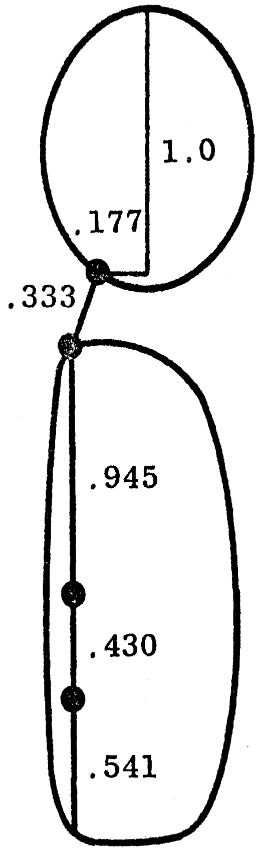
1.0
.177
.333
.945
.430
.541

Figure 22. Profile of the vehicle occupant with some of its dimensions (in feet).

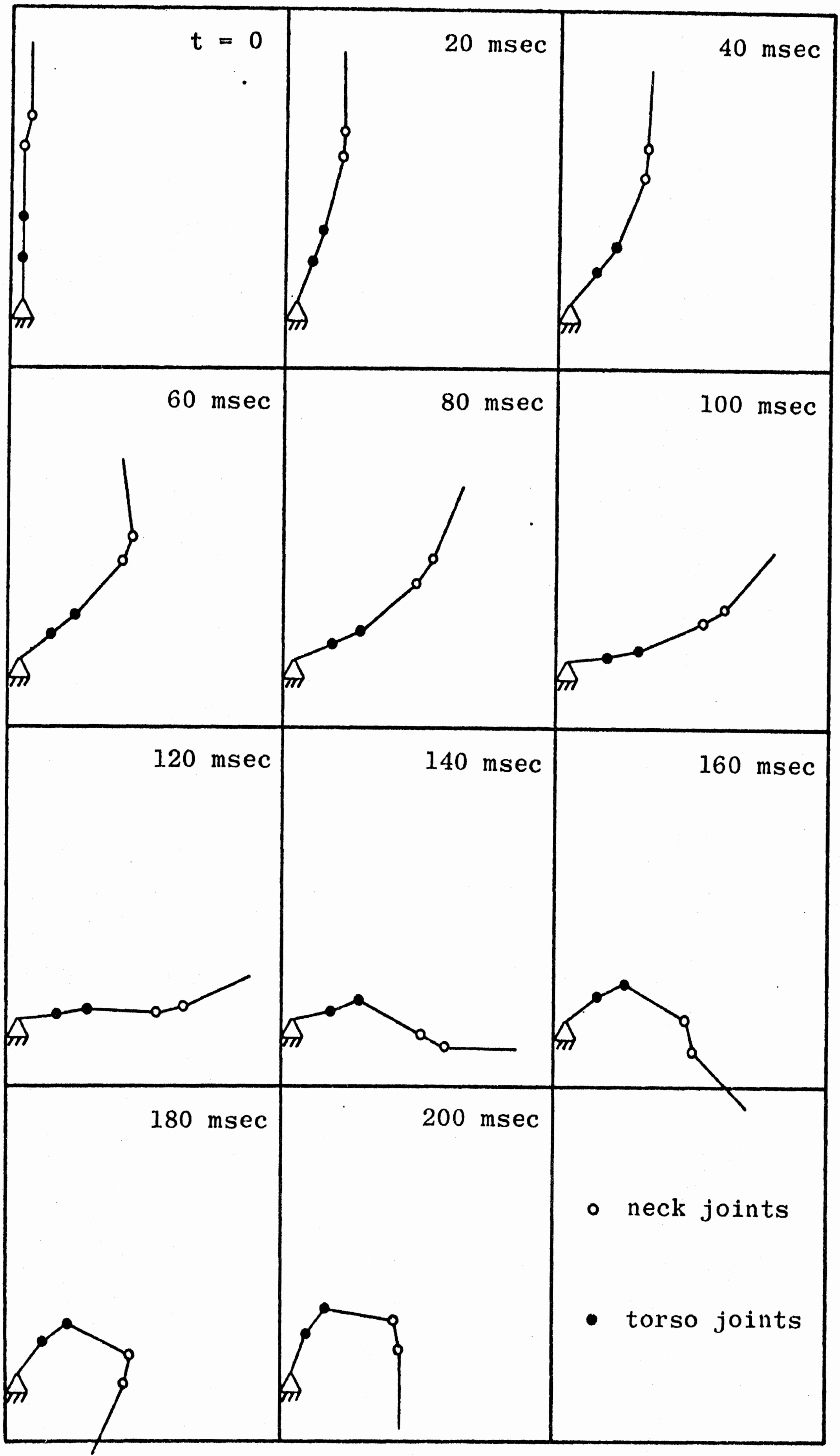
t = 0
20 msec
40 msec
60 msec
80 msec
100 msec
120 msec
140 msec
160 msec
180 msec
200 msec
○ neck joints
● torso joints

Figure 23. Frontal impact time history for pitching.

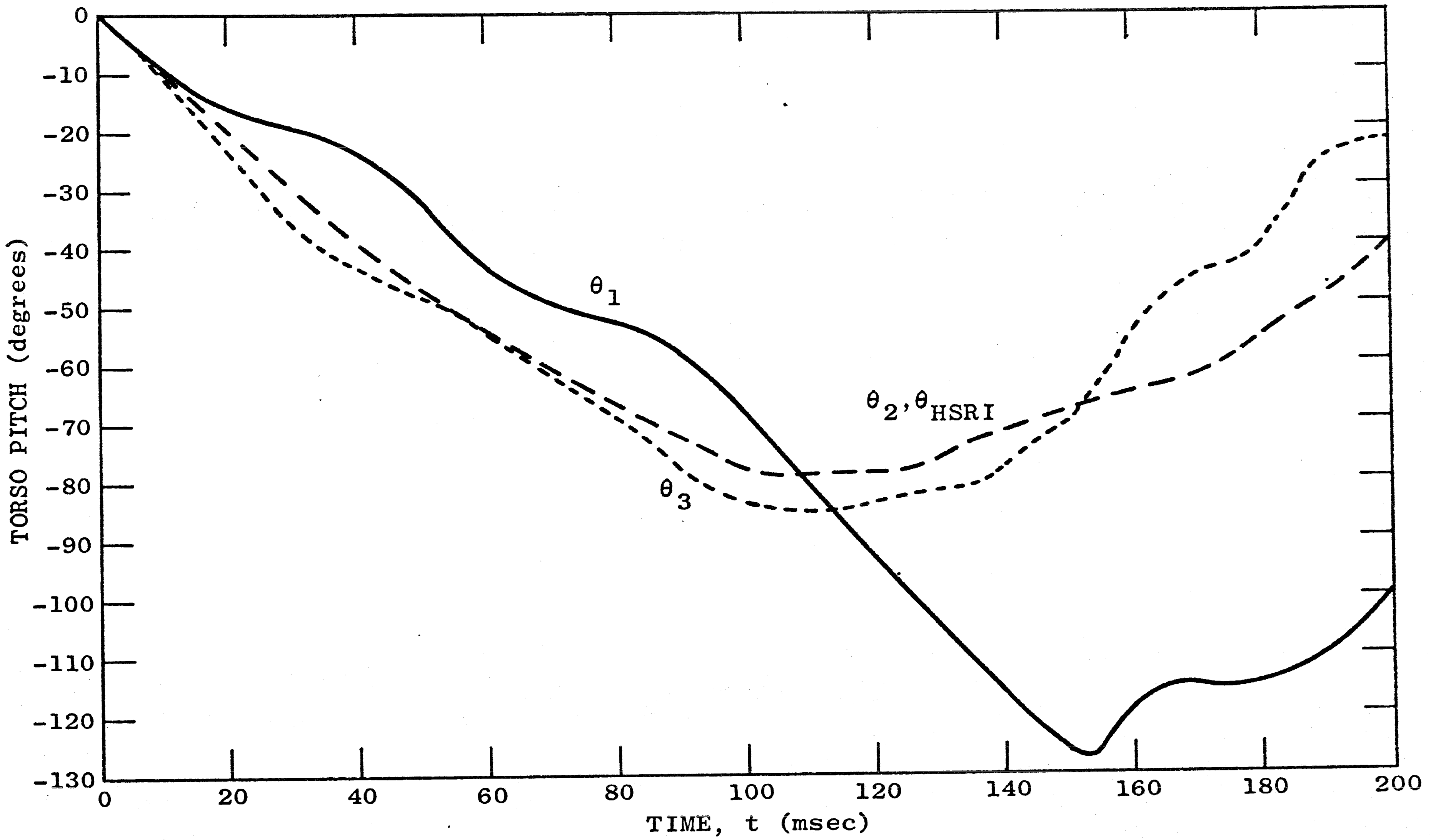

Figure 24. Torso pitching for frontal impact.

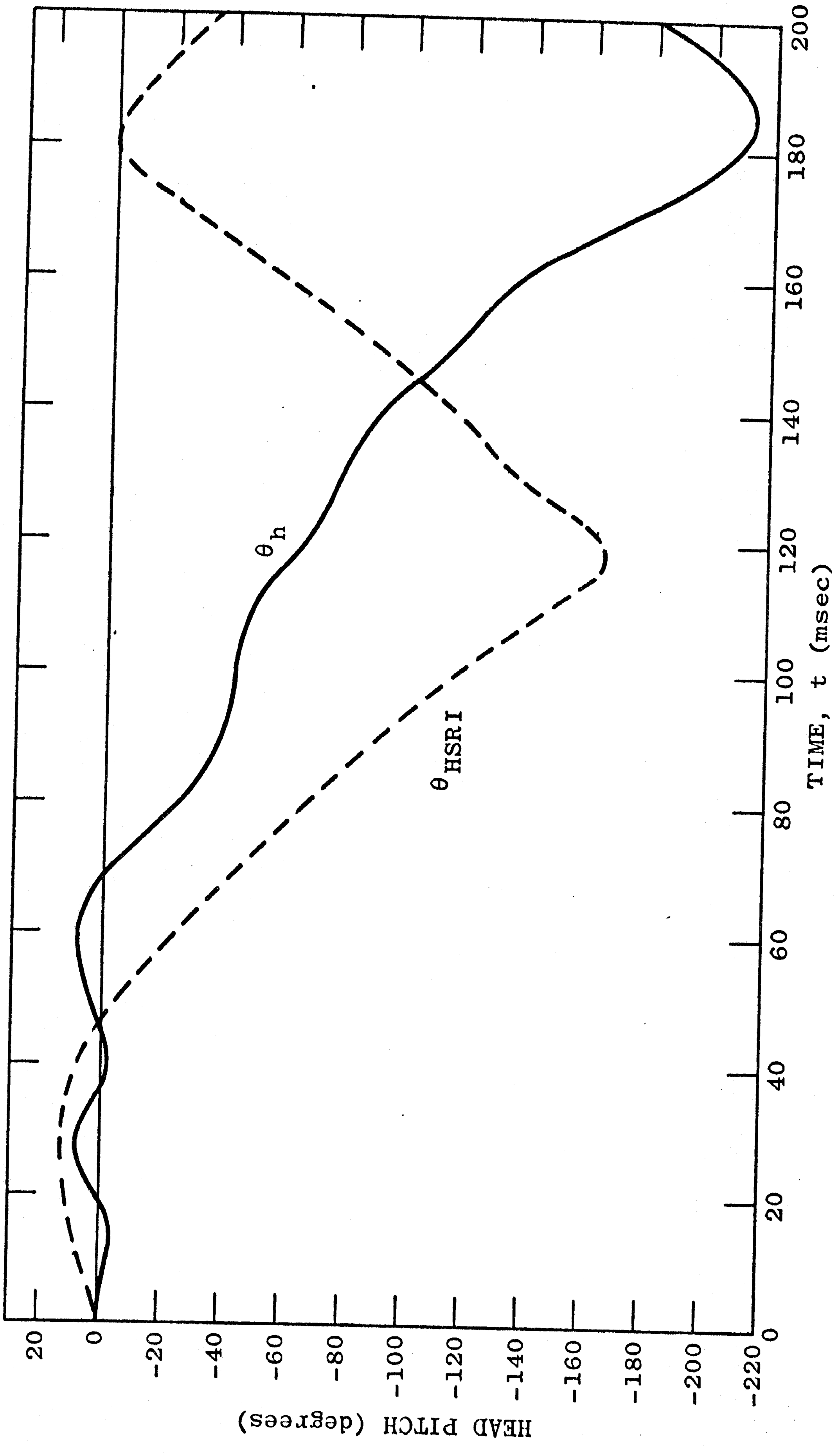

Figure 25. Head pitching for frontal impact.

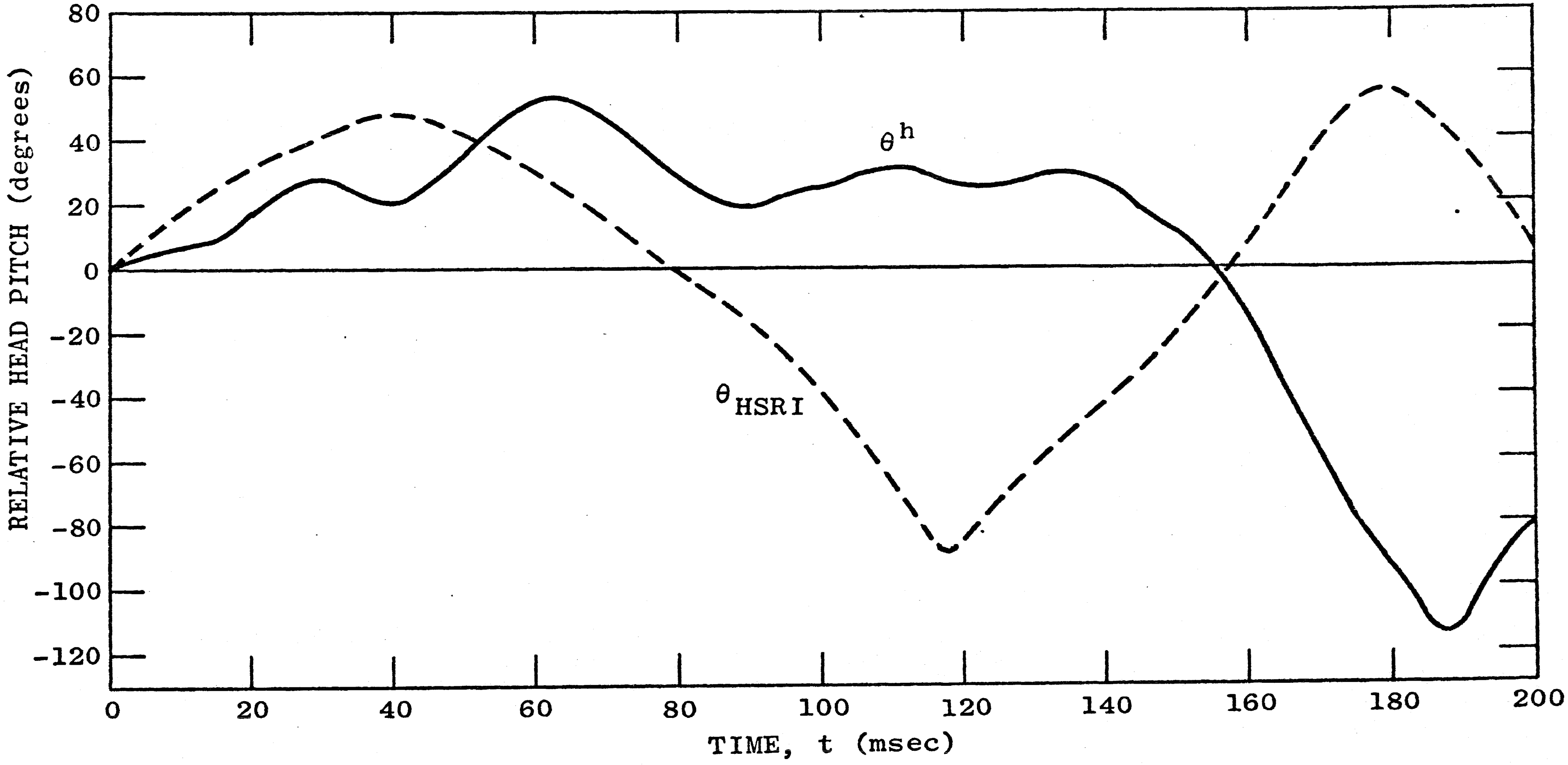

Figure 26. Pitching angle for head relative to torso.

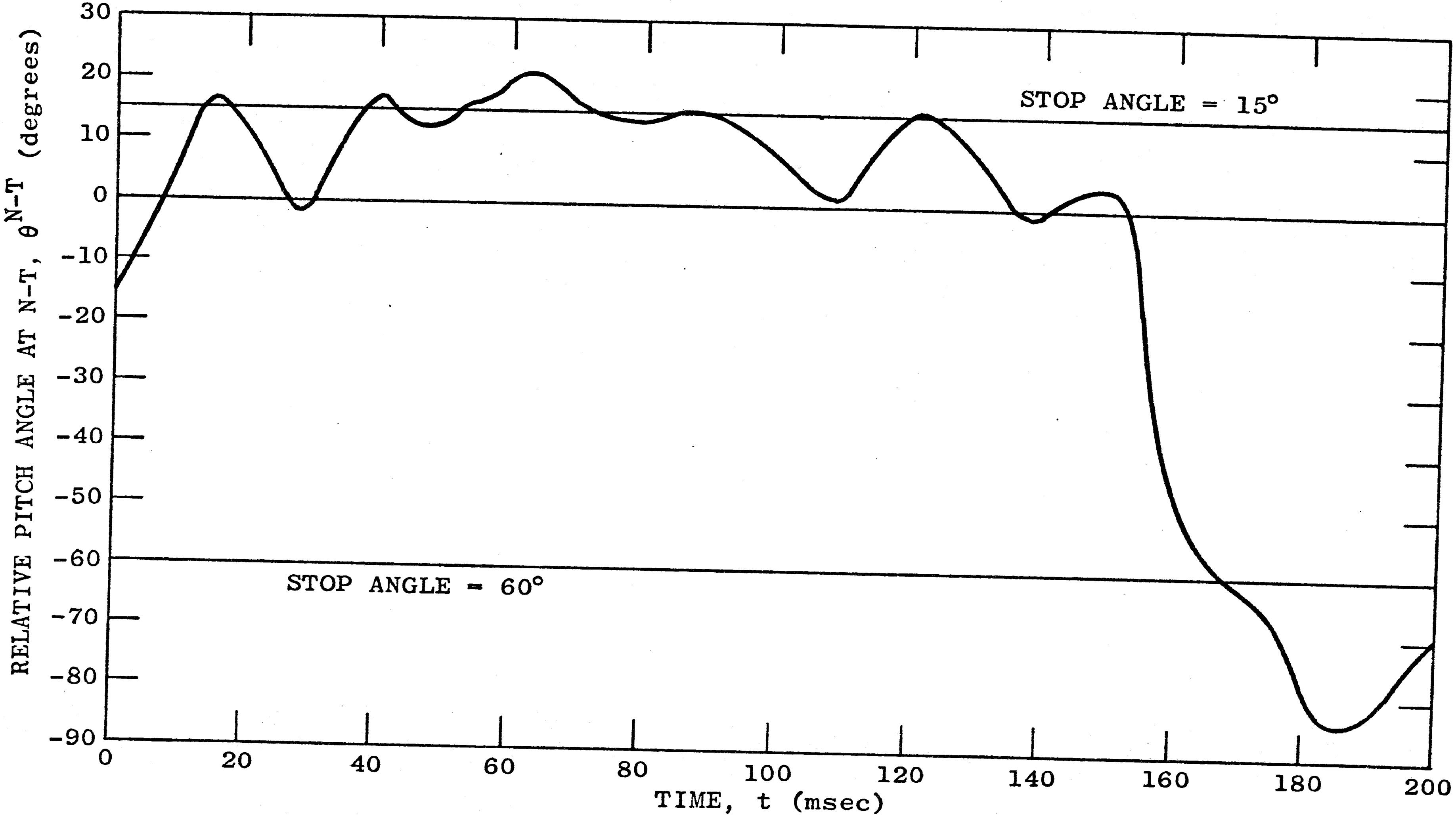

Figure 27. Relative pitching angle at neck-torso joint (N-T).

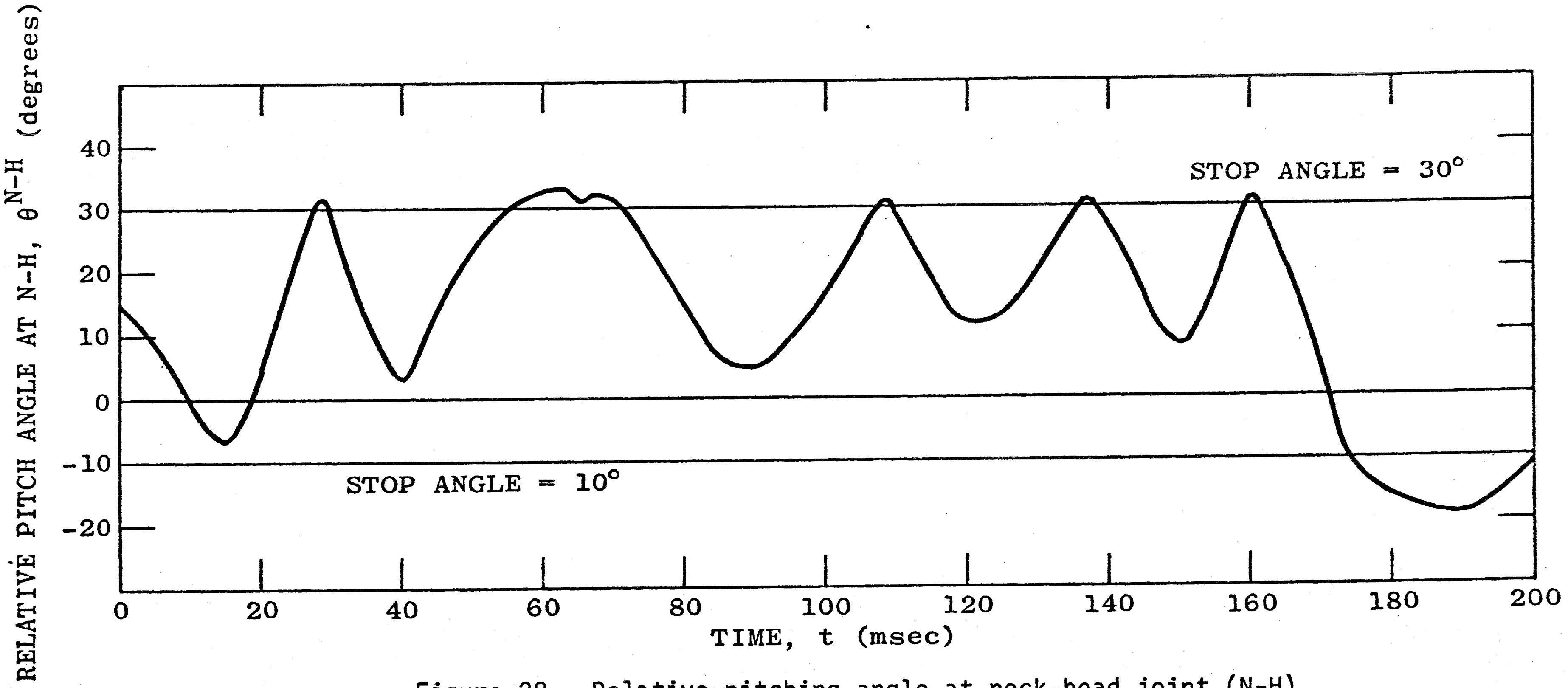

Figure 28. Relative pitching angle at neck-head joint (N-H).

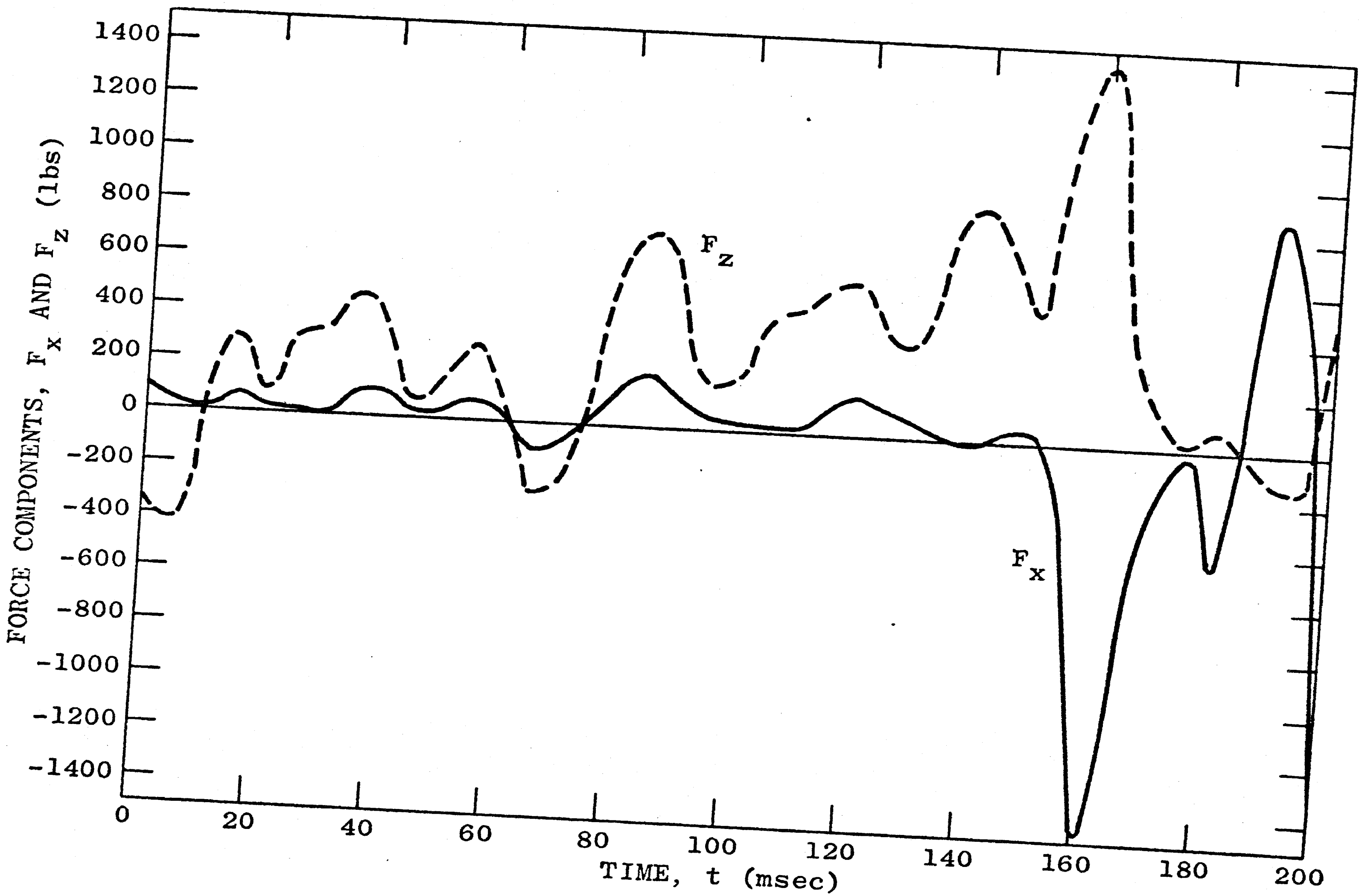

Figure 29. Components of neck compression force in e_1.

10.2 SIDE IMPACT

One crash investigation made by Robbins, Bennett, and Roberts (18) is of particular interest for this study. First, a 19 mile per hour side impact was simulated in the sled lab with a 50th-percentile-male anthropomorphic dummy. Targets were placed on the dummy's head, and the impact was filmed from two directions. Inertial head Euler angle values were found by this author, from calculations with available Vanguard film analysis results, for use in the vehicle occupant model exercise discussed in this section. These experimental results are shown in Figures 30 to 32. Robbins, Bennett, and Roberts simulated the impact sled crash with the HSRI 3-D computer model for comparison with impact sled results.

This simulation was of interest for this study for several reasons. First, both experimental and analytical results are available for possible comparison against VOM. Second, a real crash situation is considered. Third, a particularly interesting study of the vehicle occupant model neck linkage is made possible. The forcing limitations for VOM still apply, of course, so experimental and analytical HSRI results must be used carefully. In particular, torso interaction with the seat back and shoulder harness cannot be simulated for VOM, so only the head-neck motion can be studied. So that head-neck motion can be compared directly with dummy or HSRI 3-D head motion it is necessary that the torsos undergo identical motion. Since no torso motion data was available for the dummy, the HSRI 3-D torso motion $(x, y, z, \psi, \theta, \phi)$ was used to force the torso for VOM. It might still be reasonable to compare VOM head motion against dummy head motion but only if it could be shown or inferred that dummy torso motion is very similar to HSRI 3-D

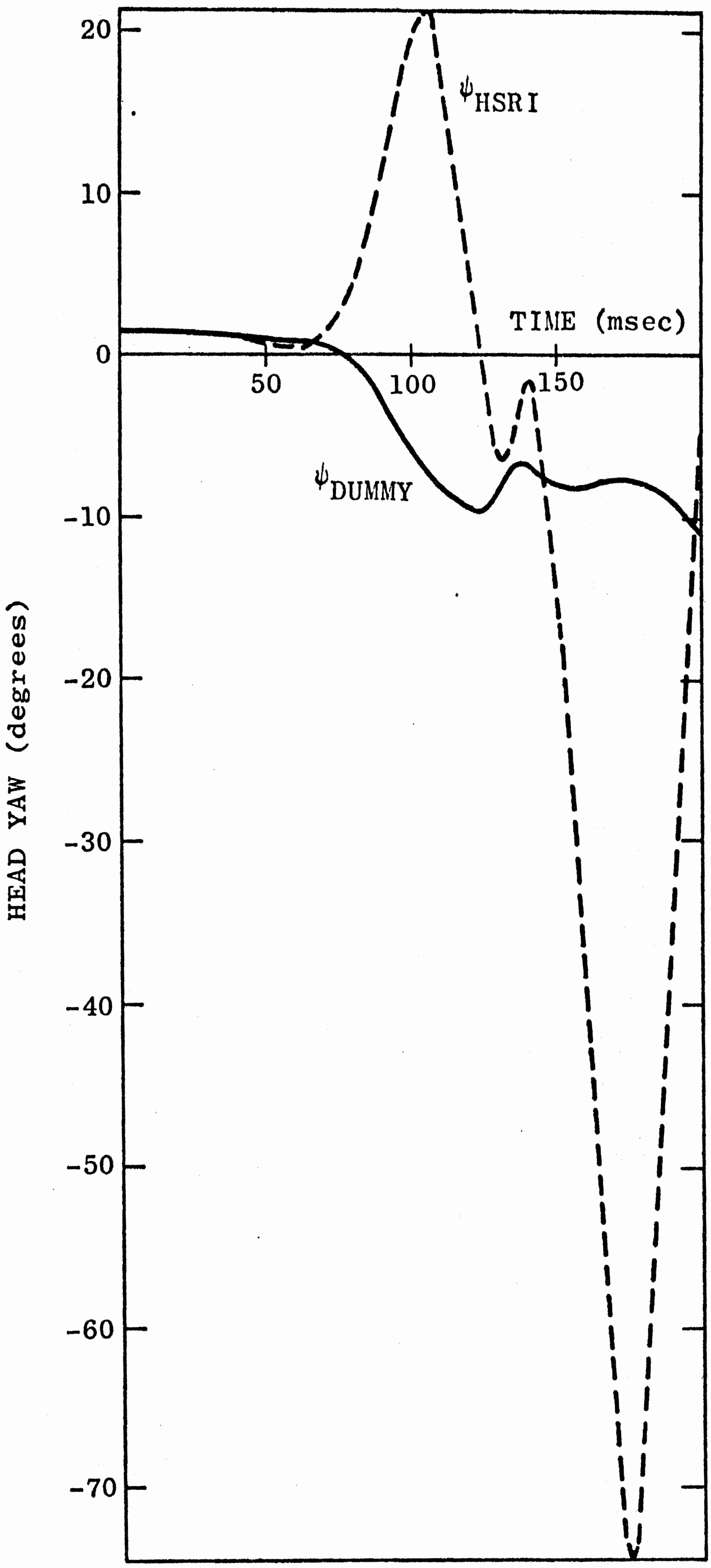

Figure 30. HSRI 3-D and dummy head yaw for side impact.

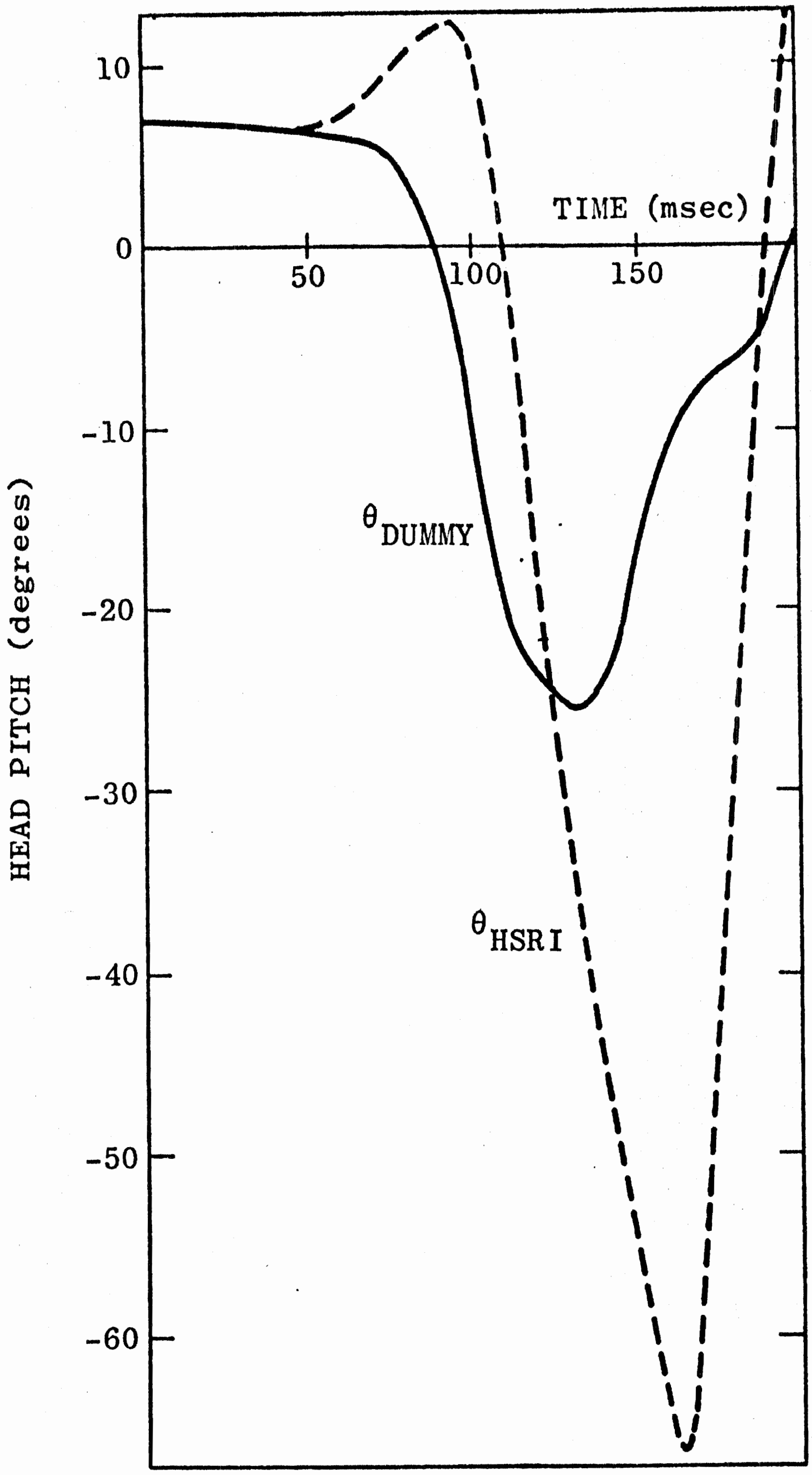

Figure 31. HSRI 3-D and dummy head pitch for side impact.

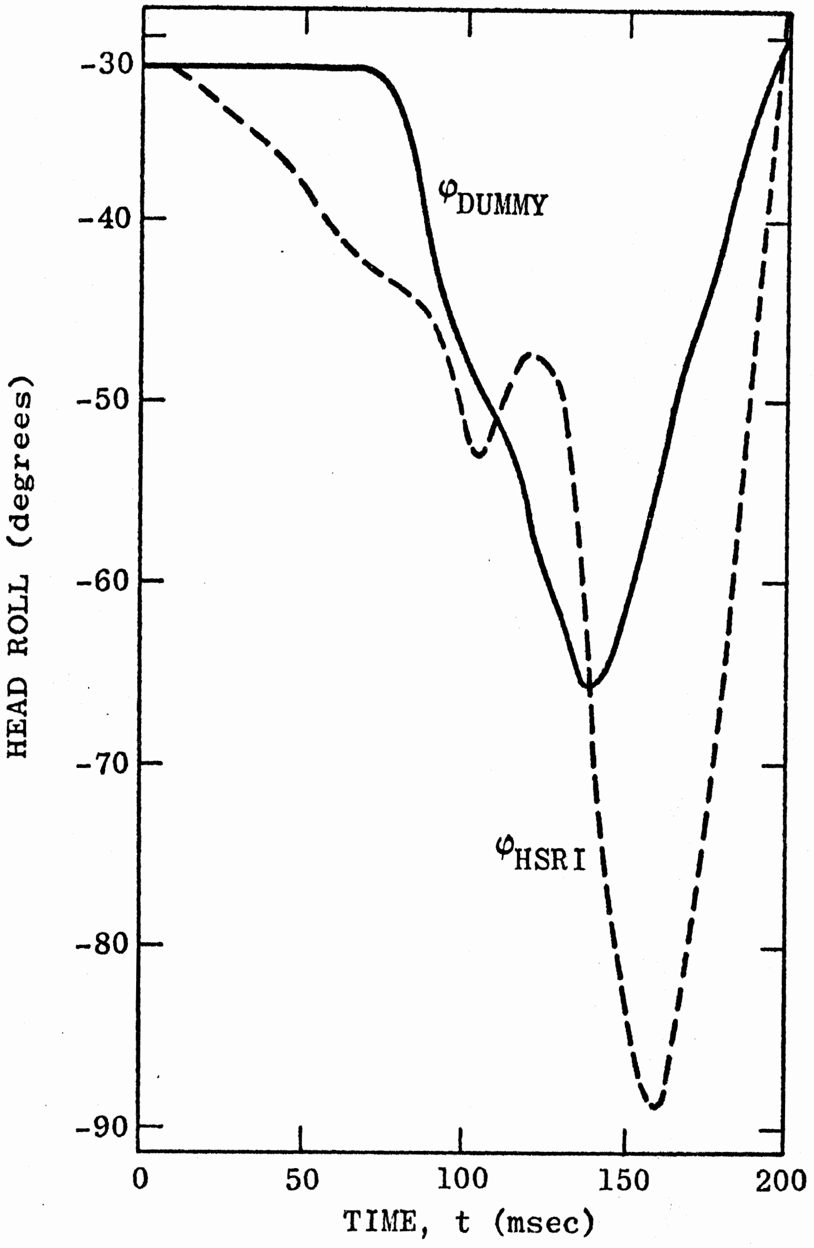

Figure 32. HSRI 3-D and dummy head roll for side impact.

torso motion. Also, it should be noted that comparison of VOM head motion with either HSRI experimental or analytical results - even as restricted above - will not be strictly valid after such time as the head, in either case, strikes any part of the vehicle interior. Since the HSRI 3-D head struck the seat back at 90 msec, it was not thought of value to run the vehicle occupant computer model much past 90 msec; integration was terminated at 150 msec.

The crash victim's vehicle has zero yaw, pitch, and roll and also no x- or z-motion. The y-acceleration history is positive, however, and $\dot{y}(0)$ is -19 mph, so the vehicle can be considered to be sliding directly toward the left at 19 mph and then impacting a nearly stationary object.

Figures 30 to 32 show the HSRI 3-D computer model results and impact sled results for inertial head yaw, pitch, and roll. The head is initially nodded forward and to the left (as can be seen from the values of yaw, pitch, and roll at $t = 0$). Robbins, Bennett, and Roberts indicate that the mathematical model results for θ could be brought into closer agreement with the dummy motion by choosing a smaller value for the pitching joint stop angle; in particular, the valley in θ_{HSRI} would then be less deep. (Roll motion (φ) could be "improved" in the same manner.) The disagreement in yaw motion (ψ) is felt by this author to be caused primarily by the way the lap and shoulder belts are represented analytically. They are considered to be fastened securely to the vehicle occupant, i.e., they cannot slide. In fact, however, the belts do slide considerably over and around the vehicle occupant; this is seen easily in observing slow motion film of the sled lab crash. (This should affect yawing much more than pitching or rolling for nearly all crashes.) Visual comparison of the film of the sled lab crash with the HSRI computer-generated film for motion of the mathematical crash victim model shows that the analytical belt restraint representation - presumedly - does cause a substantial disagreement in the torso yaw motions. In consequence, HSRI 3-D and dummy head yaw cannot be expected to be in good agreement. Further, since HSRI 3-D (and not dummy) torso motion serves as the excitation for VOM, it becomes clear that there can be no useful purpose in comparing VOM head results with dummy head results.

The bioparameter values used in the HSRI 3-D side impact simulation were the ones which guided selection of the VOM values given in Section 8.1.2. (Note that elastic k's for the neck joints are non-zero.) Thus, with regard to bioparameter values, VOM and HSRI 3-D are matched as closely as possible. The body parameter values of Section 8.1.1 apply for this side impact simulation, but for the most part only head and neck values are important; motion of the first torso element is forced, and the unrestrained motion of the lower torso elements is of no interest. However, the length of the first torso element, l_1, is of particular importance for this simulation since the mass centers for the HSRI 3-D torso and for the first torso element of VOM must coincide if excitations to the neck-head systems are to be identical. For this reason, l_1 was set equal to twice the torso CG-to-neck joint length of the HSRI 3-D model. A similar consideration was not made for t_0, the offset of N-T from the center of gravity of the first torso element, since this is considered to be a feature of the VOM neck. (That is, t_0 was not set equal to zero.)

Figures 33 to 40 and 42 to 47 show VOM head-neck results, and HSRI 3-D results are given for comparison where appropriate. Figures 33 to 35 show inertial yaw, pitch, and roll for the head. VOM and HSRI 3-D yaw and pitch are in general agreement and require little comment. Roll motion is quite dissimilar and will be discussed later. It is noted here that the HSRI 3-D head interaction with the seat back at 90 msec apparently did not significantly affect head motion. This may be deduced from the fact that the yaw and pitch results for the two models do not come into disagreement after t = 90 msec. Results for VOM to 200 msec would therefore have been valid for comparison against HSRI 3-D.

The relative head Euler angles are shown in Figures 36 to 38. The most interesting feature of the relative yaws is the difference in the curves between 105 and 140 msec. It is difficult to isolate the cause of some characteristics of three-dimensional motion of any complex model, and it is particularly difficult for this side impact simulation since it is in no way a symmetric or idealized situation. However, the difference in the relative yaws is most likely mainly a reflection of the non-zero offset lengths t_0 and d and of the non-zero neck length l. The relative pitch curves differ mainly in maximum values of relative (forward) head pitch. This is primarily an indication of basic differences between the joint models. Namely: 1) the VOM neck model has two joints with independent joint stops; and 2) bending joint stop moments for VOM depend on the anatomically meaningful "generalized pitching angles" R and R' rather than on the arbitrarily defined Euler angles for relative pitch and roll. The composite forward neck flexion stop for VOM is 70° (60° for N-T and 10° for N-H; see Section 8.1.2), which agrees with the 70° forward stop for HSRI 3-D relative pitch in a planar problem. Relative roll will be discussed later, but it is mentioned here that the VOM composite lateral neck flexion stop of 50° (25° + 25°) agrees with the HSRI relative roll stop of 50°.

The angular motion of the neck element, relative to the torso and head, is shown in Figures 39 and 40 in terms of R, Θ, R', and Θ'. Figure 39, for example, shows that from the initial values of R = 30° and Θ = -20° the left-side impact causes first deformation of the joint stop ellipse at t = 65 msec and toward the left, as expected.* The motion for the side impact crash is so complex that it becomes impossible to intuitively predict or interpret the later parts of the R - Θ motion. But it may be possible to detect the influence of the elastic spring elements at the joints; the effect of elastic spring moments, when they are not overpowered by other moment components, must be visible in a tendency for return to initial positions.

Inertial and relative head roll (Figures 35 and 38) can be interpreted with the aid of Figures 39 to 41. A complete explanation of the curves is impossible, as was implied earlier. If inertial yaw and pitch values were identically zero, the task would be much easier. As it is, the values are "not large" - i.e., torso yaw and pitch range between +20° and -35° and head yaw and pitch range between +23° and -28° - so it is possible to attempt an explanation. First, the inertial roll is approximately constant at about -30°. This seemingly indicates that sideward translation is taking place and that the sideward rotational mode (i.e., roll) will follow at some time after 150 msec. The oscillations in the rolls (both inertial and relative) are explained by observing that peaks and valleys correspond to deformations of the joint stop ellipses at N-T and N-H, respectively. The relative roll curve for VOM does not differ greatly from the curve for HSRI 3-D out to 150 msec except for being displaced upward. The negative-to-positive trend of the relative roll beginning at about 125 msec possibly results from the change toward less negative values of the torso roll excitation beginning at about that same time. The torso roll is shown in Figure 41. With regard to Figures 39 and 40 it may be observed that sharp changes of motion within either ellipse correspond closely to joint stop activity for the other ellipse.

---

*Appropriate initial values for R and Θ were found as described in Section 8.2. It is noted here also that it was necessary to monitor joint stop moments for maximum values between print times since deformations of the joint stop ellipses might otherwise have remained undetected.

The neck length compression force, elastic moments at the neck joints, and x-y-z head positions are shown in Figures 42 to 47. The VOM values for $x_h(t)$, $y_h(t)$, and $z_h(t)$ are biased by the amount that they differ from HSRI 3-D values at $t = 0$. The difference at $t = 0$ results, of course, from the non-zero neck length of VOM. Strictly, some sort of non-constant bias should be used since the geometry changes with time.

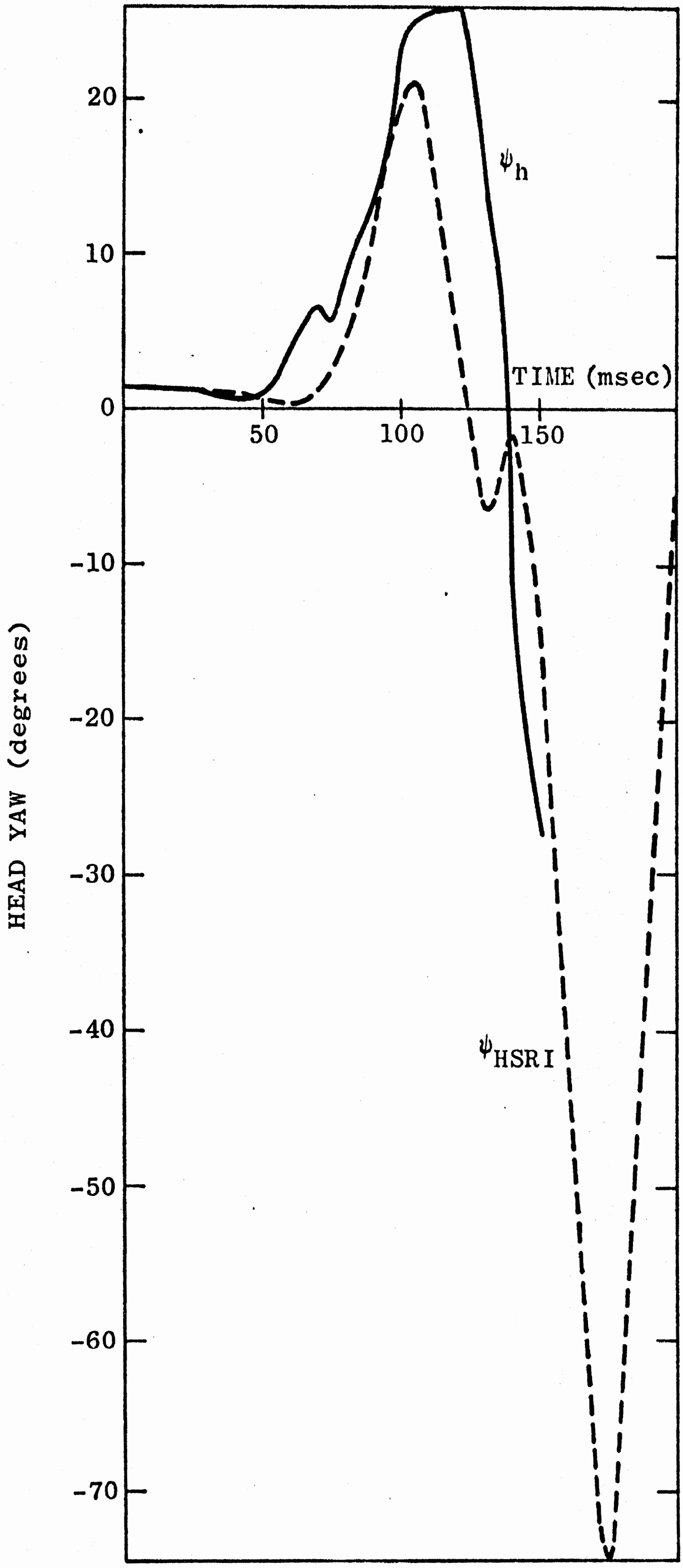

Figure 33. HSRI 3-D and VOM head yaw for side impact.

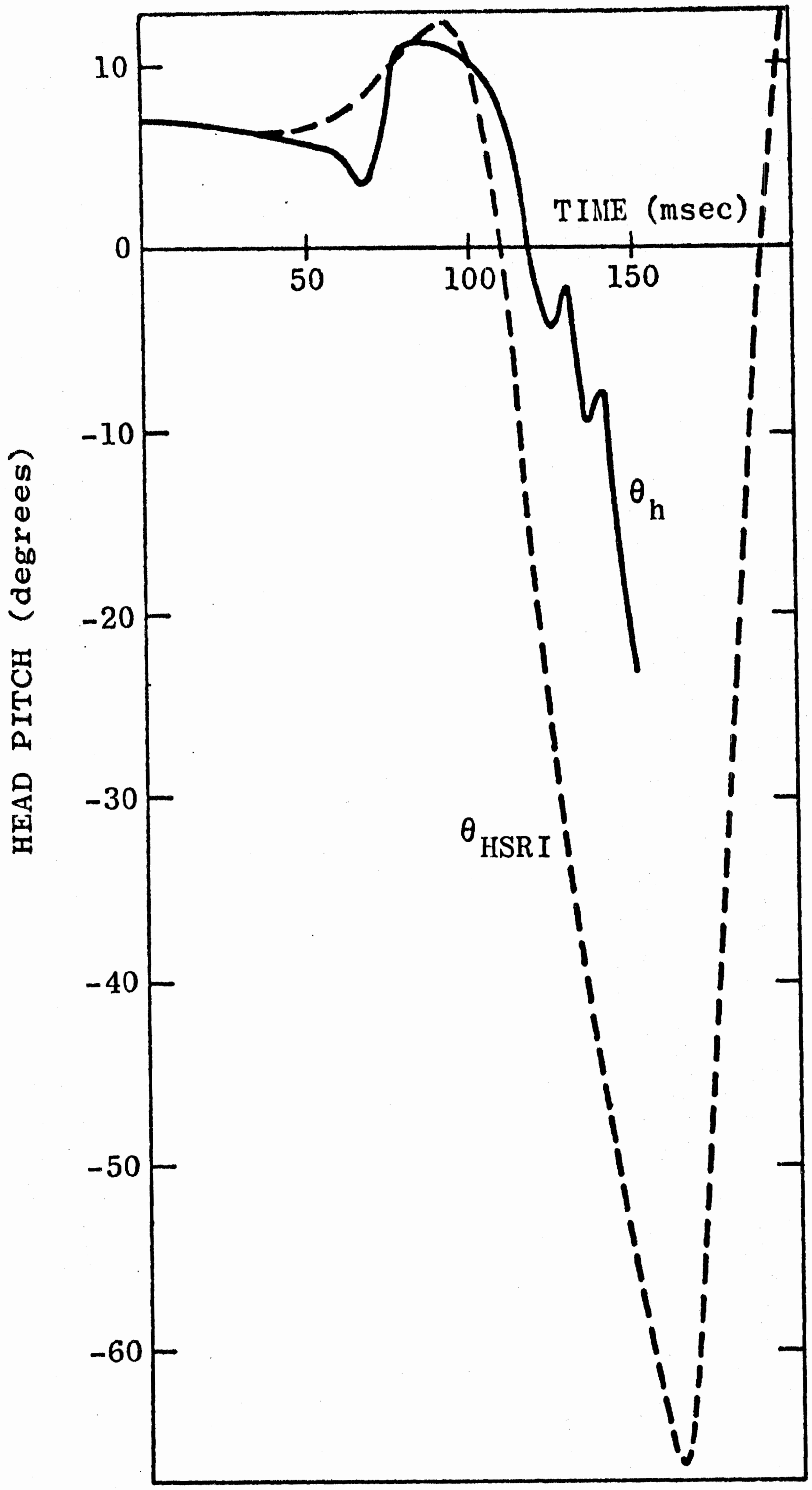

Figure 34. HSRI 3-D and VOM head pitch for side impact.

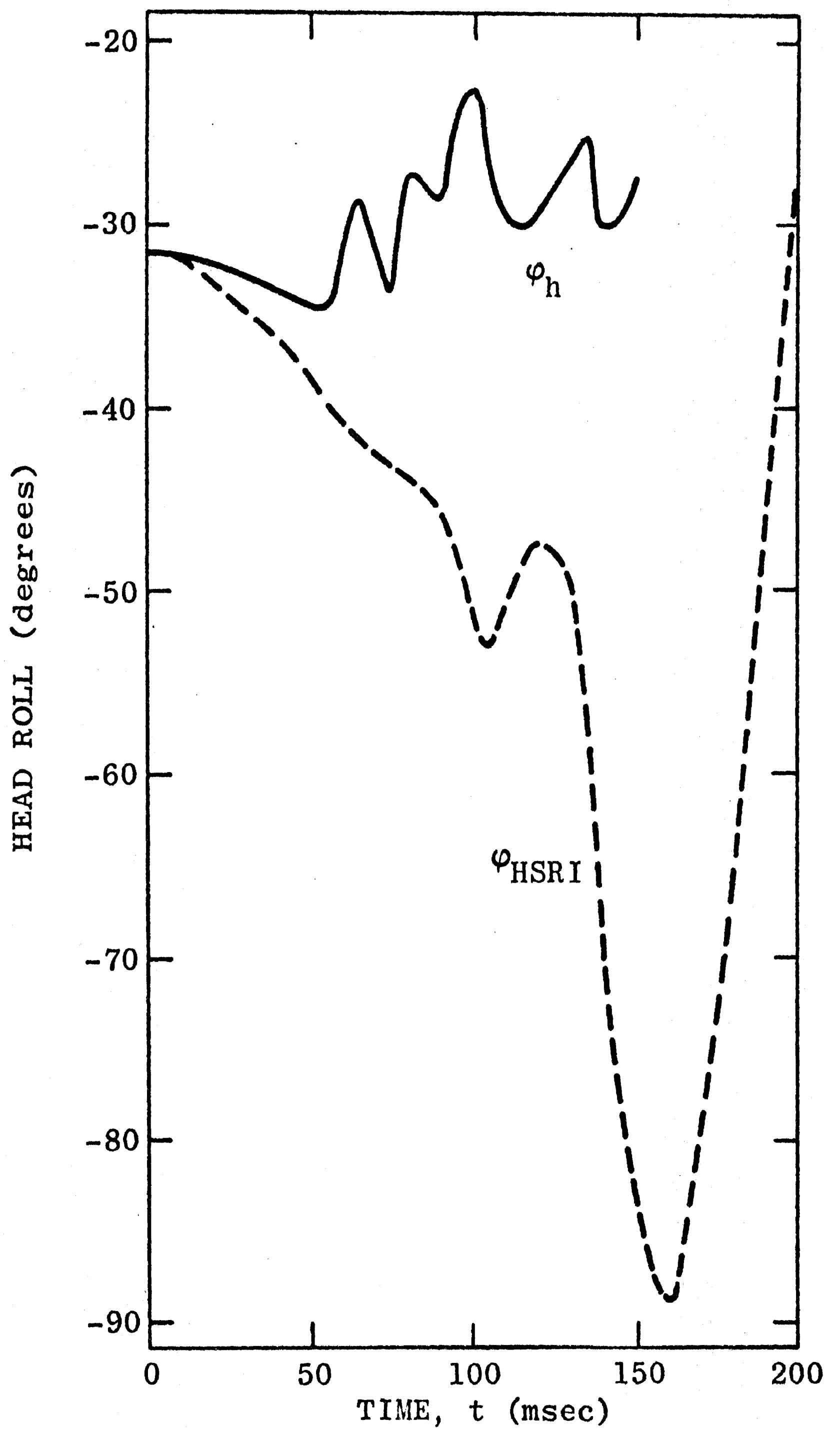

Figure 35. HSRI 3-D and VOM head roll for side impact.

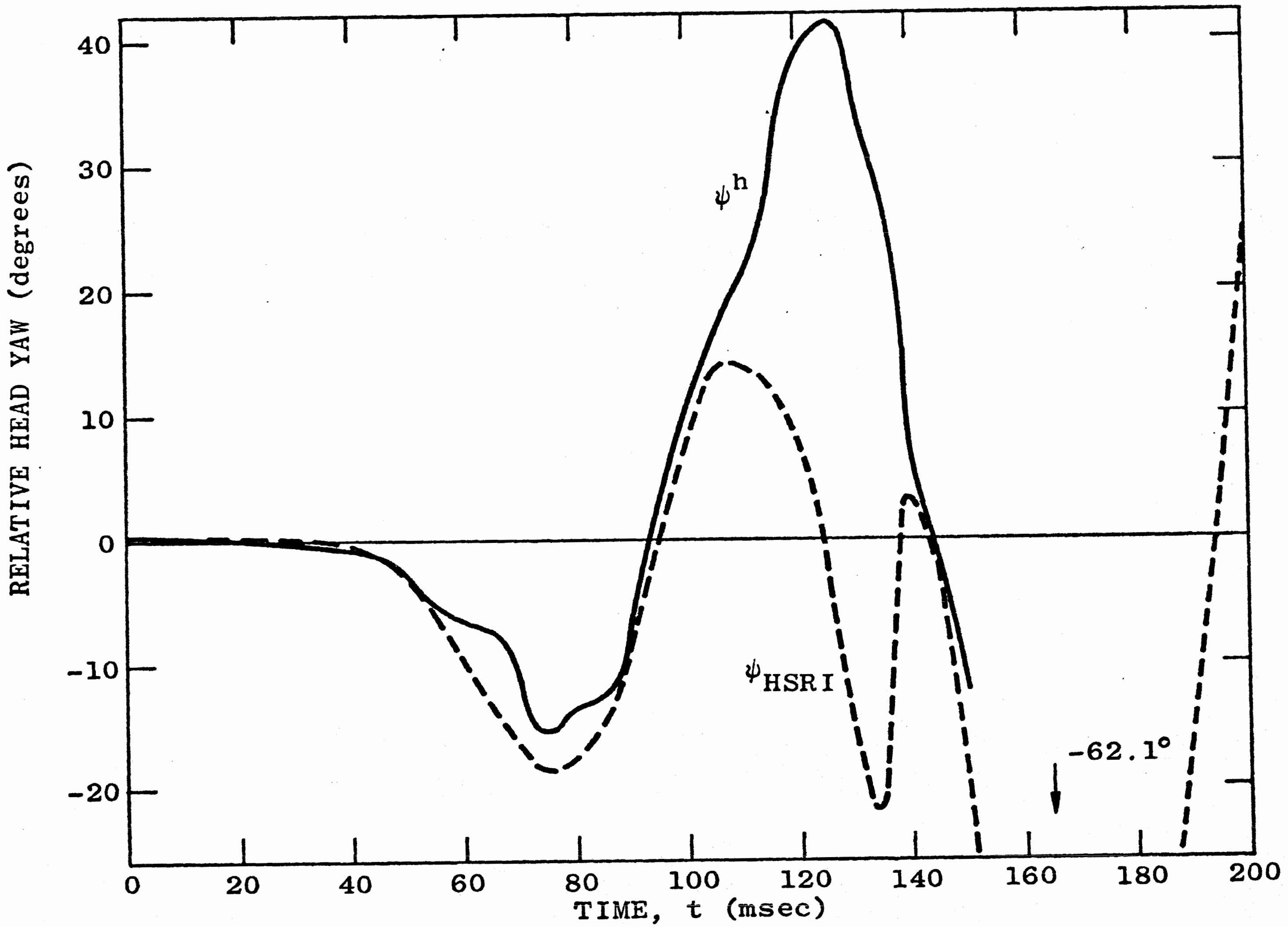

Figure 36. Head yaw relative to torso for side impact: VOM and HSRI 3-D.

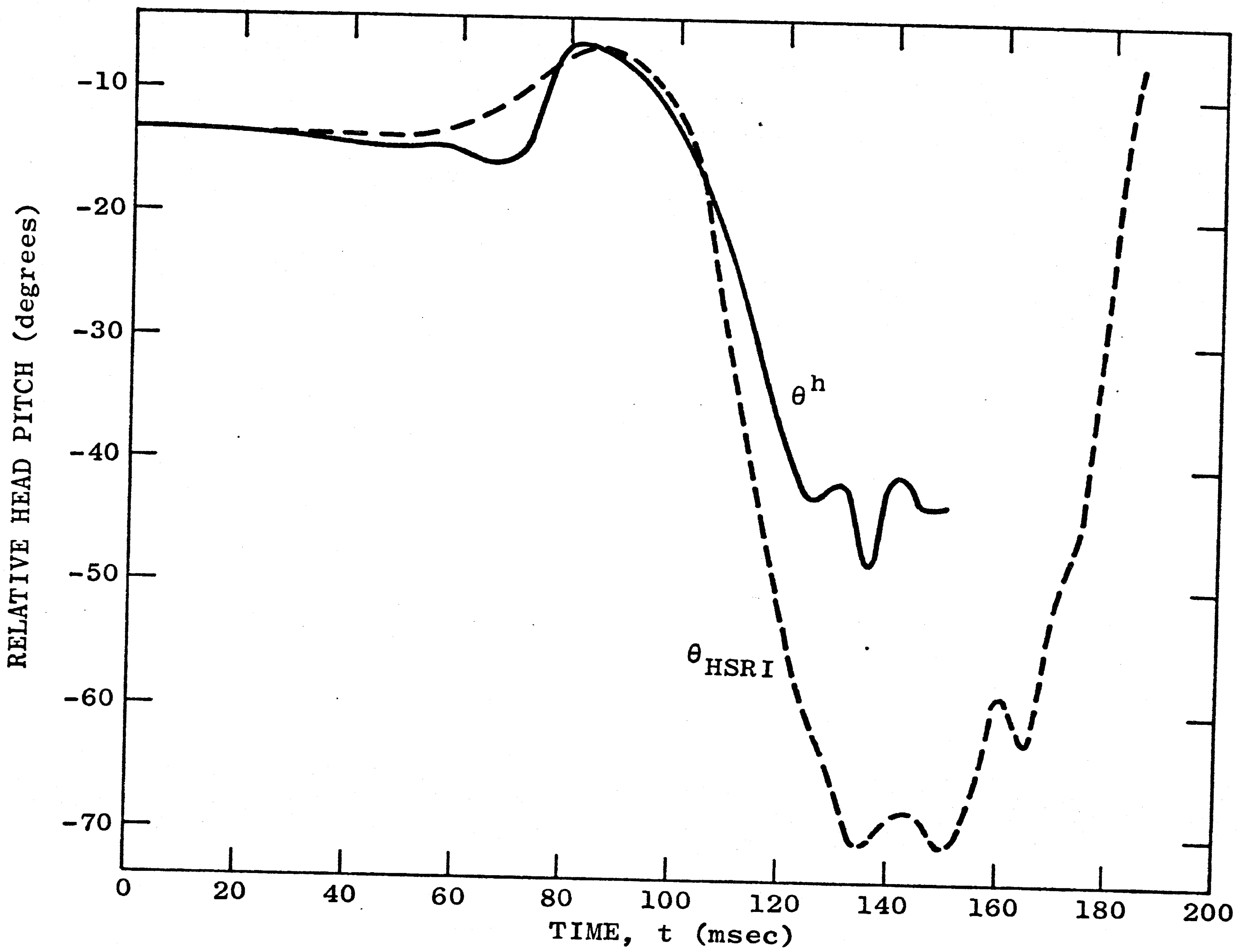

Figure 37. Head pitch relative to torso for side impact: VOM and HSRI 3-D.

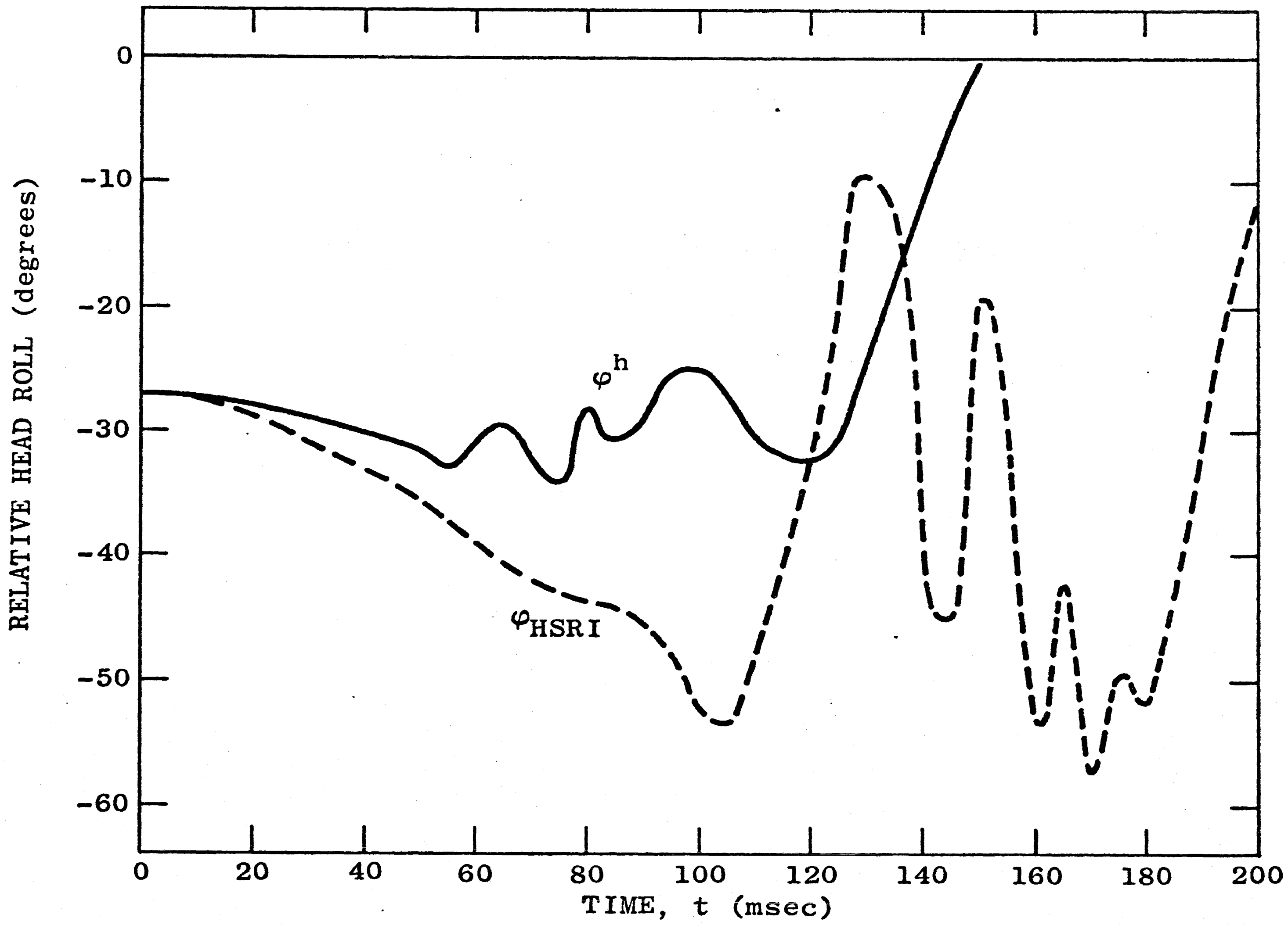

Figure 38. Head roll relative to torso for side impact: VOM and HSRI 3-D.

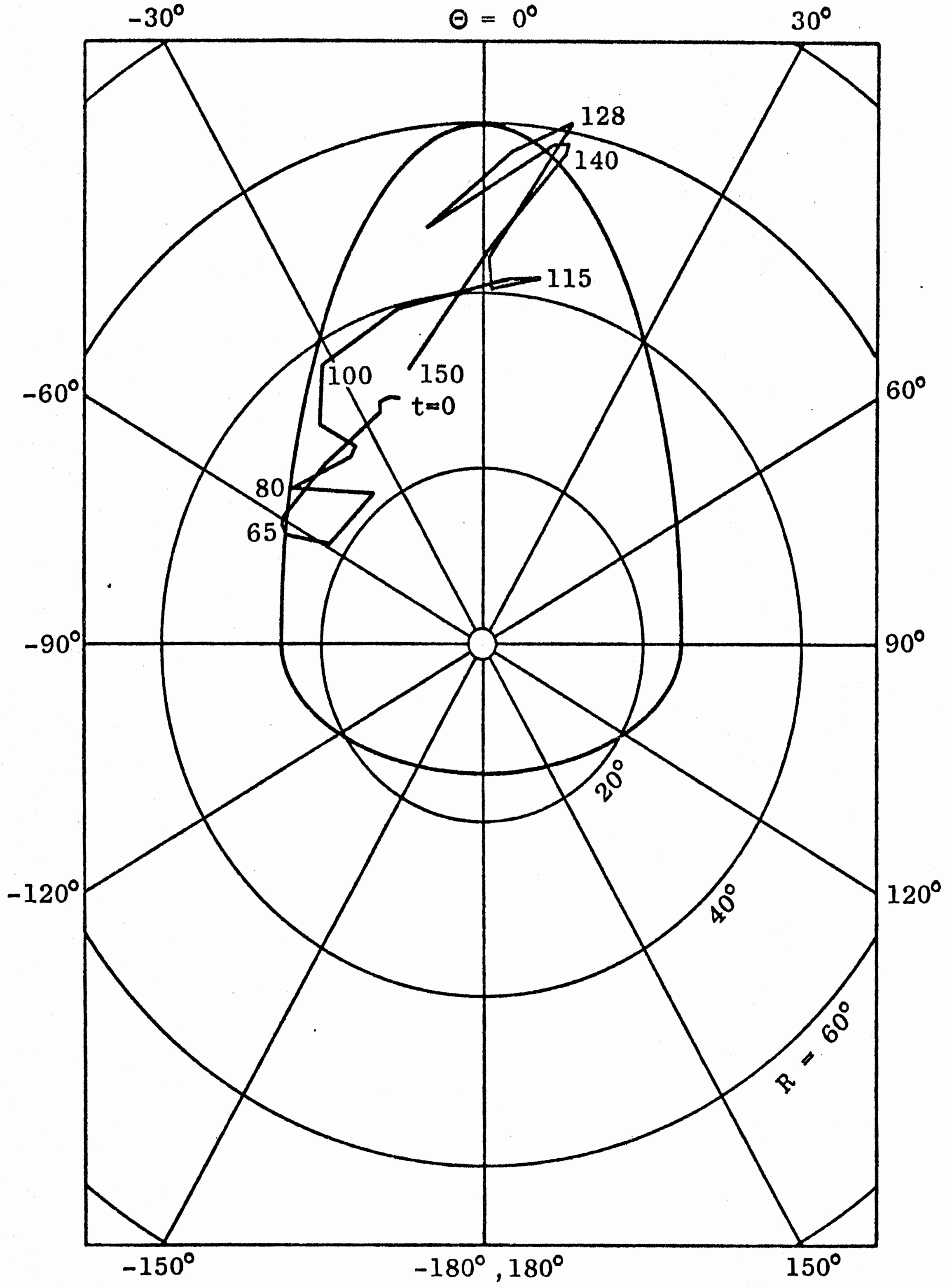

Figure 39. Generalized pitching angle R and heading angle Θ at neck-torso joint (N-T) for side impact.

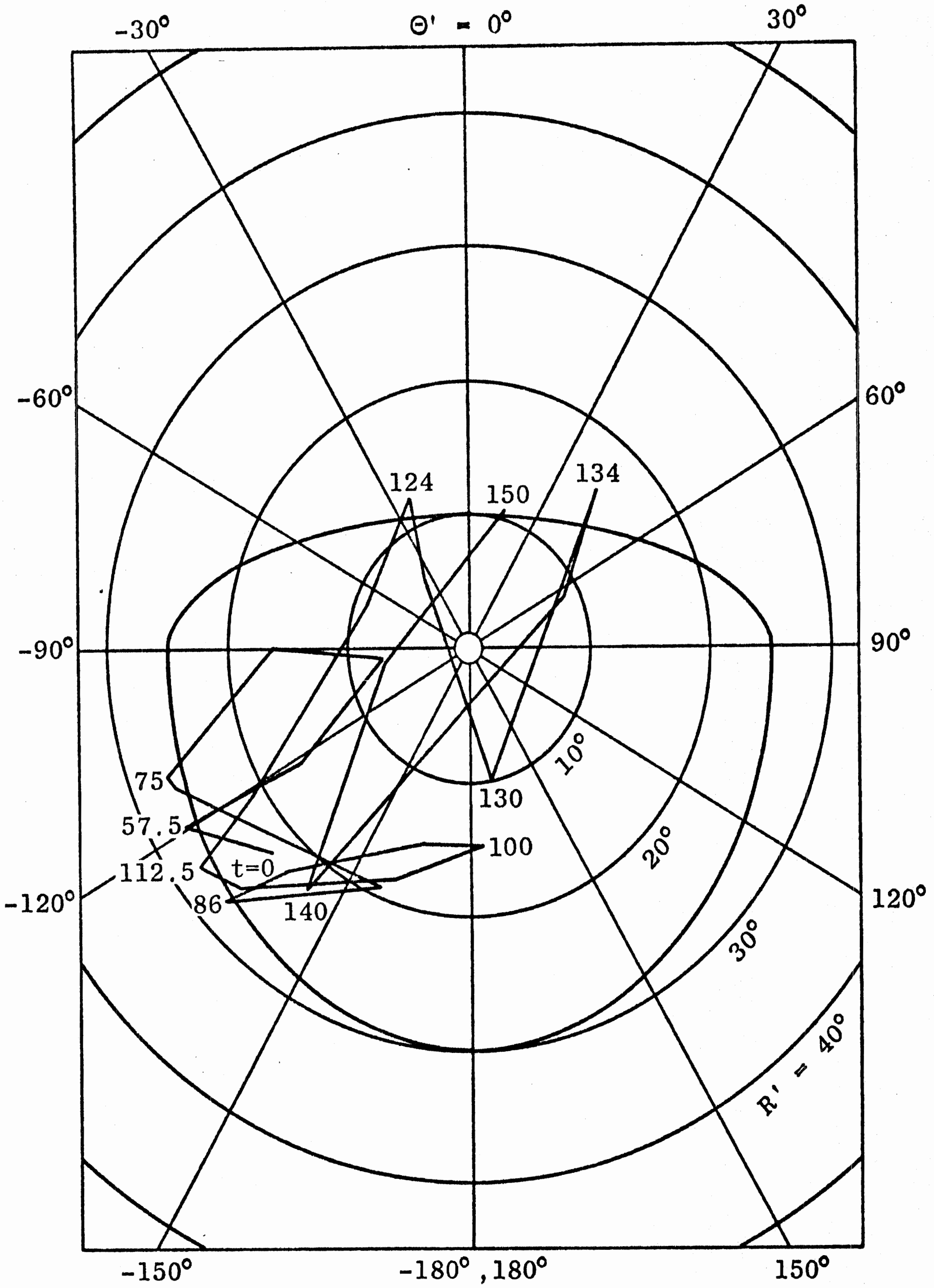

Figure 40. Generalized pitching angle R' and heading angle Θ' at neck-head joint (N-H) for side impact.

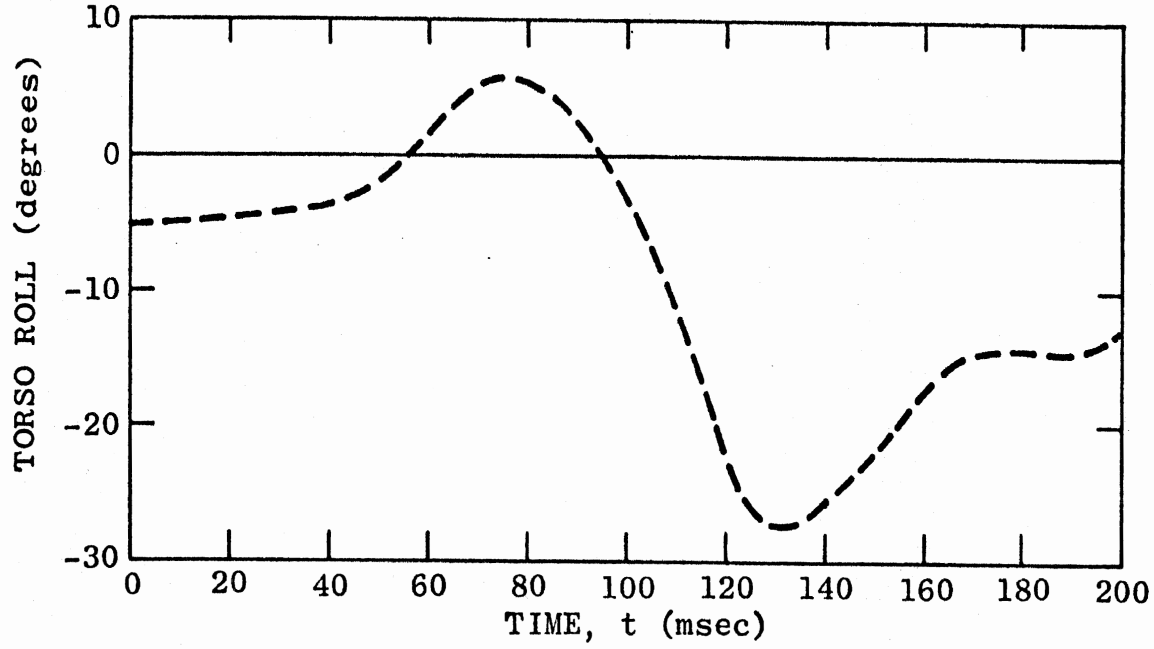

Figure 41. HSRI 3-D torso roll for side impact.

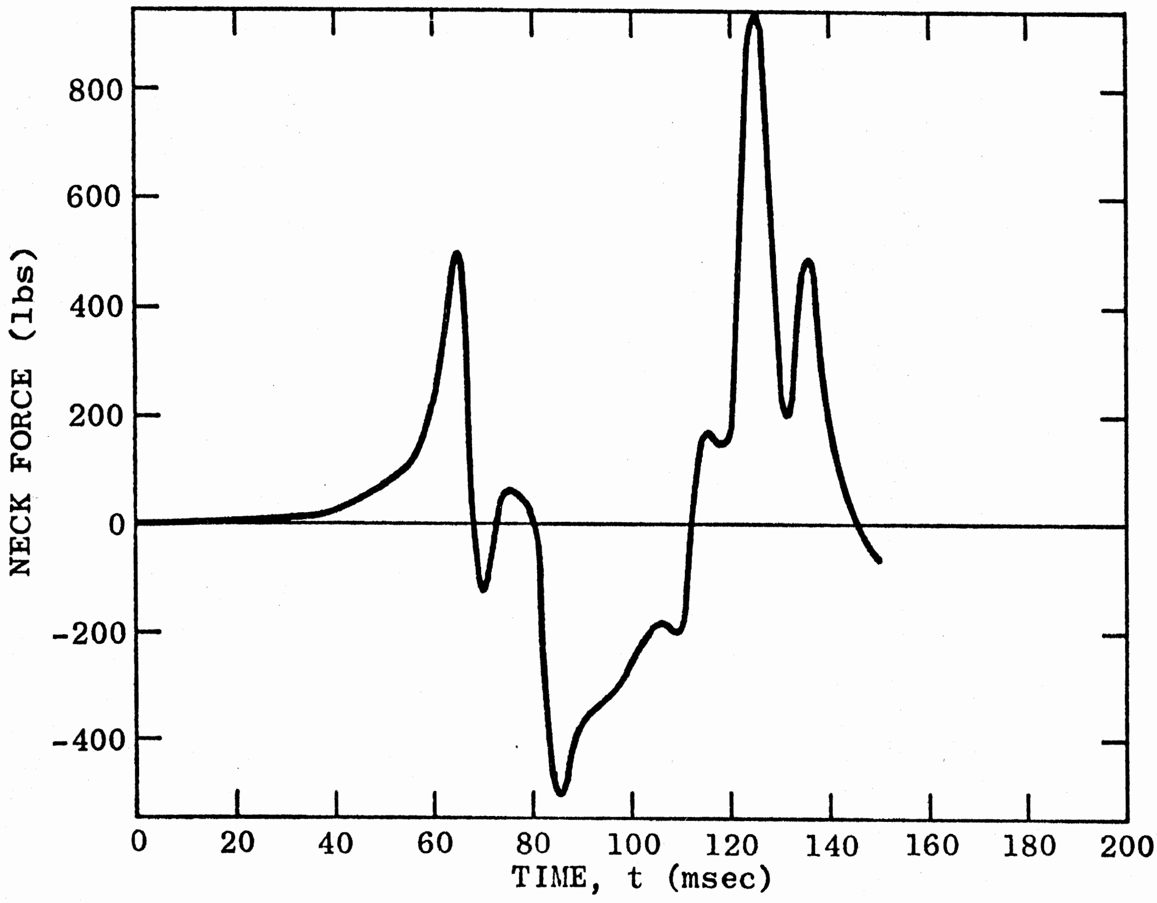

Figure 42. Neck length compression force for side impact.

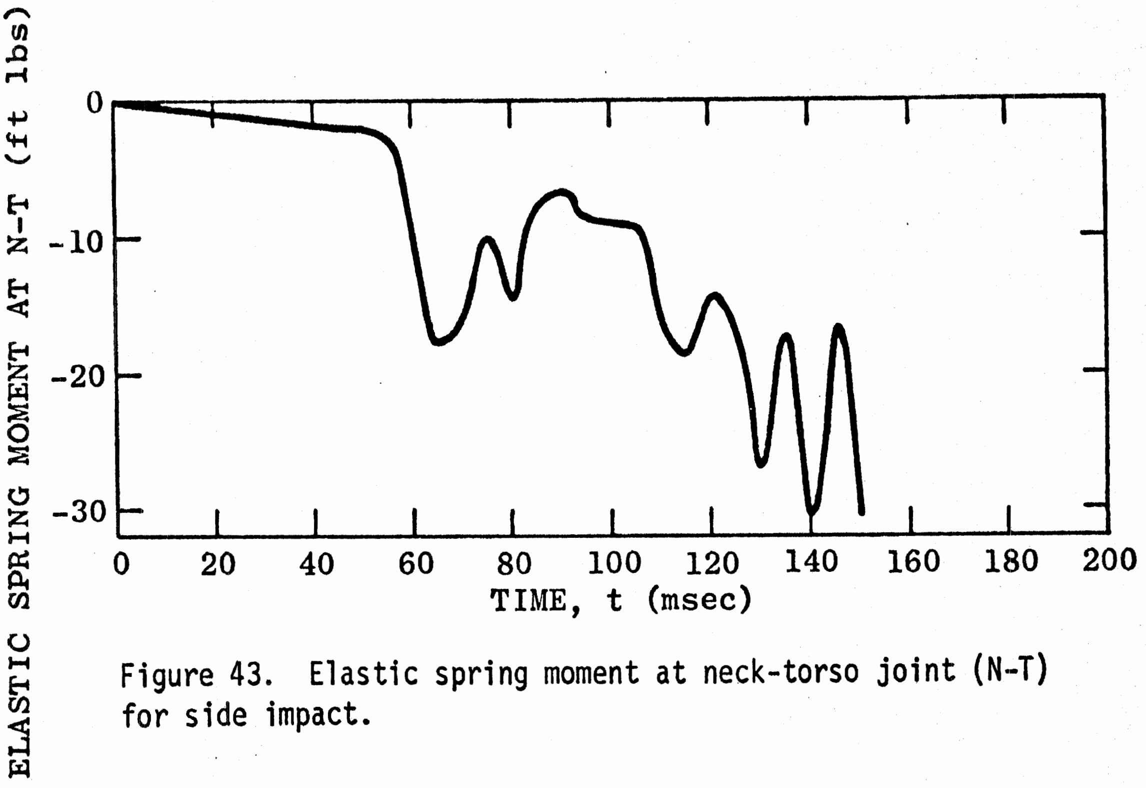

Figure 43. Elastic spring moment at neck-torso joint (N-T) for side impact.

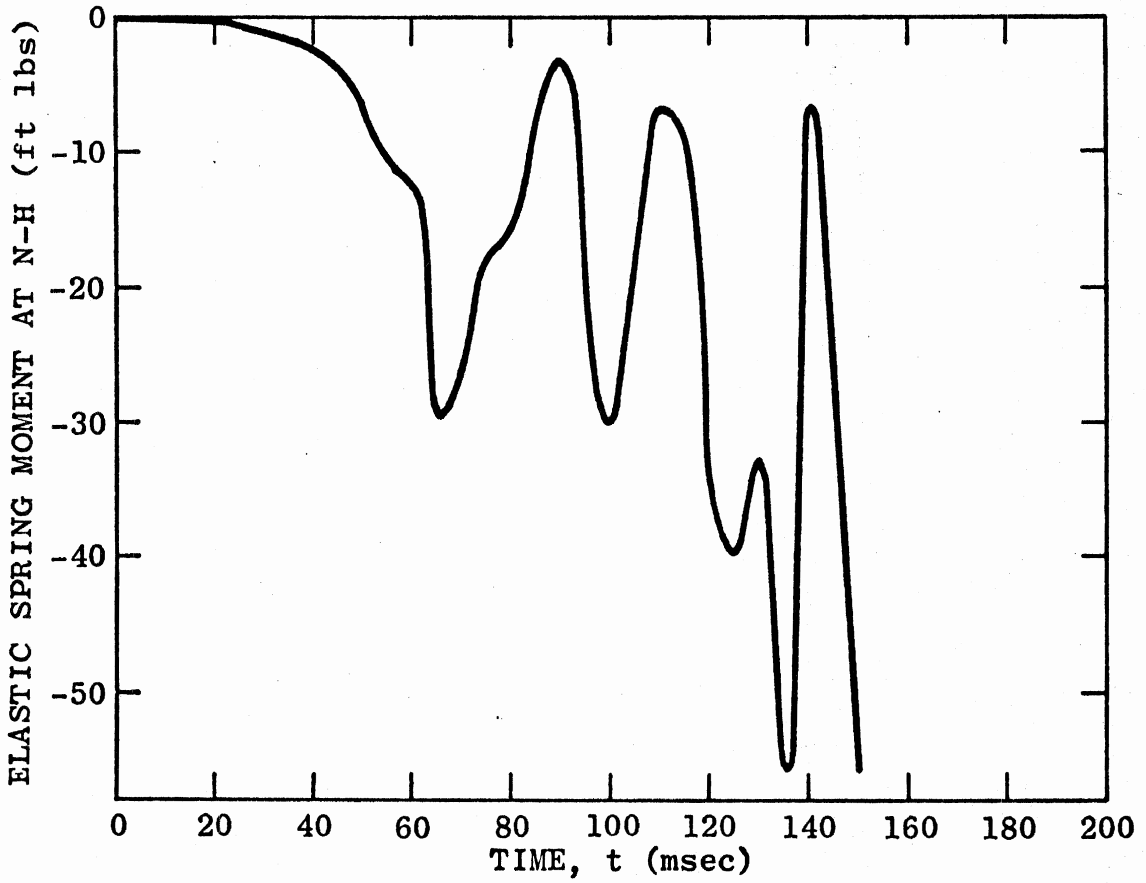

Figure 44. Elastic spring moment at neck-head joint (N-H) for side impact.

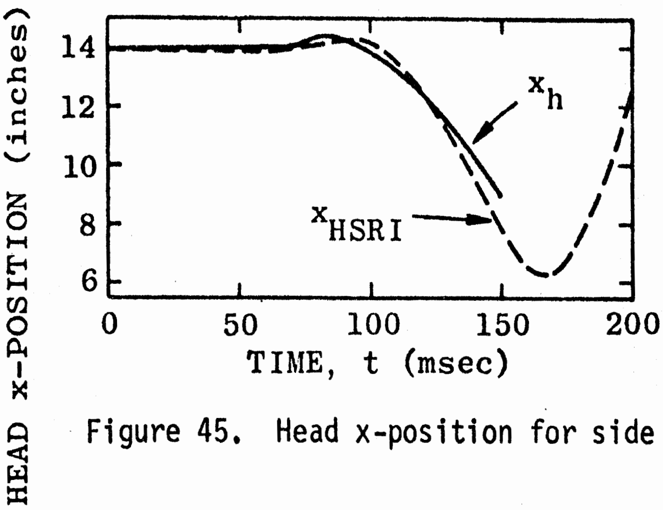

Figure 45. Head x-position for side impact.

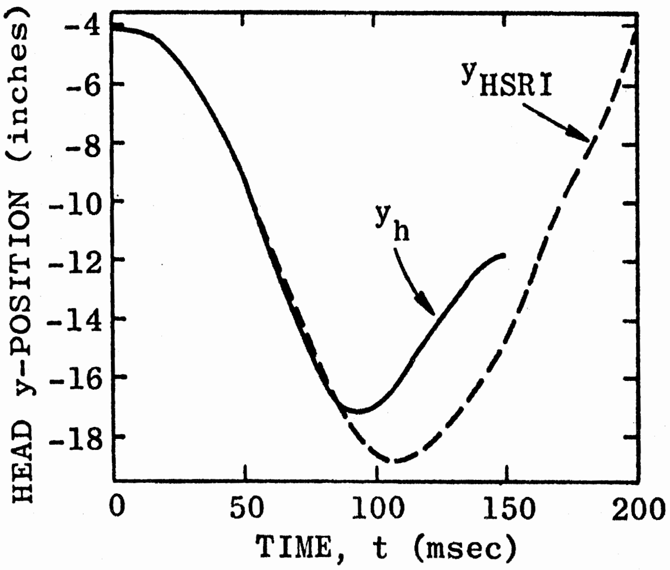

Figure 46. Head y-position for side impact.

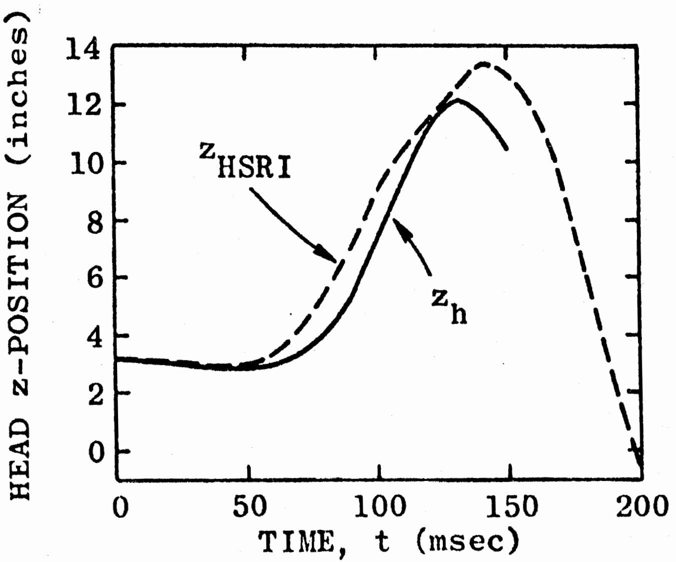

Figure 47. Head z-position for side impact.

10.3 SIDE IMPACT WITH ZERO ELASTIC NECK MOMENTS

The vehicle occupant computer model was exercised for a second side impact essentially the same as the one discussed in Section 10.2. The purpose of this exercise was to evaluate the relative contributions to the overall motion of the elastic moments and the joint stop moments, so all elastic coefficients were set to zero. The same torso excitation used for the side impact of the preceding section was used here.

This test was first made with unchanged values for the joint stop coefficients, but the values were later halved. Since the elastic springs tend to restore the initial relative orientation of the neck linkage, an effect that they have is to reduce the severity of the impact at a joint stop (especially the first impact). With elastic neck moments equal to zero the original set of joint stop coefficients caused the motion to be reversed too fast for the integration to follow, i.e., ten halvings of the original time step were insufficient to produce the accuracy required. This difficulty could have been handled easily by 1) reducing the size of the original time step, 2) allowing more than ten halvings of the integration step size, or 3) slightly reducing the requirement on accuracy. As the first two options involve added cost and since compromising the accuracy of the integration may not be desirable, the stops were instead softened by a factor of 2. Simple order-of-magnitude approximations on the basis of joint stop potential energy and moments suggest that maximum deformations for the softer stops will be greater by only a factor of about $\sqrt{2}$ with corresponding moments reduced by the same factor. The motions otherwise are probably not greatly different.

Head motion for the side impact with zero elastic neck coefficients is compared with the side impact motion of Section 10.2 in Figures 48 to 53. Setting elastic coefficients to zero is seen to affect the yaw motion more markedly than the pitch and roll motions. This is explained by the fact that the yaw stop angle moment (for H-T) is identically zero for both cases, the neck twist stop angle of 60° never being reached; elastic yaw moment thus plays a predominant role in influencing the yaw motion. Pitch and roll motions, on the otherhand, are affected significantly by activity at the generalized pitching angle stops, and elastic moments therefore make a smaller relative contribution.

The angular motion at N-T and N-H as shown in Figures 54 and 55 is generally similar to the motion of Figures 39 and 40. The motion is somewhat less complex, however, since elastic moments are not continuously pulling the neck linkage toward its original relative orientation. These figures show greater joint stop activity at the atlanto-occipital articulation (N-H) than at the seventh-cervical/first-thoracic vertebral articulation (N-T), as do Figures 39 and 40.

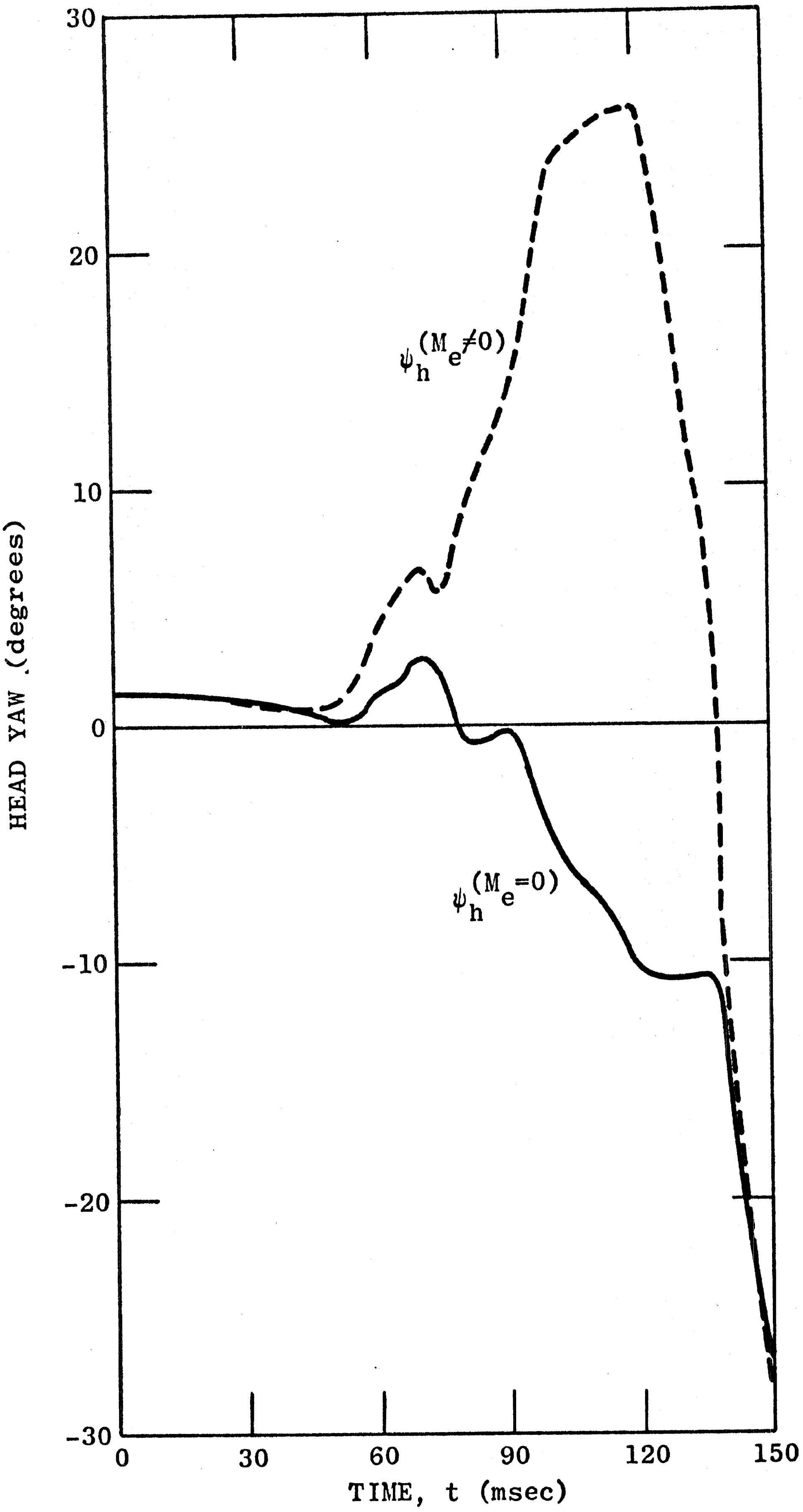

Figure 48. Head yaw for side impact, with and without elastic neck moments.

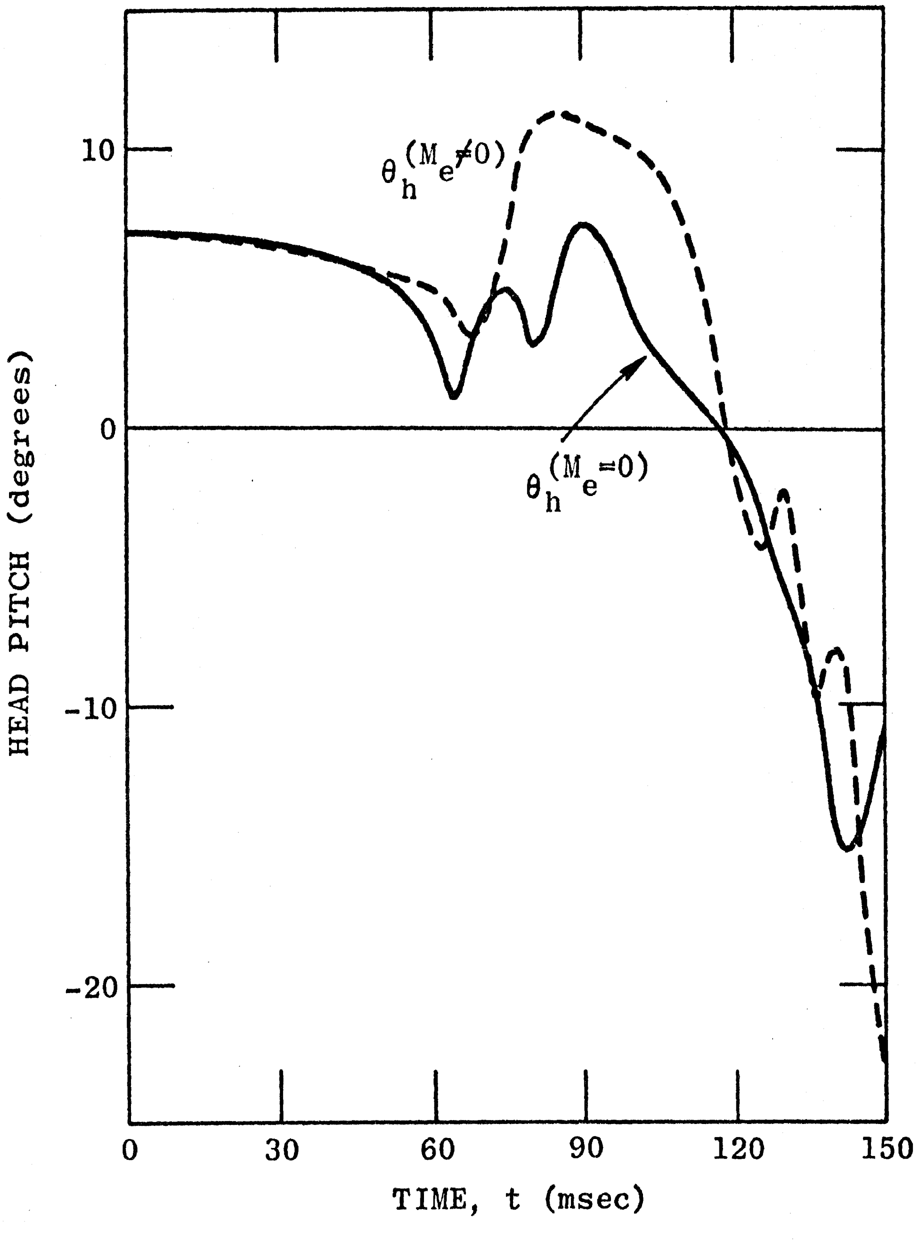

Figure 49. Head pitch for side impact, with and without elastic neck moments.

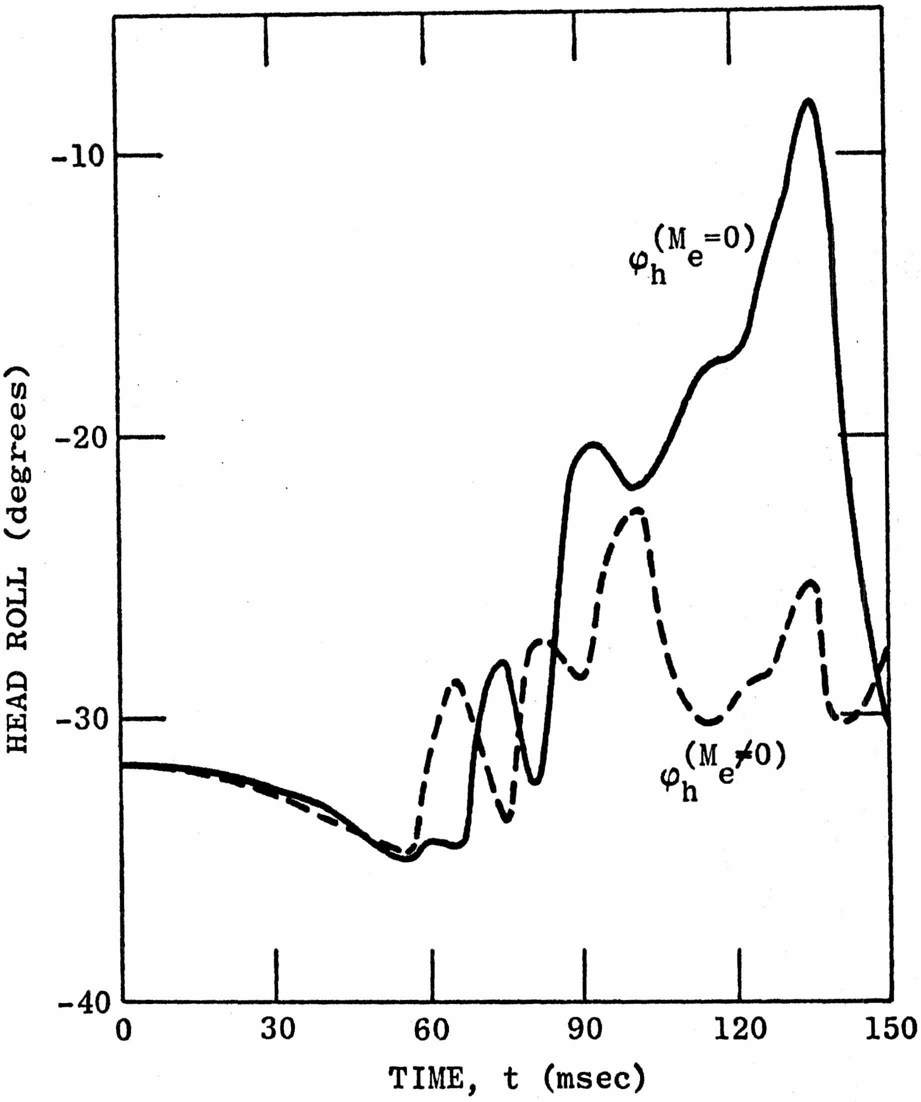

Figure 50. Head roll for side impact, with and without elastic neck moments.

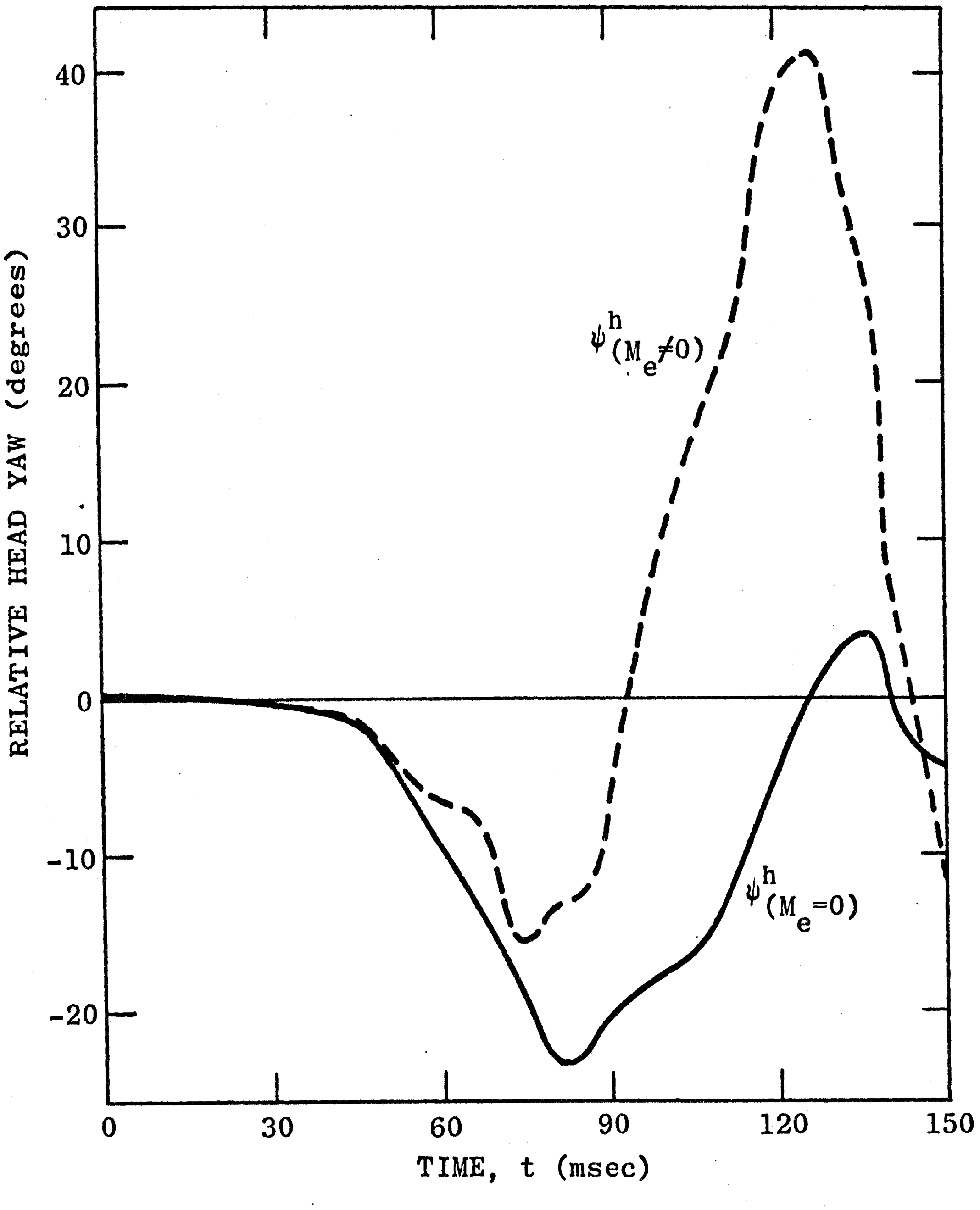

Figure 51. Relative head yaw for side impact, with and without elastic neck moments.

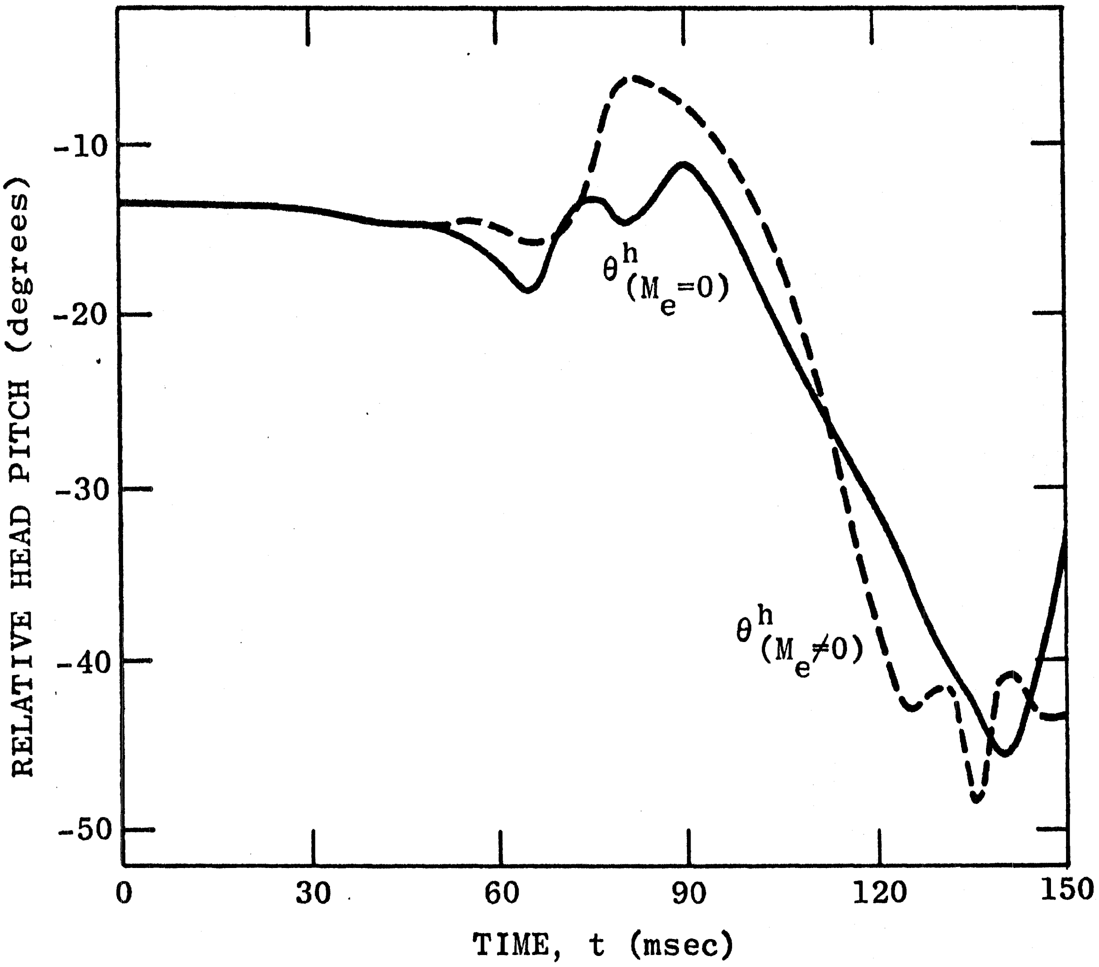

Figure 52. Relative head pitch for side impact, with and without elastic neck moments.

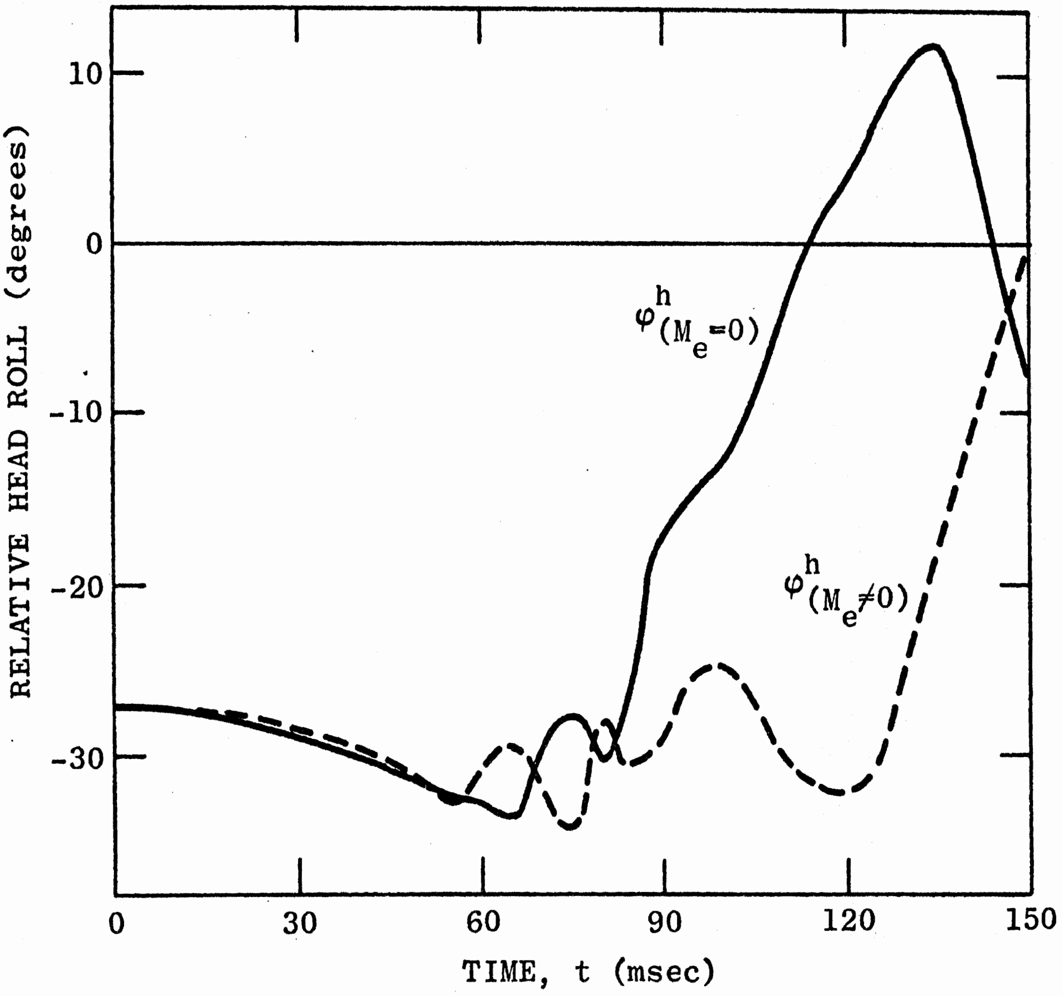

Figure 53. Relative head roll for side impact, with and without elastic neck moments.

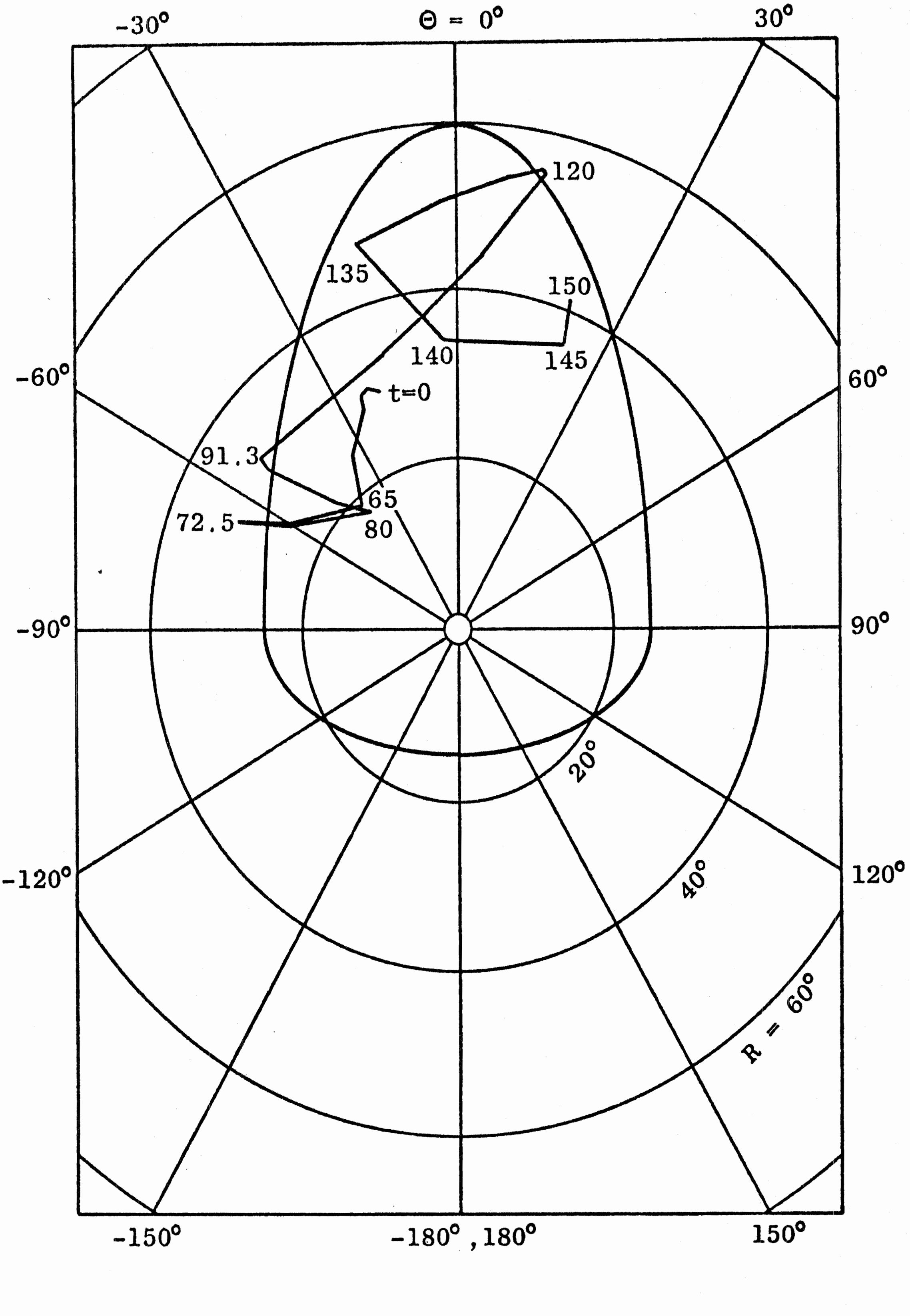

Figure 54. Generalized pitching angle R and heading angle Θ at neck-torso joint (N-T) for side impact, with zero elastic neck moments.

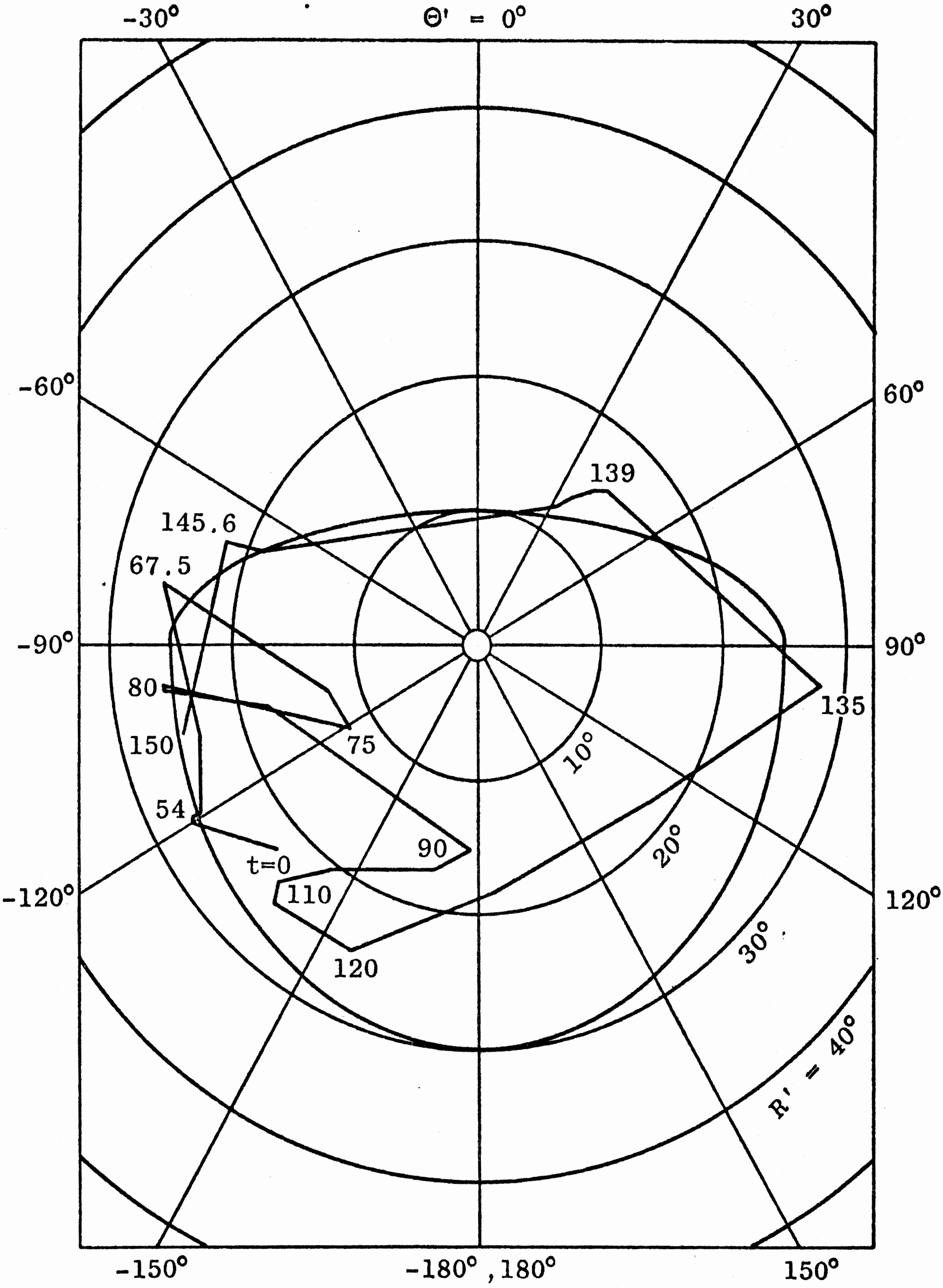

Figure 55. Generalized pitching angle R' and heading angle Θ' at neck-head joint (N-H) for side impact, with zero elastic neck moments.

10.4 SIDE IMPACT WITH NON-ZERO MUSCLE TENSION

It is generally recognized that muscle contraction can reduce the severity of likelihood of at least some types of injury in potentially traumatic situations. Hollister, Jolley, and Horne (33) produced cerebral concussion in cats by impulsive cervical stretch alone and demonstrated a clear reduction in the incidence of concussion when the neck muscles were tetanized by an electrical stimulus. Their investigation indicated that stretching of the cervical spinal cord was the probable cause of concussion. There is much debate, however, on the mechanism of concussion, and indeed there may be more than one mechanism. Several investigators have shown in experiments with animals that brain injury can be produced by rotational accelerations of the skull (2, 3, 34, 35, 36, 37). Since muscle contraction, or "tension", can be expected to reduce such accelerations in many situations, it must also effect a reduction in associated brain damage. Spinal injuries and a great variety of other injuries are produced by extreme relative rotation of body elements (3). Muscle tension should cause a reduction in these injuries as well. Mertz (4) concluded from his experiments with a volunteer that tensing of the muscles before a rear-end collision would reduce the severity of whiplash injury.

In order to investigate the effects of muscle tension in the vehicle occupant model the side impact test of Section 10.3 (zero elastic neck moments) was repeated with non-zero muscle tension parameter values. Appropriate parameter values for the neck are not available in the literature, but Moffatt, Harris, and Haslam (24) give experimentally determined values for the knee joint. These values were used along with other available experimental data to obtain rough, order-of-magnitude values for corresponding neck quantities. This analysis is presented in Appendix E. The numerical results of that analysis are summarized below. The notation is the same as in Section 3.3.3.

$a_1^{(R)} = a_1^{(R')} = 0.0129$ sec/deg

$a_2^{(R)} = a_2^{(R')} = 0.123$ ft.lb/deg

$a_3^{(R)} = a_3^{(R')} = 0.153$/deg

$a_1^{(\psi^h)} = 0.0129$ sec/deg

$a_2^{(\psi^h)} = 0.0308$ ft.lb/deg

$a_3^{(\psi^h)} = 0.153$/deg

$a_1^{(\ell)} = 4.44$ sec/ft

$a_2^{(\ell)} = 508$ lb/ft

$a_3^{(\ell)} = 52.7$/ft

$|M_{max}^{(R)}| = |M_{max}^{(R')}| = 17.5$ ft.lb

$|M_{max}^{(\psi^h)}| = 4.375$ ft.lb

$|F_{max}^{(\ell)}| = 210$ lb

The above bioparameter values, a_i, were adopted. For a particular (living) vehicle occupant these values are constants. The muscle tension parameters, $|M|$ and $|F|$, can be between zero and the indicated maximum values although they must be constants for the duration of a given crash. Moment values, M, for N-T, N-H, and H-T were selected for near maximum muscle contraction: 16.0, 16.0, and 4.0 ft.lb, respectively. The effect of muscle tension for the neck length was not investigated in this exercise, $F^{(\ell)}$ being set to zero.

Inertial and relative head Euler angles are shown in Figures 56 to 61. (The subscripts "MT" indicate "muscle tension.") The differences in the curves of Figures 59 to 61 are attributable solely to muscle contraction. The elastic coefficients are zero for each case. Figures 62 to 64 show the moments which result from the contraction of the neck muscles.

Figures 65 to 69 are of particular interest because they show how muscle contraction can limit the extent of injuries caused by extreme relative motion of body elements. Comparison of Figures 65 and 66 with Figures 54 and 55 shows a considerable change in the character of the angular motion at the neck joints. Of more tangible significance from an injury probability standpoint is a comparison of joint stop moments. Moments produced at the hard, anatomical stops should be good indications of the probability and extent of injury.* Neck-torso joint stop moments are shown in Figure 67.** The moments which result from a "relaxed" state (MT = 0) are seen to be considerably greater than for the

---

*Mertz (4, 38) concluded from his investigation that neck torque at the occipital condyles (N-H) was the predominant parameter in evaluating the possibility of neck injury (rather than shear force of axial force).

**The base widths of the spikes are only approximate.

"tensed" state (MT $\neq$ 0). The joint stop moments at N-H for the "relaxed" and "tensed" situations are shown in Figures 68 and 69, respectively. As a rather arbitrary means of indicating the possible effectiveness of muscle contraction in reduction of injury, the average maximum moment values for the spikes of the respective cases have been determined. At N-T the results are -84 ft.lbs and -262 ft.lbs, in favor of muscle contraction. At N-H, the averages are -281 ft.lbs and -399 ft.lbs, in favor of muscle contraction. More properly, joint stop moment spikes below some minimum injury level should probably be omitted from the averaging; and if this is done for *any* level, the averages swing even more to the favor of muscle contraction.

There may also be some indication that concussion resulting from large values of angular acceleration of the head becomes less likely when the neck muscles are tensed prior to impact. The magnitudes of the maximum occurring values for inertial head yaw, pitch, and roll accelerations were about 13%, 183%, and 54% greater, respectively, for the "relaxed" state than for the "tensed" state.* The maximum angular acceleration occurred for roll (relaxed state) - 3.52×10^4 rad/sec^2 at about 135 msec. Ommaya, *et al.* (36), however, have shown that the *duration* of acceleration above a given level affects the probability of concussion. Later work by Ommaya and Hirsch (37) indicates that peak rotational velocity values may be better indicators of concussion probability for acceleration peaks of short duration - less than about 20 msec. Ommaya and Hirsch predict that the 50% concussion probability level for long duration rotational acceleration (for man) is about 1800 rad/sec^2. Although maximum acceleration values for the VOM exercises with and without muscle tension exceed this value several times during the crash (in one instance reaching twenty times that value), at no time in either exercise does an acceleration peak remain above 1800 rad/sec^2 for longer than about 5 msec. Comparison of peak rotational velocity values for the two side impact tests may therefore be the better way of evaluating the effect of muscle contraction in regard to concussion. On this basis muscle contraction is not clearly shown to be beneficial, maximum yaw, pitch, and roll velocities for the "relaxed" state being 68%, 98%, and 189% of the "tensed" state values. It should be noted, however, that no values exceed 36.4 rad/sec and that calculations based on values given by Ommaya and Hirsch indicate a 50% concussion probability threshold for rotational velocity of about 57 rad/sec. (A value of 70 rad/sec is given by Ommaya and Hirsch for chimpanzees.)

---

*The angular accelerations $\dot{\alpha}_h$, $\dot{\beta}_h$, and $\dot{\gamma}_h$ would be somewhat better indicators. They were calculated but not printed out.

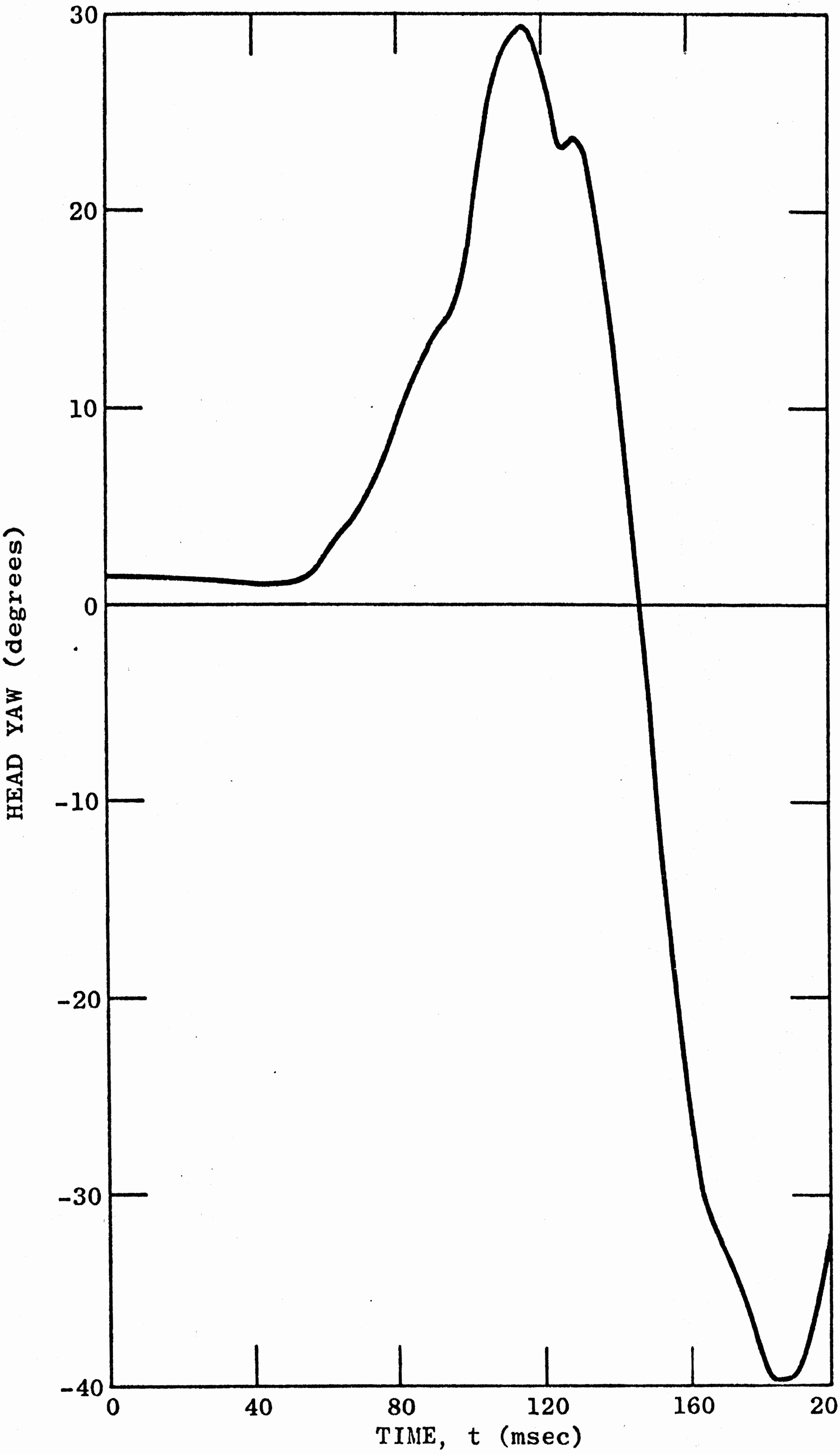

Figure 56. Head yaw for side impact with non-zero muscle tension.

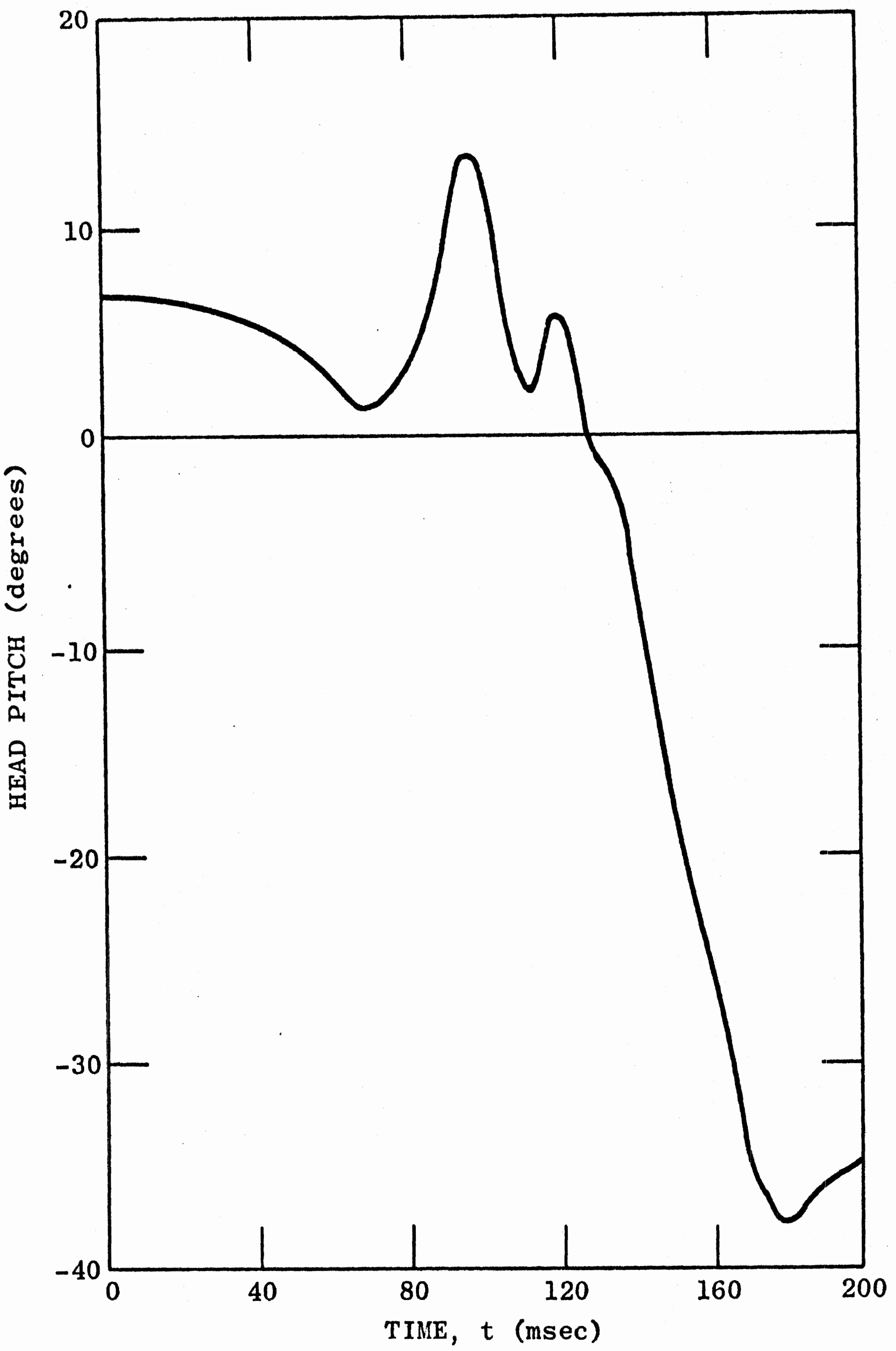

Figure 57. Head pitch for side impact with non-zero muscle tension.

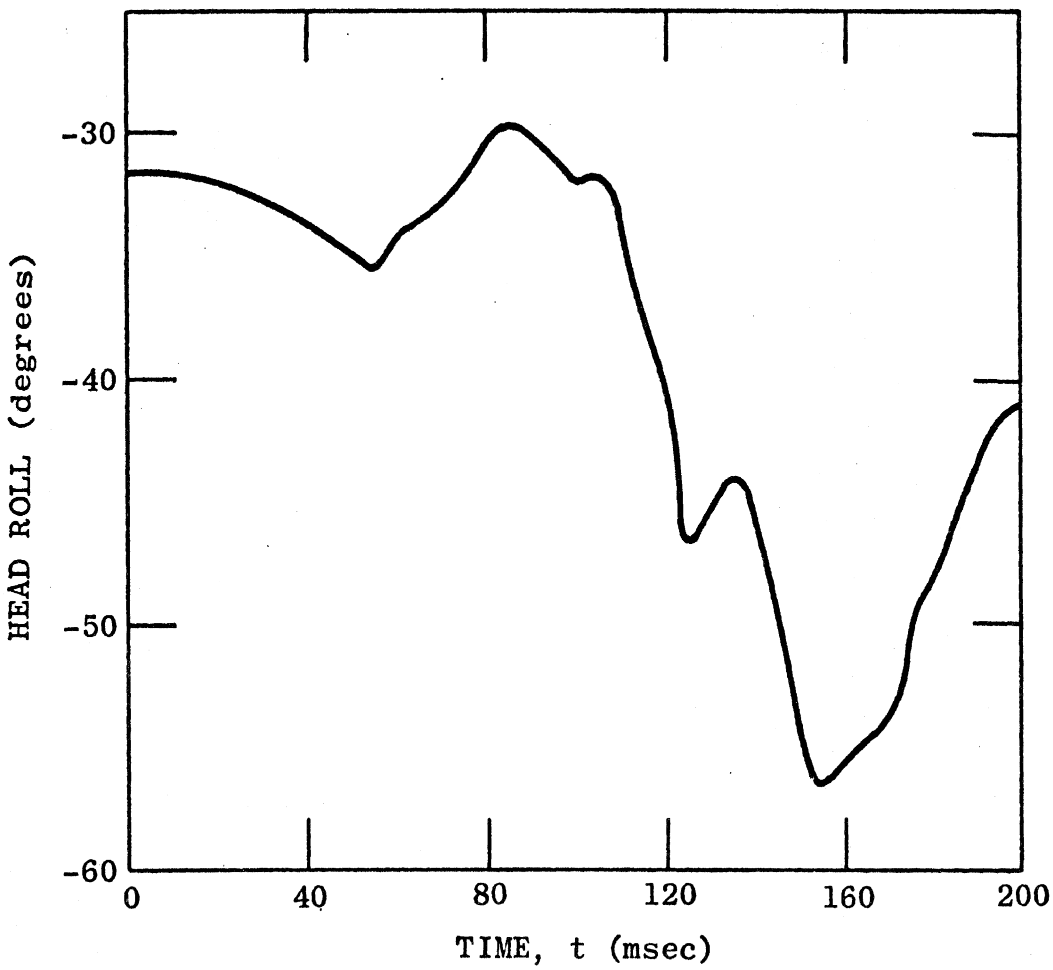

Figure 58. Head roll for side impact with non-zero muscle tension.

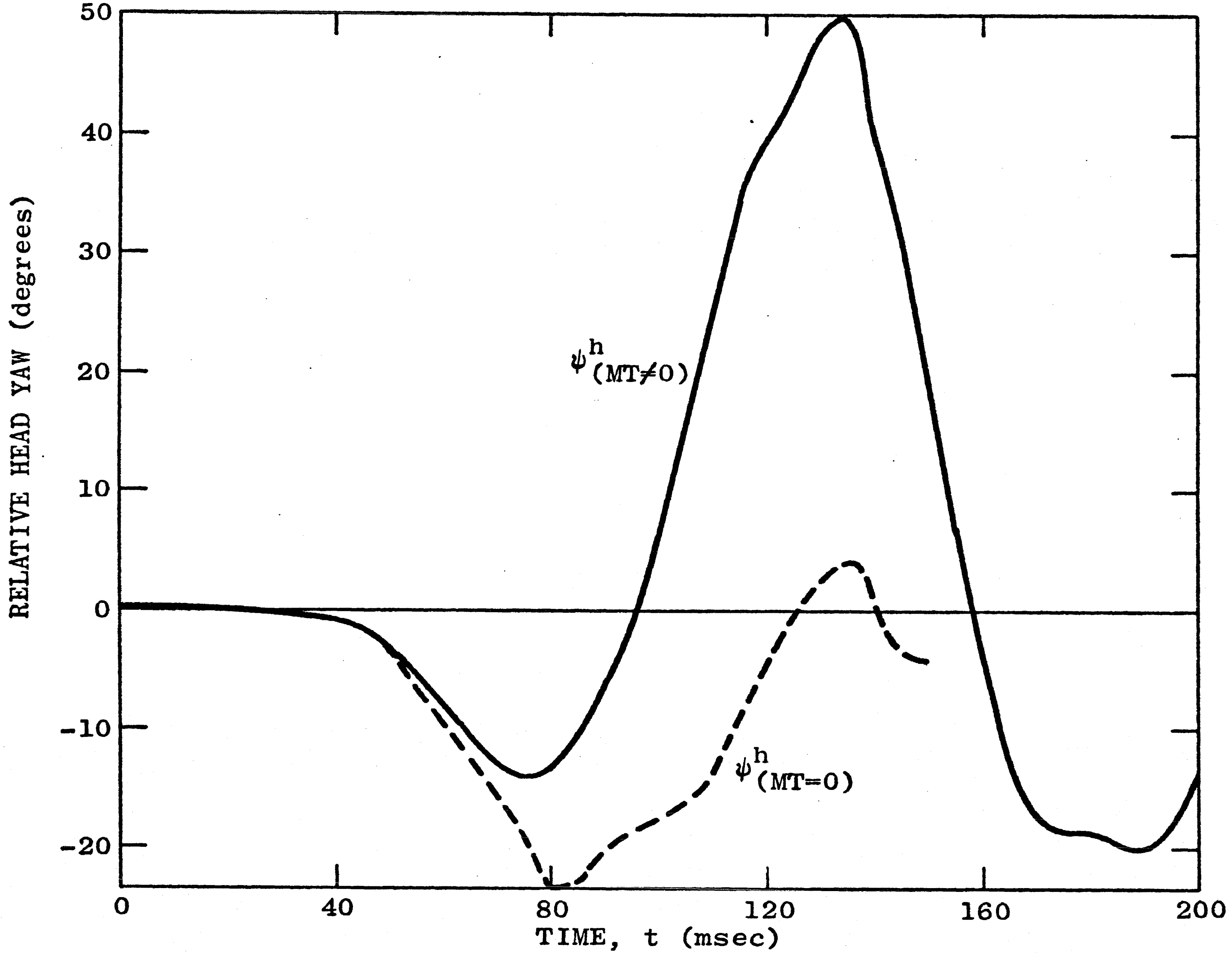

Figure 59. Relative head yaw for side impact with non-zero muscle tension.

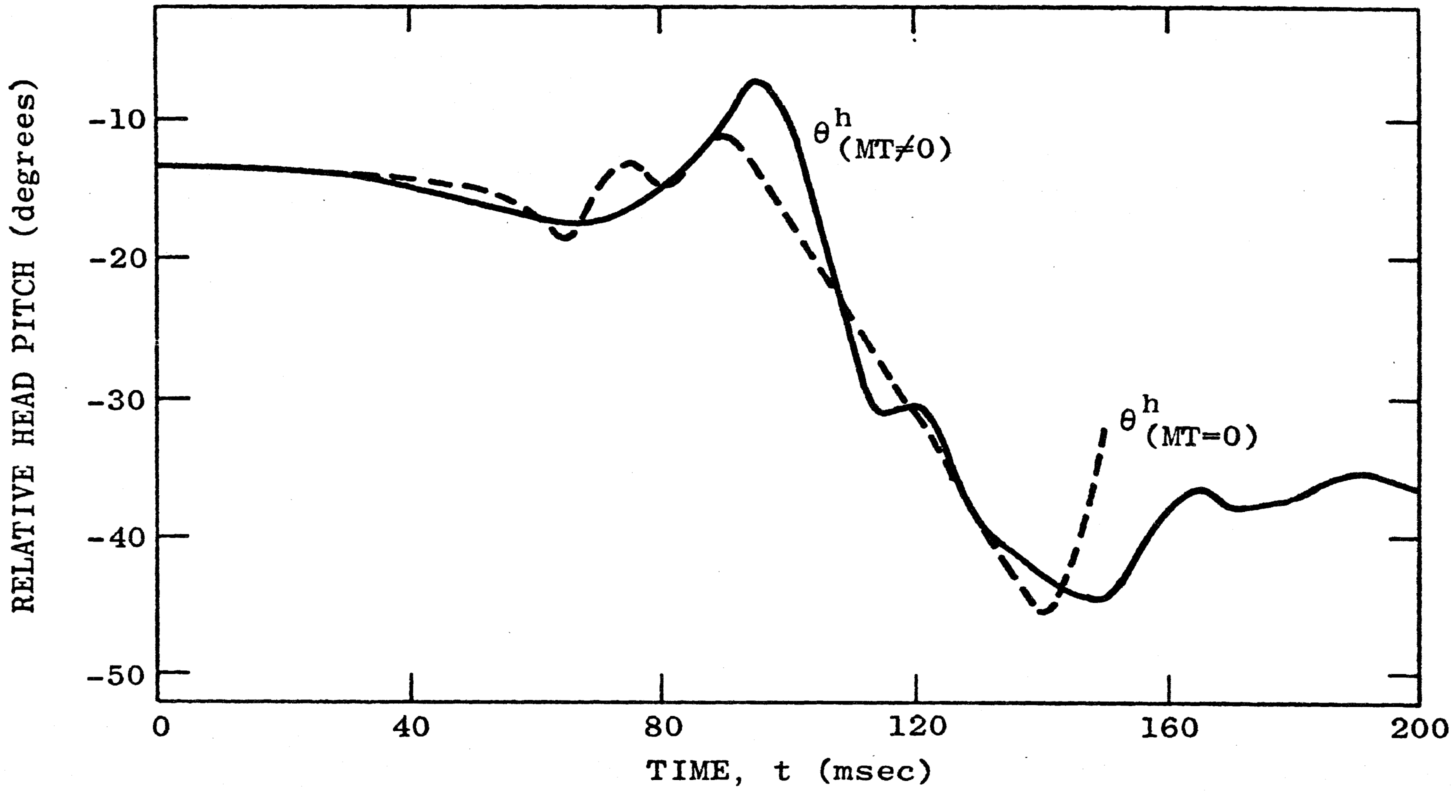

Figure 60. Relative head pitch for side impact with non-zero muscle tension.

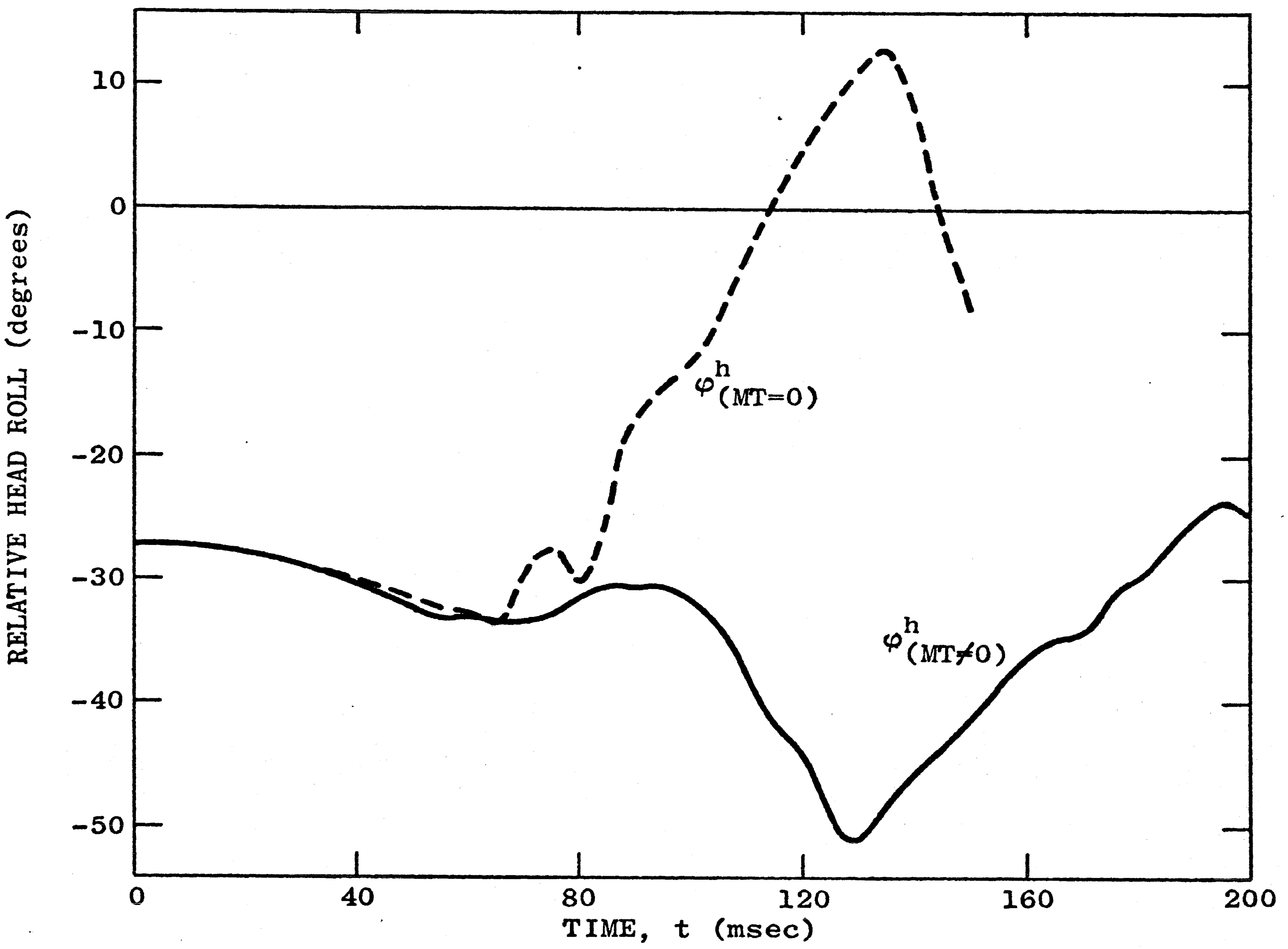

Figure 61. Relative head roll for side impact with non-zero muscle tension.

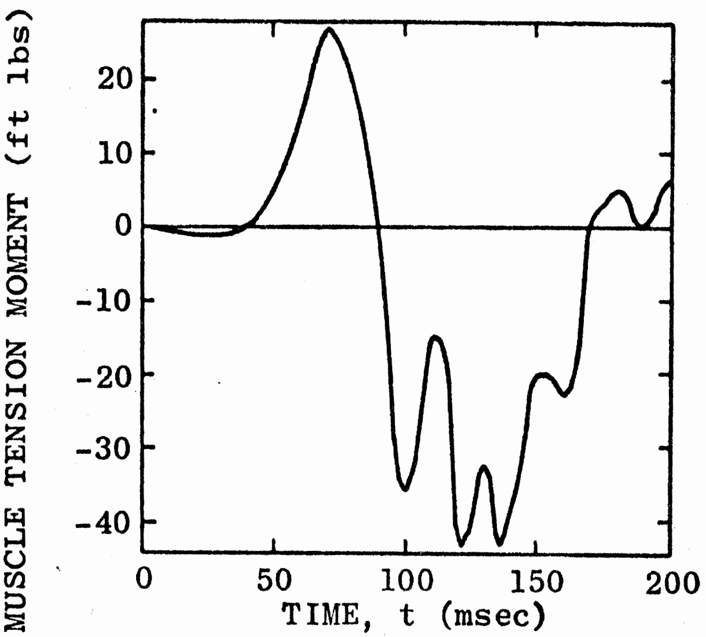

Figure 62. Muscle tension moment for generalized pitching at the neck-torso joint (N-T).

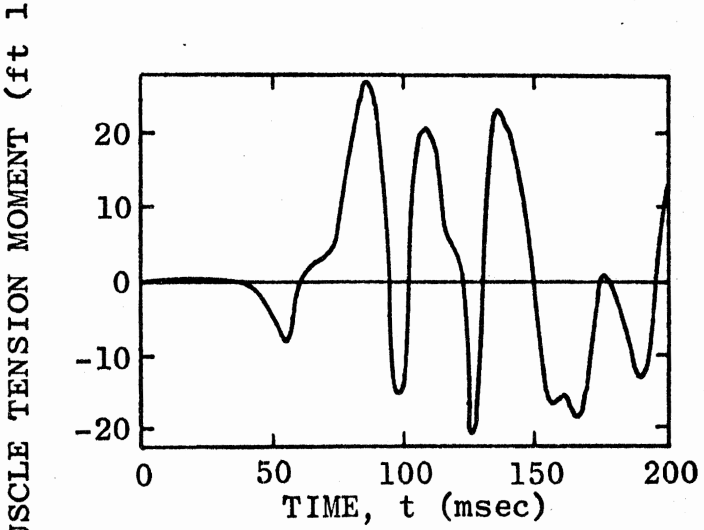

Figure 63. Muscle tension moment for generalized pitching at the neck-head joint (N-H).

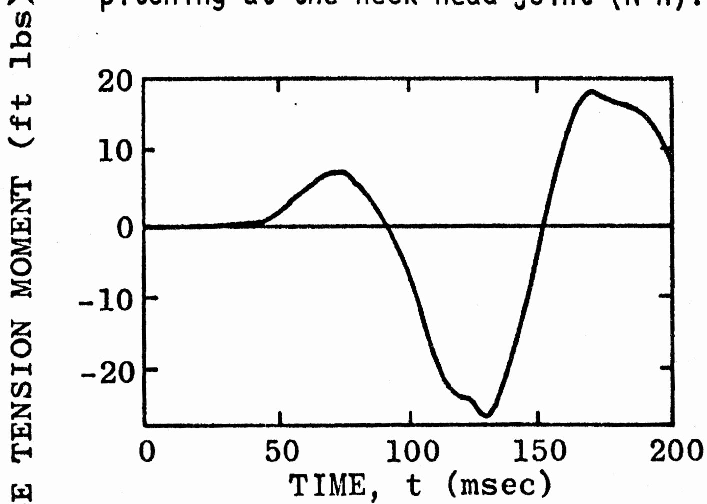

Figure 64. Muscle tension moment for twisting at the head-torso joint (H-T).

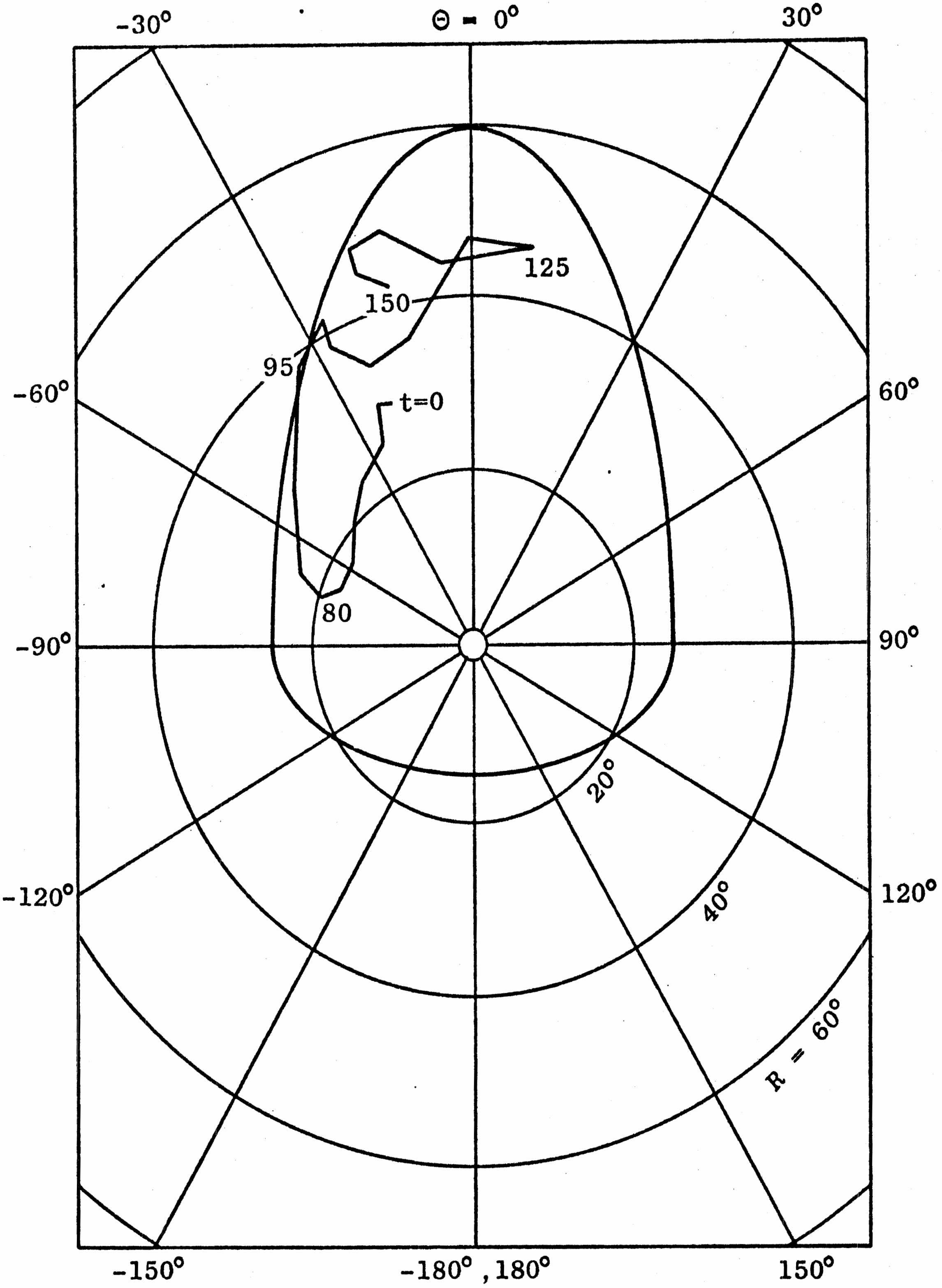

Figure 65. Generalized pitching angle R and heading angle Θ at neck-torso joint (N-T) for side impact, with non-zero muscle tension.

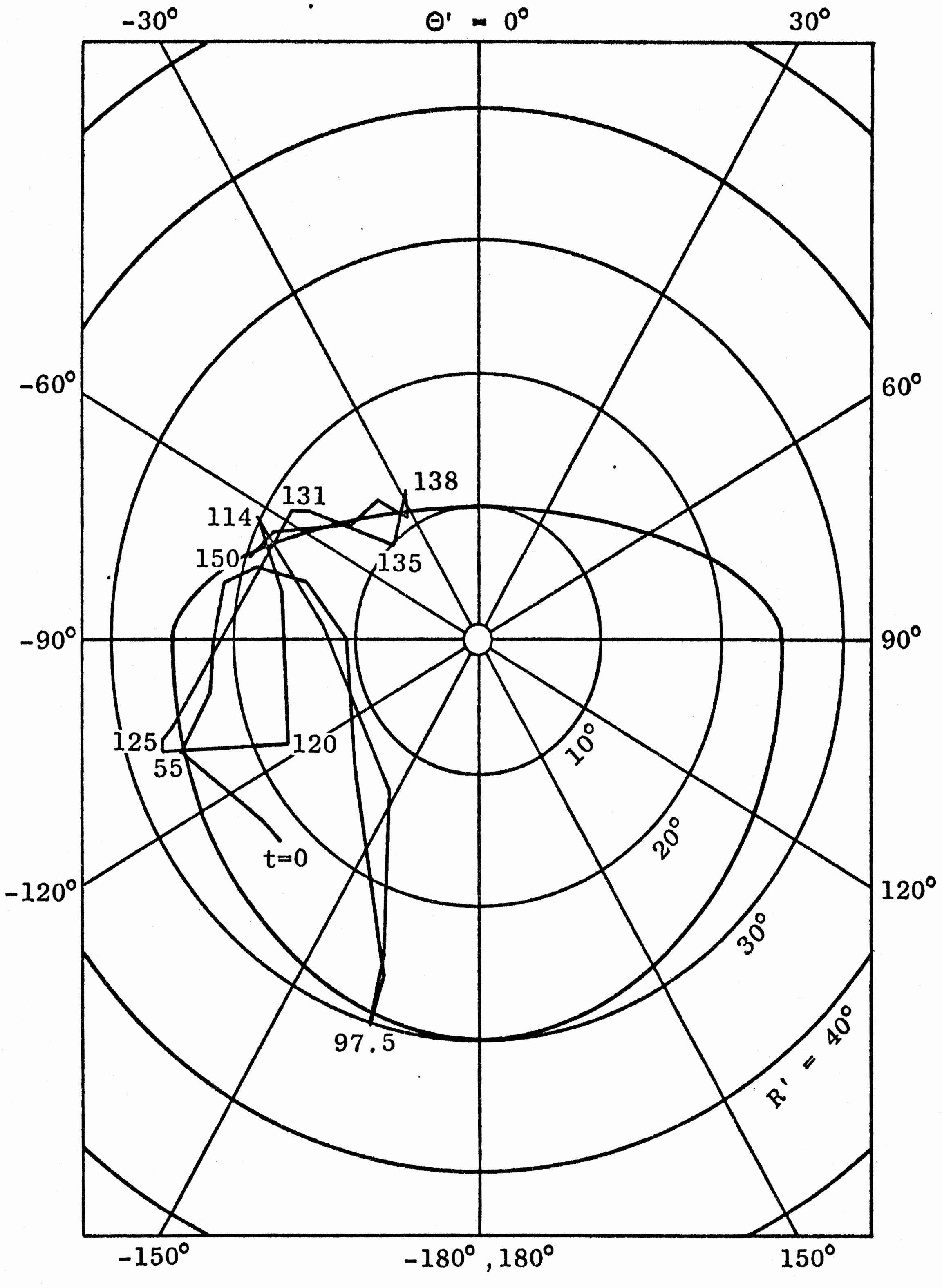

Figure 66. Generalized pitching angle R' and heading angle Θ' at neck-head joint (N-H) for side impact, with non-zero muscle tension.

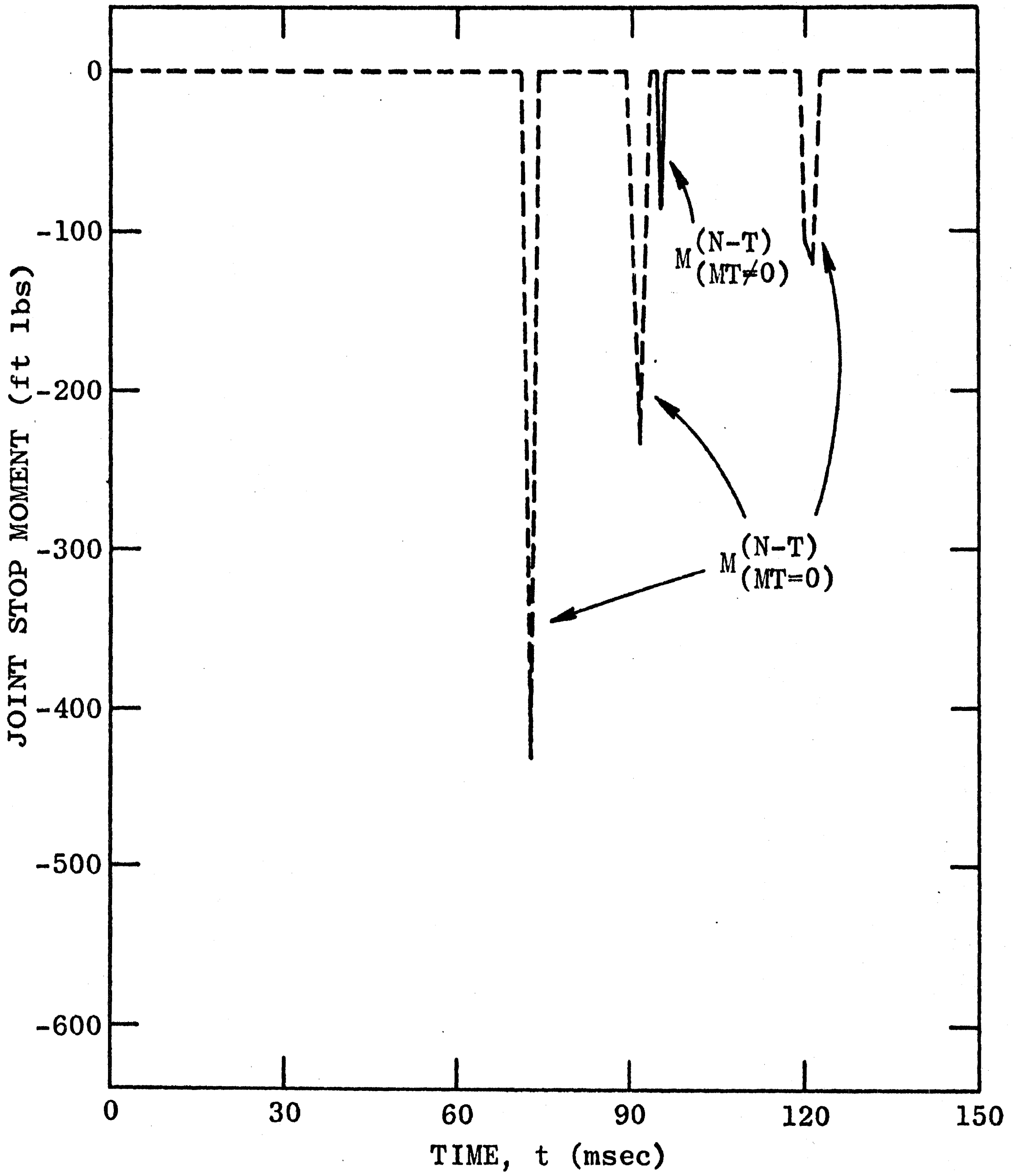

Figure 67. Neck-torso joint stop moments, with and without muscle tension.

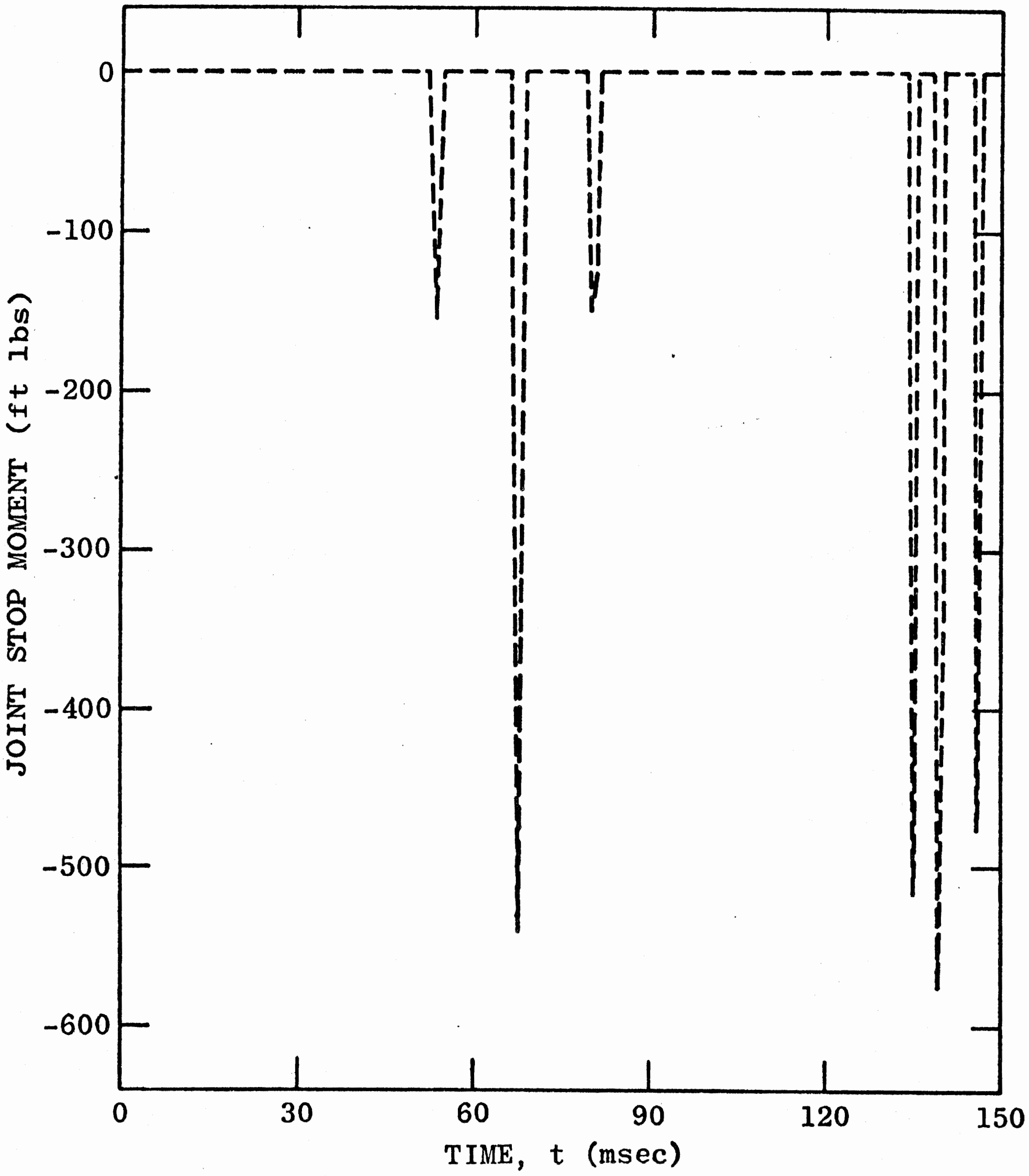

Figure 68. Neck-head joint stop moment for zero muscle tension.

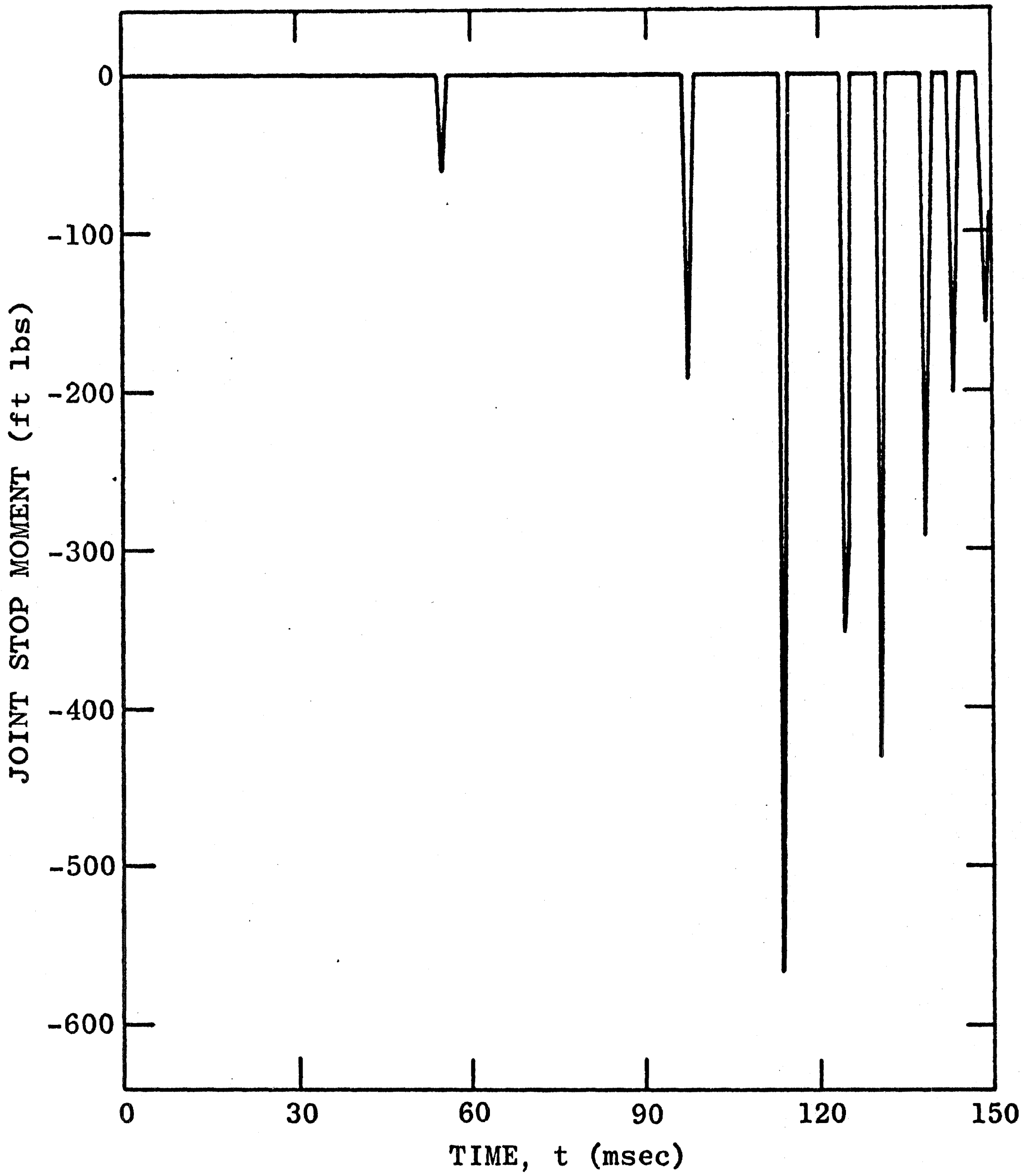

Figure 69. Neck-head joint stop moment for non-zero muscle tension.

10.5 OBLIQUE IMPACT: EXCITATION AT LOWER TORSO

The vehicle occupant model exercises discussed in this section and in Section 10.6 investigate the response to yawing excitation. An idealized crash was again simulated with the HSRI 3-D computer model, and output was used as the excitation for VOM.

Consider three identical, symmetrical vehicles involved in the collision illustrated in Figure 70. The crash victim is in the central vehicle, which is motionless at the instant that it is simultaneously struck by the other vehicles. The reason for treatment of this problem is that a reasonable vehicle yawing motion for a crash situation is required as excitation to the HSRI 3-D model. The necessity of the special nature of the illustrated collision will be made clear later.

Pure yaw will result for the central vehicle, and there will be no motion of the vehicle's center in x-y-z. Let a, b, and l be the vehicle dimensions shown in the figure, l being measured from the axis of rotation to the center of a tire contact patch. Masses and yawing moments of inertia are m and I. The impact velocities are v_0, and velocities at the end of the impact phase of the collision kinematics are v and $\dot{\psi}_r = \dot{\psi}(t_r)$. (It will be assumed that no angular velocity is imparted to the striking vehicles.) Before impact the kinetic energy of the system is

$$KE_i = m v_o^2 \quad . \tag{10.5.1}$$

Just at the end of the impact phase, when the vehicles have separated, the kinetic energy is

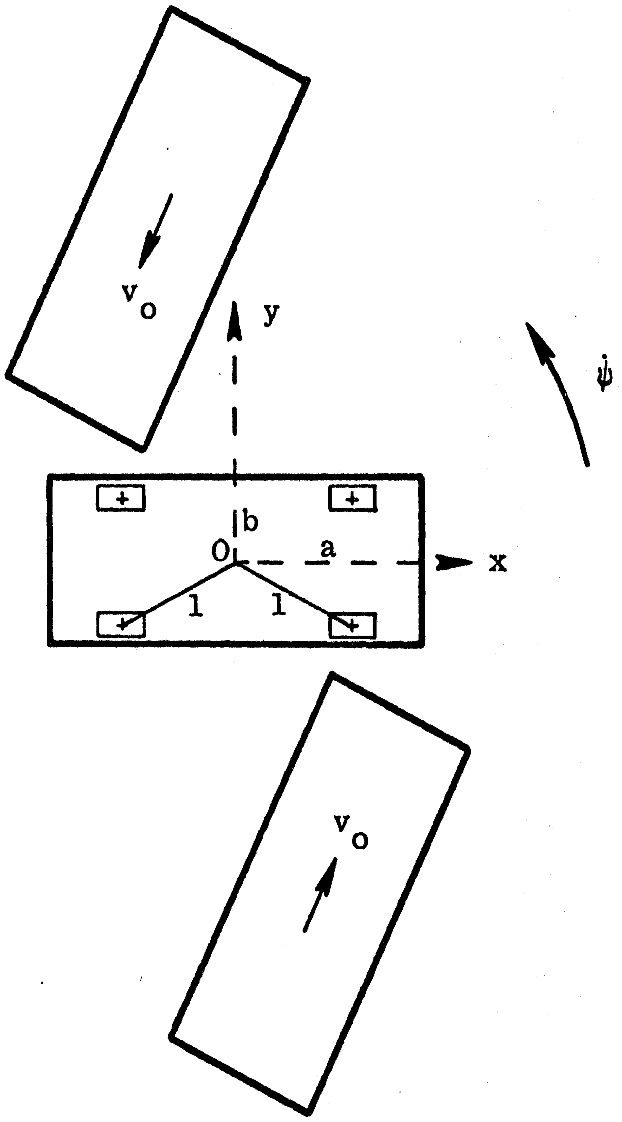
v_o
y
$\dot{\psi}$
b
O
a
x
l
l
v_o

Figure 70. Simultaneous oblique impact by two vehicles.

$$KE = mv^2 + \frac{1}{2} I \dot{\psi}_r^2 = (1-\eta) m v_0^2 \quad , \qquad (10.5.2)$$

where η is the fraction of the initial energy lost in the collision:

$$\eta = \frac{KE_i - KE}{KE_i} \quad . \qquad (10.5.3)$$

If tire friction is assumed negligible during the impact phase, $0 < t < t_r$, then conservation of angular momentum about point 0 gives

$$2 m v (\ell + b) + I \dot{\psi}_r = 2 m v_0 (\ell + b) \quad . \qquad (10.5.4)$$

We may eliminate v from equations (10.5.2) and (10.5.4) to obtain

$$\dot{\psi}_r = \frac{v_0\left[1 + \sqrt{1 - \eta\left[\frac{2m(\ell+b)^2}{I} + 1\right]}\right]}{(\ell+b)\left[1 + \frac{I}{2m(\ell+b)^2}\right]} \quad . \qquad (10.5.5)$$

Here, the plus sign has been used for the solution of a quadratic equation since we expect that for zero energy lost to crushing, etc., we should have a maximum for $\dot{\psi}_r$.

We cannot expect $\eta = 1$ in any crash of this sort. Since angular momentum is conserved, and since it is non-zero before the crash, there must always be at least some rotational kinetic energy after the impact phase. This is reflected in equation (10.5.5) by the constraint that

$$\eta \leq \frac{I}{2m(\ell+b)^2 + I} \quad . \tag{10.5.6}$$

For a right angle front-side collision (one impacting vehicle) Emori and Tani (39) give a percent energy loss in collision of 29% as typical. For a rear-side collision they give 21%. Two facts suggest that η will be smaller than these amounts for the collision under consideration. First, the initial angular momentum is greater than for a side impact (at the wheel) at 90° by the factor $[l + b]/[\sqrt{l^2 - b^2} + b]$. Second, for the symmetrical situation shown, each of the two impacting vehicles shares in causing motion of the central vehicle so that crush for each of them should be less.

The assumption will be made that the angular velocity of the impacted vehicle increases from zero to $\dot{\psi}_r$ linearly with t between 0 and t_r. After t_r it is assumed that rotational kinetic energy is dissipated by tire friction until $\dot{\psi} = 0$. Let W = mg be the weight of the vehicle. The frictional force at each tire may then be taken as $f = \mu W/4$, where μ is the coefficient of friction for tires against pavement. (Assume locked wheels and locked steering.) The total moment resisting yawing is therefore $M = -(\mu W)l$, and

$$I\ddot{\psi}(t_r \leq t \leq t_{max}) = -\mu W \ell \quad . \tag{10.5.7}$$

t_{max} is the time that $\dot{\psi}$ becomes zero and may be shown to be

$$t_{max} = t_r + \frac{I\dot{\psi}_r}{\mu W l} \quad . \qquad (10.5.8)$$

The velocity and acceleration curves therefore look in general as shown in Figure 71. t_r is an adjustable parameter, and $\dot{\psi}_r$ and t_{max} are as determined.

The numerical values required for the positive and negative accelerations were obtained by assuming the following parameter values.*

$2a = 17$ ft

$2b = 7$ ft

$l \simeq \sqrt{a^2 + b^2} = 7.4$ ft

$t_r = 0.06$ sec

$v_0 = 50$ mph $= 73.3$ ft/sec

$\mu = 0.5$

$W = 3800$ lb

$m = 118$ slugs

$I = m[(2a)^2 + (2b)^2]/12$

$= 3320$ lb-ft-sec^2

Equation (10.5.6) implies that the fractional energy loss must be less than 0.0769, i.e., 7.69%. Maximum energy loss may as well be assumed, so with $\eta = 0.0769$, we obtain

$$\begin{aligned} \dot{\psi}_r &= 7.20 \text{ rad/sec} \\ t_{max} &= 1.76 \text{ sec} \\ \ddot{\psi}(0 < t < 0.06) &= 120 \text{ rad/sec}^2 \\ \ddot{\psi}(0.06 < t < 1.76) &= -4.24 \text{ rad/sec}^2 \end{aligned} \qquad (10.5.9)$$

Figure 72 shows $\psi(t)$ for the 50 mph impact.

---

*The HSRI 3-D computer model integrates the accelerations to obtain required velocities.

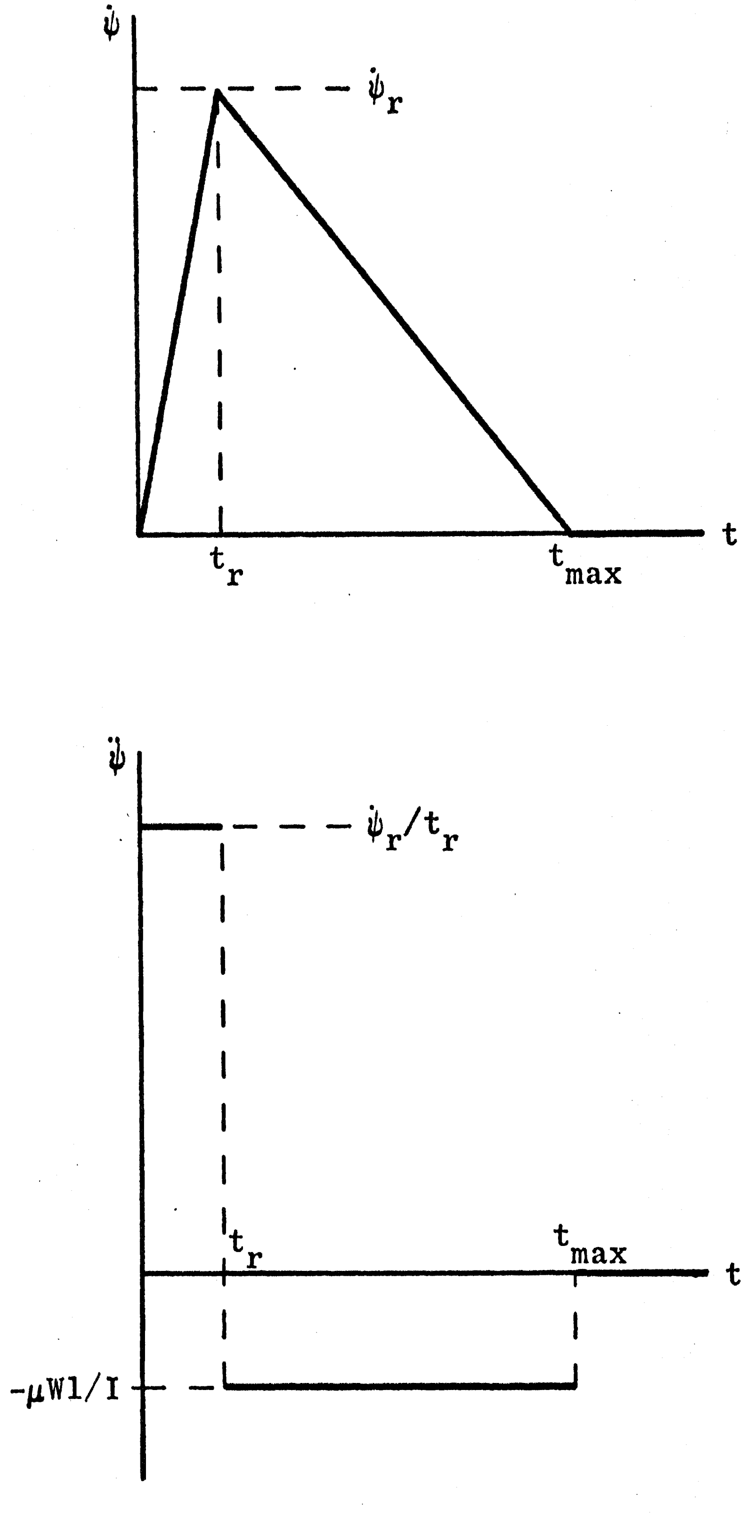

Figure 71. Vehicle yawing velocity and acceleration profiles.

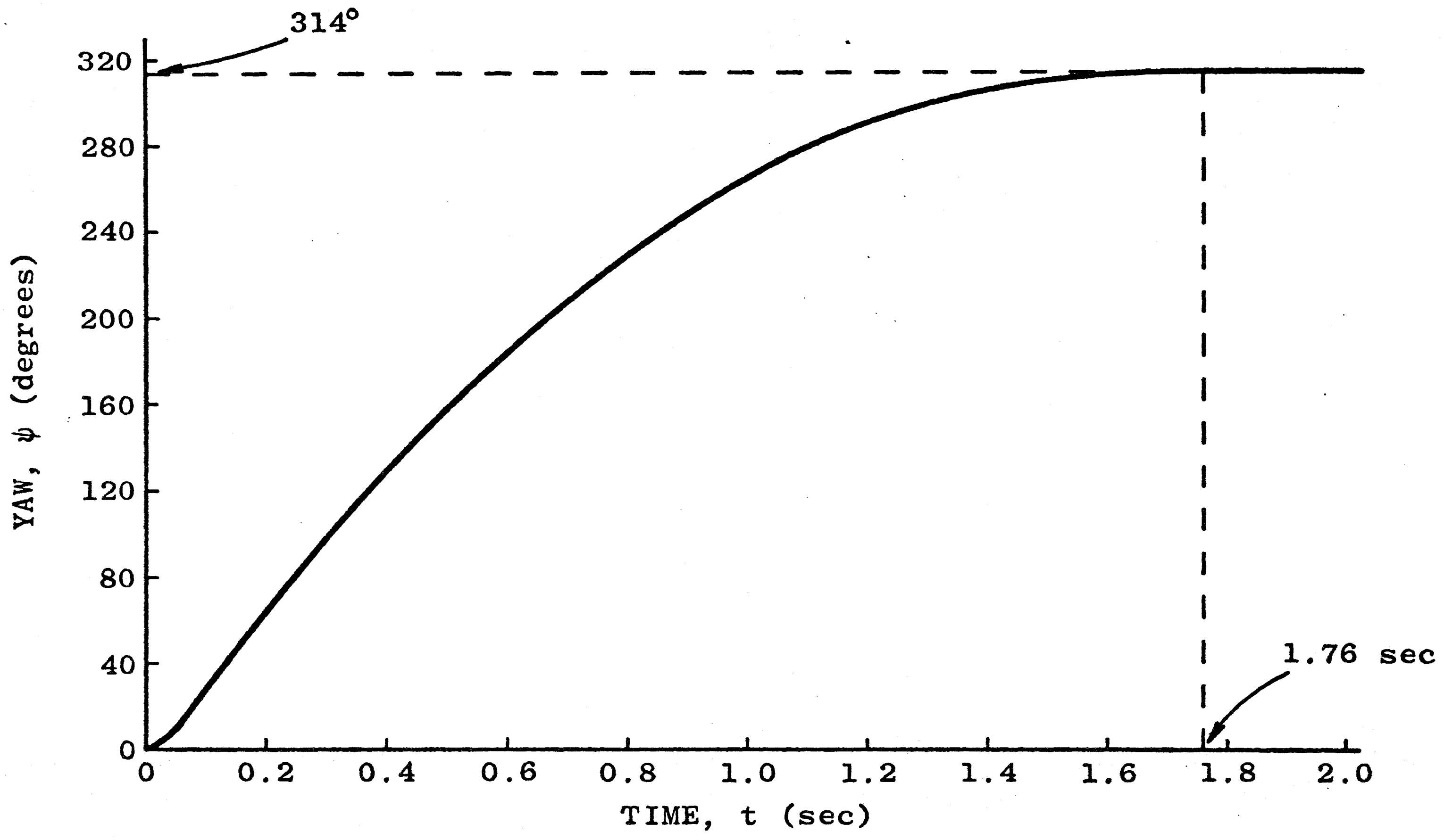

Figure 72. Vehicle yaw for double oblique impact at 50 mph.

Since the x-y-z motion of the lower torso element of the vehicle occupant model cannot be forced, it is made to be negligible as in the frontal impact test by choosing a large value for m_3 and by setting g equal to zero. Correspondingly, x-y-z motion for the HSRI 3-D occupant is made to be zero by making all initial angles equal to zero and by positioning the occupant at the center of rotation of the vehicle. The vehicle yaw determined in the foregoing caused pure yawing of the HSRI occupant since the lap belts were attached symmetrically and extended directly toward the sides. (Note: Clockwise (positive) vehicle yaw was used for the HSRI simulation - opposite from that shown in Figure 70.) The question now arises: Does the HSRI 3-D one-mass torso yawing motion correspond more closely to the lower, middle, or upper element torso motion for VOM? That is, which torso element of the vehicle occupant model is most reasonably forced by the HSRI 3-D motion? Since there is really no clear answer to this question, the motion for both lower and upper (pelvic and chest) elements was forced in separate tests. The results presented in this section are for forcing at the lower element, which allows investigation of both torso twisting and head motion. Section 10.6 gives results for forcing at the upper element.

Figure 73 illustrates the wind-up of the torso. Maximum twist over the whole length of the torso is about 40 degrees at about 165 msec.* Relative yaw angles for the torso joints are shown in Figures 74 and 75. The more immediate relative yawing occurs at the second (lower) joint since twisting moment is transmitted upward from the forced pelvic element. Even though elastic coefficients are zero, there is found to be some yawing of the first and second elements even before the yawing stop at the second joint is reached. This results because the joints are not on the longitudinal centerline but are offset by t_1 and t_2. Positioning the joints along the spine also accounts for the bending motion seen in Figures 76 and 77. Torso bending can occur even for an oblique impact resulting in pure vehicle yaw.

---

*Maximum lap belt forces occur at about t_r (60 msec) when HSRI 3-D torso yaw relative to the vehicle is about -12 degrees.

Figures 78 to 83 show inertial and relative head Euler angles. Pitch and roll motions are seen to be non-zero. This results because of non-zero torso pitch and roll and because of the offsets t_0 and d and the initial value $R(0) \neq 0$. Of more particular interest is that the head yaw stop is not reached for VOM. This stop angle is 60° for both VOM and the HSRI 3-D model. Figure 81 shows that the HSRI stop is reached at about 150 msec but that the relative head yaw for VOM has reached only about -36° by 200 msec. This is explained by the HSRI model having a one-mass torso, inflexible to twisting, and again by the fore-aft asymmetry of VOM, which causes participation of pitch and roll in the total motion.

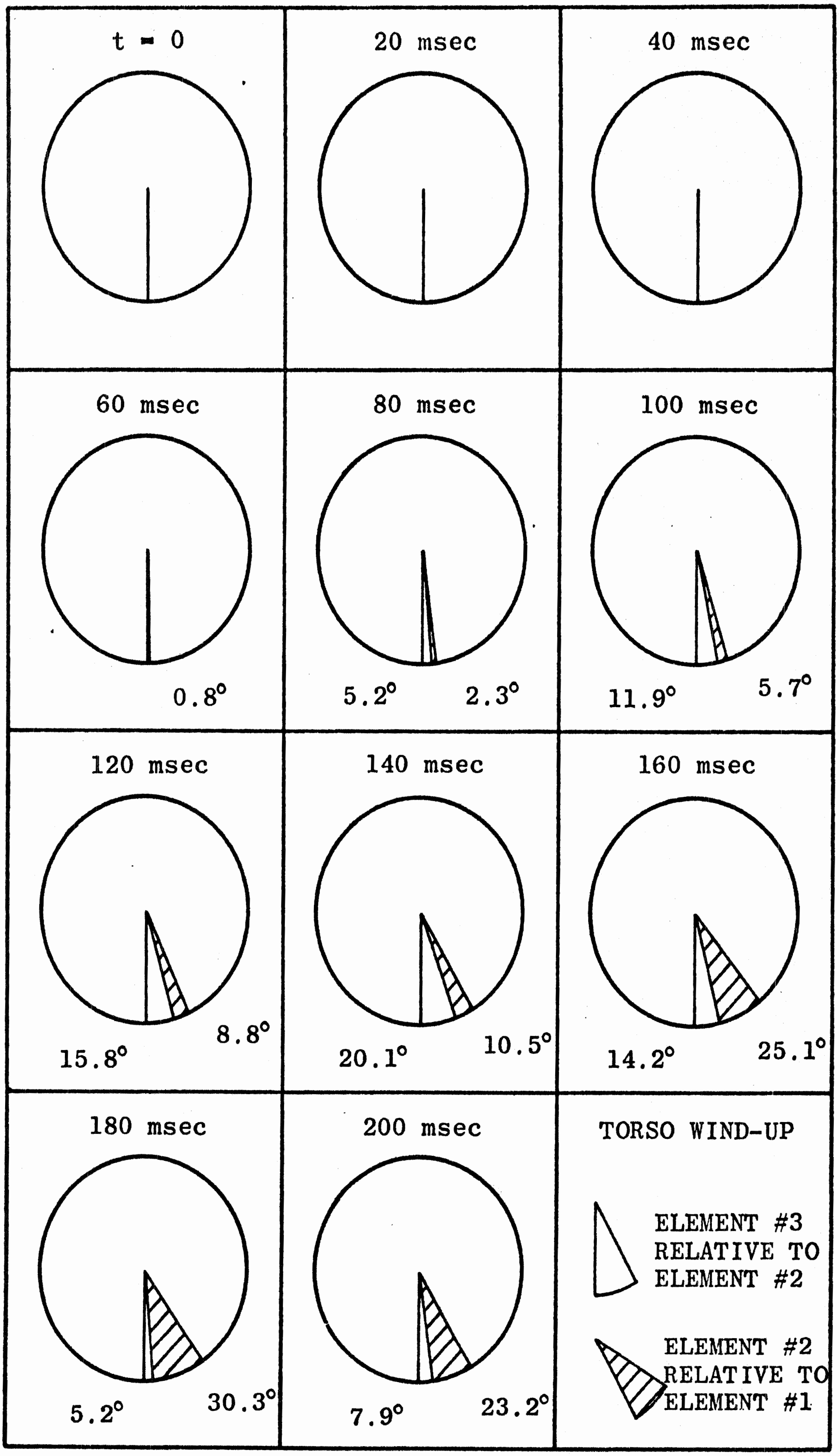
t = 0
20 msec
40 msec
60 msec
0.8°
80 msec
5.2°
2.3°
100 msec
11.9°
5.7°
120 msec
15.8°
8.8°
140 msec
20.1°
10.5°
160 msec
14.2°
25.1°
180 msec
5.2°
30.3°
200 msec
7.9°
23.2°
TORSO WIND-UP
ELEMENT #3 RELATIVE TO ELEMENT #2
ELEMENT #2 RELATIVE TO ELEMENT #1

Figure 73. Torso wind-up for oblique impact: excitation at lower torso.

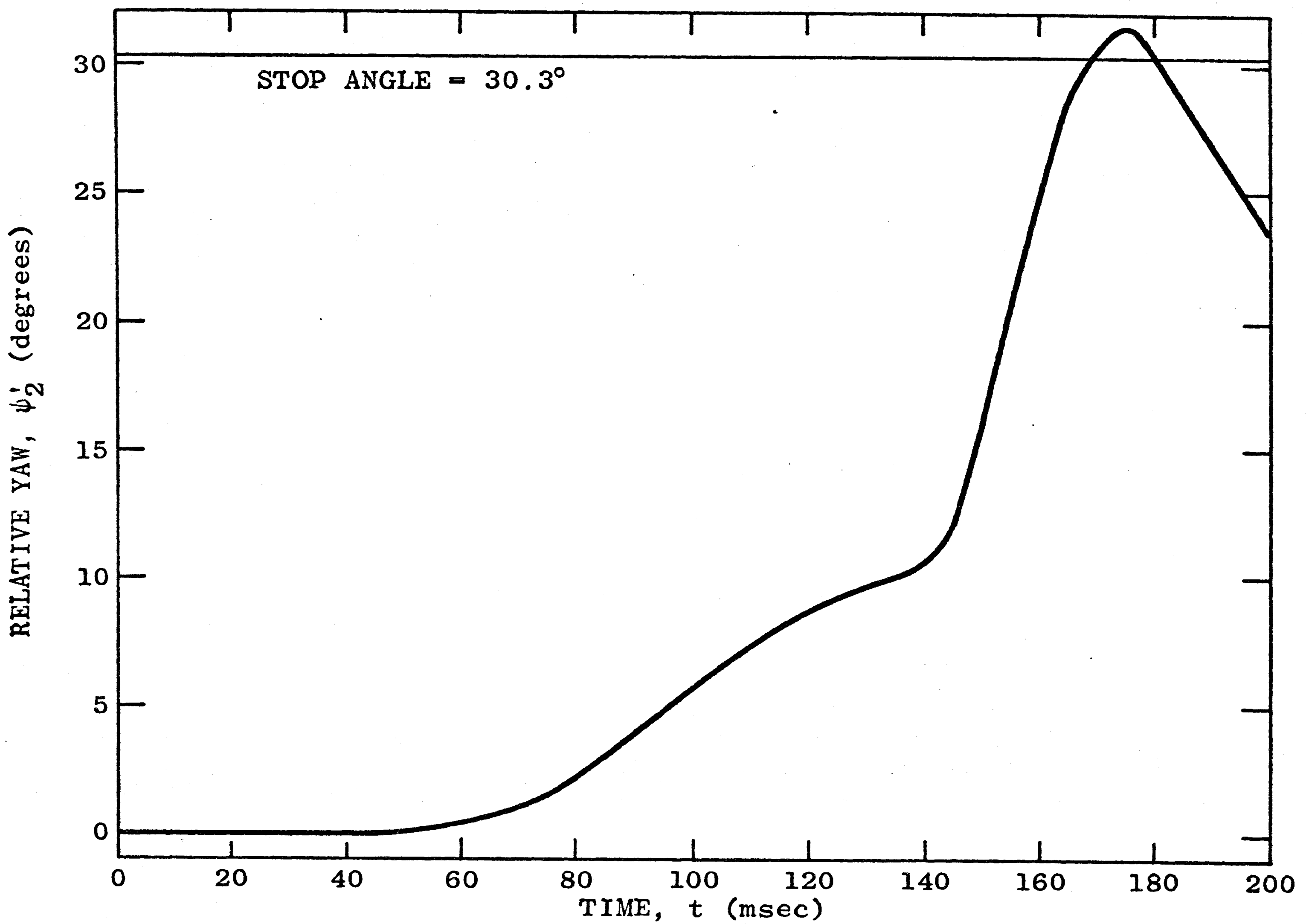

Figure 74. Yaw for second torso element relative to first torso element.

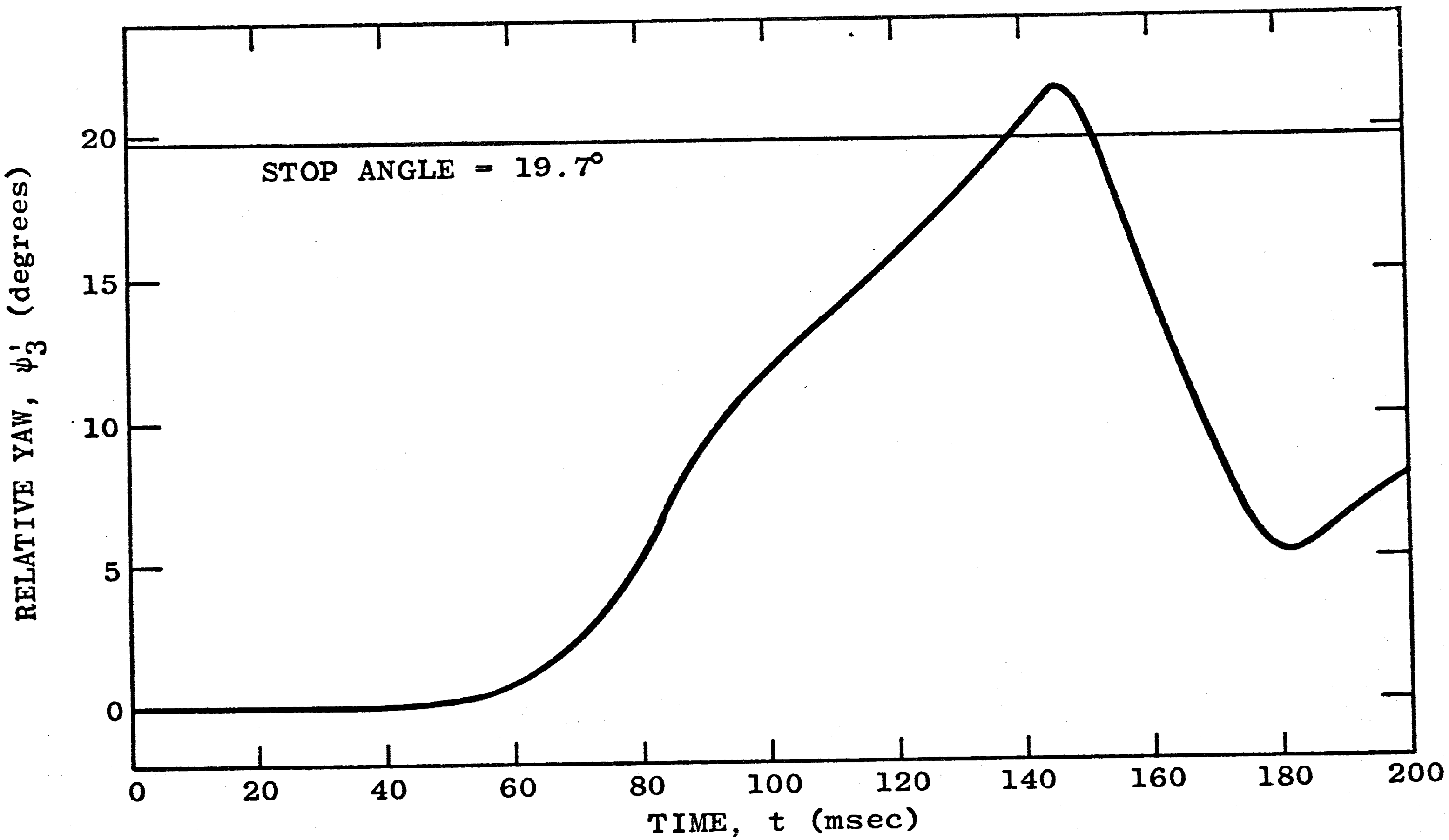

Figure 75. Yaw for third torso element relative to second torso element.

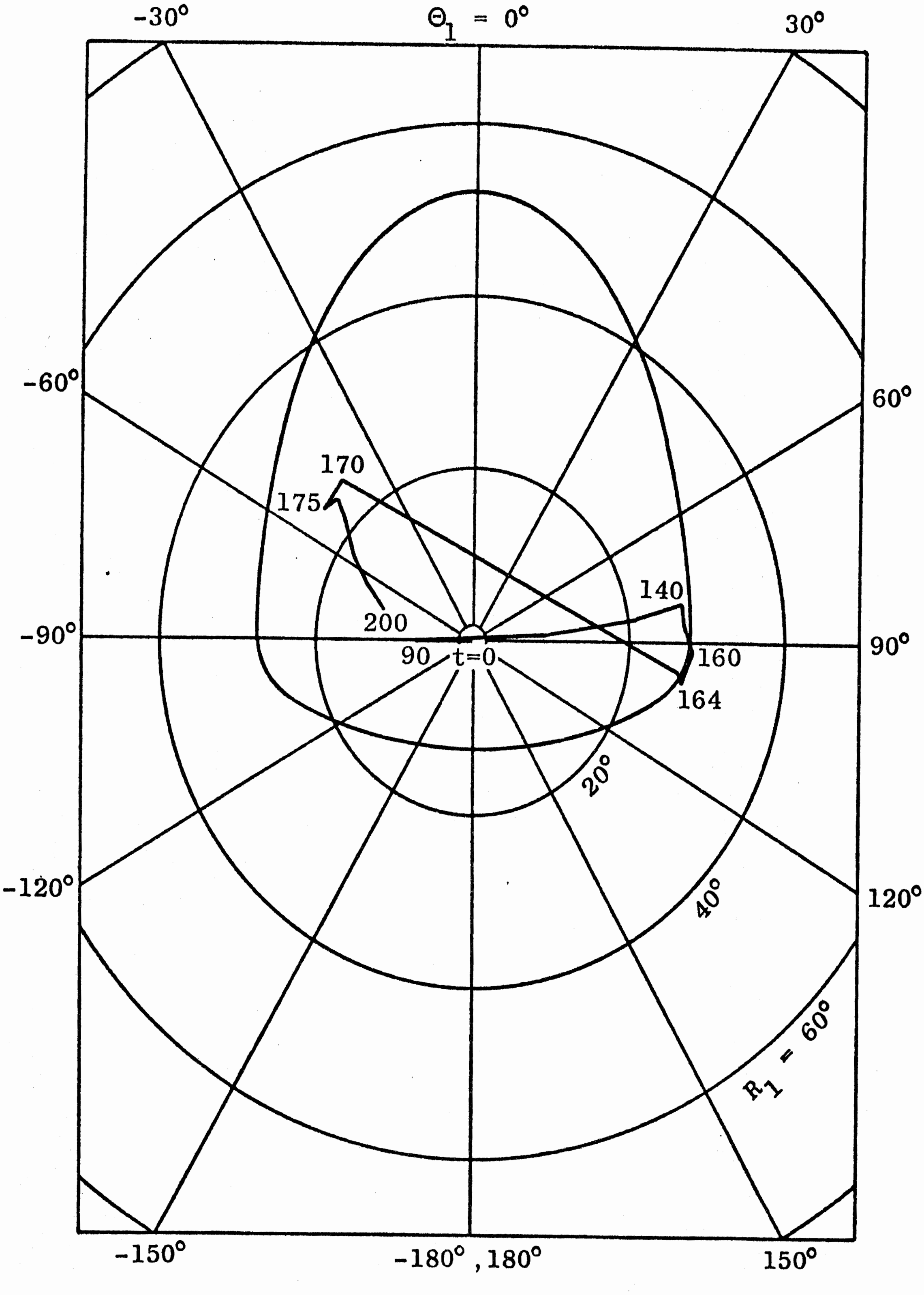

Figure 76. Generalized pitching angle R_1 and heading angle Θ_1 at first torso joint for oblique impact.

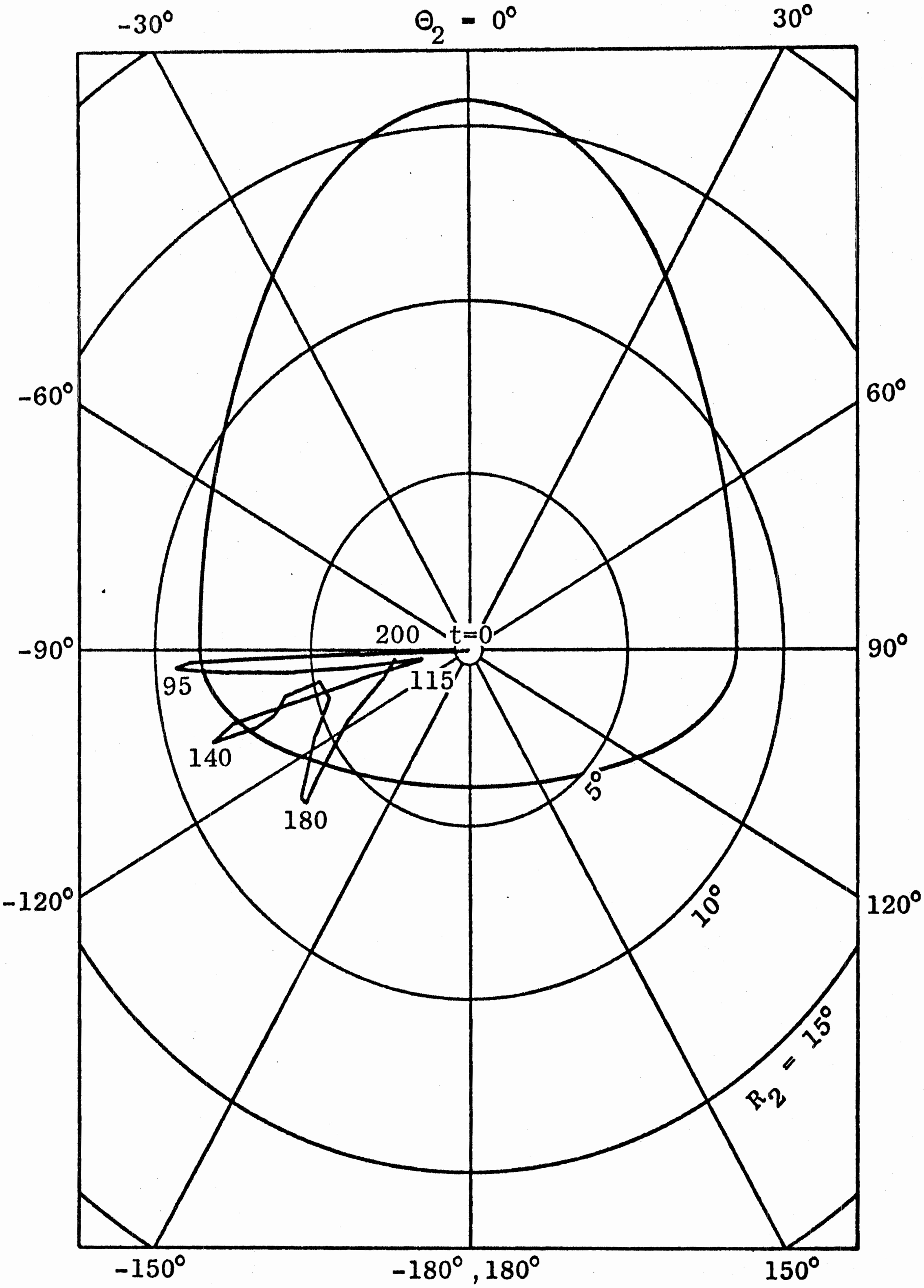

Figure 77. Generalized pitching angle R_2 and heading angle Θ_2 at second torso joint for oblique impact.

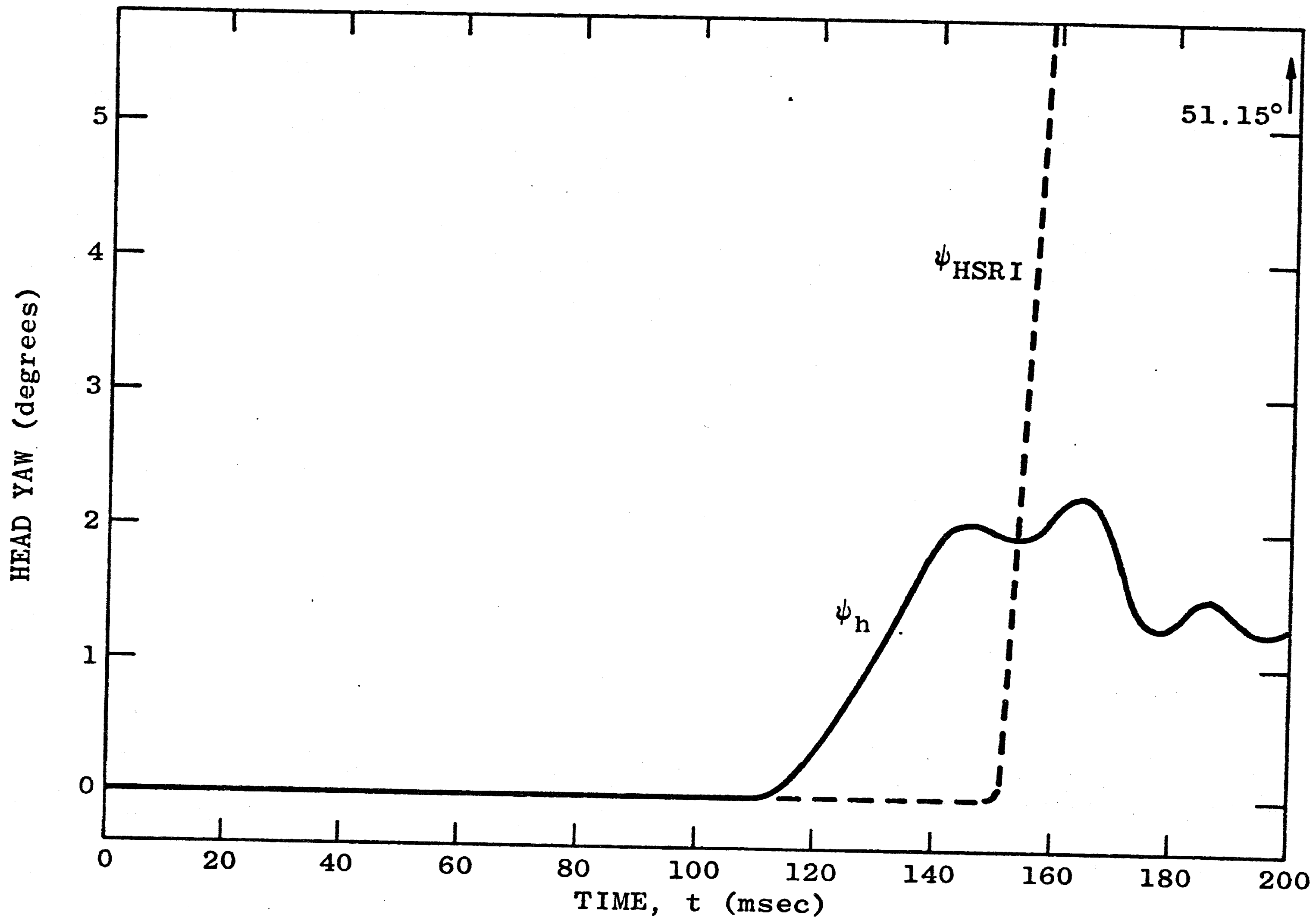

Figure 78. HSRI 3-D and VOM head yaw for oblique impact: excitation at lower torso.

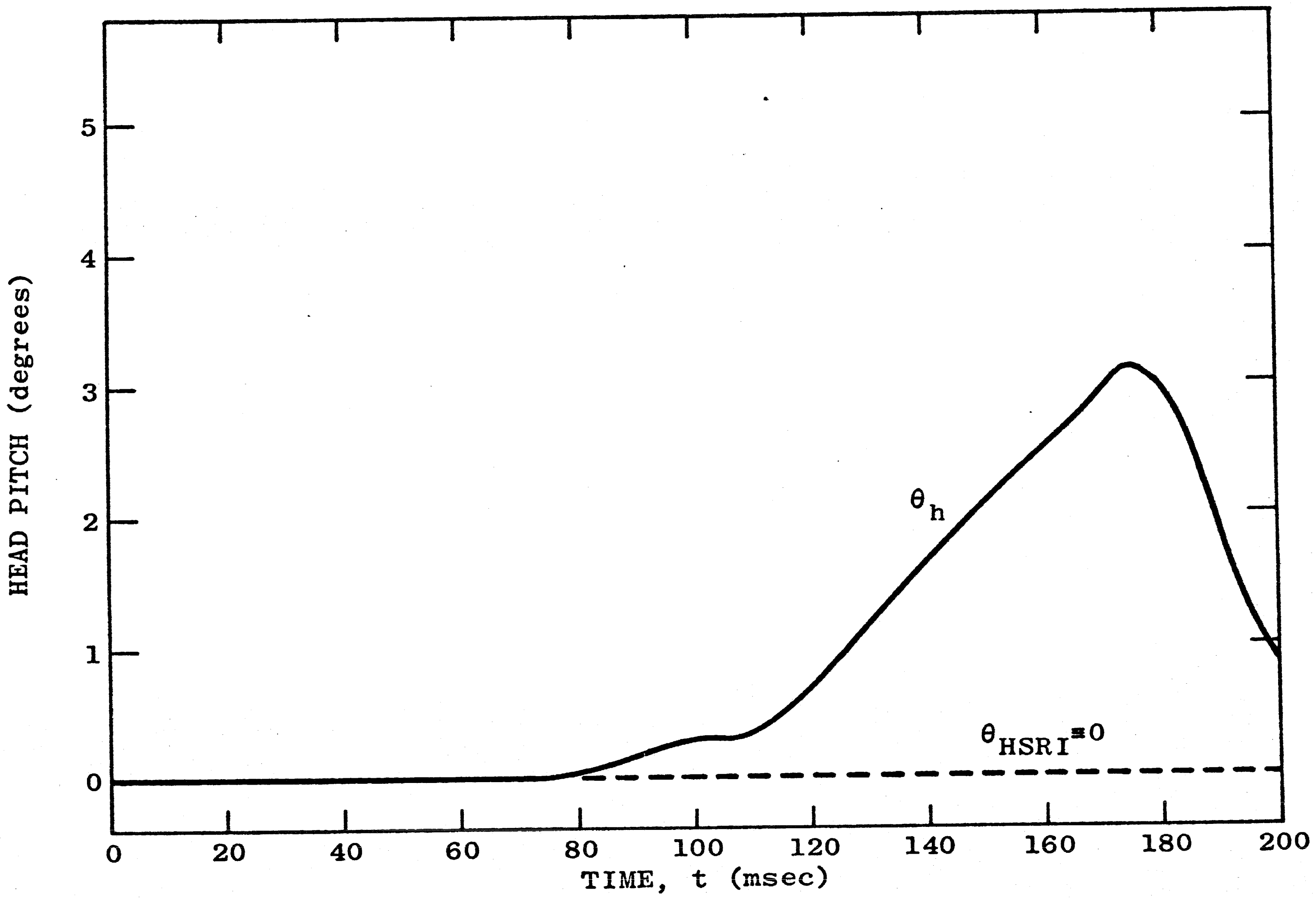

Figure 79. HSRI 3-D and VOM head pitch for oblique impact: excitation at lower torso.

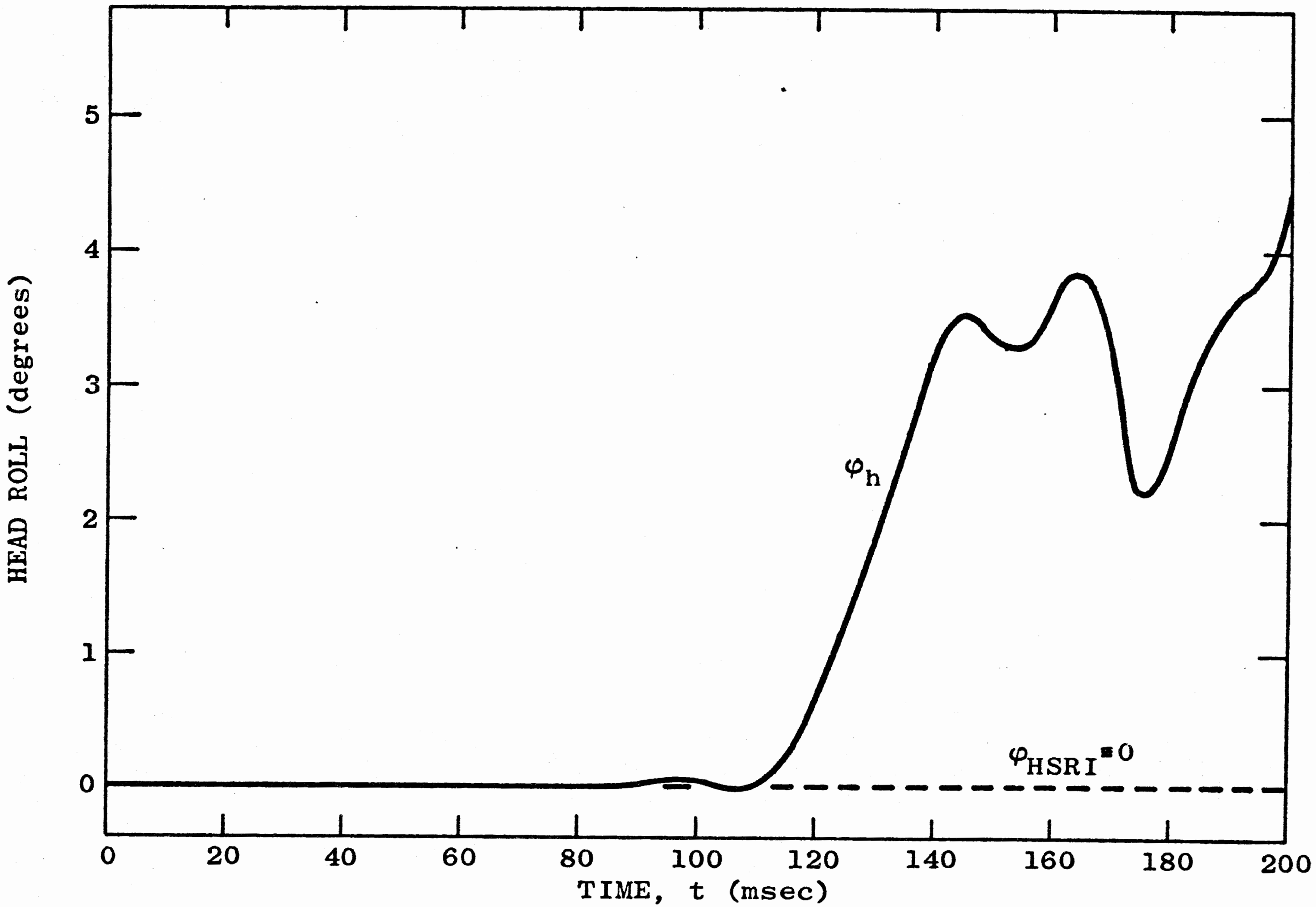

Figure 80. HSRI 3-D and VOM head roll for oblique impact: excitation at lower torso.

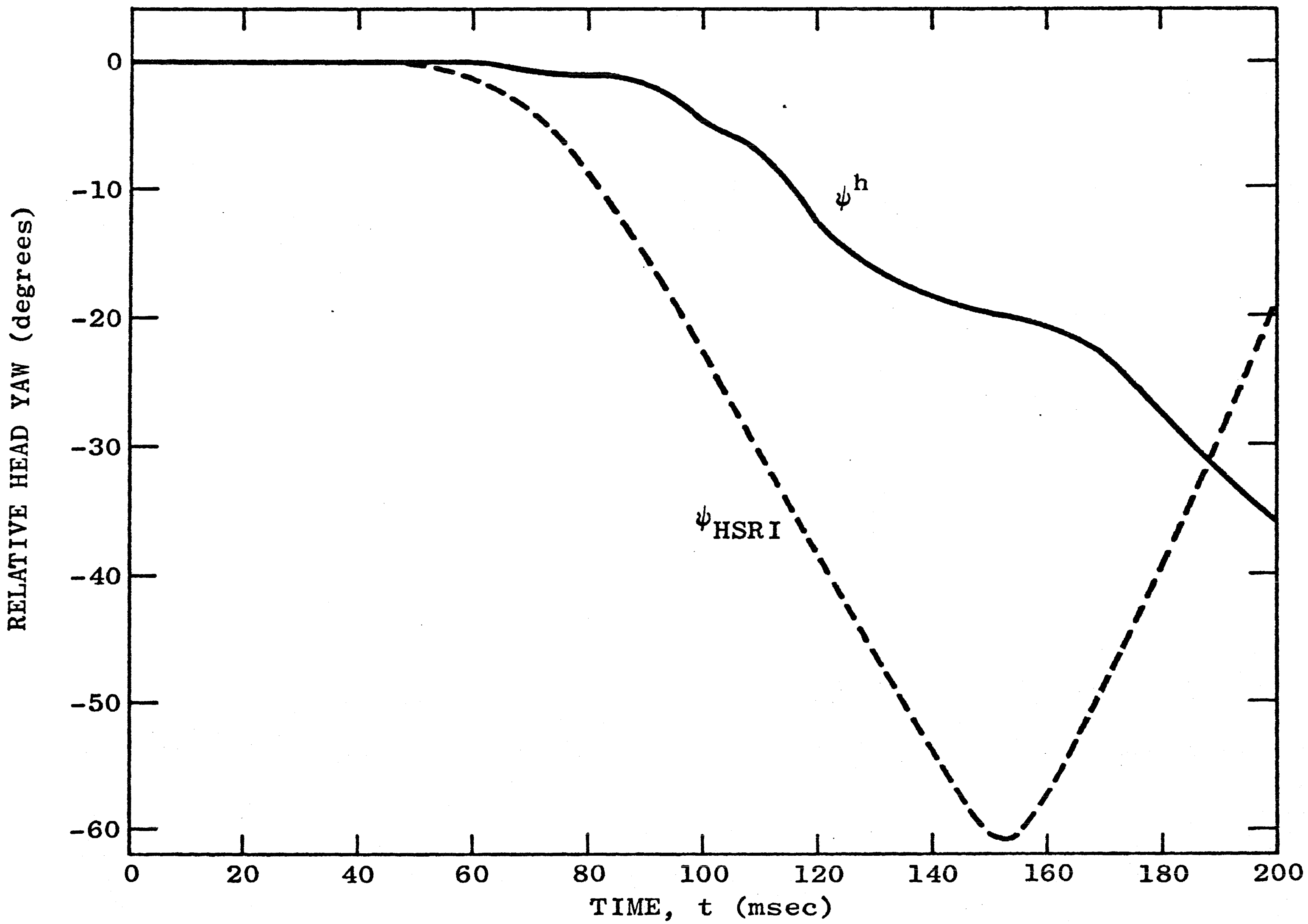

Figure 81. Head yaw relative to torso for oblique impact: excitation at lower torso.

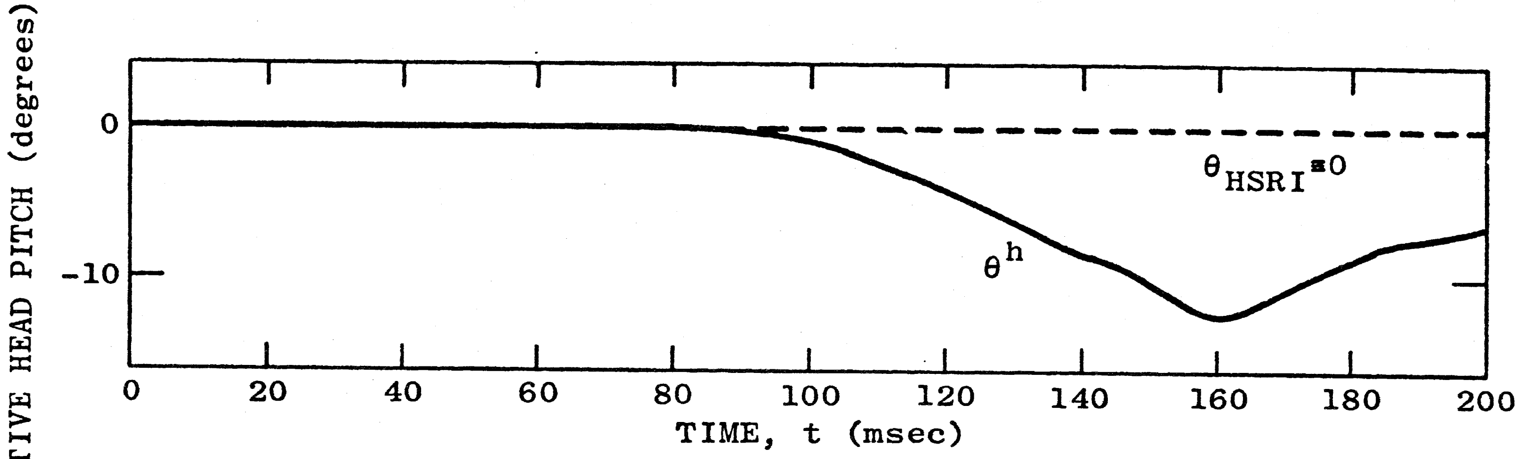

Figure 82. Head pitch relative to torso for oblique impact: excitation at lower torso.

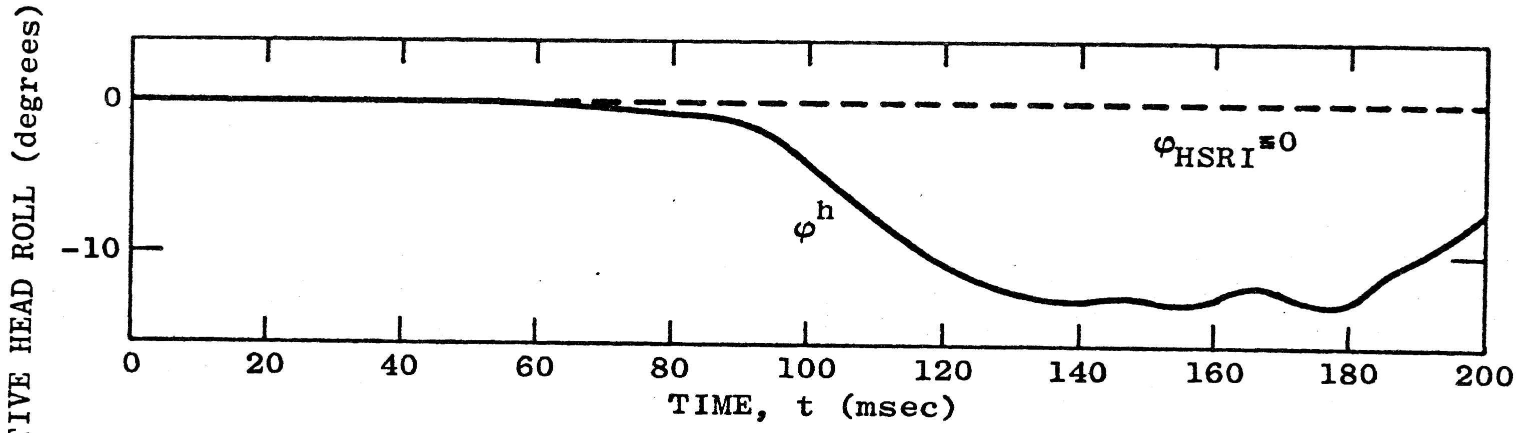

Figure 83. Head roll relative to torso for oblique impact: excitation at lower torso.

10.6 OBLIQUE IMPACT: EXCITATION AT UPPER TORSO

This exercise of the model differs from the one of the preceding section only in that the HSRI 3-D torso motion is used to force the *chest* motion for VOM. Thus, motion of the lower torso elements will be of no interest, and head motion is isolated from the effects of torso flexibility.

Head motions for the vehicle occupant model and the HSRI 3-D model are compared in Figures 84 to 89. Figure 87 shows that even direct yawing excitation of the vehicle occupant model upper torso element does not cause the neck yawing stop to be reached. The relative head yaw for the HSRI 3-D model reaches -60° by 150 msec while the relative yaw for VOM is only -53.2° at 200 msec. The neck linkage for VOM causes generalized pitching motion to be of greater importance for this simulated impact, at least with regard to possible injury. Figure 89 shows that relative head roll reaches a peak value of over 30° at about 165 msec. A maximum neck-head joint stop moment of -189.7 ft.lb is reached at just after 165 msec; the generalized pitching angle at N-H is then 27.4° and pitching at N-H is toward the right and backward - $\Theta' = 125.0°$. Lesser N-H joint stop activity occurs at 105 msec toward the left and at 132 msec toward the left and front. There is no joint stop activity at the neck-torso joint.

Head motions in x-y-z are all less than 0.5 inches for VOM and identically zero for the HSRI model.

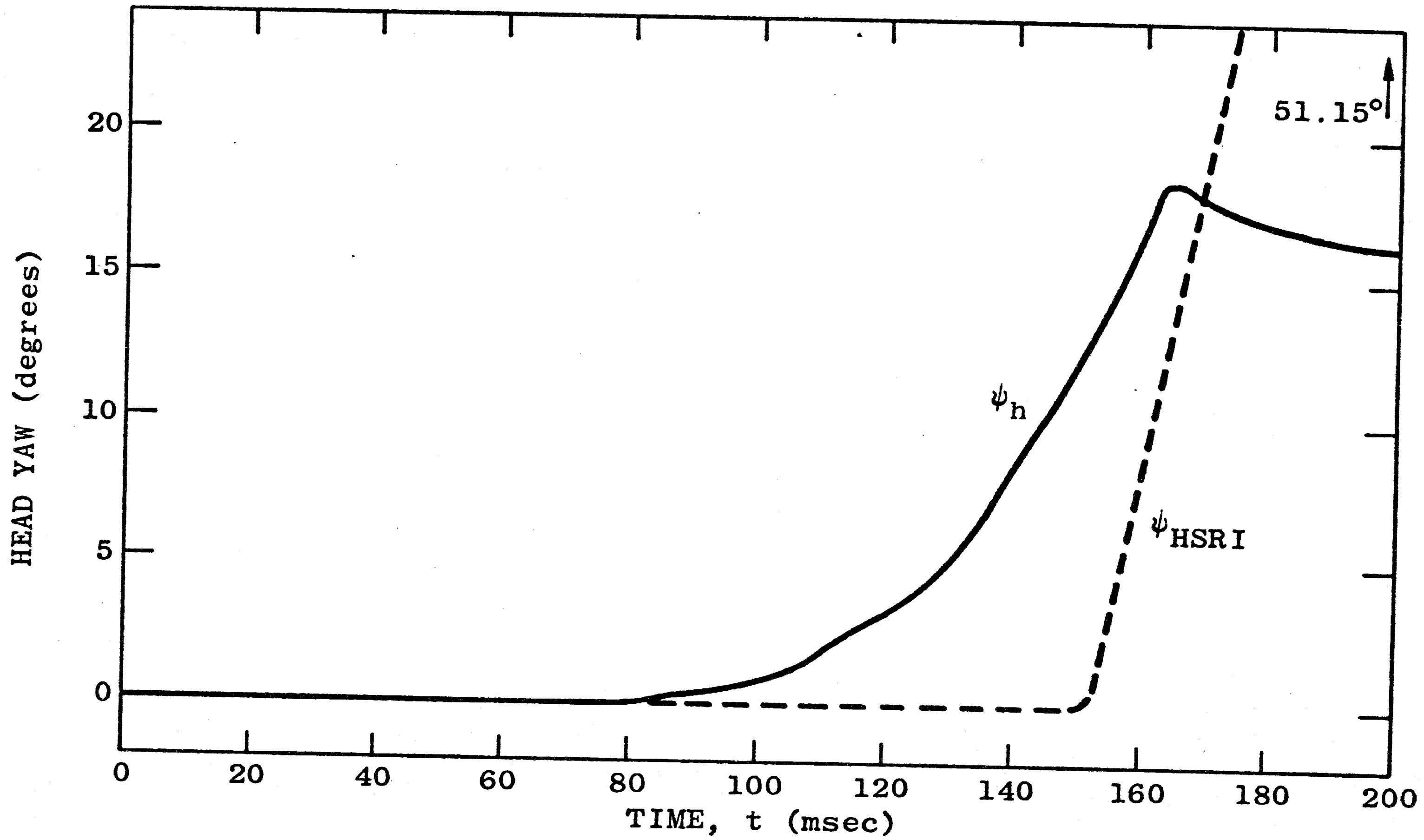

Figure 84. HSRI 3-D and VOM head yaw for oblique impact: excitation at upper torso.

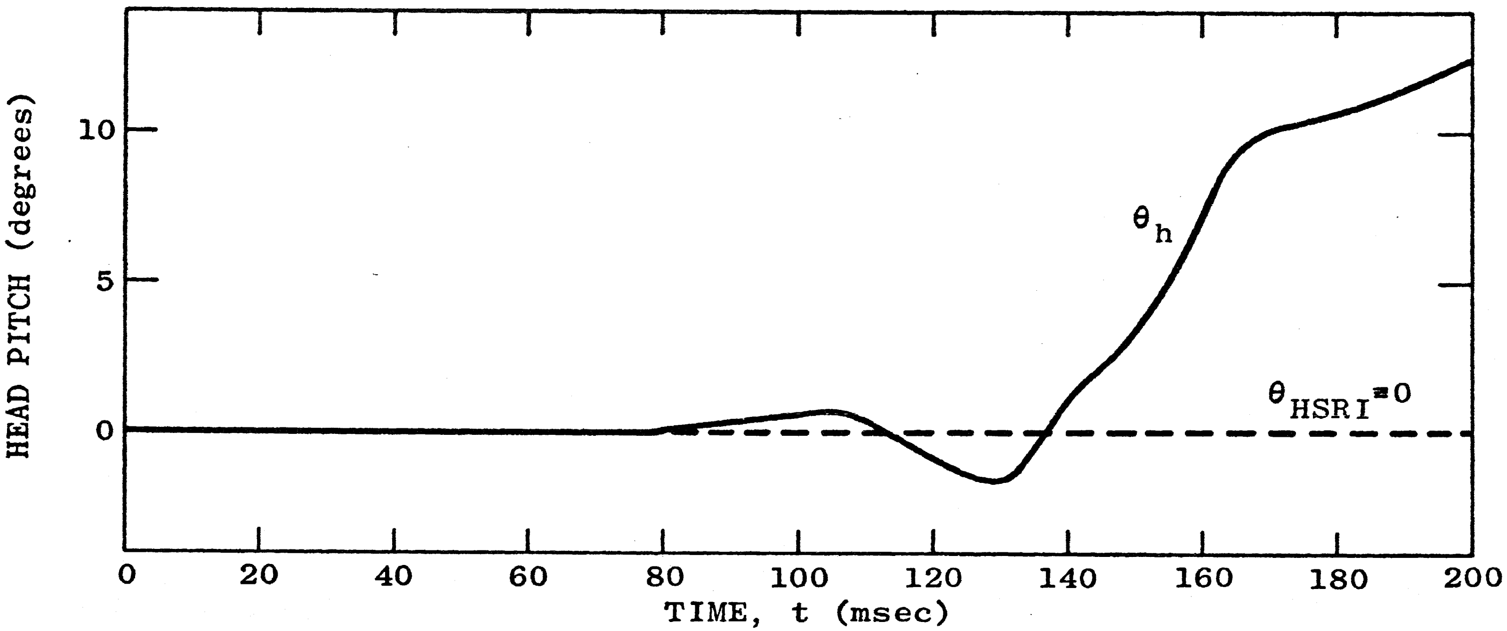

Figure 85. HSRI 3-D and VOM head pitch for oblique impact: excitation at upper torso.

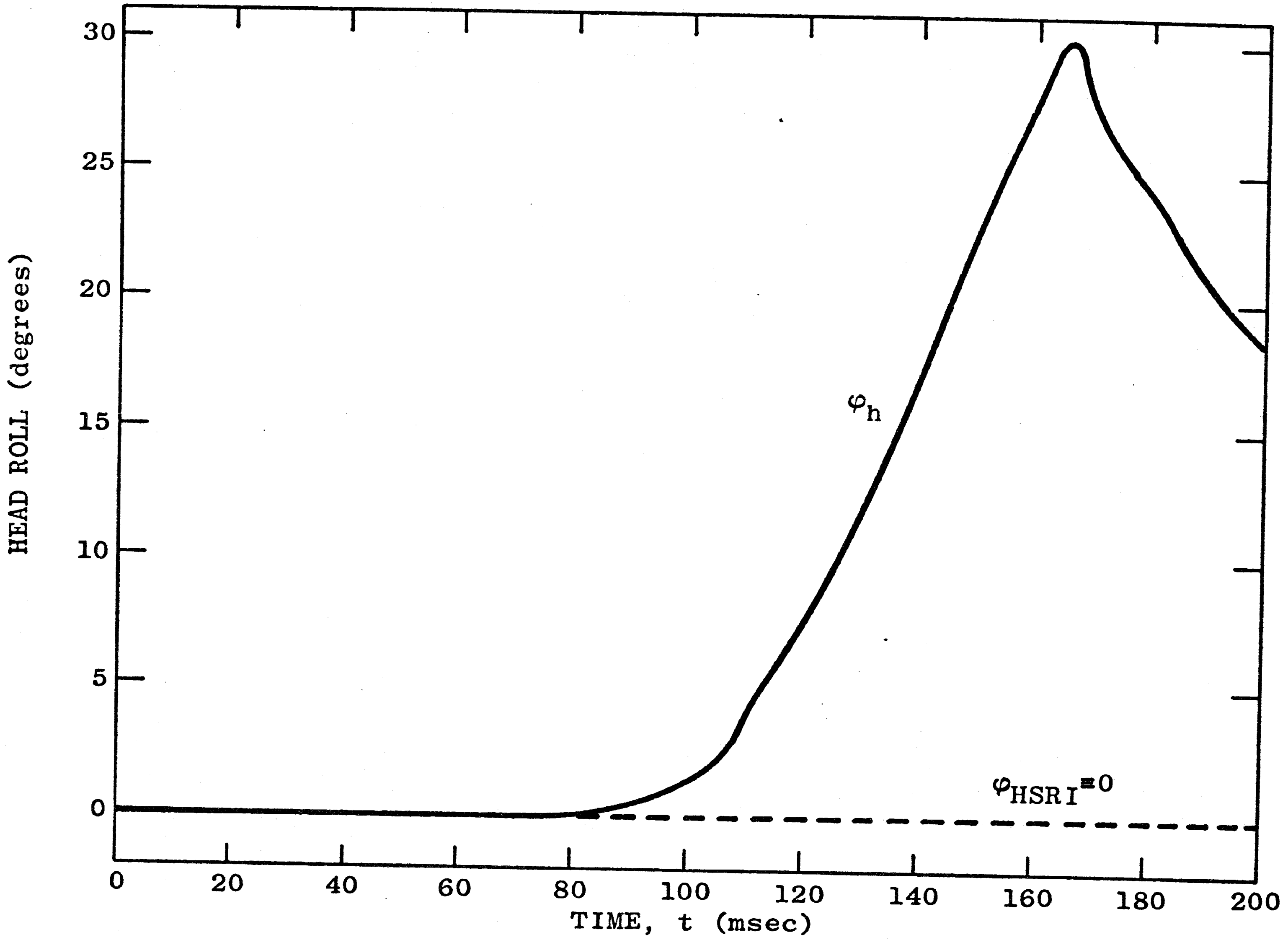

Figure 86. HSRI 3-D and VOM head roll for oblique impact: excitation at upper torso.

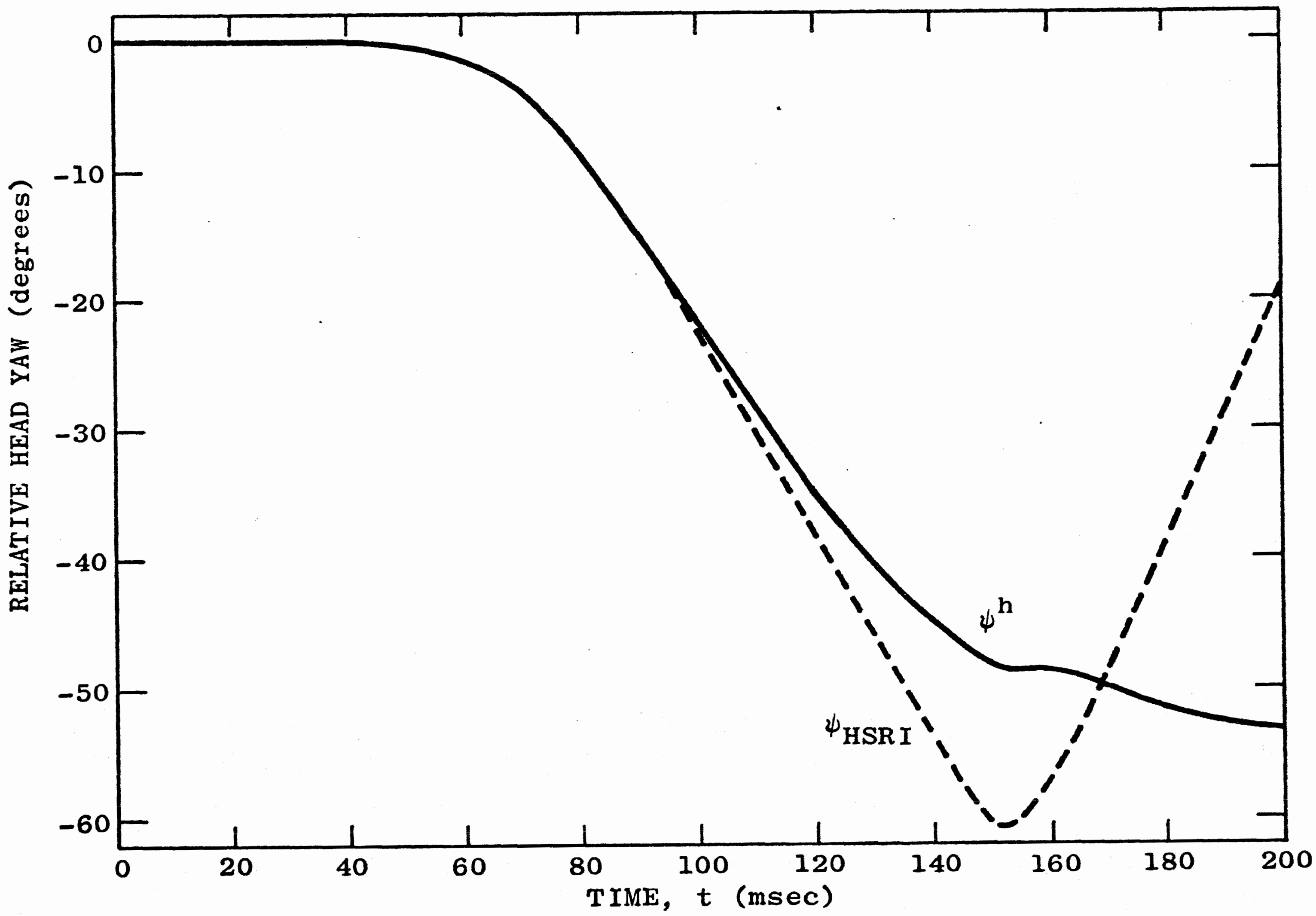

Figure 87. Head yaw relative to torso for oblique impact: excitation at upper torso.

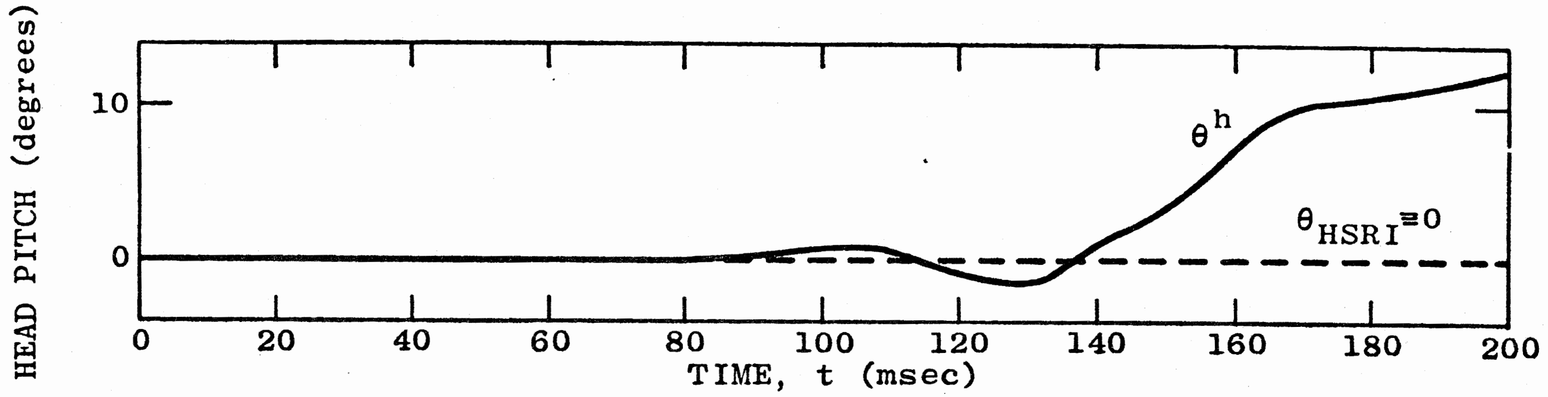

Figure 88. Head pitch relative to torso for oblique impact: excitation at upper torso.

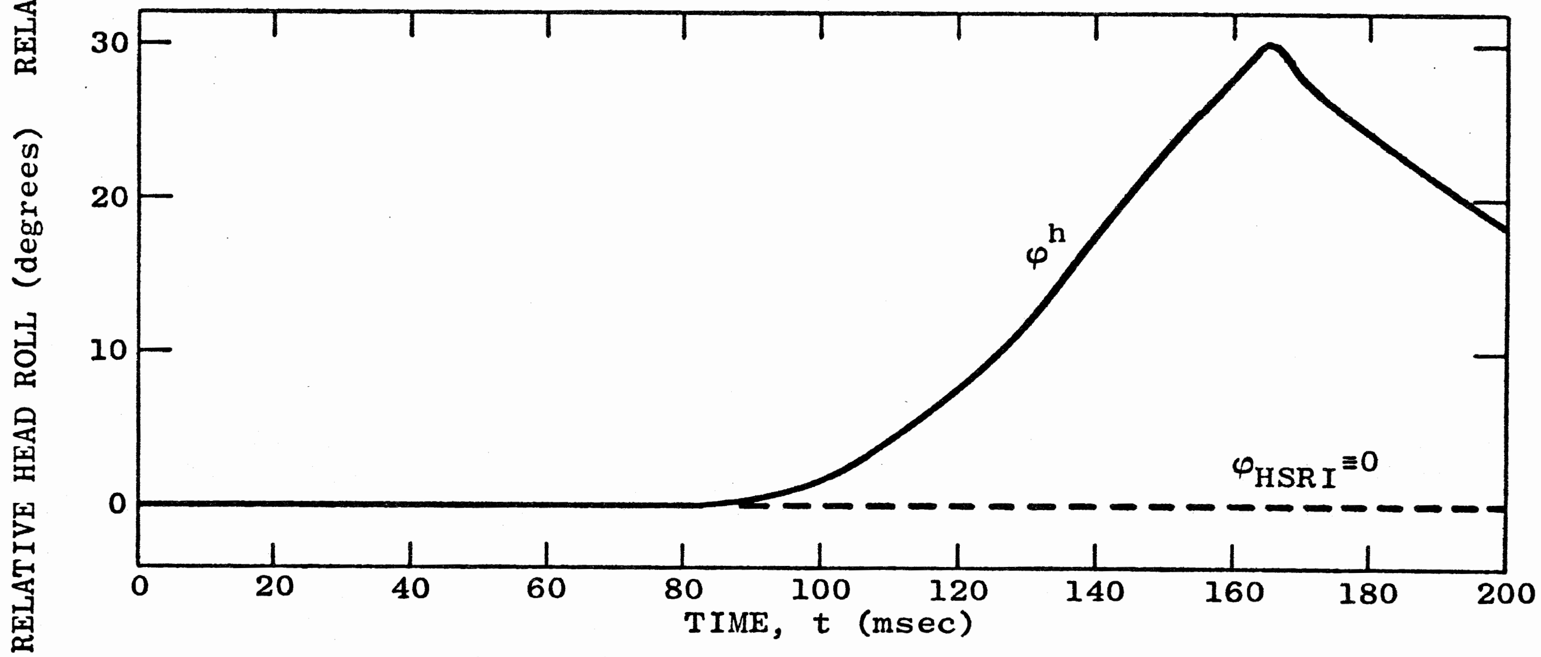

Figure 89. Head roll relative to torso for oblique impact: excitation at upper torso.

CHAPTER 11

CONCLUSIONS AND SUGGESTIONS FOR EXTENDED RESEARCH

11.1 CONCLUSIONS

The results of this investigation show that the proposed vehicle occupant model predicts the translational modes of head-neck motion observed by Ewing, et al., Tisserand and Wisner, and Schulman, et al. Quantitative comparison against their experimental results was prevented by lack of required experimental detail. The successfully represented qualitative nature of the kinematics cannot be predicted by any of the various simpler crash victim models.

For the two-joint neck model it was determined that relative rotational motion at the atlanto-occipital articulation (the neck-head juncture) is no less important than at the seventh-cervical/first-thoracic vertebral articulation (the neck-torso juncture). Injury due to extreme relative rotation may well occur at either joint in a sufficiently severe crash situation.

Fore-aft asymmetry of the vehicle occupant model was found to result in pitch and roll participation in the kinematics resulting from pure yawing excitation. The results indicate that injuries incurred in oblique "intersection collisions" are as likely (or more likely) to result from extreme relative "bending" at body joints as from extreme relative "twisting."

Results predict that muscle contraction prior to impact can cause a reduction in the severity of injuries resulting from extreme relative rotation at joints. There is also some evidence that the likelihood of cerebral concussion is reduced.

Several opinions regarding human crash victim representation by the analytical model have been reached by this author over the course of the investigation. 1) Both "elastic" moments based on an equilibrium orientation and joint stop moments are important at torso joints for best representing the continuous human torso with spinal support. 2) The relatively "loose" neck linkage should not have elastic moments associated with it; joint stops at the neck joints are of prime importance. 3) Normal levels of muscle tension for a person in a sitting position (with partial support for his back) should be taken as minimum values for a conscious crash victim since even a vehicle occupant not anticipating an impact maintains a level of muscle contraction sufficient to balance external forces. 4) Three torso masses and a single leg of one or two masses are probably sufficient to adequately represent the human torso and legs.

11.2 SUGGESTIONS FOR EXTENDED RESEARCH

An obvious extension of the investigation reported here would be to include the crash victim model as a part of a vehicle-occupant system. However, this would not necessarily precede further study of the crash victim model itself.

Only limited parameter study has been done to this point, i.e., no real effort has yet been made to "tune" the model so as to make it represent the living human system to the best of its ability. Primarily, this means that the best possible values for joint coefficients should be determined; this might involve direct measurement of joint properties or empirical adjustment of the analytically predicted kinematics of various forced motions to corresponding laboratory tests with volunteers.

Some use may also be made of limited existing experimental results. It seems likely that higher levels of velocity-dependent damping than have been used thus far would be more realistic. It has been previously mentioned that normal levels of muscle tension should be determined for all joints so that a minimum muscular resistance to relative joint motion can always be represented. It may also be of value to make use of the non-linear form assumed for joint stop moments in conjunction with smaller values for joint stop angles so that the "hard" anatomical stops could be "softened" by appropriate amounts.

Various improvements upon the analytical model itself might also be considered. For example, it is possible to introduce greater flexibility into the neck without increasing the number of degrees of freedom. Further increasing the complexity of the neck model, however, would increase the burden of supplying proper bioparameter values. The muscle tension model might also be further developed. While it is felt to be very significantly better than any other muscle tension representation used to date in crash victim models, it is still the simplest and most limited possible realistic representation of the effect of muscle contraction on crash kinematics.

Finally, it would be of value to establish a broad set of injury criteria to be incorporated in the computer model so that the absolute effectiveness of any proposed restraint system could be evaluated.

LIST OF REFERENCES

1. Martin, D. E., and Kroell, C. K., "Vehicle Crush and Occupant Behavior." Paper 670034, Society of Automotive Engineers, Inc., New York, January 1967.

2. Martinez, J. L., Wickstrom, J. K., and Barcelo, B. T., "The Whiplash Injury--A Study of Head-Neck Action and Injuries in Animals." Transactions of The American Society of Mechanical Engineers, Paper No. 65-WA/HUF-6, 1965.

3. Martinez, J. L., and Garcia, D. J., "A Model for Whiplash." Journal of Biomechanics, Vol. 1, No. 1, January 1968, pp. 23-32.

4. Mertz, H. J., Jr., The Kinematics and Kinetics of Whiplash. A dissertation for the degree of Doctor of Philosophy, Wayne State University, Detroit, 1967.

5. Renneker, D. N., "A Basic Study of 'Energy-Absorbing' Vehicle Structure and Occupant Restraints by Mathematical Model." Paper 670897, Society of Automotive Engineers, Inc., New York, October 1967.

6. Ryan, J. J., "Reduction in Crash Forces." The Fifth Stapp Automotive Crash and Field Demonstration Conference, Minneapolis, September 1961, pp. 48-89.

7. Ryan, J. J., and Tobias, J. R., "Reduction in Crash Forces." Proceedings of the Ninth Stapp Car Crash Conference, Minneapolis, October 1965, pp. 413-419.

8. Weaver, J., "A Simple Occupant Dynamics Model." Journal of Biomechanics, Vol. 1, No. 3, August 1968, pp. 185-191.

9. Roberts, V. L., and Robbins, D. H., "Multidimensional Mathematical Modeling of Occupant Dynamics Under Crash Conditions." Paper 690248, Society of Automotive Engineers, Inc., New York, January 1969.

10. McHenry, R. R., "Analysis of the Dynamics of Automotive Passenger-Restraint Systems." Proceedings of the Seventh Stapp Conference, Springfield, Illinois, 1963.

11. McHenry, R. R., and Naab, K. N., "Computer Simulation of the Automobile Crash Victim in a Frontal Collision--A Validation Study." CAL No. YB-2126-V-1R, Cornell Aeronautical Laboratory, Inc., Buffalo, N. Y., July 1966.

12. McHenry, R. R., and Naab, K. N., "Computer Simulation of the Crash Victim--A Validation Study." Proceedings of Tenth Stapp Car Crash Conference. Paper 660792, Society of Automotive Engineers, Inc., New York, 1966.

13. Roberts, S. B., Ward, C. C., and Nahum, A. M., "Head Trauma--A Parametric Dynamic Study." Journal of Biomechanics, Vol. 2, No. 4, October 1969, pp. 397-415.

14. Becker, J. M., and Robbins, D. H., "Mathematical Simulation of Collision, I." Final Report to National Highway Safety Bureau on Contract FH-11-6685. Highway Safety Research Institute, The University of Michigan, 1967.

15. Robbins, D. H., Bennett, R. O., and Roberts, V. L., "HSRI Two-Dimensional Crash Victim Simulator: Analysis, Verification, and Users' Manual." HSRI Report No. BioM-70-8, Highway Safety Research Institute, The University of Michigan, 1971.

16. Thompson, J. E., "Occupant Response Versus Vehicle Crush: A Total System Approach." Proceedings of Twelfth Stapp Car Crash Conference. Paper 680780, Society of Automotive Engineers, Inc., New York, 1968.

17. Young, R. D., "A Three-Dimensional Mathematical Model of an Automobile Passenger." Research Report 140-2, Texas Transportation Institute, Texas A&M University, College Station, Texas, 1970.

18. Robbins, D. H., Bennett, R. O., and Roberts, V. L., "HSRI Three-Dimensional Crash Victim Simulator: Analysis, Verification, Users' Manual, and Pictorial Section." HSRI Report No. BioM-70-9, Highway Safety Research Institute, The University of Michigan, 1971.

19. Ewing, C. L., et al., "Dynamic Response of the Head and Neck of the Living Human to $-G_X$ Impact Acceleration." Proceedings of the Twelfth Stapp Car Crash Conference. Paper 680792, Society of Automotive Engineers, Inc., New York, 1968.

20. Tisserand, M., and Wisner, A., "Comportement du Rachis Cervical lors de Chocs Dorsaux." Centre de Physiologie du Travail de l'Institut National de Securite, Report No. 73, 1966.

21. Jackson, R., The Cervical Syndrome. Charles C Thomas, Springfield, Illinois, 1966.

22. Tarrière, C., and Sapin, C., "Biokinetic Study of the Head to Thorax Linkage." Proceedings of Thirteenth Stapp Car Crash Conference. Paper 690815, Society of Automotive Engineers, Inc., New York, 1969.

23. Schulman, M., et al., "Determination of Human Tolerance to Negative Impact Acceleration." U.S. Naval Air Engineering Center - Aerospace Crew Equipment Laboratory Report NAEC-ACEL-510, November 1963.

24. Moffatt, C. A., Harris, E. H., and Haslam, E. T., "An Experimental and Analytic Study of the Dynamic Properties of the Human Leg." Journal of Biomechanics, Vol. 2, No. 4, October 1969, pp. 373-387.

25. Johns, R. J., and Wright, V., "An Analytical Description of Joint Stiffness." Biorheology, Vol. 2, November 1964, pp. 87-95.

26. Goldstein, H., Classical Mechanics. Addison-Wesley Publishing Company, Inc., Reading, Massachusetts, 1950.

27. Orne, D., and Liu, Y. K., "A Mathematical Model of Spinal Response to Impact." Transactions of The American Society of Mechanical Engineers, Paper No. 70-BHF-1, 1970.

28. Von Gierke, H. E., "Biodynamic Response of the Human Body." Applied Mechanics Reviews, Vol. 17, No. 12, December 1964.

29. Orne, D., and Liu, Y. K., "A Mathematical Model of Spinal Response to Impact." Journal of Biomechanics, Vol. 4, No. 1, January 1971, pp. 49-71.

30. McKenzie, J. A., and Williams, J. F., "The Dynamic Behaviour of the Head and Cervical Spine During 'Whiplash'" (unpublished paper, June 1971).

31. Markolf, K. L., and Steidel, R. F., Jr., "The Dynamic Characteristics of the Human Intervertebral Joint." Transactions of The American Society of Mechanical Engineers, Paper No. 70-WA/BHF-6, 1970.

32. Maté, P. I., and Popp, L. E., "Third Generation of Automotive Test Dummies." Proceedings of Fourteenth Stapp Car Crash Conference. Paper 700908, Society of Automotive Engineers, Inc., New York, 1970.

33. Hollister, N. R., Jolley, W. P., and Horne, R. G., "Biophysics of Concussion." WADC Technical Report No. ASTIA 203385, Part I, September 1958.

34. Ommaya, A. K., Hirsch, A. E., and Martinez, J. L., "The Role of Whiplash in Cerebral Concussion." Proceedings of Tenth Stapp Car Crash Conference. Paper 660804, Society of Automotive Engineers, Inc., New York, 1966.

35. Wickstrom, J. K., "Acceleration-Deceleration Injuries of the Cervical Spine in Animals." Proceedings of the Seventh Stapp Conference, Springfield, Illinois, 1963.

36. Ommaya, A. K., et al., "Scaling of Experimental Data on Cerebral Concussion in Sub-Human Primates to Concussion Threshold for Man." 11th Stapp Car Crash Conference. Paper 670906, Society of Automotive Engineers, Inc., New York, 1967.

37. Ommaya, A. K., and Hirsch, A. E., "Tolerances for Cerebral Concussion from Head Impact and Whiplash in Primates." Journal of Biomechanics, Vol. 4, No. 1, January 1971, pp. 13-21.

38. Mertz, H. J., Jr., and Patrick, L. M., "Investigation of the Kinematics and Kinetics of Whiplash." 11th Stapp Car Crash Conference. Paper 670919, Society of Automotive Engineers, Inc., New York, 1967.

39. Emori, R. I., and Tani, M., "Vehicle Trajectories After Intersection Collision Impact." Paper 700176, Society of Automotive Engineers, Inc., New York, January 1970.

40. Hamming, R. W., Numerical Methods for Scientists and Engineers. McGraw-Hill Book Company, Inc., New York, 1962.

41. Williams, M., and Lissner, H. R., Biomechanics of Human Motion. W. B. Saunders Company, Philadelphia, 1962.

42. Patrick, L. M., and Mertz, H. J., "Human Tolerance to Impact." Human Anatomy, Impact Injuries, and Human Tolerances, Society of Automotive Engineers, Inc., New York, 1970, pp. 90-103.

43. Aquino, C. F., "A Dynamic Model of the Lumbar Spine to Aid in the Study of Injury Due to Automobile Seat Belt Restraint." A dissertation for the degree of Doctor of Philosophy, The University of Michigan, 1969.

44. Crowe, A., "A Mechanical Model of Muscle and Its Application to the Intrafusal Fibres of the Mammalian Muscle Spindle." Journal of Biomechanics, Vol. 3, No. 5, October 1970, pp. 583-592.

45. Holbourn, A. H. S., "Mechanics of Head Injuries." Lancet, Vol. 245, October 1943, pp. 438-441.

46. Liu, Y. K., "Dynamic Response of the Human Body Considered as a Non-Linear System." Biomechanics Research Center Report, Wayne State University, 1962.

47. Morrison, J. B., "The Mechanics of Muscle Function in Locomotion." Journal of Biomechanics, Vol. 3, No. 4, July 1970, pp. 431-451.

48. Payne, P. R., "The Dynamics of Human Restraint Systems." Impact Acceleration Stress, National Academy of Sciences - National Research Council Publication NAS-NRC 977, 1962, pp. 195-258.

49. Payne, P. R., "Personnel Restraint and Support System Dynamics." Aerospace Medical Research Laboratories Tech. Rept. 65-127, Wright-Patterson A. F. B., Ohio, October 1965.

50. Robbins, D. H., "Three-Dimensional Simulation of Advanced Automotive Restraint Systems." 1970 International Automobile Safety Conference Compendium. Paper 700421, Society of Automotive Engineers, Inc., New York, 1970.

51. Schultz, A. B., and Galante, J. O., "A Mathematical Model for the Study of the Mechanics of the Human Vertebral Column." Journal of Biomechanics, Vol. 3, No. 4, July 1970, pp. 405-416.

52. Versace, J., "Experimental Validation of Dynamic Models." Automotive Safety Dynamic Modeling Symposium. Paper 670896, Society of Automotive Engineers, Inc., New York, October 1967.

APPENDIX A

DERIVATIVES

The rotation matrix determined in Chapter 4 has elements as follows:

$$a_{11,i} = \cos\psi_i \cos\theta_i$$

$$a_{12,i} = \sin\psi_i \cos\theta_i$$

$$a_{13,i} = -\sin\theta_i$$

$$a_{21,i} = \cos\psi_i \sin\theta_i \sin\phi_i - \sin\psi_i \cos\phi_i$$

$$a_{22,i} = \sin\psi_i \sin\theta_i \sin\phi_i + \cos\psi_i \cos\phi_i$$

$$a_{23,i} = \cos\theta_i \sin\phi_i$$

$$a_{31,i} = \cos\psi_i \sin\theta_i \cos\phi_i + \sin\psi_i \sin\phi_i$$

$$a_{32,i} = \sin\psi_i \sin\theta_i \cos\phi_i - \cos\psi_i \sin\phi_i$$

$$a_{33,i} = \cos\theta_i \cos\phi_i \quad .$$

The components in e_i of the angular velocity vectors were found to be as follows (see equations (4.3.6)):

$$\alpha_i = \dot{\phi}_i - \dot{\psi}_i \sin\theta_i$$

$$\beta_i = \dot{\psi}_i \cos\theta_i \sin\phi_i + \dot{\theta}_i \cos\phi_i$$

$$\gamma_i = \dot{\psi}_i \cos\theta_i \cos\phi_i - \dot{\theta}_i \sin\phi_i \quad .$$

The various time derivatives and partial derivatives of the above required in the equations of motion are presented in this appendix. Since the $a_{jk,i}$ are functions of $(\psi_i, \theta_i, \varphi_i)$ only, and since α_i, β_i, and γ_i are functions of $(\psi_i, \theta_i, \varphi_i, \dot{\psi}_i, \dot{\theta}_i, \dot{\varphi}_i)$ only, the subscript "i" can be omitted without confusion.

$$\dot{a}_{11} = -(\cos\psi \sin\theta\, \dot{\theta} + \sin\psi \cos\theta\, \dot{\psi})$$

$$\dot{a}_{12} = -\sin\psi \sin\theta\, \dot{\theta} + \cos\psi \cos\theta\, \dot{\psi}$$

$$\dot{a}_{13} = -\cos\theta\, \dot{\theta}$$

$$\dot{a}_{21} = \cos\psi \cos\theta \sin\varphi\, \dot{\theta} - a_{22}\dot{\psi} + a_{31}\dot{\varphi}$$

$$\dot{a}_{22} = \sin\psi \cos\theta \sin\varphi\, \dot{\theta} + a_{21}\dot{\psi} + a_{32}\dot{\varphi}$$

$$\dot{a}_{23} = \cos\theta \cos\varphi\, \dot{\varphi} - \sin\theta \sin\varphi\, \dot{\theta}$$

$$\dot{a}_{31} = \cos\psi \cos\theta \cos\varphi\, \dot{\theta} - a_{32}\dot{\psi} - a_{21}\dot{\varphi}$$

$$\dot{a}_{32} = \sin\psi \cos\theta \cos\varphi\, \dot{\theta} + a_{31}\dot{\psi} - a_{22}\dot{\varphi}$$

$$\dot{a}_{33} = -(\cos\theta \sin\varphi\, \dot{\varphi} + \sin\theta \cos\varphi\, \dot{\theta})$$

$$\begin{aligned} \ddot{a}_{11} = {} & -\cos\psi \sin\theta\, \ddot{\theta} - \sin\psi \cos\theta\, \ddot{\psi} - [(\cos\psi \cos\theta\, \dot{\theta} \\ & - \sin\psi \sin\theta\, \dot{\psi})\dot{\theta} + (-\sin\psi \sin\theta\, \dot{\theta} \\ & + \cos\psi \cos\theta\, \dot{\psi})\dot{\psi}] \end{aligned}$$

$$\begin{aligned}
\ddot{a}_{12} &= -\sin\psi\sin\theta\,\ddot{\theta} + \cos\psi\cos\theta\,\ddot{\psi} - \Big[(\sin\psi\cos\theta\,\dot{\theta} \\
&\quad + \cos\psi\sin\theta\,\dot{\psi})\,\dot{\theta} + (\cos\psi\sin\theta\,\dot{\theta} \\
&\quad + \sin\psi\cos\theta\,\dot{\psi})\,\dot{\psi}\Big] \\
\ddot{a}_{13} &= -\cos\theta\,\ddot{\theta} + \sin\theta\,\dot{\theta}^2 \\
\ddot{a}_{21} &= a_{31}\ddot{\phi} + \cos\psi\cos\theta\sin\phi\,\ddot{\theta} - a_{22}\ddot{\psi} \\
&\quad + \dot{\theta}\big(-\sin\psi\cos\theta\sin\phi\,\dot{\psi} - \cos\psi\sin\theta\sin\phi\,\dot{\theta} \\
&\quad + \cos\psi\cos\theta\cos\phi\,\dot{\phi}\big) - \dot{a}_{22}\dot{\psi} + \dot{a}_{31}\dot{\phi} \\
\ddot{a}_{22} &= a_{32}\ddot{\phi} + \sin\psi\cos\theta\sin\phi\,\ddot{\theta} + a_{21}\ddot{\psi} + \dot{a}_{21}\dot{\psi} \\
&\quad + \dot{a}_{32}\dot{\phi} + \dot{\theta}\big(\sin\psi\cos\theta\cos\phi\,\dot{\phi} \\
&\quad - \sin\psi\sin\theta\sin\phi\,\dot{\theta} + \cos\psi\cos\theta\sin\phi\,\dot{\psi}\big) \\
\ddot{a}_{23} &= \cos\theta\cos\phi\,\ddot{\phi} - \sin\theta\sin\phi\,\ddot{\theta} - \dot{\phi}\big(\sin\theta\cos\phi\,\dot{\theta} \\
&\quad + \cos\theta\sin\phi\,\dot{\phi}\big) - \dot{\theta}\big(\cos\theta\sin\phi\,\dot{\theta} + \sin\theta\cos\phi\,\dot{\phi}\big) \\
\ddot{a}_{31} &= -a_{32}\ddot{\psi} + \cos\psi\cos\theta\cos\phi\,\ddot{\theta} - a_{21}\ddot{\phi} - \dot{a}_{32}\dot{\psi} \\
&\quad - \dot{a}_{21}\dot{\phi} - \dot{\theta}\big(\cos\psi\cos\theta\sin\phi\,\dot{\phi} \\
&\quad + \cos\psi\sin\theta\cos\phi\,\dot{\theta} + \sin\psi\cos\theta\cos\phi\,\dot{\psi}\big) \\
\ddot{a}_{32} &= a_{31}\ddot{\psi} - a_{22}\ddot{\phi} + \sin\psi\cos\theta\cos\phi\,\ddot{\theta} + \dot{a}_{31}\dot{\psi} \\
&\quad - \dot{a}_{22}\dot{\phi} + \dot{\theta}\big(-\sin\psi\cos\theta\sin\phi\,\dot{\phi} \\
&\quad - \sin\psi\sin\theta\cos\phi\,\dot{\theta} + \cos\psi\cos\theta\cos\phi\,\dot{\psi}\big)
\end{aligned}$$

$$\ddot{a}_{33} = -\cos\theta \sin\varphi \ddot{\varphi} - \sin\theta \cos\varphi \ddot{\theta} - \dot{\varphi}(\cos\theta \cos\varphi \dot{\varphi} - \sin\theta \sin\varphi \dot{\theta}) - \dot{\theta}(\cos\theta \cos\varphi \dot{\theta} - \sin\theta \sin\varphi \dot{\varphi})$$

$$\dot{\alpha} = \ddot{\varphi} - \ddot{\psi} \sin\theta - \dot{\psi}\dot{\theta} \cos\theta$$

$$\dot{\beta} = \ddot{\psi} \sin\varphi \cos\theta + \ddot{\theta} \cos\varphi + \dot{\psi}(\dot{\varphi} \cos\varphi \cos\theta - \dot{\theta} \sin\varphi \sin\theta) - \dot{\theta}\dot{\varphi} \sin\varphi$$

$$\dot{\gamma} = \ddot{\psi} \cos\varphi \cos\theta - \ddot{\theta} \sin\varphi - \dot{\psi}(\dot{\varphi} \sin\varphi \cos\theta + \dot{\theta} \cos\varphi \sin\theta) - \dot{\theta}\dot{\varphi} \cos\varphi$$

The following partial derivatives are required:

$$\frac{\partial a_{jk}}{\partial q}, \quad \frac{\partial \dot{a}_{jk}}{\partial \dot{q}}, \quad \frac{\partial \dot{a}_{jk}}{\partial q}, \quad \frac{d}{dt}\frac{\partial \dot{a}_{jk}}{\partial \dot{q}} .$$

It is easily demonstrated that the first and third of these are identical to the second and fourth, respectively. Thus, it suffices to give the second and its time derivative (the fourth). These are below.

$$\frac{\partial \dot{a}_{11}}{\partial \dot{\psi}} = -\sin\psi \cos\theta \qquad \frac{d}{dt}: \ -\dot{\psi} \cos\psi \cos\theta + \dot{\theta} \sin\psi \sin\theta$$

$$\frac{\partial \dot{a}_{11}}{\partial \dot{\theta}} = -\cos\psi \sin\theta \qquad \frac{d}{dt}: \ \dot{\psi} \sin\psi \sin\theta - \dot{\theta} \cos\psi \cos\theta$$

$$\frac{\partial \dot{a}_{11}}{\partial \dot{\varphi}} = 0 \qquad \frac{d}{dt}: \quad 0$$

$$\frac{\partial \dot{a}_{12}}{\partial \dot{\psi}} = \cos\psi\cos\theta \qquad \frac{d}{dt}: -(\dot{\psi}\sin\psi\cos\theta + \dot{\theta}\cos\psi\sin\theta)$$

$$\frac{\partial \dot{a}_{12}}{\partial \dot{\theta}} = -\sin\psi\sin\theta \qquad \frac{d}{dt}: -(\dot{\psi}\cos\psi\sin\theta + \dot{\theta}\sin\psi\cos\theta)$$

$$\frac{\partial \dot{a}_{12}}{\partial \dot{\varphi}} = 0 \qquad \frac{d}{dt}: \quad 0$$

$$\frac{\partial \dot{a}_{13}}{\partial \dot{\psi}} = 0 \qquad \frac{d}{dt}: \quad 0$$

$$\frac{\partial \dot{a}_{13}}{\partial \dot{\theta}} = -\cos\theta \qquad \frac{d}{dt}: \quad \dot{\theta}\sin\theta$$

$$\frac{\partial \dot{a}_{13}}{\partial \dot{\varphi}} = 0 \qquad \frac{d}{dt}: \quad 0$$

$$\frac{\partial \dot{a}_{21}}{\partial \dot{\psi}} = -a_{22} \qquad \frac{d}{dt}: \quad -\dot{a}_{22}$$

$$\frac{\partial \dot{a}_{21}}{\partial \dot{\theta}} = \cos\psi\cos\theta\sin\varphi \qquad \frac{d}{dt}: \quad \dot{\psi}(-\sin\psi\cos\theta\sin\varphi)$$

$$-\dot{\theta}\cos\psi\sin\theta\sin\varphi + \dot{\varphi}\cos\psi\cos\theta\cos\varphi$$

$$\frac{\partial \dot{a}_{21}}{\partial \dot{\varphi}} = a_{31} \qquad \frac{d}{dt}: \quad \dot{a}_{31}$$

$$\frac{\partial \dot{a}_{22}}{\partial \dot{\psi}} = a_{21} \qquad \frac{d}{dt}: \quad \dot{a}_{21}$$

$$\frac{\partial \dot{a}_{22}}{\partial \dot{\theta}} = \sin\psi \cos\theta \sin\varphi \qquad \frac{d}{dt}: \ \dot{\psi} \cos\psi \cos\theta \sin\varphi$$

$$- \dot{\theta} \sin\psi \sin\theta \sin\varphi + \dot{\varphi} \sin\psi \cos\theta \cos\varphi$$

$$\frac{\partial \dot{a}_{22}}{\partial \dot{\varphi}} = a_{32} \qquad \frac{d}{dt}: \ \dot{a}_{32}$$

$$\frac{\partial \dot{a}_{23}}{\partial \dot{\psi}} = 0 \qquad \frac{d}{dt}: \ 0$$

$$\frac{\partial \dot{a}_{23}}{\partial \dot{\theta}} = -\sin\theta \sin\varphi \qquad \frac{d}{dt}: \ -(\dot{\theta} \cos\theta \sin\varphi + \dot{\varphi} \sin\theta \cos\varphi)$$

$$\frac{\partial \dot{a}_{23}}{\partial \dot{\varphi}} = \cos\theta \cos\varphi \qquad \frac{d}{dt}: \ -(\dot{\theta} \sin\theta \cos\varphi + \dot{\varphi} \cos\theta \sin\varphi)$$

$$\frac{\partial \dot{a}_{31}}{\partial \dot{\psi}} = -a_{32} \qquad \frac{d}{dt}: \ -\dot{a}_{32}$$

$$\frac{\partial \dot{a}_{31}}{\partial \dot{\theta}} = \cos\psi \cos\theta \cos\varphi \qquad \frac{d}{dt}: \ -(\dot{\psi} \sin\psi \cos\theta \cos\varphi$$

$$+ \dot{\theta} \cos\psi \sin\theta \cos\varphi + \dot{\varphi} \cos\psi \cos\theta \sin\varphi)$$

$$\frac{\partial \dot{a}_{31}}{\partial \dot{\varphi}} = -a_{21} \qquad \frac{d}{dt}: \ -\dot{a}_{21}$$

$$\frac{\partial \dot{a}_{32}}{\partial \dot{\psi}} = a_{31} \qquad \frac{d}{dt}: \ \dot{a}_{31}$$

$$\frac{\partial \dot{a}_{32}}{\partial \dot{\theta}} = \sin\psi \cos\theta \cos\varphi \qquad \frac{d}{dt}: \ \dot{\psi} \cos\psi \cos\theta \cos\varphi$$

$$- \dot{\theta} \sin\psi \sin\theta \cos\varphi - \dot{\varphi} \sin\psi \cos\theta \sin\varphi$$

$$\frac{\partial \dot{a}_{32}}{\partial \dot{\varphi}} = -a_{22} . \qquad \frac{d}{dt}: \quad -\dot{a}_{22}$$

$$\frac{\partial \dot{a}_{33}}{\partial \dot{\psi}} = 0 \qquad \frac{d}{dt}: \quad 0$$

$$\frac{\partial \dot{a}_{33}}{\partial \dot{\theta}} = -\sin\theta\cos\varphi \qquad \frac{d}{dt}: \; -(\dot{\theta}\cos\theta\cos\varphi - \dot{\varphi}\sin\theta\sin\varphi)$$

$$\frac{\partial \dot{a}_{33}}{\partial \dot{\varphi}} = -\cos\theta\sin\varphi \qquad \frac{d}{dt}: \; \dot{\theta}\sin\theta\sin\varphi - \dot{\varphi}\cos\theta\cos\varphi$$

The required derivatives of α, β, and γ are now presented.

$$\frac{\partial \alpha}{\partial \psi} = 0$$

$$\frac{\partial \alpha}{\partial \theta} = -\dot{\psi}\cos\theta$$

$$\frac{\partial \alpha}{\partial \varphi} = 0$$

$$\frac{\partial \beta}{\partial \psi} = 0$$

$$\frac{\partial \beta}{\partial \theta} = -\dot{\psi}\sin\varphi\sin\theta$$

$$\frac{\partial \beta}{\partial \varphi} = \dot{\psi}\cos\varphi\cos\theta - \dot{\theta}\sin\varphi$$

$$\frac{\partial \gamma}{\partial \psi} = 0$$

$$\frac{\partial\gamma}{\partial\theta} = -\dot\psi\cos\varphi\sin\theta$$

$$\frac{\partial\gamma}{\partial\varphi} = -\dot\psi\sin\varphi\cos\theta - \dot\theta\cos\varphi$$

$$\frac{\partial\alpha}{\partial\dot\psi} = -\sin\theta \qquad \frac{d}{dt}: \quad -\cos\theta\,\dot\theta$$

$$\frac{\partial\alpha}{\partial\dot\theta} = 0 \qquad \frac{d}{dt}: \quad 0$$

$$\frac{\partial\alpha}{\partial\dot\varphi} = 1 \qquad \frac{d}{dt}: \quad 0$$

$$\frac{\partial\beta}{\partial\dot\psi} = \sin\varphi\cos\theta \qquad \frac{d}{dt}: \quad \dot\varphi\cos\varphi\cos\theta - \dot\theta\sin\varphi\sin\theta$$

$$\frac{\partial\beta}{\partial\dot\theta} = \cos\varphi \qquad \frac{d}{dt}: \quad -\sin\varphi\,\dot\varphi$$

$$\frac{\partial\beta}{\partial\dot\varphi} = 0 \qquad \frac{d}{dt}: \quad 0$$

$$\frac{\partial\gamma}{\partial\dot\psi} = \cos\varphi\cos\theta \qquad \frac{d}{dt}: \quad -(\dot\varphi\sin\varphi\cos\theta + \dot\theta\cos\varphi\sin\theta)$$

$$\frac{\partial\gamma}{\partial\dot\theta} = -\sin\varphi \qquad \frac{d}{dt}: \quad -\cos\varphi\,\dot\varphi$$

$$\frac{\partial\gamma}{\partial\dot\varphi} = 0 \qquad \frac{d}{dt}: \quad 0$$

Finally, derivatives of $\dot{x}_h$, $\dot{y}_h$, and $\dot{z}_h$ are given.

$$\frac{\partial \dot{x}_h}{\partial \dot{x}} = a_{11,1}$$

$$\frac{\partial \dot{x}_h}{\partial \dot{y}} = a_{21,1}$$

$$\frac{\partial \dot{x}_h}{\partial \dot{z}} = a_{31,1}$$

$$\dot{q} = (\dot{\psi}_1, \dot{\theta}_1, \dot{\varphi}_1):$$

$$\frac{\partial \dot{x}_h}{\partial \dot{q}} = (x - x_0)\frac{\partial \dot{a}_{11,1}}{\partial \dot{q}} + y\frac{\partial \dot{a}_{21,1}}{\partial \dot{q}} - \left(-z + \frac{\ell_1}{2}\right)\frac{\partial \dot{a}_{31,1}}{\partial \dot{q}}$$

$$\dot{q} = (\dot{\psi}_h, \dot{\theta}_h, \dot{\varphi}_h):$$

$$\frac{\partial \dot{x}_h}{\partial \dot{q}} = d\,\frac{\partial \dot{a}_{11,h}}{\partial \dot{q}} - \frac{\partial \dot{a}_{31,h}}{\partial \dot{q}}$$

The preceding results hold for $\dot{y}_h$ and $\dot{z}_h$ if all second subscripts are changed to 2 and 3, respectively. Also,

$$\frac{\partial \dot{x}_h}{\partial \dot{x}_1} = \frac{\partial \dot{y}_h}{\partial \dot{y}_1} = \frac{\partial \dot{z}_h}{\partial \dot{z}_1} = 1 \quad .$$

APPENDIX B

SOLUTION FOR MUSCLE TENSION FORCE BY REDUCTION TO QUADRATURE

In some circumstances it might not be desired to solve equation (4.8.6) as part of a system of differential equations. It may be solved alternatively by quadrature as long as $\dot{x}(t)$ is known. Equation (4.8.6), repeated here as equation (B.1), is dealt with alone in this appendix, and it is put into the best form for a numerical quadrature solution. Any number of numerical methods are then suitable for obtaining F(t).

$$\dot{F} + \frac{k}{c} F = -k\dot{x} \tag{B.1}$$

$e^{kt/c}$ is an integrating factor for the left-hand side of (B.1). By multiplying the equation by $e^{kt/c}$ and integrating from 0 to t, we obtain

$$\left. e^{kt/c} F \right]_0^t = -k\int_0^t e^{k\tau/c}\, \dot{x}(\tau)\, d\tau \quad , \tag{B.2}$$

or

$$F(t) = F_0\, e^{-kt/c} - k\, e^{-kt/c}\int_0^t e^{k\tau/c}\, \dot{x}(\tau)\, d\tau. \tag{B.3}$$

The integral in (B.3) is not in a form well suited to numerical integration. The integrand values are likely to change quite rapidly because of both factors, the exponential and the velocity $\dot{x}$.

Define I and a as follows;

$$I = e^{-kt/c}\int_0^t e^{k\tau/c}\, \dot{x}(\tau)\, d\tau \tag{B.4}$$

$$a = k/c \quad . \tag{B.5}$$

Then,

$$I = \int_0^t e^{-a(t-\tau)} \dot{x}(\tau)\, d\tau \quad . \tag{B.6}$$

An integration by parts then yields

$$I = x(\tau)\, e^{-a(t-\tau)} \Big]_0^t - a \int_0^t x(\tau)\, e^{-a(t-\tau)} d\tau \, , \tag{B.7}$$

or

$$I = x - x_0 e^{-at} - a \int_0^t x(\tau)\, e^{-a(t-\tau)} d\tau \quad . \tag{B.8}$$

Therefore, equation (B.3) becomes

$$\begin{aligned} F(t) = -kx + \left(F_0 + kx_0\right) e^{-kt/c} \\ + \frac{k^2}{c} \int_0^t x(\tau)\, e^{-k(t-\tau)/c}\, d\tau \quad . \end{aligned} \tag{B.9}$$

This form is considerably better than (B.3) for numerical integration since both factors in the integrand will change less rapidly than their counterparts in (B.3).

Depending on how x(t) is obtained, values for x may or may not be available for evenly spaced values of time. Since virtually all numerical quadrature formulas to be found in references on numerical analysis involve constant integration step size, a three-point quadrature formula is developed here for variable step size. If greater accuracy is required, then a five-point integration formula could be derived in a simular manner. The error terms for this type of integration decrease in order of magnitude by pairs, four-point being little better than three-point.

The Lagrange interpolation formula (40), equation (B.10), is used to fit a second-degree polynomial f(t) through three points with abscissas t_0, t_1, t_2 and ordinates f_0, f_1, f_2, where f_i are integrand values.

$$f(t) = \sum_{i=0}^{2} L_i(t) f_i \tag{B.10}$$

Here,

$$\begin{aligned} L_0(t) &= \frac{(t-t_1)(t-t_2)}{(t_0-t_1)(t_0-t_2)} \\ L_1(t) &= \frac{(t-t_0)(t-t_2)}{(t_1-t_0)(t_1-t_2)} \\ L_2(t) &= \frac{(t-t_0)(t-t_1)}{(t_2-t_0)(t_2-t_1)} \end{aligned} \tag{B.11}$$

Unequal step sizes h_1 and h_2 are assumed, i.e.,

$$t_1 = t_0 + h_1$$
$$t_2 = t_1 + h_2 = t_0 + h_1 + h_2 \quad . \tag{B.12}$$

Integration of (B.10) from t_0 to t_2 gives

$$\int_{t_0}^{t_2} f(t)\,dt = \sum_{i=0}^{2} f_i \int_{t_0}^{t_2} L_i(t)\,dt \quad . \tag{B.13}$$

Now, the polynomials $L_i(t)$ in the right-hand side of (B.13) are available from (B.11) and, after expansion, may be integrated easily. After tedious but straightforward algebraic manipulation of the results, all t_i may be eliminated in favor of h_1 and h_2 by relations (B.12). The final result of this procedure is given by equation (B.14), where the summation in (B.13) is expanded.

$$\int_{t_0}^{t_2} f(t)\,dt = \frac{h_1+h_2}{6h_1}(2h_1-h_2)f_0 + \frac{(h_1+h_2)^3}{6h_1h_2}f_1 + \frac{h_1+h_2}{6h_2}(2h_2-h_1)f_2 \quad . \tag{B.14}$$

This result if seen to reduce to Simpson's Rule if $h_1 = h_2 = h$, and it predicts properly that the integral is equal to $h_1 + h_2$ in the case that $f_0 = f_1 = f_2 = 1$.

APPENDIX C

A SIMPLE DYNAMIC SYSTEM INVOLVING A MAXWELL ELEMENT

Figure 90 below may be compared with Figure 15 of Section 4.8. The Maxwell elements are identical; M_1, M_2, M_3, K, and C in Figure 90 represent the "black boxes" in Figure 15; and X(t) is a displacement excitation.

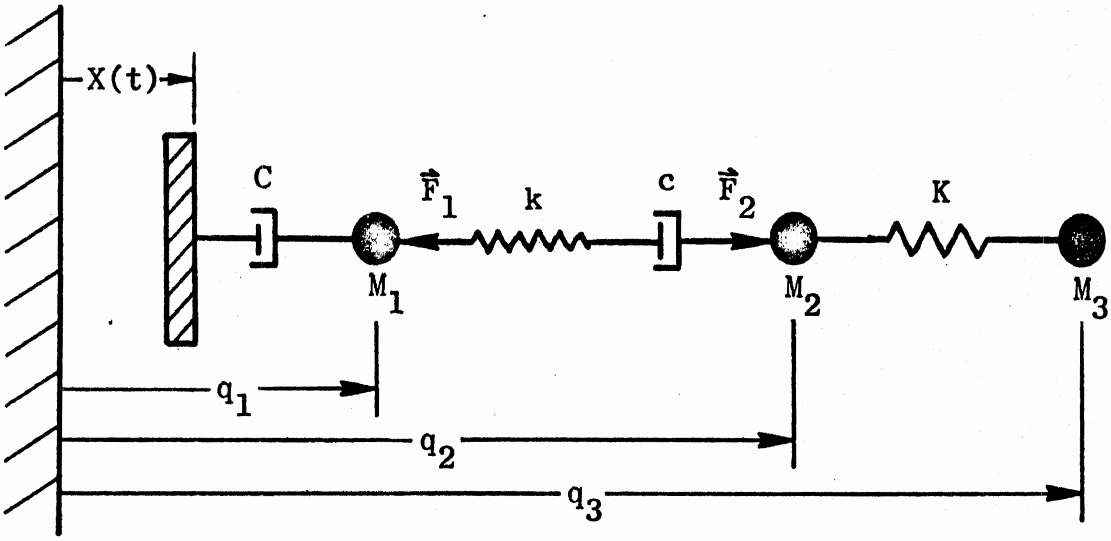

Figure 90. A simple dynamic system with Maxwell element.

Let l_0 be the equilibrium length of the spring joining M_2 and M_3. Then, the kinetic energy, potential energy, and dissipation function of the system are

$$\begin{aligned} T &= \tfrac{1}{2} M_1 \dot{q}_1^2 + \tfrac{1}{2} M_2 \dot{q}_2^2 + \tfrac{1}{2} M_3 \dot{q}_3^2 \\ V &= \tfrac{1}{2} K (q_3 - q_2 - \ell_0)^2 \\ D &= \tfrac{1}{2} C (\dot{q}_1 - \dot{X})^2 \end{aligned} \qquad (C.1)$$

.

Where F is defined by

$$\vec{F}_2 = -\vec{F}_1 = F\hat{\ell} \quad , \tag{C.2}$$

the Lagrange equations of motion are then

$$\begin{aligned}
\frac{d}{dt}\frac{\partial T}{\partial \dot{q}_1} + \frac{\partial D}{\partial \dot{q}_1} &= -F(t) \\
\frac{d}{dt}\frac{\partial T}{\partial \dot{q}_2} + \frac{\partial V}{\partial q_2} &= F(t) \\
\frac{d}{dt}\frac{\partial T}{\partial \dot{q}_3} + \frac{\partial V}{\partial q_3} &= 0 \quad ,
\end{aligned} \tag{C.3}$$

or

$$\begin{aligned}
M_1\ddot{q}_1 + C(\dot{q}_1 - \dot{X}) &= -F(t) \\
M_2\ddot{q}_2 - K(q_3 - q_2 - \ell_0) &= F(t) \\
M_3\ddot{q}_3 + K(q_3 - q_2 - \ell_0) &= 0 \quad .
\end{aligned} \tag{C.4}$$

Corresponding to equation (4.8.6), the differential equation for F is

$$\dot{F} + \frac{k}{c}F = -k(\dot{q}_2 - \dot{q}_1) \quad . \tag{C.5}$$

Equations (C.4) with (C.5), then, are the system of governing differential equations for the dynamic system in Figure 90.

APPENDIX D

ANALYTICAL SOLUTIONS FOR SPECIAL CASES

This appendix contains the analysis for some of the preliminary model verification tests mentioned in Chapter 6. All of these are free motion problems.

D.1 Gravity test

Suppose that the elements of the entire dynamic system, including the head-neck portion, are oriented in space by random values of the Euler angle coordinates. If the linkage is then allowed to fall in a gravitational field, all angle coordinates must be constant in time and the system as a whole must fall with acceleration g, velocity gt, and distance $\frac{1}{2} gt^2$.

D.2 Twisting test

Suppose three identical (torso) elements to be positioned as shown in Figure 91 at t = 0. The stop angles for twisting are zero and the two joints have identical joint stop k and c values for linear terms (quadratic and cubic terms equal to zero). Elements 1 and 3 are rotated (yawed) by equal amounts in opposite directions against the stops and released at t = 0. Then, by symmetry, ψ_2 must be identically zero and ψ_3 must be identically the negative of ψ_1. The problem therefore reduces to determining ψ_1, or ψ, as illustrated in Figure 91.

The equation of motion is

$$\ddot{\psi} + \frac{c}{I}\dot{\psi} + \frac{k}{I}\psi = 0 \,, \qquad \text{(D.2.1)}$$

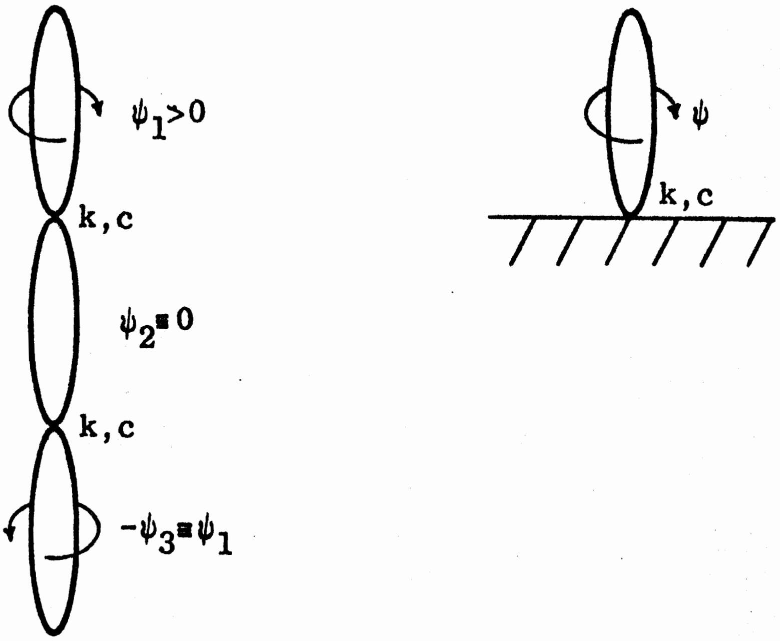

Figure 91. Twisting test.

where I is the moment of inertia for yawing. The general solution of (D.2.1) is

$$\psi = A e^{-ct/2I} \cos(\omega t + \varphi) \quad , \qquad (D.2.2)$$

where

$$\omega = \frac{\sqrt{4kI - c^2}}{2I} \quad . \qquad (D.2.3)$$

Application of the initial conditions $\psi(0) = \psi_0$ and $\dot{\psi}(0) = 0$ to (D.2.2) gives

$$A = \psi_0 / \cos\varphi \qquad (D.2.4)$$

$$0 = \sqrt{4kI - c^2} \sin\varphi + c \cos\varphi \quad . \qquad (D.2.5)$$

The sign of $\cos\varphi$ is not uniquely determined by (D.2.5). However, in order to have A positive, we may choose sgn $(\cos\varphi)$ = sgn ψ_0. Thus, as

ψ_0 will be taken as positive, we obtain

$$A = \psi_0 \sqrt{\frac{4kI}{4kI - c^2}} \quad . \tag{D.2.6}$$

Note that (D.2.5) indicates that $\sin\varphi$ and $\cos\varphi$ are of opposite sign, i.e., φ is in the second or fourth quadrant. Since $\cos\varphi$ has arbitrarily been taken as positive, φ must be in the fourth quadrant. Hence,

$$\varphi = \tan^{-1} \frac{(-c)}{\sqrt{4kI - c^2}} \quad . \tag{D.2.7}$$

$\psi(t)$ is thus determined. Computer model results are also compared with $\dot{\psi}$, which is given by equation (D.2.8).

$$\begin{aligned} \dot{\psi} = & -A \frac{\sqrt{4kI - c^2}}{2I} e^{-ct/2I} \sin(\omega t + \varphi) \\ & -A \frac{c}{2I} e^{-ct/2I} \cos(\omega t + \varphi) \end{aligned} \tag{D.2.8}$$

The total energy dissipation can also be calculated and compared with computer model results. The energy dissipated for the three-element system is

$$Diss = 2\int_0^t c\,\dot{\psi}^2\,dt \quad . \tag{D.2.9}$$

Equation (D.2.9) could be evaluated by integrating $\dot{\psi}^2$, but a simpler method is available. Since $\dot{\psi}$ is an integrating factor for the first and third terms of (D.2.1), multiplication of that equation by $\dot{\psi}dt$ gives

$$d(\dot{\psi}^2) + \frac{2}{I} c \dot{\psi}^2 dt + \frac{k}{I} d(\psi^2) = 0 \ . \qquad \text{(D.2.10)}$$

Therefore, by (D.2.9) and (D.2.10), we have

$$\mathrm{Diss} = -I \int_0^t \left[\frac{k}{I} d(\psi^2) + d(\dot{\psi}^2) \right] \qquad \text{(D.2.11)}$$

or

$$\mathrm{Diss} = \Big[k\psi^2 + I\dot{\psi}^2 \Big]_t^0 \ . \qquad \text{(D.2.12)}$$

Then, Diss may be evaluated directly by (D.2.12) after values for $\psi(t)$ and $\dot{\psi}(t)$ have been found. Alternatively, it may be written out as an explicit function of t. Its simplest form is given by (D.2.13) and may be obtained from (D.2.12) by using the results (D.2.2) and (D.2.8) for $\psi(t)$ and $\dot{\psi}(t)$. Considerable algebraic and trigonometric manipulation, together with two applications of (D.2.5), yields

$$\begin{aligned} \mathrm{Diss} = \frac{A^2}{4I} \Big\{ (4kI - c^2) - e^{-ct/I} \Big[& (4kI - c^2) \\ & + 2c^2 \cos^2(\omega t + \varphi) \\ & + c\sqrt{4kI - c^2}\, \sin 2(\omega t + \varphi) \Big] \Big\}, \end{aligned} \qquad \text{(D.2.13)}$$

where A is in radians.

D.3 Pitching test, elastic k

Three identical elements of length l are positioned in a plane as shown in Figure 92 at t = 0. The joints have identical elastic spring rates for pitching. The initial configuration is symmetric and initial

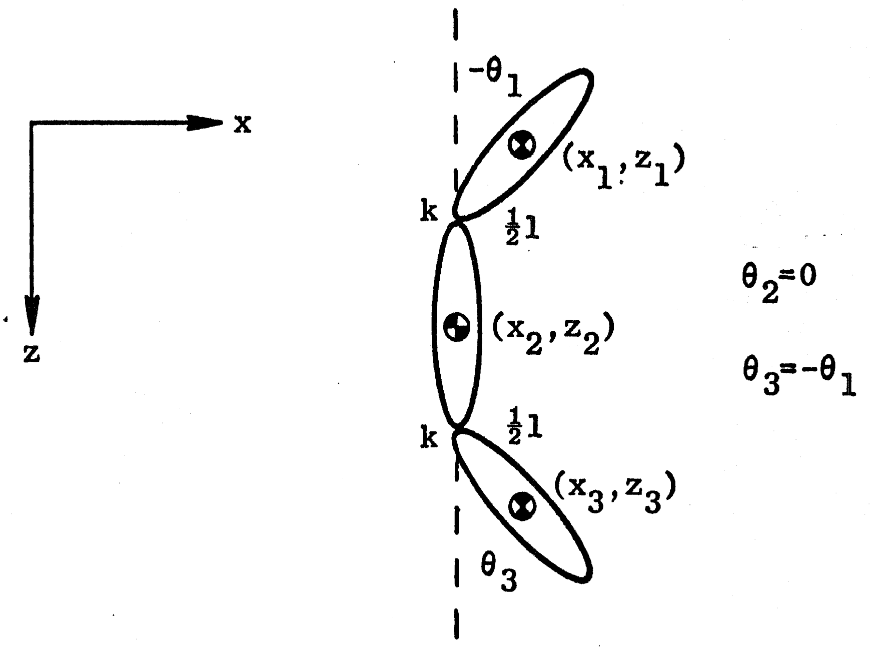
x
z
$-\theta_1$
(x_1,z_1)
k
$\frac{1}{2}l$
(x_2,z_2)
k
$\frac{1}{2}l$
(x_3,z_3)
θ_3
$\theta_2=0$
$\theta_3=-\theta_1$

Figure 92. Pitching test, elastic k.

velocities $\dot{\theta}_1(0)$ and $\dot{\theta}_3(0) = -\dot{\theta}_1(0)$ are prescribed. The problem is clearly reduced, essentially, to one angular and one linear degree of freedom (say, θ_1 and x_1).

By the symmetry and the constraints of this problem we have immediately that

$$
\begin{aligned}
X_2 &= X_1 + \frac{\ell}{2}\sin\theta_1 \\
\dot{X}_2 &= \dot{X}_1 + \frac{\ell}{2}\dot{\theta}_1\cos\theta_1 \\
X_3 &= X_1 \\
\dot{X}_3 &= \dot{X}_1 \\
\theta_2 &= \dot{\theta}_2 = 0 \\
\theta_3 &= -\theta_1 \\
\dot{\theta}_3 &= -\dot{\theta}_1 \qquad .
\end{aligned}
\tag{D.3.1}
$$

Now, note that requiring conservation of x-momentum gives

$$
\begin{aligned}
m\dot{X}_1 + m\dot{X}_2 + m\dot{X}_3 = &- m\frac{\ell}{2}\cos\theta_1(0)\,\dot{\theta}_1(0) \\
&+ m\frac{\ell}{2}\cos\theta_3(0)\,\dot{\theta}_3(0) .
\end{aligned}
\tag{D.3.2}
$$

By (D.3.14) this becomes

$$
3\dot{X}_1 + \frac{\ell}{2}\dot{\theta}_1\cos\theta_1 = -\ell\cos\theta_1(0)\,\dot{\theta}_1(0) , \tag{D.3.3}
$$

or

$$
3\,dX_1 + \frac{\ell}{2}\cos\theta_1\,d\theta_1 = -\ell\cos\theta_1(0)\,\dot{\theta}_1(0)\,dt . \tag{D.3.4}
$$

Integrating and determining the arbitrary constant of integration in terms of initial conditions (t = 0), we obtain finally

$$
\begin{aligned}
3X_1 + \frac{\ell}{2}\sin\theta_1 = &-\ell\cos\theta_1(0)\,\dot{\theta}_1(0)\,t \\
&+ 3X_1(0) + \frac{\ell}{2}\sin\theta_1(0) \quad .
\end{aligned}
\tag{D.3.5}
$$

While this is not a complete solution, it does indicate an explicit t-dependence for a simple function of x_1 and θ_1. Satisfaction of this time-dependent constraint represents a partial verification of computer model results.

D.4 Pitching test, joint stop c

Consider another three-mass, free motion problem. Suppose that the first and second elements have very large masses and moments of inertia in comparison with the third, and suppose that the first two elements are initially at rest. This system is shown in Figure 93. Motion of the third element should cause only slight motion of the massive elements. As the mass and pitching moment of inertia for the second element are made larger and larger, the motion of the third element - given a set of initial conditions - should approach more and more closely the motion of an identical element with a solid anchor.

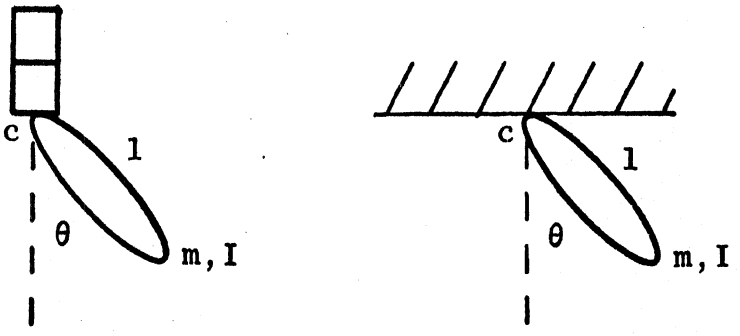

Figure 93. Pitching test, joint stop c.

Since joint stop damping will be assumed, but no spring, as indicated in the figure, the only possible motions are for $\dot{\theta}(t) \leq 0$ or $\dot{\theta}(t) \geq 0$. No oscillation is possible. It will be sufficient to solve the problem for $\dot{\theta}(t) \geq 0$, arbitrarily, and $\theta \geq 0$. Let the joint stop angle for forward pitching be zero so that the deformation will be θ itself. The first-order joint stop damping coefficient is

$$\begin{aligned} c &= \frac{\theta}{\Delta} C \,, & \theta &\le \Delta \\ c &= C \,, & \theta &> \Delta \,. \end{aligned} \tag{D.4.1}$$

Here, Δ and C are the constants defined in the footnote in Section 4.6.2.

The kinetic energy is

$$T = \frac{1}{2}\left(I + m\frac{\ell^2}{4}\right)\dot{\theta}^2 \,, \tag{D.4.2}$$

where $I = I_{CG}$. The dissipation function is

$$\begin{aligned} D &= \frac{1}{2}\frac{\theta}{\Delta} C \dot{\theta}^2 \,, & \theta &\le \Delta \\ D &= \frac{1}{2} C \dot{\theta}^2 \,, & \theta &> \Delta \,. \end{aligned} \tag{D.4.3}$$

Therefore,

$$\begin{aligned} \frac{\partial D}{\partial \dot{\theta}} &= \frac{\theta}{\Delta} C \dot{\theta} \,, & \theta &\le \Delta \\ \frac{\partial D}{\partial \dot{\theta}} &= C \dot{\theta} \,, & \theta &> \Delta \,. \end{aligned} \tag{D.4.4}$$

The equation of motion, then, is

$$\left(I + m\frac{\ell^2}{4}\right)\ddot{\theta} + C\dot{\theta}\,\min\left\{1, \frac{\theta}{\Delta}\right\} = 0 \,. \tag{D.4.5}$$

Solutions must be obtained for the two regions $\theta \leq \Delta$ and $\theta > \Delta$ and matched at $\theta = \Delta$.

$\underline{\theta \leq \Delta}$:

The equation of motion (D.4.5) becomes

$$a\ddot{\theta} + C\dot{\theta}\frac{\theta}{\Delta} = 0 \; , \tag{D.4.6}$$

where

$$a = I + m\frac{\ell^2}{4} \; . \tag{D.4.7}$$

By the change of variable $p = \dot{\theta}$, equation (D.4.6) can be reduced to quadrature:

$$t + C_2 = -\frac{2a\Delta}{C}\int \frac{d\theta}{\theta^2 - \frac{2a\Delta C_1}{C}} \; . \tag{D.4.8}$$

C_1 and C_2 are constants of integration, and

$$C_1 = \dot{\theta} + \frac{C}{2a\Delta}\theta^2 = \dot{\theta}_o + \frac{C}{2a\Delta}\theta_o^2 \; . \tag{D.4.9}$$

Since a, Δ, and C are positive, the form of the integral in (D.4.8) depends upon the sign of C_1. But since $\dot{\theta}$ and θ are both positive, equation (D.4.9) indicates that C_1 is positive. Therefore, where

$$d = \sqrt{\frac{2a\Delta C_1}{C}} \; , \tag{D.4.10}$$

we obtain

$$t + C_2 = \frac{a\Delta}{C} \frac{1}{d} \log \frac{d+\theta}{d-\theta} \quad . \tag{D.4.11}$$

Equation (D.4.11) gives, for t = 0,

$$C_2 = \frac{a\Delta}{C} \frac{1}{d} \log \frac{d+\theta_0}{d-\theta_0} \quad . \tag{D.4.12}$$

Eliminating C_2 in (D.4.11) and solving for θ, we obtain

$$\theta(t) = d \frac{h(t)-1}{h(t)+1} \tag{D.4.13}$$

where

$$h(t) = \frac{d+\theta_0}{d-\theta_0} \exp\left[\frac{Cd}{a\Delta} t\right] \quad . \tag{D.4.14}$$

The solution for $\theta \leq \Delta$ is complete.

$\theta > \Delta$:

The equation of motion (D.4.5) becomes

$$a\ddot{\theta} + C\dot{\theta} = 0 \quad . \tag{D.4.15}$$

The general solution may be written as

$$\theta = C_3 + C_4 e^{-C(t-t_R)/a} \quad , \tag{D.4.16}$$

where t_R is defined to be the time at which $\theta = \Delta$ occurs in the first range of the motion, $\theta \leq \Delta$. It can be shown from (D.4.13) and (D.4.14) that

$$t_R = \frac{a\Delta}{Cd} \log\left[\frac{d-\theta_0}{d+\theta_0} \; \frac{d+\Delta}{d-\Delta}\right] \quad . \tag{D.4.17}$$

Let θ_R and $\dot{\theta}_R$ be the corresponding values of θ and $\dot{\theta}$, i.e.,

$$\theta_R = \Delta \tag{D.4.18}$$

and, from (D.4.9) and (D.4.18),

$$\dot{\theta}_R = C_1 - \frac{C\Delta}{2a} \quad . \tag{D.4.19}$$

Evaluation of $\dot{\theta}$ and $\dot{\theta}$ at t_R from equation (D.4.16) yields C_3 and C_4, so that the solution for $\theta > \Delta$ is complete:

$$\theta(t) = \theta_R + \frac{a}{C}\, \dot{\theta}_R\left(1 - e^{-C(t-t_R)/a}\right) \quad . \tag{D.4.20}$$

D.5 Joint stop damping in three planes

One test performed was for a problem identical to the one illustrated by Figure 92 except that joint stop c's replaced the elastic k's. The analytical solution is not presented here. Of greater interest is that the computer model was used to obtain the motion for identical problems set up in the inertial planes, x-z, x-y, y-z; the resultant motions were equivalent, as they should be.

D.6 Symmetric mass matrix

It can be demonstrated that the generalized mass matrix [G(t)] (Chapter 5) must be symmetric, i.e., $G(t)_{ik} = G(t)_{ki}$. The symmetry may be checked for any forced or free motion exercise of the computer model.

D.7 Maxwell element tests

The implementation in the computer model of Maxwell elements for muscle tension was checked by two tests. Both involved the element for the neck length. The elements were allowed to resist compression in contrast to the "tension only" provision (Section 4.8.2) which is applied to neck length muscle tension whenever the computer model is used to simulate a vehicle occupant rather than some other dynamic system. Both tests involved setting the torso masses equal to large values so that the systems illustrated by Figures 94 and 95 could be approximated. The masses in these figures represent the head mass.

A Maxwell element

Since

$$F = m\ddot{x} \quad , \tag{D.7.1}$$

the equation

$$\dot{F} + \frac{k}{c}F = -k\dot{x} \tag{D.7.2}$$

(i.e., equation (4.8.10)) becomes

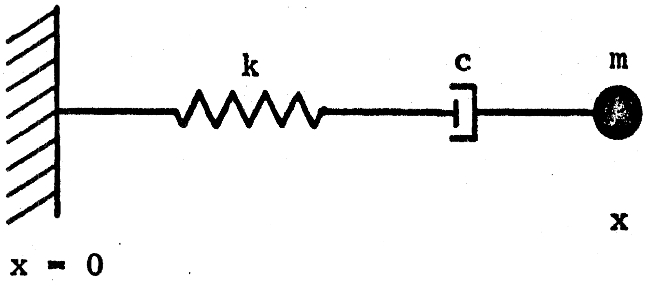

Figure 94. A Maxwell element.

$$m\dddot{x} + \frac{k}{c} m\ddot{x} + k\dot{x} = 0 \quad . \tag{D.7.3}$$

Suppose that initial values x_0, $\dot{x}_0$, and F_0 are given. Equation (D.7.3) can be immediately reduced to second order with a right-hand side integration constant of

$$C_1 = F_0 + \frac{k}{c} m\dot{x}_0 + kx_0 \quad . \tag{D.7.4}$$

The second-order equation with constant coefficients then has the general solution

$$x = e^{-bt}\left(A\cos\omega t + B\sin\omega t\right) + \frac{C_1}{k} , \tag{D.7.5}$$

where

$$b = \frac{k}{2c} \tag{D.7.6}$$

and

$$\omega = \sqrt{\frac{k}{m} - \left(\frac{k}{2c}\right)^2} \quad . \tag{D.7.7}$$

The integration constants A and B are found to be

$$A = -\frac{F_0}{k} - \frac{m}{c}\dot{x}_0 \tag{D.7.8}$$

and

$$B = \frac{m}{k\omega}\left(\omega^2 - \beta^2\right)\dot{x}_0 - \frac{F_0}{2c\omega} \quad . \tag{D.7.9}$$

A three-parameter solid

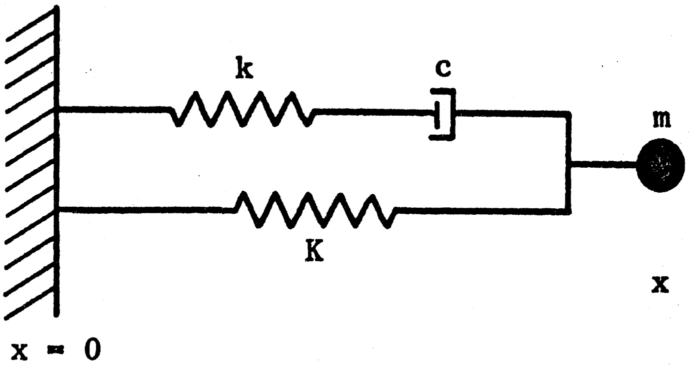

Figure 95. A three-parameter solid.

The procedure demonstrated in Appendix C results in the following governing equations:

$$\begin{aligned} \dot{F} + \frac{k}{c}F &= -k\dot{x} \\ m\ddot{x} &= -K(x - \ell_0) + F \quad , \end{aligned} \tag{D.7.10}$$

where l_0 is the equilibrium length for spring K. These equations could be solved for x as an explicit function of t, but solution of a cubic equation is involved so the analysis would be quite lengthy. A short computer program was written, instead, to solve these equations and the results were compared against the equivalent computer model exercise.

APPENDIX E

ESTIMATION OF NECK MUSCLE TENSION PARAMETER VALUES

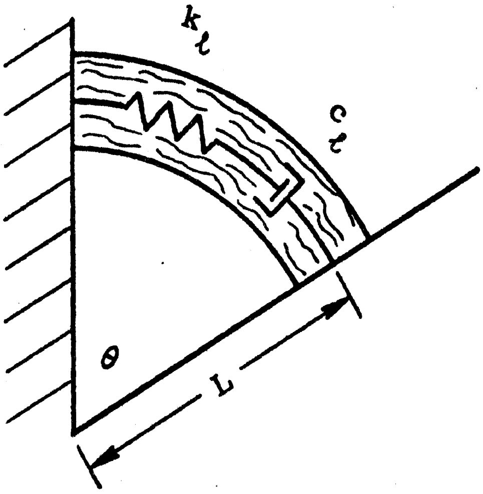

Figure 96. Muscle at a joint.

The effect of muscle tension at a joint is modeled by a Maxwell element with components k_θ and c_θ, where

$$c_\theta = a_1^{(\theta)} |M^{(\theta)}| \tag{E.1}$$

$$k_\theta = a_2^{(\theta)} + a_3^{(\theta)} |M^{(\theta)}| , \tag{E.2}$$

and $M^{(\theta)}$ is the steady, voluntary moment exerted by the subject. The $a_i^{(\theta)}$ are constants for the subject and the joint. This model, based directly on θ-motion, is somewhat artificial in that the moment investigated is really a result of linear action of muscle with a moment arm. Strictly, the effective moment arm, L, is a function of θ, but it will be assumed here to be constant. Figure 96 shows L and the linear components k_ℓ and c_ℓ.

An interpretation of the coefficients $a_i^{(\theta)}$ is now sought. Consider first that

$$c_\ell = a_1^{(\ell)} |F^{(\ell)}| \tag{E.3}$$

$$k_\ell = a_2^{(\ell)} + a_3^{(\ell)} |F^{(\ell)}| \quad . \tag{E.4}$$

Consider a case $k_\ell \longrightarrow \infty$ so that the Maxwell element contributes

$$F = c_\ell (L\dot{\theta}) \quad . \tag{E.5}$$

The corresponding moment is

$$M = F\ell = L^2 \dot{\theta} c_\ell \quad . \tag{E.6}$$

The angular model gives directly

$$M = c_\theta \dot{\theta} \quad , \tag{E.7}$$

so

$$c_\theta = L^2 c_\ell \quad , \tag{E.8}$$

where c_θ, of course, has dimensions of torque per radian velocity. Now,

$$M^{(\theta)} = L F^{(\ell)} \quad , \tag{E.9}$$

and therefore (E.1) becomes

$$c_\theta = a_1^{(\theta)}\left(L\left|F^{(\ell)}\right|\right) . \tag{E.10}$$

From equations (E.3), (E.8), and (E.10) we then obtain

$$a_1^{(\theta)} = L\, a_1^{(\ell)} . \tag{E.11}$$

If we similarly consider $c_\ell \to \infty$, $a_2 = 0$, we get

$$a_3^{(\theta)} = L\, a_3^{(\ell)} . \tag{E.12}$$

Taking $c_\ell \to \infty$ and $a_3 = 0$ gives

$$a_2^{(\theta)} = L^2\, a_2^{(\ell)} . \tag{E.13}$$

So as to eliminate possible confusion it is pointed out that k_ℓ and c_ℓ are not material properties; their values depend on the size, or strength, of a particular muscle, the values being larger for larger muscles and smaller for smaller muscles. Their component parts - $a_1^{(\ell)}|F^{(\ell)}|$, $a_2^{(\ell)}$, and $a_3^{(\ell)}|F^{(\ell)}|$ - have this same character (equations (E.3) and (E.4)). Now, consider two different muscles, one with a maximum possible contraction force $F_{max}^{(\ell)}$ of, say, ten times that of the other. It is reasonable to assume that the maximum c_ℓ for the larger muscle should be ten times c_ℓ for the smaller muscle. It is concluded, therefore, that the constants $a_1^{(\ell)}$ for the two muscles are equal, i.e., that $a_1^{(\ell)}$ is a material property. The constant $a_3^{(\ell)}$ is similarly expected to be a material property, not dependent on the particular muscle. The constant $a_2^{(\ell)}$, on the otherhand, may be expected to be proportional to the maximum potential strength of a particular muscle:

$$a_2^{(\ell)} = a_2'^{(\ell)} \left| F_{max}^{(\ell)} \right| \quad . \tag{E.14}$$

The quantities $a_1^{(\ell)}$, $a_2'^{(\ell)}$, and $a_3^{(\ell)}$ are essentially muscle tissue properties - material properties - and as such may not differ greatly from joint to joint in an individual. If these values are assumed constant from joint to joint, it becomes possible to estimate values for $a_1^{(\theta)}$, $a_2^{(\theta)}$, $a_3^{(\theta)}$ at a second joint if the values at the first joint and values of certain other quantities can be estimated. This is done as follows.

Suppose that for joint number I the following are known: L_I, $a_{1,I}^{(\theta)}$, $a_{2,I}^{(\theta)}$, $a_{3,I}^{(\theta)}$, and $M_{max,I}^{(\theta)}$. For the second joint (II) suppose that L_{II} and $M_{max,II}^{(\theta)}$ are known. Then,

$$\begin{aligned} a_{1,I}^{(\theta)} &= L_I \, a_1^{(\ell)} \\ a_{2,I}^{(\theta)} &= L_I^2 \, a_2'^{(\ell)} \left| F_{max,I}^{(\ell)} \right| \\ a_{3,I}^{(\theta)} &= L_I \, a_3^{(\ell)} \end{aligned} \tag{E.15}$$

by equations (E.11) to (E.14). Also,

$$\begin{aligned} a_{1,II}^{(\theta)} &= L_{II} \, a_1^{(\ell)} \\ a_{2,II}^{(\theta)} &= L_{II}^2 \, a_2'^{(\ell)} \left| F_{max,II}^{(\ell)} \right| \\ a_{3,II}^{(\theta)} &= L_{II} \, a_3^{(\ell)} \quad . \end{aligned} \tag{E.16}$$

Subscripts "I" or "II" are not necessary in (E.15) and (E.16) since $a_1^{(\ell)}$, $a_2'^{(\ell)}$, and $a_3^{(\ell)}$ are assumed constant from joint to joint. These equations then combine to give

$$
\begin{aligned}
a_{1,II}^{(\theta)} &= \left(\frac{L_{II}}{L_I}\right) a_{1,I}^{(\theta)} \\
a_{2,II}^{(\theta)} &= \left(\frac{L_{II}}{L_I}\right)^2 a_{2,I}^{(\theta)} \frac{\left|F_{max,II}^{(\ell)}\right|}{\left|F_{max,I}^{(\ell)}\right|} \\
a_{3,II}^{(\theta)} &= \left(\frac{L_{II}}{L_I}\right) a_{3,I}^{(\theta)} \quad .
\end{aligned}
\tag{E.17}
$$

By (E.9), we can eliminate the ratio of maximum contraction forces:

$$
\frac{\left|F_{max,II}^{(\ell)}\right|}{\left|F_{max,I}^{(\ell)}\right|} = \frac{L_I}{L_{II}} \frac{\left|M_{max,II}^{(\theta)}\right|}{\left|M_{max,I}^{(\theta)}\right|} \quad . \tag{E.18}
$$

Since experimental values of $a_1^{(\theta)}$, $a_2^{(\theta)}$, $a_3^{(\theta)}$ are available for the knee joint, an effort will be made to obtain crude values for other joints from these relations.

It may be deduced from a problem given by Williams and Lissner (41) (pp. 85, 86) that $L_{knee} \simeq 4'' \times \sin 20° = 1.37''$. Also, Williams and

Lissner indicate that a 90 pound exercise load on the foot - with a 24 inch moment arm to the knee - is about maximum for an average man (p. 86). This represents a maximum knee moment of

$$|M^{(\theta)}_{max,knee}| = 180 \text{ ft lb} \quad . \tag{E.19}$$

It is estimated very roughly (from scale drawings in anatomy references) that the effective moment arms for both the neck-torso "joint" and the head-neck "joint" are two inches. Also, Patrick and Mertz (42) give an experimental maximum neck torque value which should closely approximate $|M^{(\theta)}_{max,N-T}|$:

$$|M^{(\theta)}_{max,N-T}| = 17.5 \text{ ft lb} \quad . \tag{E.20}$$

Patrick and Mertz also give maximum static torque values at the occipital condyles (N-H). These values vary from 10.5 ft.lb to 26.0 ft.lb, depending on the position of the head and the sign of the applied moment for bending (fore-aft). The neck-torso value, 17.5 ft.lb, will be assumed for N-H as well. Since both L and M_{max} have been taken as equal for the two neck joints, all $a_i^{(\theta)}$ results will be the same for N-T and N-H.

Moffatt, Harris, and Haslam (24) obtained the following approximate experimental results for the knee:

$$\begin{aligned} a^{(\theta)}_{1,knee} &\simeq 0.5 \text{ sec/rad} = 0.0088 \text{ sec/deg} \\ a^{(\theta)}_{2,knee} &\simeq 600 \text{ in lb/rad} = 0.87 \text{ ft lb/deg} \\ a^{(\theta)}_{3,knee} &\simeq 6/\text{rad} = 0.105/\text{deg} \quad . \end{aligned} \tag{E.21}$$

(Values are given here for [deg^{-1}] only because the vehicle occupant computer program accepts input in terms of degrees.) Using these values and the values for moment arms and maximum static moments we obtain the following results for N-T and N-H from equations (E.17) and (E.18):

$$\begin{aligned} a^{(\theta)}_{1;\,N-T,\,N-H} &= 0.0129 \text{ sec/deg} \\ a^{(\theta)}_{2;\,N-T,\,N-H} &= 0.123 \text{ ft lb/deg} \\ a^{(\theta)}_{3;\,N-T,\,N-H} &= 0.153/\text{deg} \quad . \end{aligned} \tag{E.22}$$

These values are hoped to be reasonable for bending type deformation of the neck.

The neck is also capable of muscular resistance to twisting. The effective moment arm for the muscles will be taken as two inches. It will also be assumed rather arbitrarily that the neck can resist a static twisting moment of only one-fourth the maximum bending moment, i.e., $|M^{(\theta)}_{\max,H-T}| = 17.5/4 = 4.375$ ft.lb. Accordingly,

$$\begin{aligned} a^{(\theta)}_{1,\,H-T} &= 0.0129 \text{ sec/deg} \\ a^{(\theta)}_{2,\,H-T} &= 0.0308 \text{ ft lb/deg} \\ a^{(\theta)}_{3,\,H-T} &= 0.153/\text{deg} \quad . \end{aligned} \tag{E.23}$$

The model of the neck also allows for muscular resistance to stretching. The coefficients $a^{(\ell)}_i$ are required.

It is assumed that the muscles which resist stretching are essentially the same as those resisting bending. It is assumed further, however, that only about half the muscle helps to resist bending in any direction while all of the muscle helps to resist stretching; hence, a factor of 2 is introduced for $a_2^{(\ell)}$, which depends on the amount of potentially active muscle. From equations (E.11) to (E.13) we then obtain

$$a^{(\ell)}_{1,\,neck} = \frac{a^{(\theta)}_{1,\,N-T}}{L_{N-T}} = 4.44\ sec/ft \tag{E.24}$$

$$a^{(\ell)}_{2,\,neck} = 2\,\frac{a^{(\theta)}_{2,\,N-T}}{L^2_{N-T}} = 508\ lb/ft$$

$$a^{(\ell)}_{3,\,neck} = \frac{a^{(\theta)}_{3,\,N-T}}{L_{N-T}} = 52.7/ft\ ,$$

where the results (E.22) have been first converted to [rad^{-1}] dimensions. Also, a reasonable value for $|F^{(\ell)}_{\max,\text{neck}}|$ can be assumed to be

$$\left|F^{(\ell)}_{max,\,neck}\right| = 2\,\frac{\left|M^{(\theta)}_{max,\,N-T}\right|}{L_{N-T}} = 210\ lb. \tag{E.25}$$

(Patrick and Mertz (42) give an experimentally determined value of 250 lb.)

APPENDIX F

TWO-DIMENSIONAL ANALOGUES OF THE BASIC BALL-AND-SOCKET JOINT CHARACTERISTICS

This appendix illustrates the basic joint characteristics of the three-dimensional analytical model in terms of two-dimensional analogues. The illustrations here are for torso joints in particular, but the fundamental characteristics apply for the neck joints as well - "N-T" and "N-H" for bending and "H-T" for twisting. Extensions to the three-dimensional ball-and-socket joint are described in general terms in Chapter 3 and in analytical detail in Chapter 4.

F.1 Joint stop moments

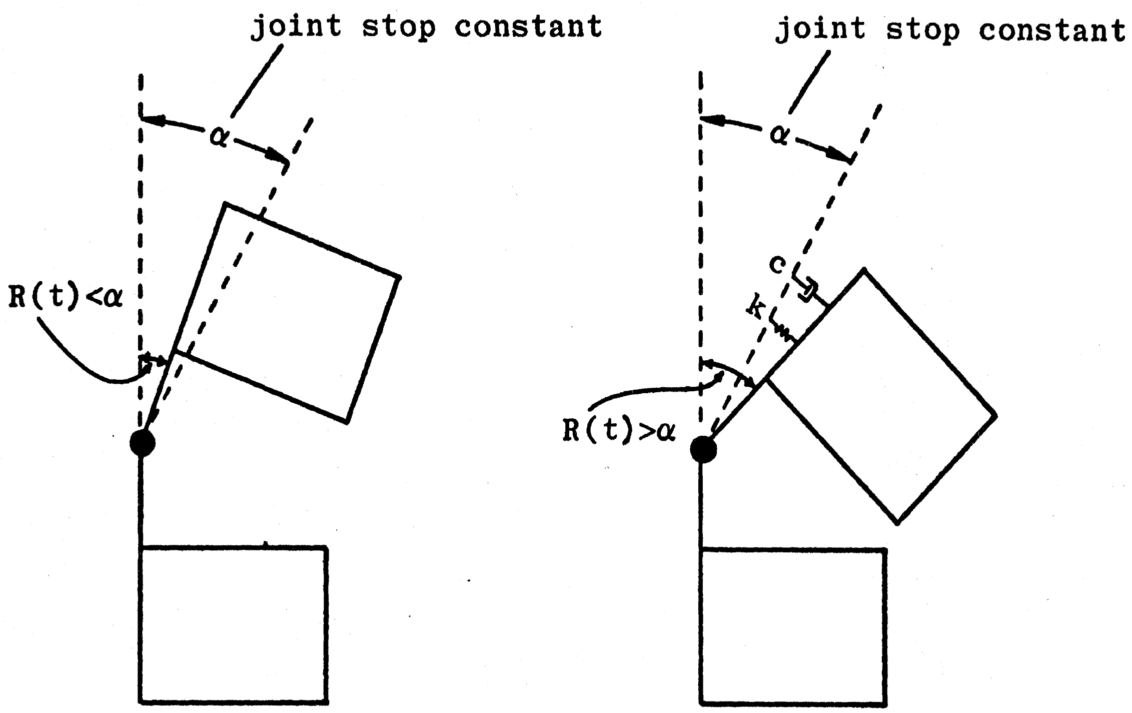

zero deformation

$$M = 0$$

non-zero deformation

$$M = k_{nonlinear}(R-\alpha) + c_{nonlinear}\dot{R}$$

Figure 97. Two-dimensional analogue for joint stop resistance to bending at a typical torso joint.

Figure 97 shows the character of "joint stop" resistance to bending deformation. Relative bending occurs freely until the bending angle exceeds a constant value, the joint stop angle. Figure 98 illustrates a similar joint stop resistance to relative twisting of the elements. It is noted here that the three-dimensional extension for twisting deformation is essentially the same as illustrated while the extension to bending in three dimensions of necessity differs considerably.

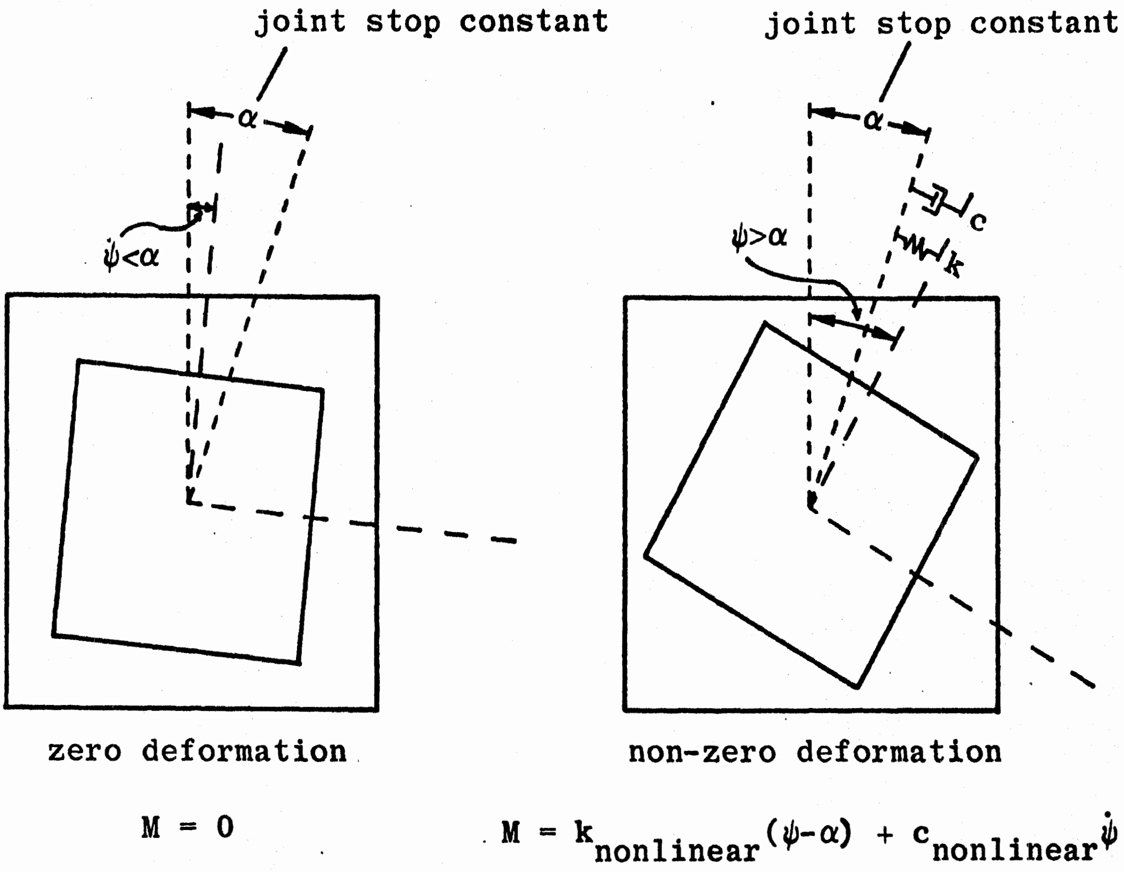

zero deformation

$M = 0$

non-zero deformation

$M = k_{nonlinear}(\psi-\alpha) + c_{nonlinear}\dot{\psi}$

Figure 98. Joint stop resistance to twisting at a typical torso joint (top view of two connected body elements).

F.2 Elastic moments

A second joint characteristic of the anlytical model is the tendency for return to an equilibrium position, the orientation at t = 0. Deformations for this "elastic" bending and twisting are shown in Figures 99 and 100.

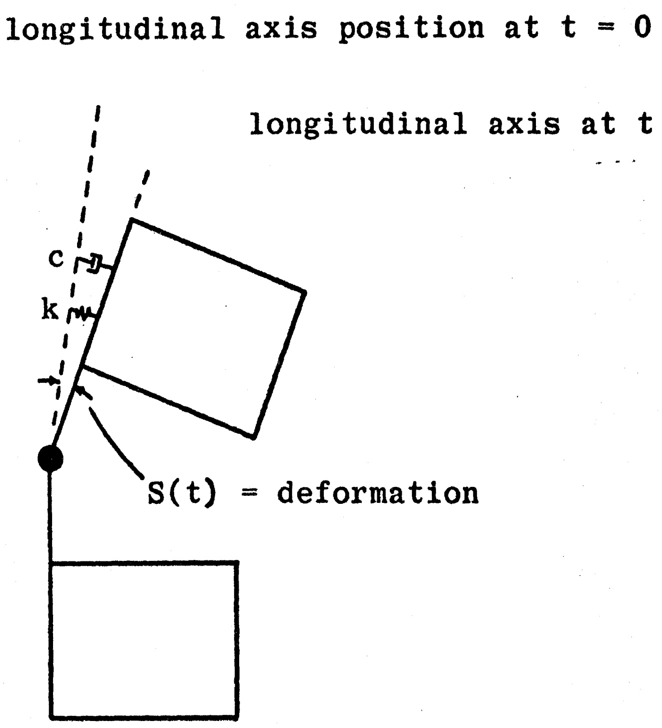
longitudinal axis position at t = 0
longitudinal axis at t
c
k
S(t) = deformation

$$M = k_{\text{nonlinear}}S + c_{\text{nonlinear}}\dot{S}$$

Figure 99. Two-dimensional analogue for elastic resistance to bending deformation away from equilibrium at a typical torso joint.

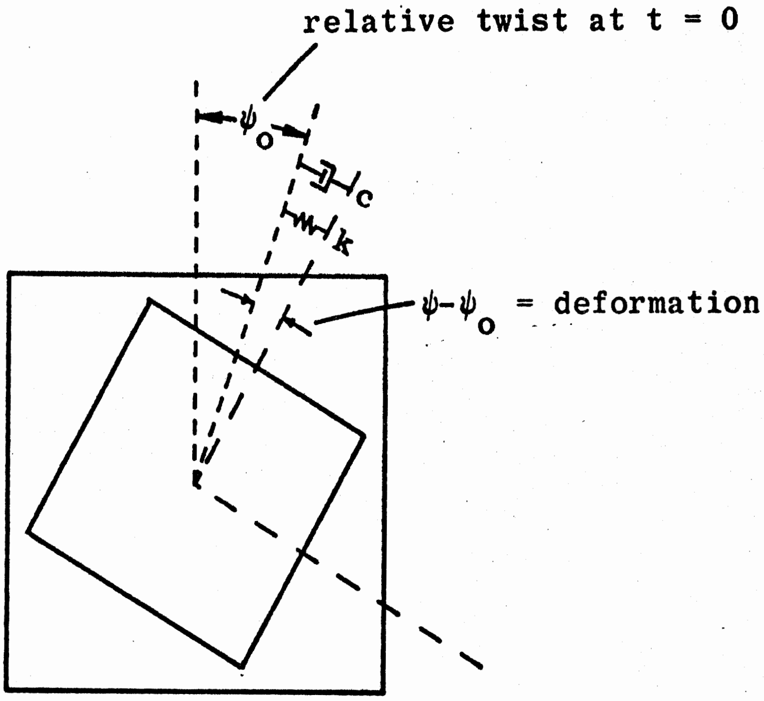
relative twist at t = 0
ψ_o
c
k
$\psi-\psi_o$ = deformation

$$M = k_{nonlinear}(\psi-\psi_o) + c_{nonlinear}\dot{\psi}$$

Figure 100. Elastic resistance to twisting deformation away from equilibrium at a typical torso joint (top view of two connected elements).

F.3 Neck length extension and compression

The character of resistance to change of the neck length is illustrated by Figure 101. The series spring and damper represent the effect of muscle contraction; the coefficients are functions of a parameter F which indicates the degree of muscle tightening.

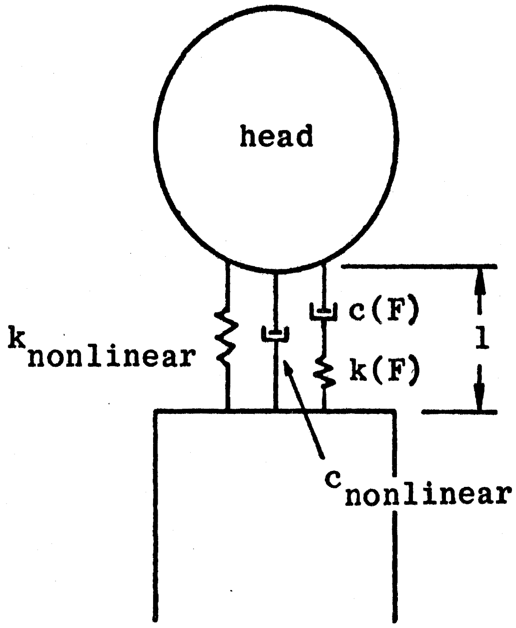

Figure 101. Resistance to change of neck length.

F.4 Muscle tension moments

Rotational Maxwell elements analogous to the linear element shown in Figure 101 represent the effect of muscle contraction on relative bending and twisting at ball-and-socket joints. Figure 96 (Appendix E) illustrates the muscle tension moment resistance to these relative angular motions at a joint.